



Extraction, modification and characterization of lignin from oil palm fronds as corrosion inhibitors for mild steel in acidic solution

Mohd Hazwan Bin Hussin

► To cite this version:

Mohd Hazwan Bin Hussin. Extraction, modification and characterization of lignin from oil palm fronds as corrosion inhibitors for mild steel in acidic solution. Food and Nutrition. Université de Lorraine, 2014. English. NNT: 2014LORR0135 . tel-01750984

HAL Id: tel-01750984

<https://hal.univ-lorraine.fr/tel-01750984>

Submitted on 29 Mar 2018

HAL is a multi-disciplinary open access archive for the deposit and dissemination of scientific research documents, whether they are published or not. The documents may come from teaching and research institutions in France or abroad, or from public or private research centers.

L'archive ouverte pluridisciplinaire **HAL**, est destinée au dépôt et à la diffusion de documents scientifiques de niveau recherche, publiés ou non, émanant des établissements d'enseignement et de recherche français ou étrangers, des laboratoires publics ou privés.



AVERTISSEMENT

Ce document est le fruit d'un long travail approuvé par le jury de soutenance et mis à disposition de l'ensemble de la communauté universitaire élargie.

Il est soumis à la propriété intellectuelle de l'auteur. Ceci implique une obligation de citation et de référencement lors de l'utilisation de ce document.

D'autre part, toute contrefaçon, plagiat, reproduction illicite encourt une poursuite pénale.

Contact : ddoc-theses-contact@univ-lorraine.fr

LIENS

Code de la Propriété Intellectuelle. articles L 122. 4

Code de la Propriété Intellectuelle. articles L 335.2- L 335.10

http://www.cfcopies.com/V2/leg/leg_droi.php

<http://www.culture.gouv.fr/culture/infos-pratiques/droits/protection.htm>



Faculté des Sciences et Technique

U.F.R. : Science et Technique

Ecole doctoral : RP2E

Formation doctorale : Sciences du Bois et des Fibres

THESE

Présentée pour l'obtention de grade de

Docteur de l'Université de Lorraine

En Sciences du Bois et des Fibres

Par

Mohd Hazwan BIN HUSSIN

Extraction, modification and characterization of lignin from oil palm fronds as corrosion inhibitors for mild steel in acidic solution

Extraction, modification et caractérisation de lignine de frondes de palmier à huile pour la production d'inhibiteurs de corrosion dans solution d'acidique

Soutenue publiquement le 29 Octobre 2014 à l'Université Sains Malaysia

Membres de jury :

M. Mohd Jain Noordin MOHD KASSIM	Professeur des Universités, USM
Mme. Hasnah OSMAN	Professeur des Universités, USM
M. Jean-Michel LAVOIE	Professeur des Universités, UdS
Mme. Khalijah AWANG	Professeur des Universités, UM
M. Nicolas BROSSE	Professeur des Universités, UL
Mme. Afidah ABDUL RAHIM	Professeur des Universités, USM

ACKNOWLEDGEMENTS

First and foremost, I would like to thank my supervisors Assoc. Prof. Afidah Abdul Rahim from USM and Pr. Nicolas Brosse from Universite de Lorraine, France for the valuable guidance, advice, encouragement and assistance.

A million thanks to the Malaysian Ministry of Higher Education and to the Ministere Affaires Etrangeres de France for providing me scholarships (MyPhD scholarship and the Boursier du Gouvernement Francais; CampusFrance) throughout this PhD co-tutelle programme. I would like to extent my gratitude also for the financial support of this research from Universiti Sains Malaysia through USM Research University Grant – 1001/PKIMIA/854002.

I sincerely thank all administrative and technical staff of School of Chemical Sciences (especially Assoc. Prof. Mohamad Nasir Mohamad Ibrahim), Archaeology Research Centre, School of Physics, CRM2 UMR 7036 Laboratoire (Dr. Mehdi Yemloul), LERMAB (Lyne Desharnais and Dr. Dominique Perrin) who is helping me a lot during my PhD studies.

Besides, my sincere appreciation goes to all lab mates at USM (Affaizza, Zaharaddeen, Ridhwan and Helen) and UL (Francois Gambier, Yann Lebrech, Guevara Nonviho and Jean Bosco Saha), lecturers and parents. Lastly to my lovely wife Salmiah Md. Zain and my son Emil Harithah whom consistently support and always be with me in both happy and hard time. Thank you, *merci beacoup et a bientot!*

TABLE OF CONTENTS

	Page
Acknowledgements	ii
Table of contents	iii
List of Figures	viii
List of Tables	xiii
List of Appendices	xvi
List of Abbreviations	xvii
List of Symbols	xix
Abstrak	xxi
Abstract	xxiv
Résumé	xxvii
CHAPTER ONE – INTRODUCTION	1
1.1 Biomass as renewable feedstock	1
1.2 Lignocellulosic biomass	3
1.3 Oil palm (<i>Elaeis guineensis</i>)	5
1.3.1 Oil palm biomass waste and applications	8
1.3.2 Oil palm fronds (OPF)	9
1.4 Lignin	11
1.4.1 Delignification process	14
1.4.1.1 Kraft pulping	15
1.4.1.2 Soda pulping	17
1.4.1.3 Organosolv pulping	18

1.4.2	Combinative pretreatment process	19
1.4.2.1	Acid pretreatment	20
1.4.2.2	Autohydrolysis	21
1.4.2.3	Addition of organic scavengers during pretreatment	23
1.4.3	Fractionation and purification of lignin by ultrafiltration system	24
1.4.4	Applications of lignin	26
1.5	Corrosion of steels	28
1.5.1	Corrosion protection	31
1.5.2	Corrosion inhibitors	32
1.5.3	Corrosion measurement techniques	37
1.5.3.1	Weight loss measurement	37
1.5.3.2	Potentiodynamic polarization measurement	37
1.5.3.3	Electrochemical impedance spectroscopy (EIS)	40
1.6	Problem statement and motivation	43
1.7	Objectives	44
CHAPTER TWO – EXPERIMENTAL		46
2.1	Materials	46
2.2	Alkaline lignin extraction	48
2.3	Organosolv lignin extraction	49
2.4	Pretreatment of OPF	50
2.4.1	Dilute sulphuric acid pretreatment	50
2.4.2	Autohydrolysis pretreatment	50
2.4.3	Pretreatment with organic scavengers	51
2.5	Purification and fractionation of lignin by ultrafiltration unit	51

2.5.1	Fractionation of lignin (Kraft, soda and organosolv lignin) with 5 kDa membrane	52
2.6	Analytical procedures	53
2.7	High-performance anion-exchange chromatography (HPAEC) conditions	53
2.8	Characterization of lignin	54
2.8.1	Preliminary analysis of lignin	54
2.8.2	Fourier Transform Infrared (FTIR)	55
2.8.3	Nuclear Magnetic Resonance Spectroscopy (NMR)	55
2.8.4	High performance liquid chromatography (HPLC) of oxidized lignin	56
2.8.5	Gel permeation chromatography (GPC)	57
2.8.6	Thermal analysis	58
2.9	Antioxidant activity	59
2.9.1	Lignin antioxidant activity by oxygen uptake method	59
2.9.2	Lignin antioxidant activity by reducing power assay	60
2.10	Dissolution test of lignin	60
2.11	Corrosion inhibition studies	61
2.11.1	Electrochemical measurements	61
2.11.2	Weight loss measurement	63
2.11.3	Surface analysis	64
CHAPTER THREE – RESULT AND DISCUSSION		65
3.1	Characterization of oil palm fronds (OPF)	65
3.2	Characterization of lignins extracted from OPF via direct delignification processes	66
3.2.1	Composition of lignin samples (Kraft, soda and organosolv)	66

3.2.2	FTIR analysis	68
3.2.3	^1H , ^{13}C and ^{31}P NMR spectra	70
3.2.4	Molecular weight	77
3.2.5	Thermal behaviour	79
	3.2.5.1 Thermal gravimetric analysis	79
	3.2.5.2 Differential scanning calorimetry	81
3.2.6	Composition of phenolic acids and aldehydes	82
3.2.7	Lignin antioxidant activity by oxygen uptake method	84
3.2.8	Lignin antioxidant activity by reducing power assay	86
3.3	Characterization of lignins extracted from OPF via combinative pretreatment processes (with and without organic scavengers)	88
	3.3.1 Composition of pretreated OPF biomass	88
	3.3.2 Composition of lignin samples	89
	3.3.3 FTIR analysis	91
	3.3.4 ^1H , ^{13}C and ^{31}P NMR spectra	94
	3.3.5 HSQC and HMBC NMR	99
	3.3.6 Molecular weight	105
	3.3.7 Thermal behaviour	107
	3.3.7.1 Thermal gravimetric analysis	107
	3.3.7.2 Differential scanning calorimetry	109
	3.3.8 Composition of phenolic acids and aldehydes	109
	3.3.9 Lignin antioxidant activity by oxygen uptake method	113
	3.3.10 Lignin antioxidant activity by reducing power assay	115
3.4	Characterization of OPF lignins fractionated by ultrafiltration technique	116
	3.4.1 FTIR analysis	117

3.4.2	³¹ P NMR	120
3.4.3	Molecular weight	122
3.4.4	Thermal behaviour	123
3.4.4.1	Thermal gravimetric analysis	123
3.4.4.2	Differential scanning calorimetry	125
3.4.5	Lignin antioxidant activity by oxygen uptake method	126
3.4.6	Lignin antioxidant activity by reducing power assay	128
3.5	Corrosion inhibition studies of modified (AHN EOL and AHD EOL) and ultrafiltrated (Kraft, soda and organosolv fractions) OPF lignins in 0.5 M HCl	129
3.5.1	Preliminary dissolution test of lignins	130
3.5.2	Electrochemical measurements of the mild steel corrosion in 0.5 M HCl solution	132
3.5.2.1	Electrochemical impedance spectroscopy (EIS)	132
3.5.2.2	Potentiodynamic polarization measurement	139
3.5.3	Weight loss measurement	146
3.5.3.1	Thermodynamics of corrosion process	149
3.5.3.2	Adsorption studies	156
3.5.4	Surface analysis	161
3.5.5	Correlation between modified lignin properties and the mild steel corrosion inhibition and their possible mechanisms	167
CHAPTER FOUR – CONCLUSION AND FUTURE RESEARCH RECOMMENDATIONS		172
REFERENCES		178
LIST OF PUBLICATIONS , PRESENTATIONS AND AWARDS		198
APPENDICES		202

LIST OF FIGURES

	Page
Figure 1.1	Biomass utilization (www.riken.jp/bmep/english/outline/co2.html). 2
Figure 1.2	Composition of plant cell wall as lignocellulosic biomass (Sannigrahi <i>et al.</i> , 2010). 4
Figure 1.3	<i>Elaeis guineensis</i> as illustrated by Nicholaas Jacquin in 1763 (<i>Elaeis guineensis</i> , 2014). 6
Figure 1.4	Top palm oil producers, importers and consumers (Source: UNEP, 2011). 7
Figure 1.5	Lignocellulosic biomass components of oil palm tree. 8
Figure 1.6	Monolignols basic unit in lignin. (H): p-coumaryl alcohol/p-hydroxyphenyl; (G): coniferyl alcohol/guaiacyl; (S): sinapyl alcohol/syringyl. 12
Figure 1.7	Softwood lignin structure (Brunow, 2001). 13
Figure 1.8	Mechanistic change of lignin during Kraft pulping process (Tejado <i>et al.</i> , 2007). 16
Figure 1.9	The structure of Kraft lignin with thiol groups, -SH as proposed by Holladay <i>et al.</i> (2007). 17
Figure 1.10	Mechanistic change of lignin during soda pulping process (Tejado <i>et al.</i> , 2007). 18
Figure 1.11	Mechanistic change of lignin during organosolv pulping process (Tejado <i>et al.</i> , 2007). 19
Figure 1.12	Pretreatment of lignocellulosic biomass (Timilsena, 2012). 20
Figure 1.13	A possible mechanism during autohydrolysis (Samuel <i>et al.</i> , 2013). 22
Figure 1.14	Lignin repolymerization and immobilization via the incorporation of organic scavengers (El Hage <i>et al.</i> , 2010). 23
Figure 1.15	The principle of ultrafiltration. 26
Figure 1.16	Possible applications of lignin. 27
Figure 1.17	The mechanism of corrosion of steel (Ahmad, 2006). 29

Figure 1.18	Pourbaix diagram of steel which explain how corrosion protection can be achieved (Kruger, 2001).	32
Figure 1.19	Example of different modes of interaction on mild steel surface during inhibition process (Ansari and Quraishi, 2014).	35
Figure 1.20	Extrapolation of Tafel curves.	39
Figure 1.21	(a) Nyquist and (b) Bode plots of impedance (Dominquez-Benetton <i>et al.</i> , 2012).	41
Figure 1.22	Some examples of equivalent circuits used for EIS analysis. (C_{dl} : double layer capacitance; CPE: constant phase element; Z_d : diffusion resistant; R_{ct} : charge transfer resistant; R_s : solution resistant).	42
Figure 2.1	An overview of lignin extraction at Universiti Sains Malaysia and Universite de Lorraine with mass balance, w/w % (*used for corrosion study).	47
Figure 3.1	FTIR spectra of Kraft, soda and organosolv lignin in the expanded range.	69
Figure 3.2	^1H NMR spectra of acetylated alkaline lignin (Kraft and soda) and organosolv lignin from oil palm fronds	71
Figure 3.3	^{13}C NMR spectra of acetylated OPF lignin samples: (A) organosolv lignin and (B) expanded aromatic region.	73
Figure 3.4	Lignin substructures (Capanema <i>et al.</i> , 2004).	74
Figure 3.5	^{13}C NMR spectra of expanded acetyl region for: (A) Kraft; (B) soda and (C) organosolv lignin from OPF.	75
Figure 3.6	^{31}P NMR spectrum of Kraft, soda and organosolv lignin.	76
Figure 3.7	(A) TG and (B) DTG curves for Kraft, soda and organosolv lignin.	80
Figure 3.8	HPLC chromatogram of; (A) Kraft, (B) soda, (C) organosolv lignin after nitrobenzene oxidation and (D) mix standards obtained at a flow rate of 1 mL min^{-1} and 280 nm of UV detection.	83
Figure 3.9	Oxygen uptake profile of Kraft, soda and organosolv lignin.	85
Figure 3.10	Antioxidant profile of Kraft, soda and organosolv lignin by reducing power assay obtained at 700 nm.	87
Figure 3.11	Infra red spectra of organosolv OPF lignin after combinative pretreatments. Circle lines indicate region of interest.	92

Figure 3.12	¹ H NMR spectra of different pretreated organosolv lignin.	95
Figure 3.13	¹ H NMR spectra of autohydrolyzed organosolv lignin in the presence of 2-naphthol (AHN EOL) and 1,8-dihydroxyanthraquinone (AHD EOL).	96
Figure 3.14	¹³ C NMR spectra of different pretreated organosolv OPF lignin samples in expanded aromatic region. * Chemical shifts of 2-naphthol and 1,8-dihydroxyanthraquinone.	97
Figure 3.15	³¹ P NMR spectra of different pretreated organosolv OPF lignin samples in expanded region.	98
Figure 3.16	2D-HSQC NMR spectrum of (A) autohydrolyzed; (B) autohydrolyzed with 2-naphthol and (C) autohydrolyzed with 1,8-dihydroxyanthraquinone organosolv lignin.	101
Figure 3.17	2D-HMBC NMR spectrum at (A) aromatic region; (B) side chain region of autohydrolyzed lignin in presence of 2-naphthol.	102
Figure 3.18	Anthraquinone/ anthrahydroxyquinone redox cycle in presence of reducing sugars.	104
Figure 3.19	2D-HMBC NMR spectrum at side chain region of lignin with 1,8-dihydroxyanthraquinone. (Inset: Structure of 1,8-dihydroxyanthrahydroxyquinone).	105
Figure 3.20	(A) TG and (B) DTG curves for different pretreated organosolv lignin.	108
Figure 3.21	HPLC chromatogram of; (A) DAP EOL, (B) AH EOL, (C) AHN EOL and (D) AHD EOL organosolv lignins obtained at a flow rate of 1 mL min ⁻¹ and 280 nm of UV detection.	110
Figure 3.22	Oxygen uptake profile of different pretreated organosolv lignins.	114
Figure 3.23	Antioxidant profile of different pretreated and untreated organosolv lignins by reducing power assay obtained at 700 nm.	116
Figure 3.24	FTIR spectra of lignin obtained before and after ultrafiltration (5 kDa) of Kraft, soda and organosolv solutions.	118
Figure 3.25	³¹ P NMR spectra of OPF lignin fractions after ultrafiltration (5 kDa) in expanded region.	121
Figure 3.26	(A) TG and (B) DTG curves for OPF lignin fractions after ultrafiltration (5 kDa).	124

Figure 3.27	Oxygen uptake profile of different lignin fractions after ultrafiltration (5 kDa).	127
Figure 3.28	Antioxidant profile of different lignin fractions by reducing power assay obtained at 700 nm.	129
Figure 3.29	Dissolution profiles of modified, ultrafiltrated and crude lignins.	131
Figure 3.30	Nyquist plot of mild steel in 0.5 M HCl solution in absence and presence of; (A) AHN EOL and (B) AHD EOL lignin at 303 K.	135
Figure 3.31	Nyquist plot of mild steel in 0.5 M HCl solution in absence and presence of; (A) Kraft, (B) Soda and (C) Organosolv lignin fractions at 303 K.	136
Figure 3.32	The electrical equivalent circuit of Randles-CPE for EIS measurement.	138
Figure 3.33	Tafel curves of mild steel in 0.5 M HCl solution in absence and presence of; (A) AHN EOL and (B) AHD EOL lignin at 303 K.	140
Figure 3.34	Tafel curves of mild steel in 0.5 M HCl solution in absence and presence of; (A) Kraft, (B) Soda and (C) Organosolv lignin fractions at 303 K.	141
Figure 3.35	The correlation of inhibition efficiency with concentration for all lignin inhibitors at 303 K.	148
Figure 3.36	Transition-state plots of the corrosion rate (CR) of mild steel in 0.5 M HCl solution in absence and presence of; (A) AHN EOL and (B) AHD EOL lignin.	151
Figure 3.37	Transition-state plots of the corrosion rate (CR) of mild steel in 0.5 M HCl solution in absence and presence of; (A) Kraft, (B) Soda and (C) Organosolv lignin fractions.	152
Figure 3.38	Modified Arrhenius plots of the corrosion rate (CR/T) of mild steel in 0.5 M HCl solution in absence and presence of; (A) AHN EOL and (B) AHD EOL lignin.	154
Figure 3.39	Modified Arrhenius plots of the corrosion rate (CR/T) of mild steel in 0.5 M HCl solution in absence and presence of; (A) Kraft, (B) Soda and (C) Organosolv lignin fractions.	155
Figure 3.40	Langmuir adsorption plot of mild steel after 48 h of immersion in 0.5 M HCl solution in absence and presence of lignin inhibitors at 303 K.	158

Figure 3.41	Relation between C_{dl} and the applied potential on a mild steel electrode in 0.5 M HCl without and with; (A) modified and (B) ultrafiltrated lignin inhibitors.	162
Figure 3.42	SEM (top right) micrograph, XRD (below right) and EDX spectra of mild steel after 48 h of immersion in 0.5 M HCl solution in; (A) absence and presence of (B) AHN EOL and (C) AHD EOL lignin at 303 K and magnification 1000 x.	164
Figure 3.43	SEM (top right) micrograph, XRD (below right) and EDX spectra of mild steel after 48 h of immersion in 0.5 M HCl solution in presence of; (A) Kraft, (B) soda and (C) organosolv lignin fractions at 303 K and magnification 1000 x.	165
Figure 3.44	Influence of the diverse parameters studied on the inhibition efficiency of the analyzed lignins at the concentration of 500 ppm.	168
Figure 3.45	Corrosion inhibition reaction pathway of mild steel (Solmaz <i>et al.</i> , 2008).	169
Figure 3.46	Schematic adsorption and inhibition interaction mechanism of lignin molecules at; (A) syringyl unit, (B) 1,8-dihydroxyanthraquinone and (C) 2-naphthol sites on mild steel in 0.5 M HCl.	171

LIST OF TABLES

	Page
Table 1.1	Representation of different fractions of lignocellulosic materials. 4
Table 1.2	Composition of oil palm biomass (Oil palm biomass, 2011). 9
Table 1.3	Chemical composition of oil palm fronds (Wanrosli <i>et al.</i> , 2007). 10
Table 1.4	Different linkage types in softwood and hardwood lignin per 100 C9 unit (Henrikson <i>et al.</i> , 2010). 14
Table 1.5	Various adsorption isotherms for corrosion inhibition studies (Wan Adnan, 2012). 36
Table 3.1	Composition of raw material in OPF. 66
Table 3.2	Proximate analysis of Kraft, soda and organosolv lignin from oil palm fronds (% w/w on dry matter). 68
Table 3.3	Assignment of FTIR spectra of lignin from oil palm fronds. 70
Table 3.4	Signal assignment for ^{13}C NMR spectrometry of acetylated alkaline lignin and organosolv lignin from oil palm fronds. 72
Table 3.5	Lignins characterized by ^{31}P NMR. 77
Table 3.6	The yield (% dry sample, w/w) of phenolic acids and aldehydes from alkaline nitrobenzene oxidation of lignin samples. 84
Table 3.7	Composition of OPF biomass residues after prehydrolysis. 88
Table 3.8	Proximate analysis of pretreated organosolv lignin from oil palm fronds (% w/w on dry matter). 90
Table 3.9	Organosolv OPF lignins after combinative pretreatments characterized by FTIR. 93
Table 3.10	Pretreated organosolv lignins characterized by ^{31}P NMR. 99
Table 3.11	GPC results of weight-average (M_w), number-average (M_n) and polydispersity (PD) of different pretreated organosolv lignin from oil palm fronds. 106

Table 3.12	The yield (% dry sample, w/w) of phenolic acids and aldehydes from alkaline nitrobenzene oxidation of different pretreated organosolv lignin samples.	111
Table 3.13	Permeate lignin fractions characterized by ^{31}P NMR.	121
Table 3.14	GPC results of weight-average (M_w), number-average (M_n) and polydispersity (PD) of OPF lignin fractions after ultrafiltration.	123
Table 3.15	Electrochemical impedance parameters for mild steel in 0.5 M HCl solution in the absence and presence of AHN EOL and AHD EOL lignin at 303 K.	133
Table 3.16	Electrochemical impedance parameters for mild steel in 0.5 M HCl solution in the absence and presence of different ultrafiltrated lignin fractions (5 kDa) at 303 K.	133
Table 3.17	Electrochemical polarization parameters for mild steel in 0.5 M HCl solution in the absence and presence of AHN EOL and AHD EOL lignin at 303 K.	142
Table 3.18	Electrochemical polarization parameters for mild steel in 0.5 M HCl solution in the absence and presence of different ultrafiltrated lignin fractions (5 kDa) at 303 K.	143
Table 3.19	The inhibition efficiency of mild steel in 0.5 M HCl solution in the absence and presence of AHN EOL and AHD EOL lignin at 303 K.	147
Table 3.20	The inhibition efficiency of mild steel in 0.5 M HCl solution in the absence and presence of different ultrafiltrated lignin fractions (5 kDa) at 303 K.	147
Table 3.21	Activation parameters for mild steel dissolution in 0.5 M HCl solution in the absence and presence of AHN EOL and AHD EOL lignin.	153
Table 3.22	Activation parameters for mild steel dissolution in 0.5 M HCl solution in the absence and presence of different ultrafiltrated lignin fractions (5 kDa).	153
Table 3.23	Adsorption parameters for mild steel in 0.5 M HCl by weight loss measurement in the absence and presence of AHN EOL and AHD EOL lignin at 303 K.	158
Table 3.24	Adsorption parameters for mild steel in 0.5 M HCl by weight loss measurement in the absence and presence of different ultrafiltrated lignin fractions at 303 K.	159

Table 3.25	Values of E_r for the mild steel electrode in 0.5 M HCl for studied inhibitors.	163
Table 3.26	Percentage atomic contents of elements obtained from EDX spectra.	166

LIST OF APPENDICES

	Page
Appendix I: FTIR spectra of lignin samples	202
Appendix II: ^{13}C NMR spectra of lignin samples	203
Appendix III: DSC thermograms of lignin samples	207
Appendix IV: Calibration curves of all standards obtained from HPLC	211
Appendix V: Bode plots of all modified lignin samples obtained from EIS	218
Appendix VI: Effect of temperature on the mild steel corrosion inhibition	221
Appendix VII: Temkin adsorption isotherm curves	226

LIST OF ABBREVIATIONS

AH EOL	autohydrolysis organosolv lignin
AHD EOL	autohydrolysis with 1,8-dihydroxyanthraquinone organosolv lignin
AHN EOL	autohydrolysis with 2-naphthol organosolv lignin
CE	counter electrode
DAP EOL	dilute sulphuric acid prehydrolysis organosolv lignin
DSC	differential scanning calorimetry
EDX	energy dispersive X-ray spectroscopy
EIS	electrochemical impedance spectroscopy
EOL	ethanol organosolv lignin
FAO	Food and Agricultural Organization of the United Nations
FTIR	fourier transform infrared spectroscopy
GPC	gel permeation chromatography
HMBC	heteronuclear multiple bond correlation
HMW	high molecular weight
HPLC	high performance liquid chromatography
HSQC	heteronuclear single quantum correlation
LFP	lignin fraction recovery
LMW	low molecular weight
NMR	nuclear magnetic resonance spectroscopy
OPF	oil palm fronds

OUI	oxygen uptake inhibition
PZC	potential zero charge
RE	reference electrode
SCE	saturated calomel electrode
SEM	scanning electron microscopy
TGA	thermal gravimetry analysis
UNEP	United Nations Environment Programme
WE	working electrode
XRD	X-ray diffraction spectroscopy

LIST OF SYMBOLS

CPE	constant phase element
CR	corrosion rate
DTG	rate of thermal degradation weight loss
E_a	activation energy
E_{corr}	corrosion potential
E_r	Antropov ‘rational’ corrosion potential
G	guaiacyl/coniferyl alcohol unit
H	p-hydroxyphenyl/p-coumaryl alcohol unit
I_{corr}	corrosion current density
IE	inhibition efficiency
K_{ads}	adsorption constant
mA cm^{-2}	milliampere per centimetre square
mm y^{-1}	millimeters per year
M_n	average molecular number
mpy	mils of penetration per year
M_w	average molecular weight
PD	polydispersity
R_0	relative factor
R_{ct}	resistance charge transfer
S	syringyl/sinapyl alcohol unit
S_0	severity factor

T_g	glass transition
TG	thermal degradation weight loss
ΔG°_{ads}	Gibbs free energy of adsorption
ΔH^*	enthalpy activation
ΔS^*	entropy activation
θ	surface coverage
$\Omega \text{ cm}^2$	Ohm's centimetre square

**PENGEKSTRAKAN, PENGUBAHSUAIAN DAN PENCIRIAN LIGNIN
DARIPADA PELEPAH SAWIT SEBAGAI PERENCAT KARAT UNTUK
BESI LEMBUT DALAM LARUTAN BERASID**

ABSTRAK

Biomassa lignoselulosik di Malaysia boleh dianggap sebagai salah satu sumber tenaga diperbaharui. Ianya terdiri daripada selulosa, hemiselulosa dan lignin dan paling sesuai untuk tenaga dan penggunaan bahan kimia kerana ketersediaan yang mencukupi, murah dan mesra alam. Secara amnya, penghasilan biomassa lignoselulosik di Malaysia adalah tinggi yang kebanyakannya disumbangkan oleh industri sawit (dianggarkan 60 juta tan sisa sawit yang dihasilkan setiap tahun). Sisa sawit berpotensi untuk digunakan sebagai sumber alternatif bagi penghasilan kertas dan papan keras. Walau bagaimanapun, sejumlah besar lignin dibuang dalam kuantiti yang besar (oleh industri pulpa dan kertas) akibat kurangnya kesedaran mengenai potensinya. Disamping mempunyai kandungan kumpulan berfungsi yang tinggi (fenolik dan alifatik $-OH$, karbonil, karboksil, dll) serta struktur fenilpropanoida, lignin boleh memberikan alternatif baru yang lebih bersifat hijau terutama sekali dalam aplikasi industri seperti perencat kakisan. Oleh kerana pelepah kelapa sawit merupakan salah satu penyumbang sisa biomassa di Malaysia, ia telah digunakan sebagai bahan mentah dalam kajian ini.

Dalam usaha untuk meningkatkan penghasilan dan sifat lignin, pengekstrakan dijalankan dengan cara yang berbeza (melalui dilignifikasi langsung dan/atau kaedah prarawatan gabungan). Oleh kerana sifat hidrofobik lignin sangat tinggi, ia menghadkan keupayaan untuk bertindak sebagai perencat kakisan yang cekap.

Dalam pengertian ini, pengubahsuaian struktur lignin daripada pelepah sawit telah dilakukan dengan dua cara; (1) dengan memasukkan penghambat organik (2-naftol dan 1,8-dihidroksianthrakuinona) semasa autohidrolisis prarawatan sebelum rawatan organosolv (peratus hasil lignin: AHN EOL = 13.42 ± 0.71 % dan AHD EOL = 9.64 ± 0.84 %) dan (2) pemecahan lignin daripada proses dilignifikasi langsung (Kraft, soda dan organosolv) melalui teknik membran ultraturasan (peratus hasil pecahan lignin: Kraft = 5.41 ± 2.04 %; soda = 12.29 ± 0.54 % dan organosolv = 1.48 ± 0.15 %) . Sifat-sifat fizikal dan kimia lignin yang diubahsuai telah dinilai dengan menggunakan spektroskopi Inframerah Transformasi Fourier (FTIR), spektroskopi resonans nuclear magnetik (NMR), kromatografi gel penyerapan (GPC), penganalisis terma dan kromatografi cecair berprestasi tinggi (HPLC).

Pecahan lignin yang telah diubahsuai mengandungi bilangan fenolik –OH yang tinggi disamping mempunyai berat molekul serta kandungan alifatik –OH yang lebih rendah dan ia telah mempengaruhi aktiviti antioksidan. Aktiviti antioksidan ini pula bergantung kepada peningkatan fenolik –OH dan kandungan orto-metoksil lignin, melalui kestabilan radikal yang terbentuk dan keupayaan untuk menurunkan ion Fe^{3+} kepada ion Fe^{2+} . Sesungguhnya, sifat-sifat fizikokimia serta aktiviti antioksidan lignin terubahsuai memberikan sifat positif kakisan besi lembut melalui tindakan perencatan dalam larutan 0.5 M HCl yang dinilai oleh spektroskopi elektrokimia impedans (EIS), pengukuran kekutuban potensiodinamik dan penentuan kehilangan berat. Peratusan terbaik kecekapan perencatan (*IE*: 81 – 90 %) telah dicapai pada kepekatan 500 ppm untuk semua perencat lignin tetapi menurun dengan peningkatan suhu (303 – 333 K). Data termodinamik menunjukkan penjerapan lignin yang diubahsuai ke permukaan besi lembut berlaku secara spontan dan terjerap secara

fizikal (jerapan-fizik), disokong oleh tenaga pengaktifan penjerapan, E_a . Ciri-ciri perlindungan yang dipertingkatkan daripada lignin yang diubahsuai akan memberikan satu pendekatan alternatif dalam penggunaan bahan-bahan buangan semula jadi.

EXTRACTION, MODIFICATION AND CHARACTERIZATION OF LIGNIN FROM OIL PALM FRONDS AS CORROSION INHIBITORS FOR MILD STEEL IN ACIDIC SOLUTION

ABSTRACT

Lignocellulosic biomass in Malaysia can be considered as one of the promising sources of renewable energy. It is mainly composed of cellulose, hemicellulose, and lignin and best-suited for energy and chemical applications due to its sufficient availability, inexpensive and is sustainable. In general, the production of lignocellulosic biomass in Malaysia was considered high and mainly derived from the palm oil industries (approximately 60 million tonnes of oil palm waste were generated in a year). The oil palm biomass waste could possibly be used as alternative resources for the production of paper and cardboard. However, massive amounts of lignin by-product could also be discarded in huge quantities (by the pulp and paper industry) due to lack of awareness on its potential. Having high content of diverse functional groups (phenolic and aliphatic –OH, carbonyls, carboxyls, etc.) and phenylpropanoid structure, lignin can lead to substitutes in industrial applications such as in corrosion inhibition of metals and alloys. Since the oil palm fronds (OPF) are one of the largest biomass waste contributors in Malaysia, it was therefore used as raw material in this study.

In order to improve the lignin extractability and properties, the extraction was conducted in different ways (via direct delignification and/or combined pretreatment methods). Due to the high hydrophobicity of lignin, it limits the capability to act as efficient corrosion inhibitors. Hence, modifications of the OPF lignin structure were

conducted in two ways; (1) by incorporating organic scavengers (2-naphthol and 1,8-dihydroxyanthraquinone) during autohydrolysis pretreatment before organosolv treatment (percentage yield of lignin: AHN EOL = 13.42 ± 0.71 % and AHD EOL = 9.64 ± 0.84 %) and (2) fractionation of lignin from direct delignification processes (Kraft, soda and organosolv) via ultrafiltration membrane technique (percentage yield of permeate lignin fractions: Kraft = 5.41 ± 2.04 %; soda = 12.29 ± 0.54 % and organosolv = 1.48 ± 0.15 %). The physical and chemical properties of the modified lignins were evaluated by using Fourier Transform Infrared (FTIR) spectroscopy, nuclear magnetic resonance (NMR) spectroscopy, gel permeation chromatography (GPC), thermal analysis and high performance liquid chromatography (HPLC).

Modified lignin fractions with higher phenolic –OH content but lower molecular weight, polydispersity as well as aliphatic –OH content resulted in higher values of antioxidant activities. The antioxidant activity seems to be dependent on the increase of their free phenolic –OH and *ortho*-methoxyl content, through the stability of the radical formed and the ability to reduce Fe^{3+} ions to Fe^{2+} ions. Indeed, the improved physicochemical properties and antioxidant activity of modified lignin gave positive correlation with the mild steel corrosion inhibition action in 0.5 M HCl solution that were evaluated by electrochemical impedance spectroscopy (EIS), potentiodynamic polarization and weight loss measurements. The best percentage of inhibition efficiencies (*IE*: 81 – 90 %) were attained at the concentration of 500 ppm for all lignin inhibitors but decreased with the increase in temperature (303 – 333 K). Thermodynamic data indicated that the adsorption of the modified lignin onto the mild steel was spontaneous and the inhibitors were mainly physically adsorbed (physiosorption), supported by the activation energy of adsorption, E_a . The enhanced

protective properties of the modified lignin will pave way for an alternative approach for the utilization of these natural waste materials.

EXTRACTION, MODIFICATION ET CARACTERISATION DE LIGNINE DE FRONDES DE PALMIER A HUILE POUR LA PRODUCTION D'INHIBITEURS DE CORROSION DANS SOLUTION D'ACIDIQUE

RÉSUMÉ

La biomasse lignocellulosique en Malaisie peut être considérée comme l'une des sources d'énergie renouvelable prometteuse. Elle est principalement composée de cellulose, d'hémicellulose et de lignine et est adaptée pour des applications dans les domaines de l'énergie et de la chimie en raison de sa disponibilité suffisante, de son faible coût et de son caractère renouvelable. La production de biomasse lignocellulosique en Malaisie est considérée comme élevée et est issue en grande partie de l'industrie de l'huile de palme (environ 60 millions de tonnes de déchets d'huile de palme sont générés en un an). Les déchets de l'industrie de l'huile de palme pourraient être utilisés comme ressources alternatives pour la production de papier et de carton. Cependant, dans ce contexte, d'énormes quantités de lignine seraient rejetées (par l'industrie des pâtes et papier) en raison du manque de prise de conscience de son potentiel. Avec une teneur élevée en groupes fonctionnels divers (-OH phénoliques et aliphatiques, les carbonyles, les carboxyles, etc.), la lignine pourrait être utilisée en substitution de produits actuels dans des applications industrielles telles que l'inhibition de la corrosion des métaux et alliages. Les frondes de palmier à huile (OPF) étant l'un des plus gros contributeurs de déchets de biomasse en Malaisie, elles ont donc été utilisées comme matière première dans cette étude.

Afin d'améliorer l'extractabilité de la lignine et ses propriétés, l'extraction a été effectuée de différentes façons (par délignification directe et / ou des méthodes de pré-traitement combiné). Cependant, la forte hydrophobicité de la lignine limite sa capacité à agir comme inhibiteur de corrosion efficace. Par conséquent, des modifications de la structure de la lignine OPF ont été effectuées de deux manières; (1) en incorporant des piègeurs de recondensation de la lignine (2-naphtol et 1,8-dihydroxyanthraquinone) pendant le prétraitement par autohydrolyse avant le traitement organosolv (pourcentage de rendement de la lignine: AHN EOL = $13,42 \pm 0,71\%$ et AHD EOL = $9,64 \pm 0,84\%$) et (2) le fractionnement de la lignine à partir de procédés de délignification directs (Kraft, à la soude et organosolv) par l'intermédiaire d'une technique d'ultrafiltration à membrane (rendement en pourcentage de fractions de lignine perméat: Kraft = $5,41 \pm 2,04\%$; soude = $12,29 \pm 0,54\%$ et organosolv = $1,48 \pm 0,15\%$). Les propriétés physiques et chimiques des lignines modifiées ont été évaluées en utilisant l'infrarouge à transformée de Fourier (FTIR), la résonance magnétique nucléaire (RMN), chromatographie par perméation de gel (GPC), l'analyse thermique et la Chromatographie liquide à haute performance (HPLC).

Des fractions de lignine modifiée présentant des teneurs en OH phénoliques élevées, des poids moléculaires, polydispersité et contenus en OH aliphatiques faibles ont abouti à des valeurs plus élevées de l'activité antioxydante. L'activité antioxydante semble être dépendante de la teneur en OH phénolique et en ortho-méthoxyle, grâce à la stabilité du radical formé et la capacité de réduire les ions Fe^{3+} en Fe^{2+} ions. En effet, les propriétés physico-chimiques améliorées et une activité anti-oxydante de

lignine modifiée a donné une corrélation positive avec l'inhibition de la corrosion de l'acier doux dans l'action solution de HCl 0,5 M qui a été évaluée par spectroscopie d'impédance électrochimique (SIE), de polarisation et de la perte de poids mesure potentiodynamique. La meilleure efficacité de pourcentage d'inhibition (ex: 81 à 90%) a été obtenu à la concentration de 500 ppm pour les inhibiteurs de la lignine, mais a diminué avec l'augmentation de la température (303 à 333 K). Les données thermodynamiques indiquent que l'adsorption de la lignine modifiée sur l'acier doux a été spontanée et que les inhibiteurs ont été principalement adsorbés physiquement (physisorption), ce résultat étant confirmé par l'énergie d'activation de l'adsorption, E_a . Les propriétés de protection renforcées de la lignine modifiée ouvriront la voie à une approche alternative pour l'utilisation de ces déchets naturels.

CHAPTER ONE

INTRODUCTION

1.1 Biomass as renewable feedstock

The most crucial issue faced by the world today is the sustainability of consumption for energy and natural resources. As the fossil fuel creates problematic issues (due to global warming, increase in price and running out), the use of renewable resources to shift the oil-based economy into bio-based economy is an alternative choice. With a goal of reducing net greenhouse gas emission, this marks an important turning point in effort to promote the use of renewable energy to fulfill the commitments of the Kyoto Protocol (Ragauskas *et al.*, 2006; Sarkar *et al.*, 2012). Biomass has been considered as one of the potential sources of renewable energy in the world. Several agencies worldwide have recently reported an increase in the gross domestic energy and chemical production from renewable energy, especially biomass. It was reported that the European Union (EU) utilized about 66.1 % of its renewable energy from biomass which surpassed the contribution of other sources of energy like hydro, wind, geothermal and solar power (Zakzeski *et al.*, 2010). The development of technology and processes for biomass valorization is not only focusing on the production of energy but also for the production of biofuels and biomaterials (Figure 1.1).

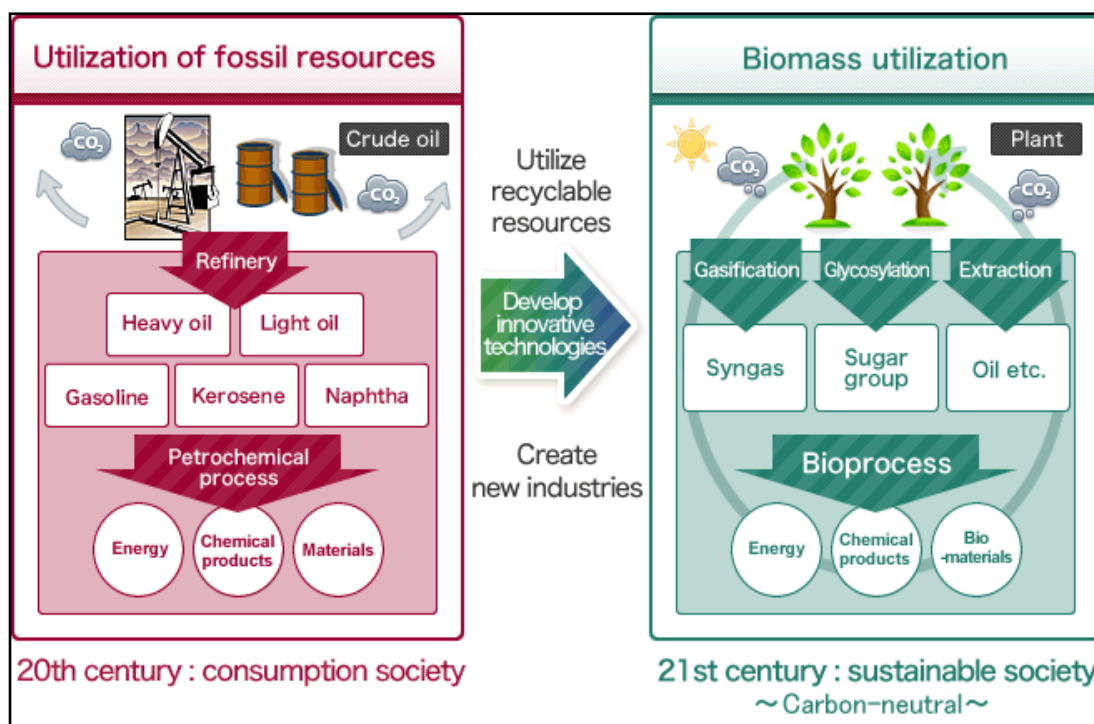


Figure 1.1: Biomass utilization (www.riken.jp/bmep/english/outline/co2.html).

Biomass can be defined as a biodegradable product, waste or residue from biological origin of agriculture, aquaculture or industrial waste (Directive 2009/28/EC, 2009). The primary production of the integrating terrestrial and oceanic components including from biomass (according to global net primary production, NPP report) in the world was estimated around 104.9×10^{15} grams of carbon per square meter per year, which is about half from the ocean and half on land (Field *et al.*, 1998). The largest source of biomass comes from wood including tree residues, wood chips and so forth. In addition, industrial crops such as miscanthus, switchgrass, corn, poplar, sorghum, sugarcane, bamboo and oil palm can also contribute as a major source of biomass (Volk *et al.*, 2000). Indeed, it is an important feedstock for the production of renewable fuels, chemicals and energy. Conversion of biomass into fuels can be achieved by employing various techniques which can be classified as thermal, chemical and biochemical methods.

1.2 Lignocellulosic biomass

Dry matter of plant can be referred as lignocellulosic biomass. It has been acknowledged as the most abundant sources of renewable energy (approximately 200×10^9 tons per year) obtained from crops, wood and agricultural waste (Zhang, 2008; Brosse *et al.*, 2010). Lignocellulosic biomass is best-suited for energy and chemical applications due to its sufficient availability, is inexpensive and environmentally safe. It is composed of cellulose, hemicellulose, and lignin with small amounts of proteins, lipids and ash that later forms a complex structure of plant cell wall (Figure 1.2). The composition of these compounds essentially depends on the origin of the plant as listed in Table 1.1.

The lignocellulosic materials (cellulose, hemicellulose and lignin) are interconnected with each other through covalent crosslinks. Recent work in this area has mainly focused on the delignification of lignocellulosic biomass separating lignin, cellulose and hemicelluloses to be used in both physical and chemical applications. The cellulose and hemicellulose can be hydrolyzed to monomeric sugars and often converted to value added products such as ethanol, additives, organic acid, and others by chemical and biochemical processes (Mussatto and Teixeira, 2010). All of these lead to the utilization of lignocellulosics not only for second generation energy, chemical and material production but also for synthesizing food additives and feed supplements (Sims, 2003).

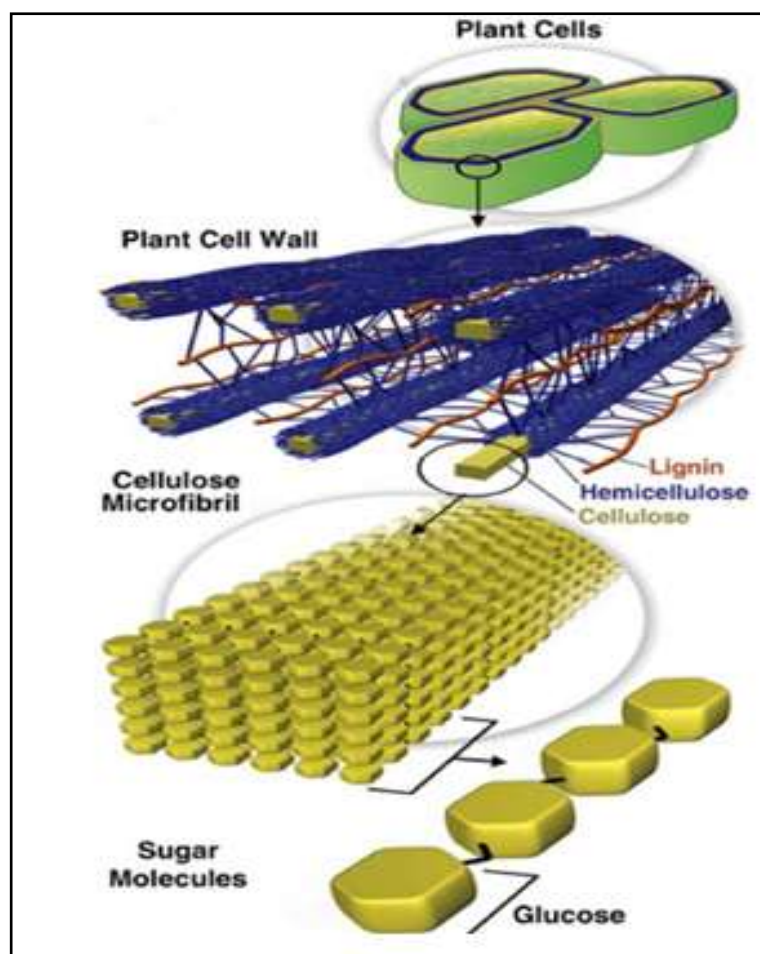


Figure 1.2: Composition of plant cell wall as lignocellulosic biomass (Sannigrahi *et al.*, 2010).

Table 1.1: Representation of different fractions of lignocellulosic materials.

Lignocellulosic materials	Cellulose (%)	Hemicellulose (%)	Lignin (%)
Hardwood stems	40-55	24-40	18-25
Softwood stems	45-50	25-35	25-35
Nut shells	25-30	25-30	30-40
Corn cobs	45	35	15
Grasses	25-40	35-50	10-30
Wheat straw	30	50	15
Cotton seed hairs	80-95	5-20	0
Coastal Bermuda grass	25	35.7	6.4
Typha capensis	34.2	11.6	26.4
Miscanthus x giganteus	38.2	24.3	25
Poplar aspen	42.3	31	16.2
Empty fruit bunch	59.7	22.1	18.1
Switch grass	45	31.4	12

*Source: Abdullah *et al.*, 2011; de Vrije *et al.*, 2002; Liu, 2002; Sun and Cheng, 2002; Zhang *et al.*, 2011).

The major component of the lignocellulosic biomass is cellulose which contains 40-60 % of its overall total weight in wood (Kamide, 2005). It is a polysaccharide organic compound (empirical formula: $(C_6H_{10}O_5)_n$) that consists of hundreds to thousands $\beta(1-4)$ linked D-glucose units. Adjacent coupling of cellulose chain (via H-bond and Van der Waals forces) forms a parallel alignment with a crystalline structure (Zhang, 2008). Cellulose plays an important role in the plant cell as a structural component. It is currently used mostly to produce cardboard, bioethanol, artificial fibers (cellulose acetate), plastics (cellulose nitrate), explosives (nitrocellulose) and gelling agent (carboxymethylcellulose, hydroxyethylcellulose and hydroxypropylmethyl cellulose) (Clasen and Kulicke, 2011). In contrast, hemicellulose is the second most abundant amorphous polysaccharide that can be found in the primary and secondary cell walls. It contains predominantly of D-pentose sugars with a small amount of L-sugars. Besides glucose, the composition of hemicellulose may include xylose, mannose, arabinose and galactose (Spiridon and Popa, 2008). Xylose sugar is the main hemicellulose in most hardwood, although mannose can also be the abundant sugar in softwood. The conversion of hemicellulose into value-added products like ethanol, xylitol and 2, 3-butanediol have recently been studied (Chandel *et al.*, 2010). Meanwhile the structure and usability of lignin will be further exposed in the next subchapter.

1.3 Oil palm (*Elaeis guineensis*)

Oil palm (*Elaeis guineensis*, Figure 1.3) is a species of palm trees that is commonly found in tropical regions in Indonesia, Malaysia, Thailand, Nigeria, Ecuador, Colombia and Papua New Guinea (FAO, 2009). Historically, the oil palm was first

introduced to Java by the Dutch (1846) and later expanded to Malaya in 1910 by William Sime and Henry Darby. The oil palm tree is un-branched with a height varying from 20-30 meters. It is cultivated on approximately 15 million hectares worldwide (Koh and Ghazoul, 2008; Fitzherber *et al.*, 2008; FAO, 2009). In Malaysia alone, it is estimated that 2.5 million hectares of land is being cultivated with oil palm trees (Mohamad Ibrahim and Azian, 2005; Mohamad Ibrahim *et al.*, 2011). The occupied area of cultivation (as shown in Figure 1.4) has been increasing throughout the years driven by the high demands from countries like India, China and the European Union (UNEP, 2011). To date, oil palm can be considered as the most productive and profitable tropical crops for the production of first generation biofuels as compared to other crops (soybean, sunflower, peanut, rapeseed and coconut) (Lester, 2006). In addition, the extract of oil palm is used for various food and household products (such as margarine, baked goods and sweets, detergent and cosmetics) as well as the production of biodiesel (UNEP 2011).



Figure 1.3: *Elaeis guineensis* as illustrated by Nicholaas Jacquin in 1763 (*Elaeis guineensis*, 2014).

In spite of the huge production, the oil content is about 10 % of the total production of biomass in the plantation. It was previously reported that approximately around 15 million tons per year of agricultural waste is being produced by oil palm milling operation in Malaysia (Figure 1.5). Massive amounts of oil palm wastes (trunks, fronds and empty fruit bunch) generated from the palm oil industry will cause a serious environmental threat since it requires a long time to decompose, thus most of it are burned in incinerators (Mohamad Ibrahim & Azian, 2005; Mohamad Ibrahim *et al.*, 2011; Rahman *et al.*, 2007). Therefore, a proper exploitation of lignocellulosic material from oil palm residues could represent a renewable source of various products and chemicals. The composition and possible applications of this biomass will be further explained in the next subchapter.

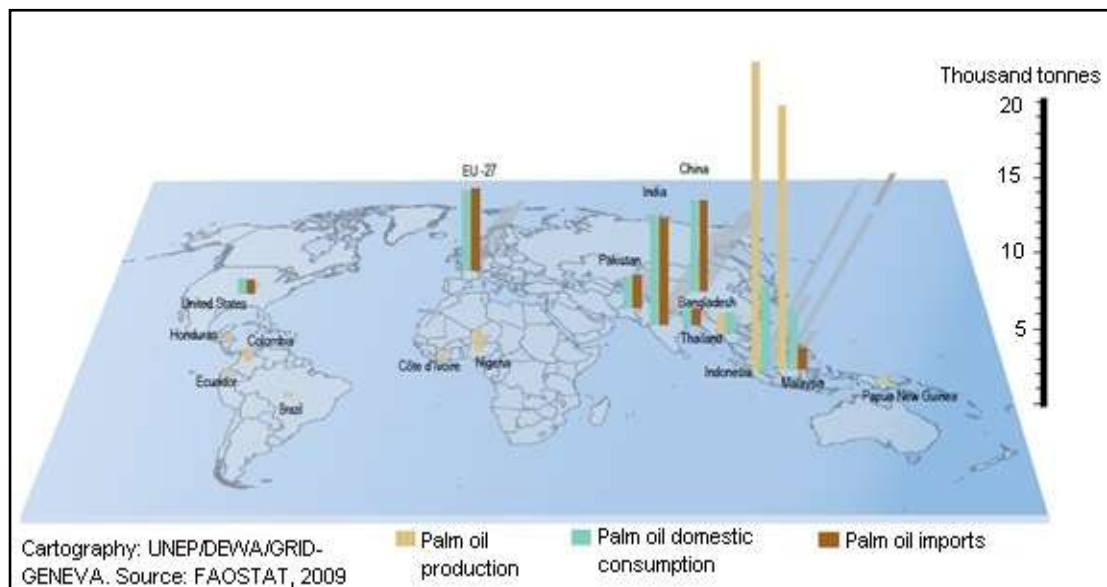


Figure 1.4: Top palm oil producers, importers and consumers (Source: UNEP, 2011).

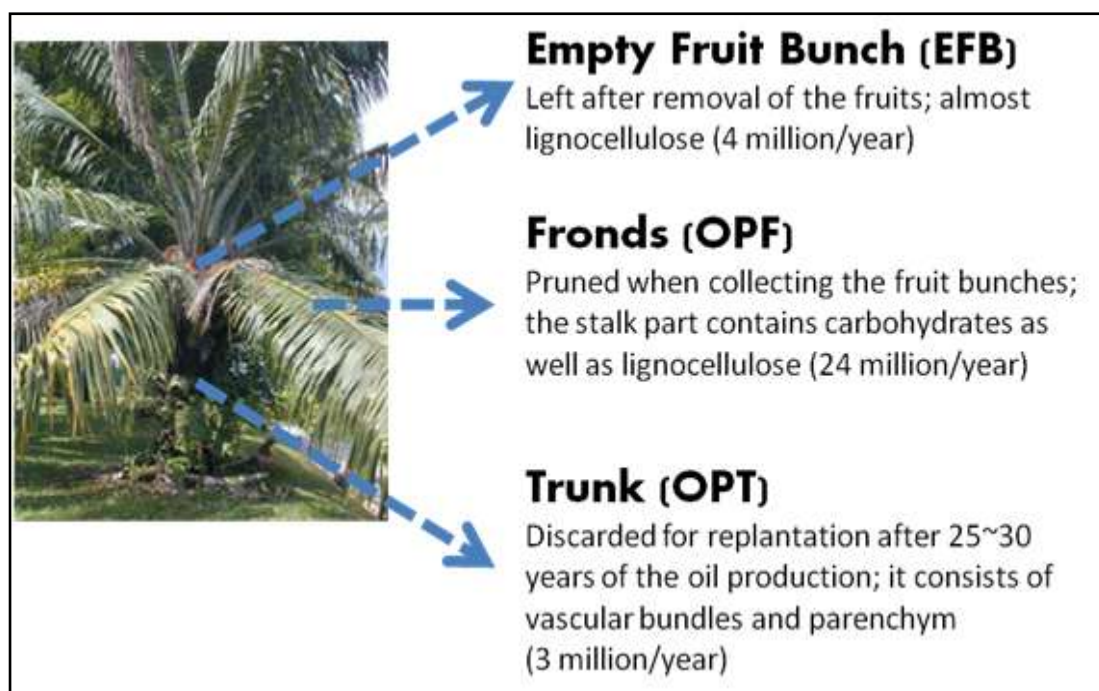


Figure 1.5: Lignocellulosic biomass components of oil palm tree.

1.3.1 Oil palm biomass waste and applications

The main contributors of biomass waste produced from oil palm plantations are oil palm shells, mesocarp fibers, empty fruit bunch (from the mills) oil palm fronds and oil palm trunk (from the field during planting). At the oil palm mill, the fresh sterilized fruit bunches will undergo a threshing process that separates the fruit nuts. The resulting emptied fruit bunches are mainly the main stalk (~20-25 %) and sharp spine spikelets (75-80 %). It is estimated that the production of empty fruit bunches from 2007 to 2020 is about 2.856 million tonnes per year. Meanwhile, oil palm trunk (~3 millions tonnes per year) and fronds (54.43 million tonnes per year) are collected during replanting and pruning activities. The oil palm tree normally passes its economic age after 25 years old and it will be cut and replanted (Oil palm biomass, 2011). The oil palm biomass contains significant amounts of lignocellulosic materials (Table 1.2). Generally, the oil palm biomass contains about 65-80 % of

holocellulose (α -cellulose and hemicellulose) and 18-21 % of lignin. Therefore the oil palm biomass is suitable as raw materials for the production of paper and pulp, composites, aromatic hydrocarbons and chemicals. Vast applications of oil palm biomass have been studied recently by several researchers. Among those are the applicability of oil palm biomass as medium density fiberboard (Onuorah, 2005; Norul Izani *et al.*, 2013), plywood (Abdul Khalil *et al.*, 2010; Loh *et al.*, 2011), particleboard (Saari *et al.*, 2014), paper and pulp (Wanrosli *et al.*, 2005, 2007) and activated carbon (Allwar *et al.*, 2008; Rahman and Yusof, 2011). Thus, it is apparent that oil palm biomass could provide a greener approach for industrial applications.

Table 1.2: Composition of oil palm biomass (Oil palm biomass, 2011).

Components (% dry weight)	Oil palm trunk	Oil palm fronds	Empty fruit bunch
Lignin	18.1	18.3	21.2
Hemicellulose	25.3	33.9	24.0
α -cellulose	45.9	46.6	41.0
Holocellulose	76.3	80.5	65.5
Ash	1.1	2.5	3.5
Alcohol-benzene solubility	1.8	5.0	4.1

1.3.2 Oil palm fronds (OPF)

Oil palm frond (OPF) is a non-woody agricultural waste discarded in large quantities in Malaysia. Despite being considered as agricultural waste, OPF is found to be a natural composite material, because it mainly consists of cellulose (46.6-47.7 %), lignin (15.2-18.3 %), hemicelluloses (~33.9 %), extractives and sugars (Wanrosli *et al.*, 2007; Goh *et al.*, 2010a; Sabiha-Hanim *et al.*, 2011) as shown in Table 1.3. As compared with other lignocellulosic materials, OPF is available at a very low cost (Goh *et al.*, 2010b). Hence, OPF represents a renewable source of various products

and chemicals and their proper exploitation could represent an alternative to crude derivatives consumption.

Table 1.3: Chemical composition of oil palm fronds (Wanrosli *et al.*, 2007).

Component	% Dry weight
Lignin	15.2
Holocellulose	82.2
α -cellulose	47.6
Alcohol-benzene extractives	1.7
Ash	0.4
Polysaccharide composition	
Arabinose	1.5
Mannose	2.2
Galactose	0.9
Glucose	66.6
Xylose	28.9

The utilization of OPF into more beneficial products has been reported recently as livestock feed (Bengaly *et al.*, 2010; Dahlan, 2000; Kawamoto *et al.*, 2001), biofuel regeneration (Goh *et al.*, 2010a, 2010b), absorbent for heavy metal ions in waste water (Salamatina *et al.*, 2010), renewable sugar (Sabiha-Hanim *et al.*, 2011; Zahari *et al.*, 2012), composite board (Rasat *et al.*, 2011; Rozman *et al.*, 1997) and it has also been recognized as one of the most promising raw materials to produce paper (Wanrosli *et al.*, 2004; Wanrosli *et al.*, 2007). Nevertheless, no study has been done previously on the extraction and utilization of lignin from OPF biomass waste as a corrosion inhibitor.

1.4 Lignin

The word lignin is derived from a Latin word for wood (*lignum*). It is a major constituent in the cell wall structure of all plants. Lignin is a natural aromatic amorphous macromolecule, a binder that holds together the lignocellulosic fibers to ensure rigidity of all vascular plants. The polyphenolic structure of lignin is known for its role to provide resistance of both chemical and biological degradations in woody biomass. Perhaps, this is due to the hydrophobic and insolubility nature of lignin in aqueous system that prevents the full access of chemicals and organisms. Generally, it is built up of three major C6-C3 (phenylpropanoid) units; p-coumaryl alcohol, coniferyl alcohol and sinapyl alcohol (Figure 1.6), which forms a randomized structure in a 3D network inside the cell wall (Ammalahti *et al.*, 1998; Garcia *et al.*, 2009; She *et al.*, 2010).

Unlike most natural polymers that consist of a single intermonomeric linkage, lignin is a branched polymer made up of many carbon-to-carbon and ether linkages (Holtmam *et al.*, 2003). The lignin structure due to its monolignol composition may be different depending on its origin. According to Dence and Lin (1992) for softwood lignin (also called guaiacyl lignin), the structure is derived from coniferyl alcohol/guaiacyl (G) with a small trace of sinapyl alcohol/syringyl (S). In turn, hardwood lignin (also called guaiacyl-syringyl lignin) is built from different ratios of coniferyl and sinapyl alcohol derived units. Similarly, grass lignin is also classified as guaiacyl-syringyl lignin however it contains additionally small quantities of p-coumaryl alcohol/p-hydroxyphenyl (H).

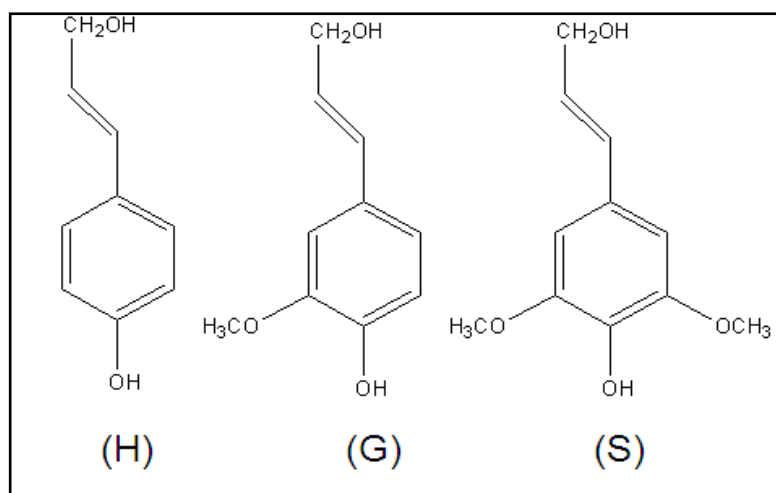


Figure 1.6: Monolignols basic unit in lignin. (H): p-coumaryl alcohol/p-hydroxyphenyl; (G): coniferyl alcohol/guaiacyl; (S): sinapyl alcohol/syringyl.

The structure of lignin can be considered to be very complex and is not exactly defined. Nevertheless, several researchers have published possible representations of the lignin structure. For example, Brunow (2001) have proposed a possible structure of softwood lignin (Figure 1.7). Some important functional groups exhibited in the unmodified lignin structure are hydroxyl (aliphatic and aromatic -OH), methoxyl (-OCH₃), carbonyl (-C=O), and carboxyl (-COOH). It was believed that the proportion of these functional groups will affect the solubility properties of lignin. In general, most lignins are dissolved in alkaline solution due to the hydroxyl and carboxyl ionizations (Gosselink, 2011).

The most abundant inter-ether unit linkage in all lignin is the β -aryl ether bond (β -O-4) (Önnerud and Gellerstedt, 2003). In addition, small proportions of lignin units remain as phenolic, being linked only by C-C bonds, such as β -5, 5-5, 4-O-5, β - β and α - β linkages. Table 1.4 shows the different linkages types in softwood and hardwood per 100 C₉ units (Henrikson *et al.*, 2010). The cleavage of ether bonds will produce new phenolic hydroxyl groups in lignin that affects the usage of lignin

(which increases lignin solubility and alters the reactivity of lignin) to be used as raw materials for various applications (Camarero *et al.*, 1999).

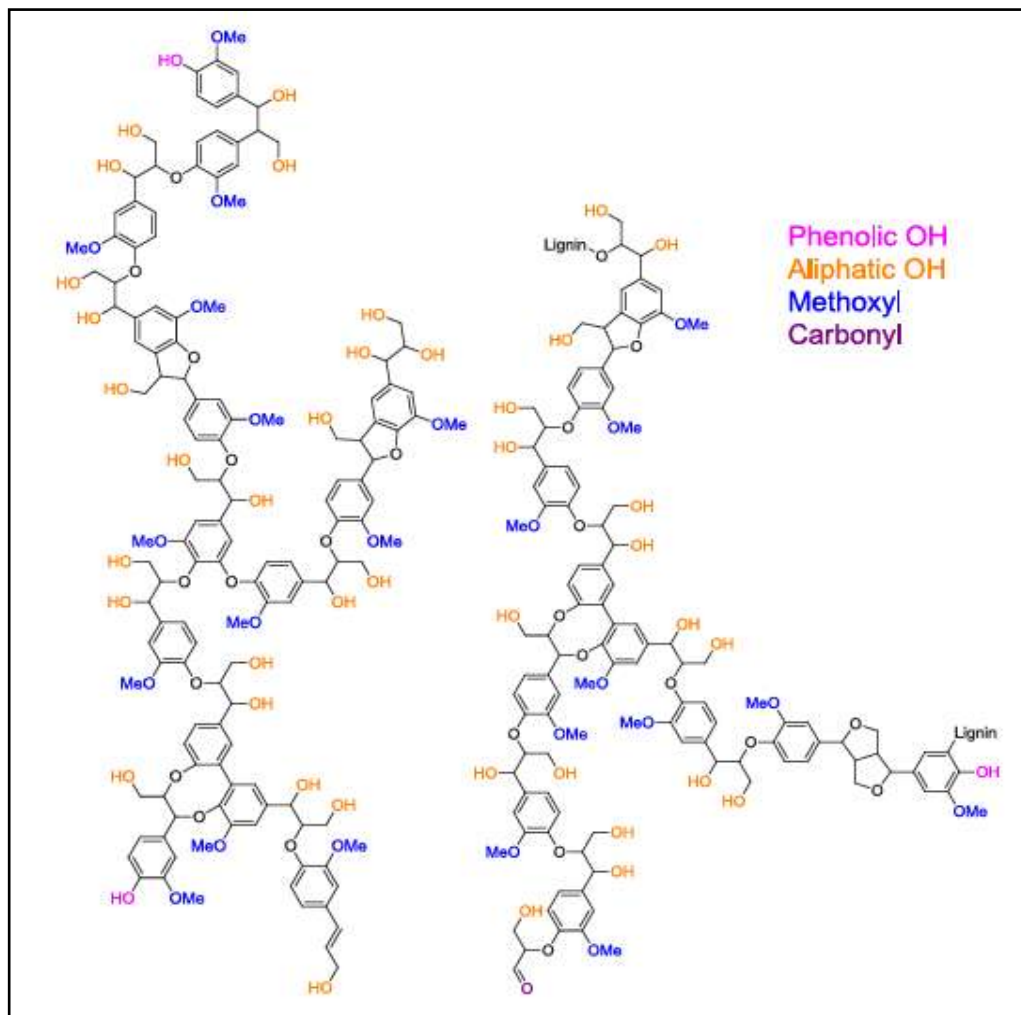
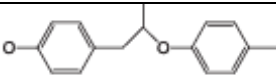
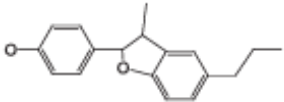
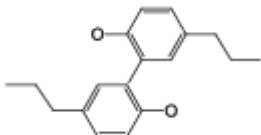
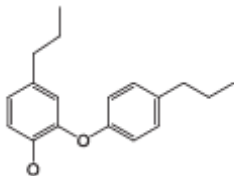
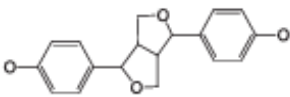
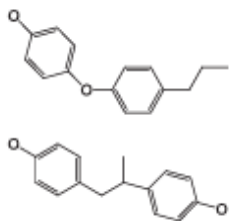


Figure 1.7: Softwood lignin structure (Brunow, 2001).

Table 1.4: Different linkage types in softwood and hardwood lignin per 100 C9 unit (Henrikson *et al.*, 2010).

Type of bond	Structure	Softwood	Hardwood
β -O-4		40-50	50-60
β -5		10-12	3
5-5		13	3
4-O-5		3	3
β - β		3	3
Bonds to 1-position		1-3	3

1.4.1 Delignification process

In general, the separation of lignin from lignocellulosic biomass can be done either by physical (mechanical) or chemical approaches. Different types of delignification (also known as pulping) process of lignocellulosic biomass will highly affect its lignin yield, structure, purity and properties. It is known that the most predominate delignification process is the chemical pulping process, accounting more than 80 % of the world pulp production (Chenier, 2002; Cleveland, 2004). The main goal of

chemical pulping is to dissolve lignin (particularly in the middle lamella) as much as possible in the black liquor without disturbing the carbohydrate component (Araujo, 2008).

During delignification process, the ether and ester linkages of larger lignin structure will be disrupted and the resulting fragments will later dissolve in the black liquor (Gosselink, 2011). The resulting lignin fragments are often referred as technical lignin. Obviously, technical lignin will be different compared to the original (native) lignin in the biomass. Meanwhile, milled wood lignin (obtained by extraction of milled wood) was commonly used to represent the total average structure of native lignin. Therefore, delignification process allows an easy separation of the lignocellulosic components from the wood biomass. Some common pulping processes that are normally used for the delignification process are listed below.

1.4.1.1 Kraft pulping

Kraft pulping was first developed in Jonkoping, Sweden in 1891 and it is the most common pulping process in the world nowadays which generally uses sodium sulfide (Na_2S) and sodium hydroxide (NaOH) as its basic chemicals. According to the Food and Agricultural Organization of the United Nations (FAO), it was estimated that 9.8×10^7 tonnes of Kraft pulp were produced worldwide in the year 2006 alone (Araujo, 2008). According to Tejado *et al.* (2007), kraft pulping processes will cleave β -O-4 and α -O-4 linkages, resulting in massive amounts of non-etherified phenolic -OH groups in the lignin structure (Figure 1.8). As the lignin has partly cleaved, the thiol groups were introduced at the β -position of the

propane side chain (Figure 1.9) that later produces a soluble fragment of lignin (Gosselink, 2011).

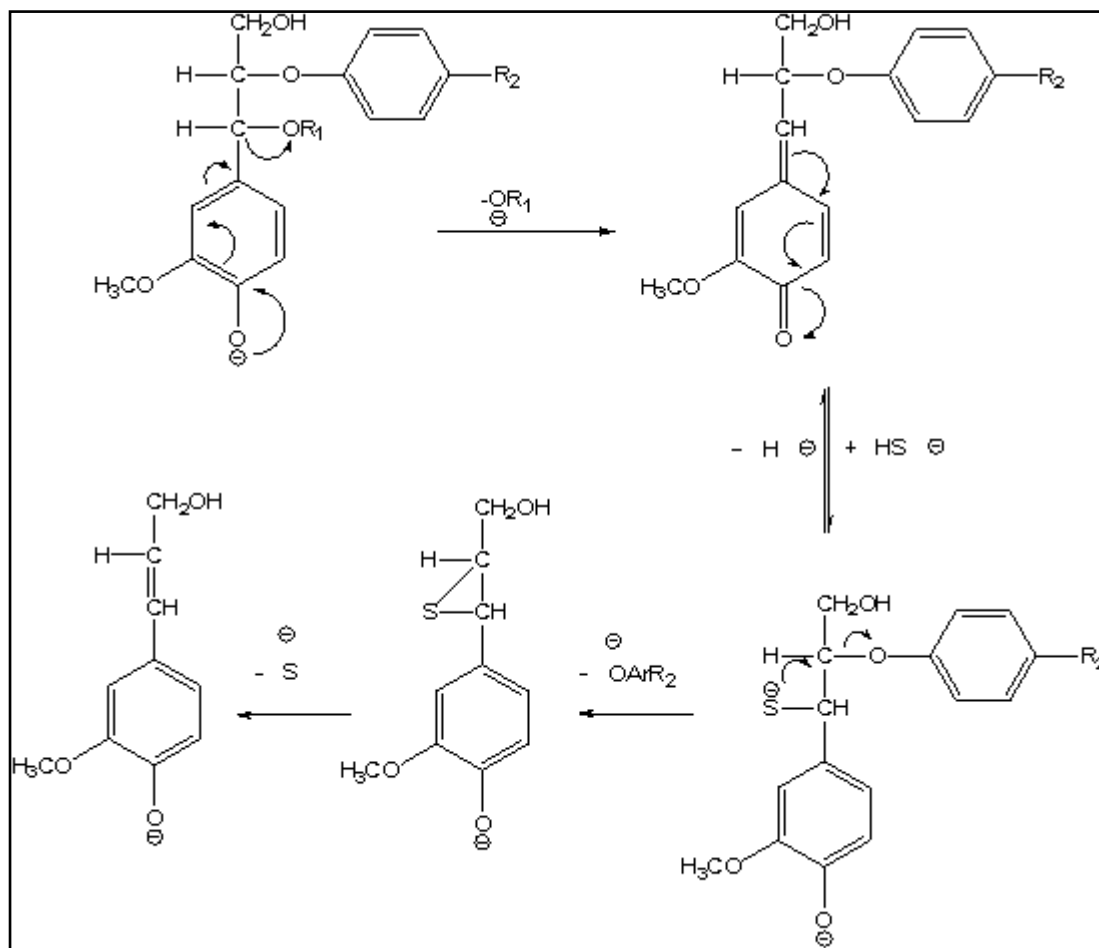


Figure 1.8: Mechanistic change of lignin during Kraft pulping process (Tejado *et al.*, 2007).

In Kraft pulping, there are two important parameters that need to be considered during the process; that is active alkali (total amount of NaOH and Na_2S) and sulphidity (ratio of Na_2S to active alkali). Generally for the Kraft pulping process, the percentage of active alkali and sulphidity should be around 15-20 % and 25-35 %, respectively which represents a 3:1 ratio of NaOH to Na_2S (Kirk-Othmer Encyclopedia, 2005; Araujo, 2008). Kraft lignin can be recovered from the

precipitation of black liquor with slight addition of mineral acids (Kringstad and Roland, 1983; Nada *et al.*, 1998; Rohella *et al.*, 1996).

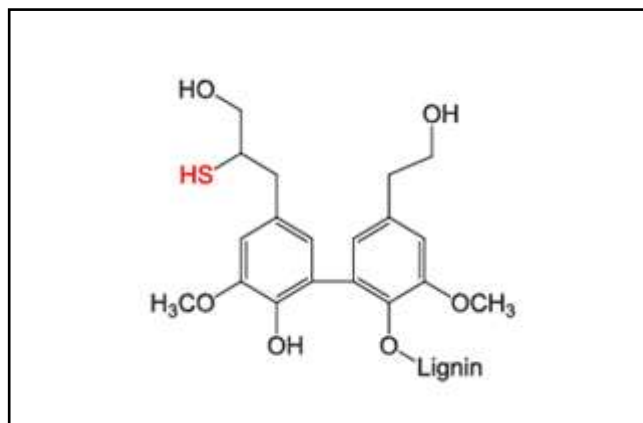


Figure 1.9: The structure of Kraft lignin with thiol groups, -SH as proposed by Holladay *et al.* (2007).

1.4.1.2 Soda pulping

In soda pulping, the process only requires sodium hydroxide (NaOH) to dissolve lignin from wood biomass. Soda pulping of wood biomass involves the cleavage of aryl-ether linkages (Figure 1.10) via the formation of small quantities of phenolic hydroxyls and the loss of primary aliphatic -OH (Tejado *et al.*, 2007). The soda pulping process produces pulp with low tearing strength because cellulose is also degraded together with lignin during the pulping process (Araujo, 2008). Therefore to decrease the degradation of cellulose, the use of anthraquinone (AQ) as an additive during soda pulping process to increase the percentage yield of lignin has been proposed (Holton, 1977). Similar to Kraft lignin, soda lignin recovery is done by precipitation of black liquor by mineral acids.

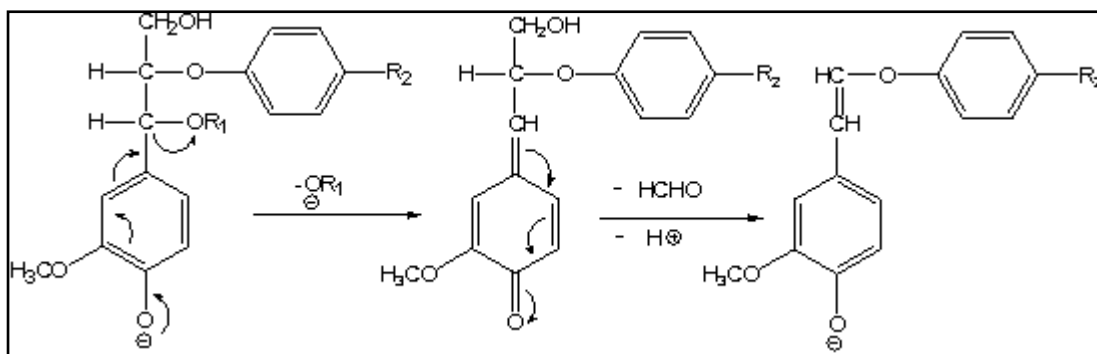


Figure 1.10: Mechanistic change of lignin during soda pulping process (Tejado *et al.*, 2007).

1.4.1.3 Organosolv pulping

Organosolv pulping uses organic solvent (e.g. aqueous ethanol, methanol, glycerol, ethylene glycol, tetrahydrofurfuryl alcohol, dimethylsulfoxide, esters, ketones and phenols) as its main chemical during the pulping process (Thring *et al.*, 1990a). The organic solvents are usually used in combination with water so that the hemicellulose sugars can be recovered in the aqueous phase portion. It was found that organosolv pulping produces high quality cellulose and lignin (Duff and Murray, 1996). In addition, organosolv pulping uses small concentrations of organic or mineral acids which act as catalysts to enhance the removal of hemicellulose and rate of delignification at very high temperatures (~180-200 °C) (Duff and Murray, 1996; Sun and Cheng, 2002). As illustrated in Figure 1.11, during organosolv pulping process the acetic acid which is released from the hemicellulose wood will initiate the dissolution of lignin. This will subsequently promote the acid hydrolysis of lignin and later generate the formation of the phenolic hydroxyl groups and new carbonyl groups in the lignin structure (Tejado *et al.*, 2007). Lignin is recovered (via precipitation) by diluting the organosolv black liquor to 1:3 of its final volume with distilled water (El Hage *et al.*, 2009).

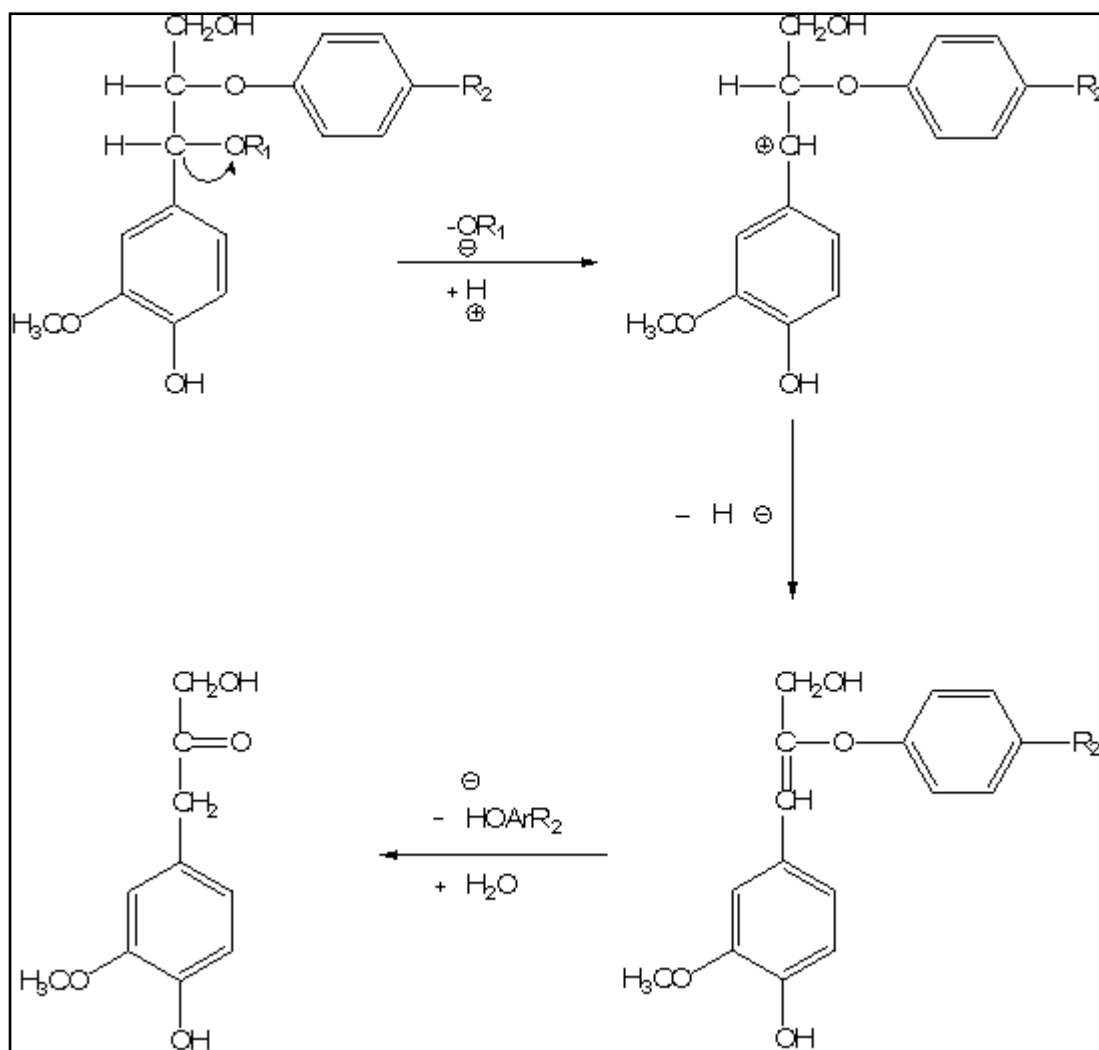


Figure 1.11: Mechanistic change of lignin during organosolv pulping process (Tejado *et al.*, 2007).

1.4.2 Combinative pretreatment process

Recently, combinative pretreatment process of lignocellulosic biomass has become an important process since it promises higher efficiency, higher delignification rate, less severity of cellulose pulp and less concentration of fermentation inhibitors (Patel and Varshney, 1989; Obama *et al.*, 2012; Timilsena *et al.*, 2013a). In this method, it involves a presoaking or prehydrolysis (as the first step) of biomass to hydrolyze the hemicelluloses and followed by delignification process (as the second step) where the solid residue from the first step is retreated (Figure 1.12). The main objective of

the two-step processes is to reduce the degradation of carbohydrate fragments into furfural and hydroxymethylfurfural (Brosse *et al.*, 2012; Timilsena *et al.*, 2013a). It was believed that the lignin deconstruction during the prehydrolysis treatment increases the extractability of organosolv lignin through the breaking of lignin-carbohydrate bonds, resulting in smaller lignin fragments. Nevertheless, the deconstruction of lignin is often associated with the repolymerization reactions through the formation of new C-C bondings (β - β , β -1 and β -5) which sometimes still affect the delignification rate and lignin structure. Some common pretreatment/prehydrolysis for combinative pretreatment processes are listed below.

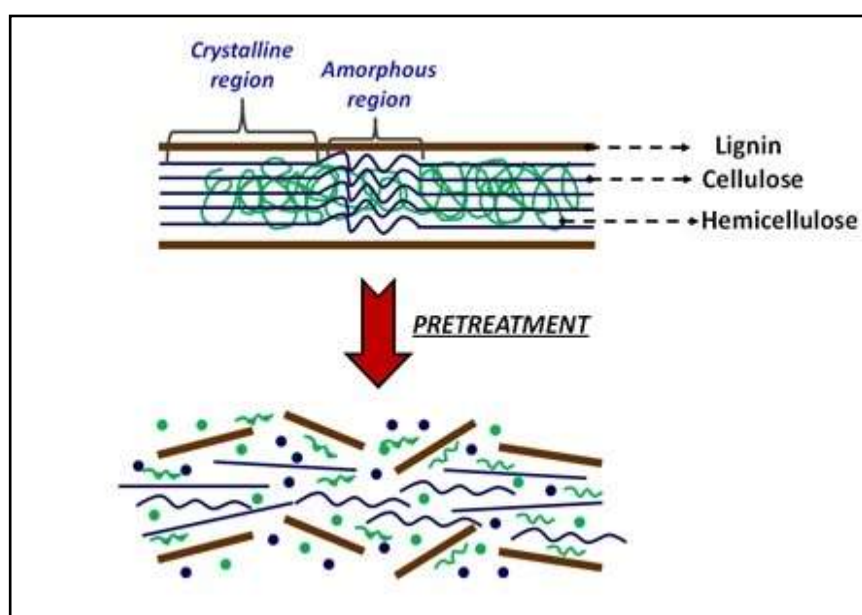


Figure 1.12: Pretreatment of lignocellulosic biomass (Timilsena, 2012).

1.4.2.1 Acid pretreatment

Acid pretreatment is the most common method that utilizes mineral acids such as hydrochloric acid (HCl) and sulphuric acid (H₂SO₄) for the treatment of biomass. According to Sun and Cheng (2002), acidic treatment of lignocellulosic biomass will

improve the enzymatic hydrolysis of pulp and at the same time gives higher recovery of fermentable sugars. However, the pretreatment with concentrated acids is not suitable in economic and environment perspectives since it is toxic, hazardous and corrosive to the reactor. Thus researchers have mainly focused on the utilization of dilute acids for the biomass pretreatment. To date, various kinds of dilute mineral acids such as sulphuric, hydrochloric, nitric, phosphoric and peracetic acid have been experimented for this pretreatment (Zheng *et al.*, 2009). Among these acids, sulphuric acid is of interest because of its low cost and efficiency (Timilsena, 2012). It was also reported that the dilute sulphuric acid can be used as an alternative for the production of furfural from biomass hemicellulose (Mosier *et al.*, 2005).

1.4.2.2 Autohydrolysis

Autohydrolysis (or also known as hydrothermal) is a biomass pretreatment with water at very severe conditions (elevated temperatures and pressures). It is more eco-friendly since it only uses water for the reaction. In this process, the lignocellulosic biomass is heated at a high temperature and pressure that will result in the solubilization of acid components, de-esterification of ester groups and formation of organic acids in the hemicellulose structure (Figure 1.13). The resulting organic acid (like acetic acid) will cause a hydrolytic breakdown of hemicellulose that is spontaneously repeated (Wayman and Lora, 1978). Due to the mechanistic action of hydronium ions on lignocellulosic biomass, it was believed that autohydrolysis process will selectively dissolve most of the hemicellulose portion which can be recovered in the residual solution (Walch *et al.*, 1992). The hemicellulose rich liquid

portion can be used potentially for the synthesis of furfural derivatives or other green chemicals (Timilsena, 2012).

The removal of hemicellulose from the lignocellulosic biomass would enhance the hydrolyzability of cellulose leaving the solid pulp rich in cellulose and insoluble lignin residue (Garrote *et al.*, 1999). Optimization of the operating conditions during autohydrolysis is considered important to ensure the effectiveness of the delignification ability of treated biomass. Brosse *et al.* (2010) have reported that the operation conditions of *Miscanthus x giganteus* during autohydrolysis have affected the removal of hemicellulose, delignification yield and the efficiency of cellulose conversion to glucose during enzymatic hydrolysis.

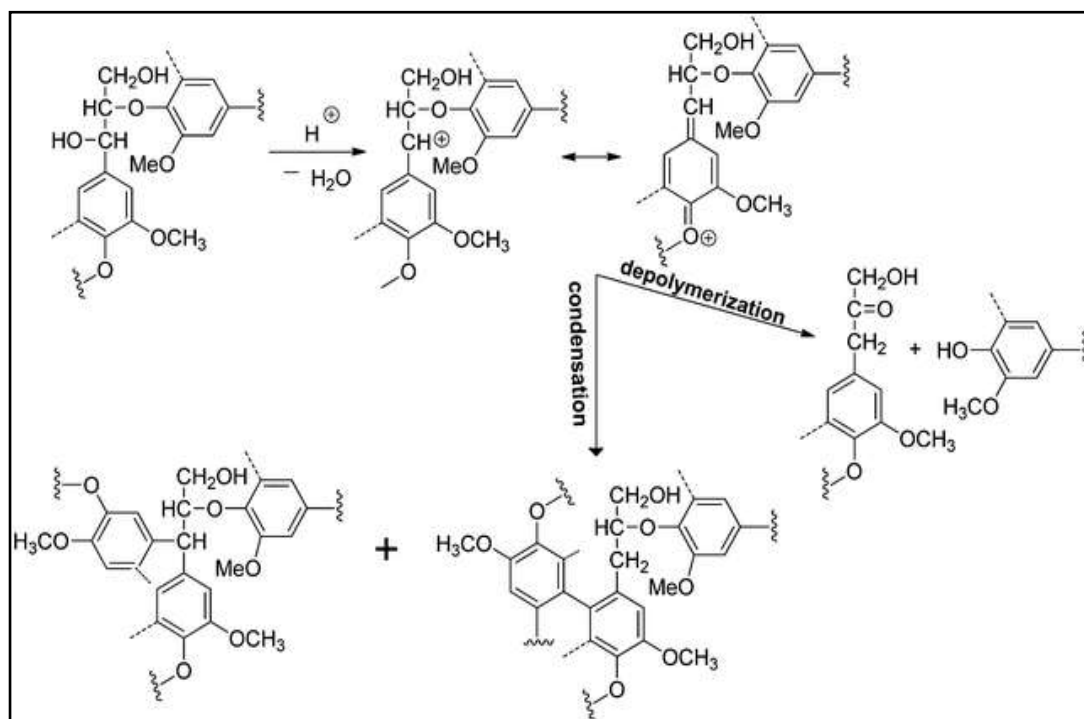


Figure 1.13: A possible mechanism during autohydrolysis (Samuel *et al.*, 2013).

1.4.2.3 Addition of organic scavengers during pretreatment

Previous studies have shown that hydrothermal treatments such as autohydrolysis could lead to the change in lignin structures and overall delignification yield due to the repolymerization of lignin (Lora and Wayman, 1979; Li and Gellerstadt, 2008; El Hage *et al.*, 2010; Timilsena *et al.*, 2013b). The repolymerization of lignin through the formation of carbonium ion intermediate will later produce new linkages of β - β , β -1 and β -5 bonds (Li and Lundquist, 2000), where the carbonium ion is formed from the lignin phenylpropane units during acidic conditions of autohydrolysis (Figure 1.14). The resulting lignin after repolymerization is highly condensed and insoluble with high molecular weight that will impair the delignification of any pulping process (Timilsena, 2012).

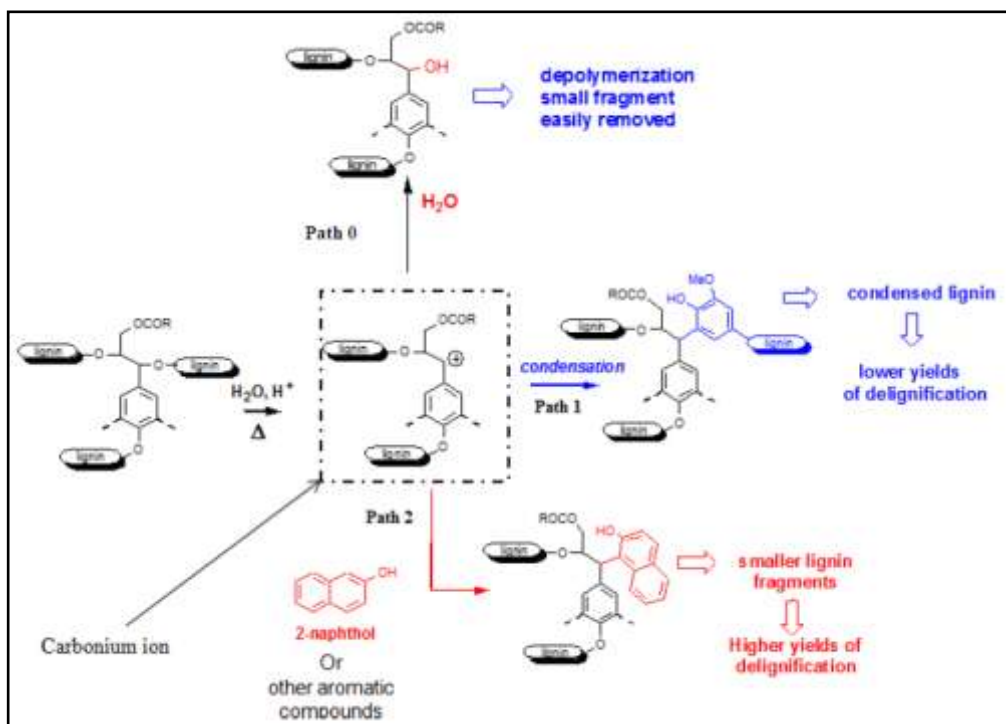


Figure 1.14: Lignin repolymerization and immobilization via the incorporation of organic scavengers (El Hage *et al.*, 2010).

It was also demonstrated that the presence of carbonium ion scavengers could substantially improve the lignin extractability. These aromatic organic compounds will compete with the aromatic rings of the lignin during the incorporation of the carbonium ion (Figure 1.14, path 2). Therefore, it will scavenge the carbonium ion intermediate from the self-condensation process during autohydrolysis. In a previous study, Wayman and Lora (1978) have tested on 40 different types of aromatic compounds in combination with the autohydrolysis pretreatment. They have revealed that 2-naphthol gave lower lignin content in the residual pulp. The utilization of 2-naphthol as lignin-lignin recondensation inhibitor in different feedstocks has been further studied by other researchers (Li and Gellerstadt, 2008; Timilsena *et al.*, 2013b). More recently, Timilsena *et al.* (2013b) have studied the effect of adding 4 different carbonium ion scavengers (o-cresol, p-cresol, hydroquinone and dihydroxyanthraquinone) on the delignification of *Miscanthus x giganteus* and it was reported that all organic scavengers used gave different lignin yields and properties.

1.4.3 Fractionation and purification of lignin by ultrafiltration system

The high non-homogeneity complex structure of lignin with high molecular weight distributions has limited its usage in the industrial sectors. It is estimated that the size of lignin molecules can vary from 1000 to 100 000 Da (Toledano, 2012). Therefore, fractionation of lignin has become a promising method to obtain a more specific molecular weight fraction with different chemical compositions and functionalities. Various methods have been proposed to fractionate the lignin molecules. These comprises of solvent extraction (Thring *et al.*, 1996; Yuan *et al.*, 2009), differential

precipitation (Sun *et al.*, 1999; Mussatto *et al.*, 2007) and membrane technology (Wallberg *et al.*, 2003; Toledano *et al.*, 2010a). The solvent extraction method was not preferred since it uses high solvent quantities, chances of contamination and operational difficulties (Toledano, 2012). Meanwhile, membrane technology via ultrafiltration was said to be a better method than differential precipitation method to obtain different fractions of lignin with specific molecular weights and low contamination (Toledano *et al.*, 2010b). The effectiveness of the ultrafiltration technology to separate the macromolecular solution is indeed beneficial for the purification and fractionation of lignin. In addition, a previous study by Garcia *et al.* (2010) has revealed that the lignin being fractionated by the ultrafiltration system will possess a good antioxidant activity than rough lignin. Thus, ultrafiltration technology would also improve the properties of lignin polymer, making it suitable for any potential applications.

Generally during the ultrafiltration process, the smaller molecules will pass through a membrane and the larger molecules will be retained if fixed pressure is applied (Baker, 2000) as shown in Figure 1.15. The operating pressure used is usually between 0.1 to 1 MPa. The solute of low molecular weight (small molecules) which passes through the membrane is called permeate while the high molecular weight solute (larger molecules) that is retained is called retentate. In some cases, the separation efficiency is not only influenced by nominal molecular weight cut-off but also by the membrane interaction with the raw solution.

Minimum energy consumption, absence of additional reagents (which can change the structure of compounds) and easy descaling makes membrane technology a

suitable fractionation-purification method to be implemented in a biorefinery. Some benefits of the membrane technology are (Mulder, 1991); i) continuous separation and energy consumption is generally low, ii) separations are carried out under mild conditions, iii) membrane properties are adjustable and available and iv) additives are not required.

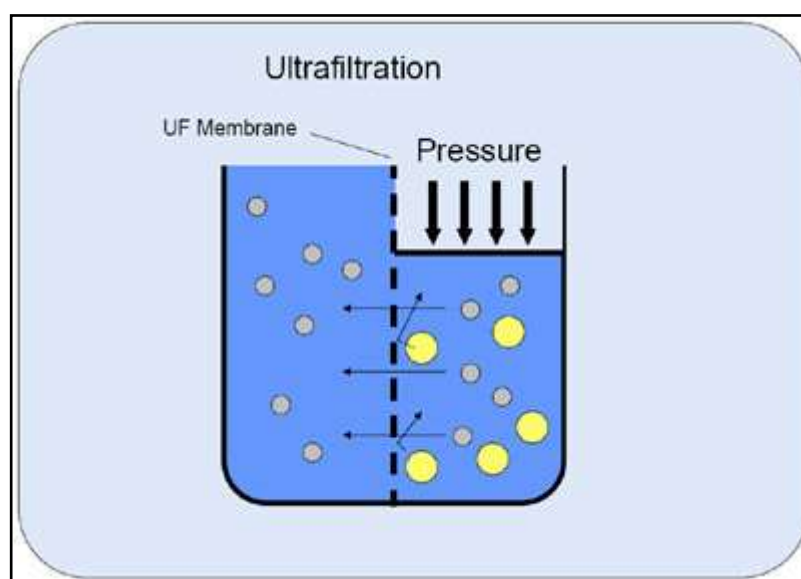


Figure 1.15: The principle of ultrafiltration.

1.4.4 Applications of lignin

Huge amounts of lignin are readily available in the pulp and paper industries and these amounts are expected to increase. However, the pulping processes which are used in the paper industries produce degraded lignin that was only employed in low-added value utilizations and energy production. A feasible economical processing of biorefinery is needed to promote a complete utilization of lignocellulosic biomass components as green materials. In this sense, lignin revalorization is one of the solutions to ensure the viability of biorefineries implementation. Many research

works are ongoing towards the use of lignin for new green approaches (Figure 1.16). These include the use of lignin as dispersant in cement (Yang *et al.*, 2007; Matsushita *et al.*, 2008), emulsifier (Boeriu *et al.*, 2004), chelating agent for heavy metals removal from industrial waste effluents (Sena-Martins *et al.*, 2008), absorbent (Mohan *et al.*, 2006) and phenol-formaldehyde adhesives (El Mansouri and Salvado, 2006; Tejado *et al.*, 2007).



Figure 1.16: Possible applications of lignin.

Lignin contains diverse functional groups of phenolic and aliphatic-OH, carbonyls, carboxyls, which can also act as a neutralizer or inhibitor in oxidation processes, via stabilizing reactions induced by oxygen radicals and their respective species. Previous studies have been done on the applicability of lignins from different sources as potential antioxidants (Urgatondo *et al.*, 2009; El Hage *et al.*, 2012). Furthermore, it was revealed that the extraction processes of lignin may give major effects on its antioxidant capacity (Garcia *et al.*, 2010). The antioxidant properties exhibited by lignin can lead to broader applications as anti-microbial, anti-aging

agents and corrosion inhibitors. Recent findings have agreed that lignin and its derivatives possess inhibitive properties towards the corrosion of metals in corrosive media (Vargin *et al.*, 2006; Ren *et al.*, 2008; Abu-Dalo *et al.*, 2013). However due to the high hydrophobic properties of lignin, its capability to act as efficient corrosion inhibitors is limited. Hence, a proper modification/alteration of the lignin structures is required to increase its efficiency.

1.5 Corrosion of steels

The usage of steels in the industrial sectors has been gradually increasing. The steel is being widely used in road constructions, railways, skyscrapers, bridges, shipbuilding, pipelines, cars and construction materials. Nevertheless, one should consider the consequences of corrosion when utilizing steel as their main material components. The corrosion of steels would cost more than billions of dollars for its maintenance. It was believed that the average costs for most industrialized nation is 3.5-4.5 % of its gross domestic product (GDP) (Davis, 2000; Ahmad, 2006). The corrosion cost in Malaysia has been estimated to be around USD 6.7 billion annually (NACE, 2002). Most of the losses are related to economic (shutdown of equipment, preventive maintenance, etc.) and social (health) aspects (Davis, 2000).

Generally, corrosion is a destructive/deterioration process of metals/alloys due to their chemical or electrochemical reactions with the environment (Uhlig, 1985; Fontana, 1986). This process will form solid scales on the metal surface, known as rusts or metal oxides. It is common that when these metals are being exposed to the environments, it will revert to its original state (normally in the form of oxides or

ores) due to its temporary unstable existence in metallic forms (Ahmad, 2006; Roberge, 2008). In the presence of oxygen and water, these unstable steels will undergo a corrosion process as shown in Figure 1.17.

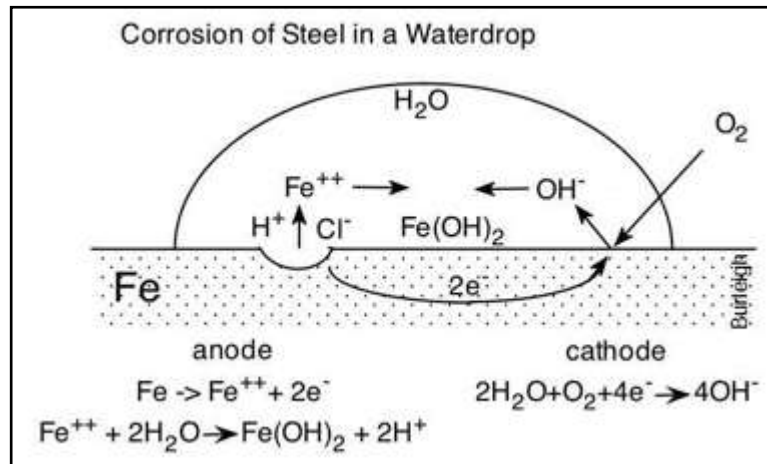


Figure 1.17: The mechanism of corrosion of steel (Ahmad, 2006).

In the first stage, the steel is oxidized to form Fe²⁺ ions at the anode terminal:



Meanwhile in neutral environments, the oxygen gas is reduced to form OH⁻ ions at the cathode terminal (Kruger, 2001):



Or if it is in acidic environments, the cathodic reaction will be as follows (Sheir *et al.*, 1994):



Hence the overall corrosion reaction will be the sum of the reduction and oxidation half equations to form an insoluble iron (II) hydroxide (also known as green rust):



But, the iron (II) ions are unstable and it can further oxidize to produce more stable iron (III) ions:



These iron (III) ions can react with hydroxide ions to yield reddish-brown color hydrated iron (III) hydroxides or ferric hydroxides/rust:



In the presence of hydrochloric acid, the reaction will produce ferrous chloride salt and hydrogen gas (Groysman, 2010):



Next, the FeCl_2 will be oxidized through anodic channels to produce ferric hydroxide (Tamura, 2008):



The formation of $\text{Fe}(\text{OH})_3$ can cause further aging process which leads to the dehydrated oxyhydroxides, FeOOH where neither acid nor base is consumed or generated. So the pH will remain unchanged during the aging process (Morgan and Stumm, 1981):



In summary, further oxidation of $\text{Fe}(\text{OH})_3$ will produce $\alpha\text{-FeOOH}$ (goethite), $\beta\text{-FeOOH}$ (akaganite), $\gamma\text{-FeOOH}$ (lepidocrocite), Fe_3O_4 (magnetite) and so forth. The corrosion of steel can be reduced by the discovery/search of corrosion-resistance materials and/or chemicals that can offer better technical practices.

1.5.1 Corrosion protection

Although it is impossible to stop the corrosion process, it can be reduced by manipulating the corrosion process. The understanding of corrosion process is essential in developing a proper method of corrosion protection. Corrosion protection can be achieved by shifting the steel overpotential to the passivity and immunity zone (Figure 1.18). The method chosen for corrosion protection must also consider both economical cost and its effectiveness. Five fundamental methods of corrosion protection have been implemented (Singley *et al.*, 1985; Davis, 2000; Kruger, 2001); i) material selection, ii) coatings, iii) inhibitors, iv) cathodic/anodic protection and v) material design. Among all types of corrosion protection, corrosion inhibitor offers good steel protection, inexpensive and easy to use. Due to these advantages, corrosion inhibitors are chosen by most corrosion scientists nowadays as an alternative to other existing protection methods.

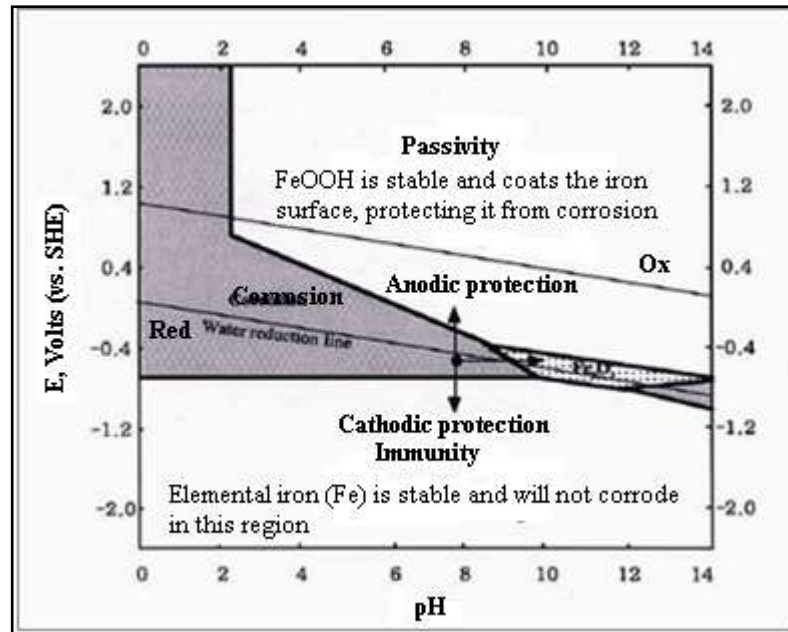


Figure 1.18: Pourbaix diagram of steel which explains how corrosion protection can be achieved (Kruger, 2001).

1.5.2 Corrosion inhibitors

The corrosion of metals can be controlled by adding sufficient amounts of specific chemicals to the corrodent which later forms a thin protective layer that can provide a barrier between the metal and water molecules. This type of corrosion protection is commonly known as inhibition and the chemical that is added to the system is called inhibitors. It is believed that the inhibitors will reduce corrosion rate of metals but it does not totally prevent the corrosion process (Singley *et al.*, 1985; Kruger, 2001; Schweitzer, 2007; Revie and Uhlig, 2008). Usually the corrosion inhibitor used is low in concentrations varying from 1 to 15000 ppm which is approximately around 0.0001 to 1.5 wt % (Sastri *et al.*, 2007; Groysman, 2010). The corrosion inhibitors are available at various ranges of pH and are commonly used in automobile cooling and boiler feedwater systems.

Generally, corrosion inhibitors can be classified into 3 major classes; i) passivators (chromates or nitrite), ii) organic inhibitors and iii) vapour phase inhibitors (Schweitzer, 2007; Revie and Uhlig, 2008). Different types of corrosion inhibitors can be employed depending on its usability and applicability. Passivators are known to be less expensive and an excellent inhibitor that is normally added as the main ingredient in coolant or paint formulations. Unlike most inhibitors that are effective only at certain conditions, the organic inhibitors offer better protection by providing a barrier to the dissolution of steel in the electrolyte. The organic inhibitors can be classified into two main categories; that is synthetic and/or natural organic inhibitors. It was revealed that synthetic inhibitors can promote good corrosion protection of steel in both acidic and near neutral solutions. Indeed, such organic derivatives like azole (Sherif and Park, 2006; Wahyuningrum *et al.*, 2008; Obot *et al.*, 2009) and imine Schiff bases (Talati *et al.*, 2005; Asan *et al.*, 2006; Behpour *et al.*, 2008; Kustu *et al.*, 2007; Hasanov *et al.*, 2007) have shown good anti corrosion activity. Nevertheless, most synthetic inhibitors are highly toxic as synthetic inhibitors may cause temporary and/or permanent damage to internal organs due to its presence in the saline system (Stupnisek-Lisec *et al.*, 2002; Bouyanzer *et al.*, 2006). It is estimated that the cost of commercial corrosion inhibitor (car coolants, paints, oils, additives or formulated chemicals) in Malaysia is around MYR 20-200 per item and considered expensive for bigger scale applications. Hence, attention has been focused to the use of naturally occurring corrosion inhibitors which are low cost and non-hazardous to both human and the environment.

Natural products as corrosion inhibitors have become a new research trend in the search of alternative inhibitors for corrosion protection. Natural inhibitors from plant

extracts like *Azadirachta indica* (Valek and Martinez, 2007), *Olea europaeae* (El-Etre, 2007), *Ammi visnaga* (El-Etre, 2006), *Nypa fruticans* (Orubite and Oforka, 2004) and *Sansevieria trifasciata* (Oguzie, 2007) have shown positive results in protecting steel/metals from corroding.

The effectiveness of organic inhibitors in corrosion protection is due to the adsorption process between the inhibitors with the steel surface. It has been postulated that the organic inhibitors will adsorb onto the steel surface (refer to Figure 1.19) either by physical adsorption (physisorption) or chemical adsorption (chemisorption). Physisorption happens as a result of electrostatic attractive forces (Van der Waals forces) between the ionic-forms of organic inhibitors with electrically charged steel surface (Schweitzer, 2007). This type of adsorption is unstable and it can easily desorb to its initial form since physisorption forces are relatively weak and possess low activation energy (Sastri *et al.*, 2007). Meanwhile chemisorption is the adsorption process which involves sharing and/or transfer of electrons from the inhibitors (as a form of nucleophile) with the steel surface that later forms a coordinate type bond. Generally the chemisorption occurs at a slower rate than physisorption and possesses high activation energy. Most of organic inhibitors having π electron or possess one or more heteroatoms (like P, Se, S, N and O) with lone pair electrons are often chemically adsorbed on the steel surface (Schweitzer, 2007; Sastri *et al.*, 2007). The other possible interaction that might occur during corrosion inhibition is the interaction of the d-orbital from Fe ion of steel to the vacant orbital of the inhibitor molecule (back-donation) (Ansari and Quraishi, 2014).

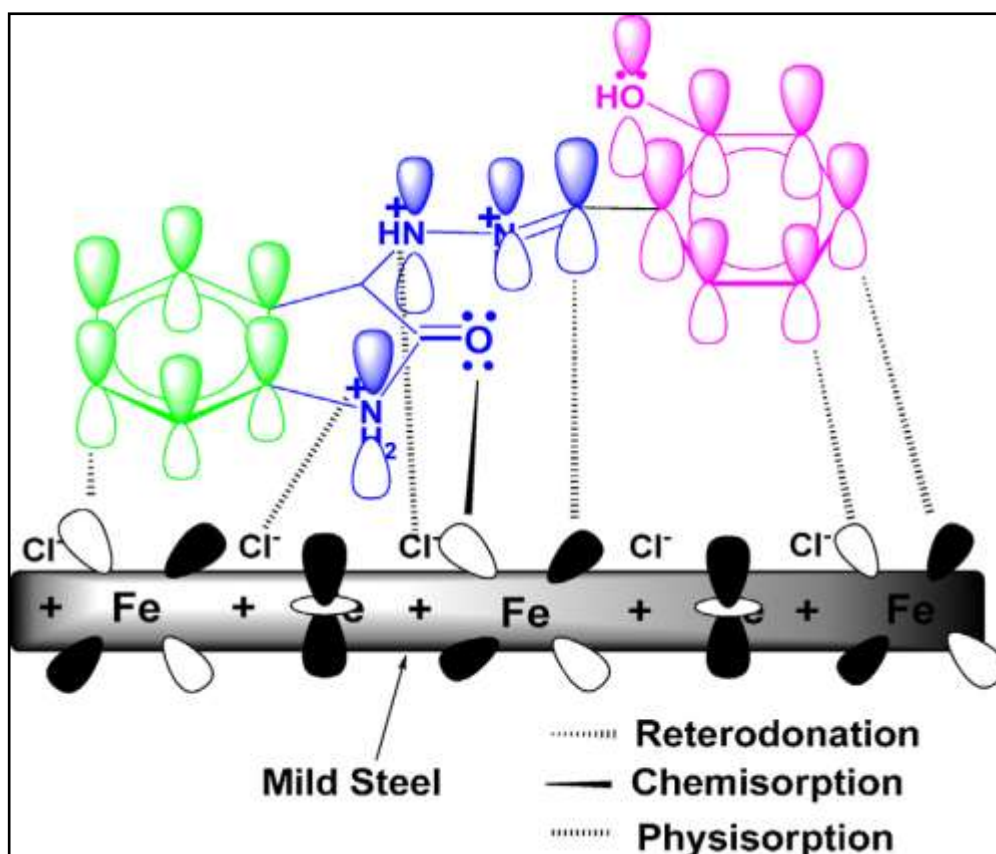


Figure 1.19: Example of different modes of interaction on mild steel surface during inhibition process (Ansari and Quraishi, 2014).

The adsorption strength of an inhibitor on the steel surface can be deduced from the adsorption isotherm. In order to evaluate the nature and the strength of adsorption, the corrosion experimental data are fitted to several isotherms and the thermodynamic parameters (especially the Gibbs free energy, ΔG_{ads}°) are evaluated from the best fit curves. The various adsorption isotherms (such as Langmuir, Frumkin, Temkin and Freundlich) which are commonly used for corrosion inhibition studies are presented in Table 1.5. It has been assumed that Langmuir adsorption isotherm is used to describe monolayer adsorption and usually appropriate for the description of physisorption or chemisorptions (Ahamad *et al.*, 2010). Meanwhile, Frumkin adsorption isotherm is often coupled with Langmuir adsorption isotherm to correlate the physisorption phenomenon that occurs on a heterogeneous surface site. Temkin adsorption isotherm characterizes the chemisorption of an unchanged

substance on a heterogenous surface, while Freundlich adsorption isotherm assumes that the adsorption occurs on a heterogenous surface site with different energy and non-identical adsorption sites (Wan Adnan, 2012).

Table 1.5: Various adsorption isotherms for corrosion inhibition studies (Wan Adnan, 2012).

Isotherm	Equation ^a	Verification plot
Langmuir	$\theta/(1-\theta) = KC$	C/θ vs C
Frumkin	$[\theta/(1-\theta)]\exp^{f\theta} = KC$	$\log [\theta/C(1-\theta)]$ vs θ
Temkin	$\exp^{f\theta} = KC$	θ vs $\log C$
Freundlich	$\theta = KC^{1/n}$	$\log \theta$ vs $\log C$

^a θ : surface coverage (%IE/100); C : bulk inhibitor concentration; f : inhibitor interaction parameter; K : equilibrium constant and n : empirical constant.

The difference in the activation energy level can be used as an indicator to identify the nature of adsorption during metal corrosion inhibition. It is believed that activation energy ranging from 40 kJ mol⁻¹ and below are often associated with a physisorption process while higher activation energy (from 80 kJ mol⁻¹) is often associated with chemisorption (Orubite and Oforka, 2004). In addition, the Gibbs free energy (ΔG_{ads}°) values can also be used to indicate the types of adsorption processes. The calculation for these values will be explained in Chapter 3. It is well-known that the values of ΔG_{ads}° around -20 kJ mol⁻¹ or less negative is attributed to physisorption while those around -40 kJ mol⁻¹ or more negative are attributed to chemisorption (Cheng *et al.*, 2007; Wahyuningrum *et al.*, 2008; Obot *et al.*, 2009; Ahamad *et al.*, 2010). If the ΔG_{ads}° values are in between -20 to -40 kJ mol⁻¹, both physisorption and chemisorption processes are possible or involved (semi-physisorption or semi-chemisorption) (Wahyuningrum *et al.*, 2008).

1.5.3 Corrosion measurement techniques

Different approaches or techniques are available in order to evaluate the applicability of organic inhibitors in corrosion processes. These techniques encompass both theoretical and practical concepts of corrosion electrochemistry so that they can provide better understanding to the inhibition phenomenon. There are several related techniques that can be employed for the corrosion measurement depending on the types of test environments. Some of the more relevant techniques are weight loss, electrochemical impedance and potentiodynamic polarization measurements.

1.5.3.1 Weight loss measurement

The weight loss or gravimetric measurement is known as the simplest method used for corrosion monitoring (Okafor and Ebenso, 2006; Bendahou *et al.*, 2006). This method involves direct immersion of steel (specimens) to the corrosive media at a fixed period of time. The rate of corrosion from this method can be determined by measuring the weight changes of the steel. In order to obtain a precise data from the weight loss measurement, one should consider certain important variables such as specimen dimension, immersion time, pre-treatment and post-treatment of steel. In addition, the volume of the corrosive media also must be appropriately used.

1.5.3.2 Potentiodynamic polarization measurement

The potentiodynamic polarization is one of the primary electrochemical techniques used to study the corrosion phenomenon (like pitting and passivity) by disturbing the

corrosion potential and measures the external flowing current (Schweitzer, 2007). This technique measures the corrosion rate of metal via current-potential relationships. The term ‘polarization’ arises when the reaction is assumed to induce deviation/polarized (due to the passage of electrical current through electrochemical cell) within ± 250 mV from its corrosion potential, E_{corr} that will cause changes in the metal (Perez, 2004; Ahmad, 2006). In definition, E_{corr} is the potential at which the rate of oxidation is similar to the rate of reduction. These current-potential correlations can be represented in a logarithm curve known as Tafel curves (Figure 1.20). The Tafel curve represents the combination of oxidation (anodic) and reduction (cathodic) linear curves. The slopes of anodic and cathodic curves are noted as β_a and β_c . These anodic and cathodic current slopes can be calculated using Equation 1.11 and 1.12, derived from the Butler-Volmer equation (Equation 1.10):

$$i = i_0 \left[\exp \left(\frac{\alpha n F}{RT} \eta \right) - \exp \left(- \frac{(1-\alpha) n F}{RT} \eta \right) \right] \quad (1.10)$$

$$\beta_a = \frac{2.303 RT}{\alpha n F} \quad (1.11)$$

$$\beta_c = \frac{2.303 RT}{(1-\alpha) n F} \quad (1.12)$$

Where i is the electrode current (A), i_0 is the exchange current density (A cm^{-2}), α is the charge transfer coefficient, n is number of electrons, F is Faraday constant ($9.65 \times 10^4 \text{ C mol}^{-1}$), R is universal gas constant ($8.314 \text{ J mol}^{-1} \text{ K}^{-1}$) and T is absolute temperature (K). In addition, from the Tafel curves the value of corrosion current density (i_{corr}) can be determined by extrapolating both anodic and cathodic linear

curves towards E_{corr} . Determination of i_{corr} is considered important in order to evaluate the corrosion rate and the corrosion inhibition.

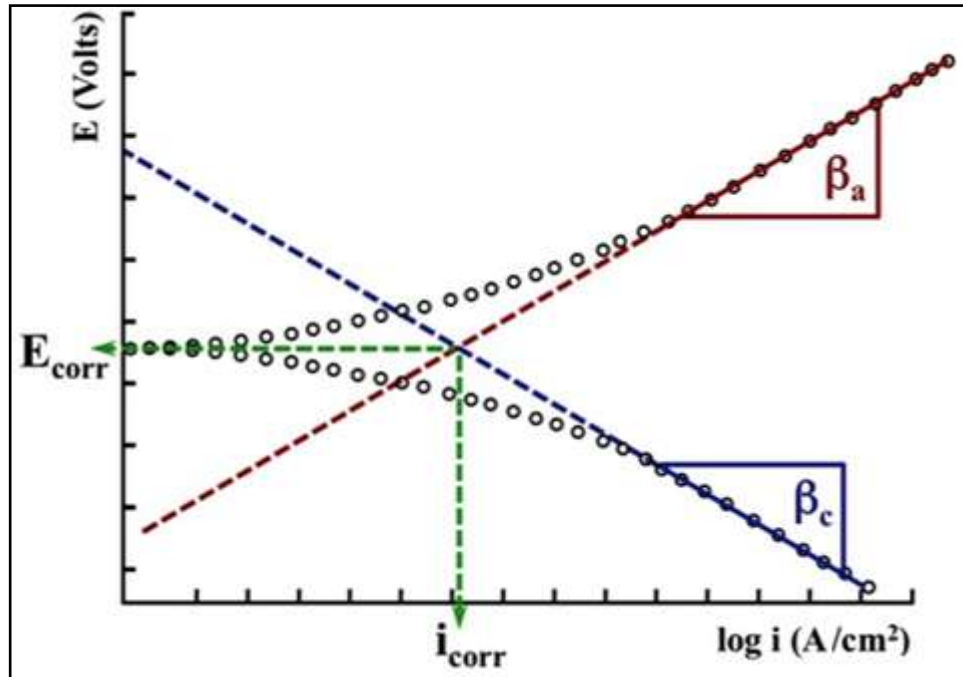


Figure 1.20: Extrapolation of Tafel curves.

Apart from the determination of corrosion rate, Tafel curves can also be used to explain the behavior of the corrosion inhibition process. There are three major types of inhibition processes that can be observed from the Tafel curves; cathodic, anodic and mixed inhibitions. Generally, the inhibition processes are identified if the linear slope of anodic and/or cathodic shows a greater slope reduction as a response to low current density. Cathodic inhibition is when the inhibitor inhibits the corrosion reduction process (either hydrogen gas evolution in acidic solution or formation of hydroxide ions in neutral or alkaline solution as in Equation 1.2 and 1.3). As for anodic inhibition, this will occur when the inhibitor inhibits the corrosion oxidation process (dissolution of metals) while for mixed inhibition, the inhibitor inhibits both oxidation and reduction processes.

1.5.3.3 Electrochemical impedance spectroscopy (EIS)

Electrochemical impedance spectroscopy (also known as AC impedance) is another electrochemical method used to evaluate the corrosion process by determining the electrical impedance of steel/metals to electrolyte interface at various alternating current (AC) frequencies (Schweitzer, 2007). The EIS measurement is also capable of characterizing the corrosion interface in low conductive solution or high resistivity of coatings (Schweitzer, 2007; Revie and Uhlig, 2008). In an alternating circuit, the amplitude of current and the proportionality factor between current (I , ampere) and potential (E , volts) will be determined by the impedance (Revie and Uhlig, 2008; Groysman, 2010):

$$E = IZ \quad (1.13)$$

Impedance can be defined as a complete number where the resistance is the real component and the combined capacitance and inductance act as its imaging component (Ahmad, 2006). Two different plots can be obtained in the impedance analysis, namely the Nyquist and Bode plots (Figure 1.21). For Nyquist plots, the impedance data are represented as the correlation of imaginary impedance ($-Z''$) to real impedance (Z'). Subsequently, the Bode plot shows the correlation between the impedance magnitude ($|Z|$) to log frequency and phase angle (θ) to log frequency.

The phase angle θ , refers to the difference between the points on the x-axis where the voltage-current curves amplitudes are equal to zero.

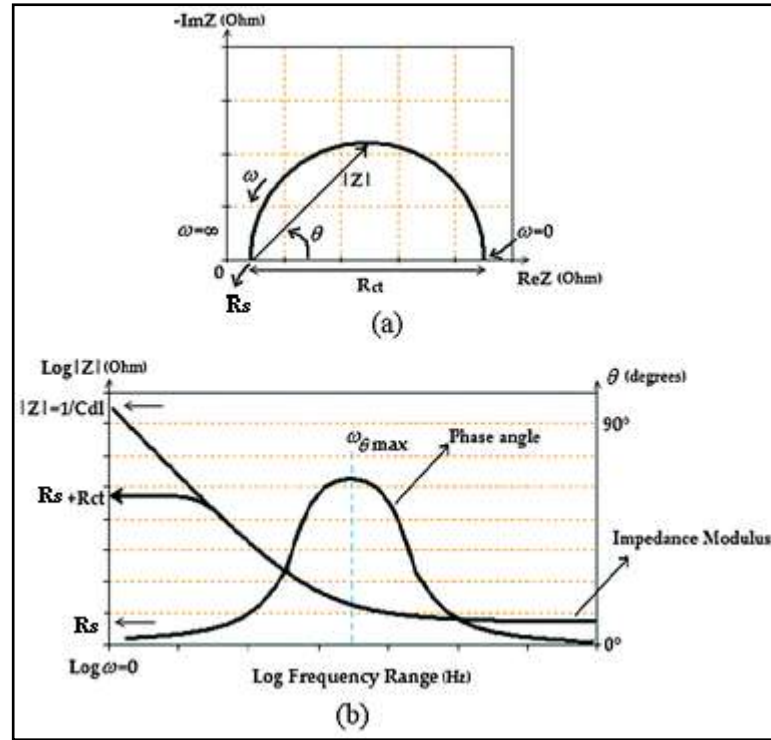


Figure 1.21: (a) Nyquist and (b) Bode plots of impedance (Dominquez-Benetton *et al.*, 2012).

The response of an electrode to the alternating potential signals (at various frequencies) is later interpreted with the basic circuit models of electrode to electrolyte interphase (Perez, 2004; Revie and Uhlig, 2008). Basically, the electronic circuit (as shown in Figure 1.22) consists of a capacitance that stores the electron charge and resistance which controls the current flow. The manipulation of this electronic circuit model is important in order to determine the actual resistant charge transfer (R_{ct}) and capacitance (C) values. In the charge transfer circuit, the capacitance C corresponds to the capacitance of double layer (C_{dl}) hence the impedance for this system can be denoted by (Marcus and Mansfeld, 2006):

$$Z = R_s + \frac{R_{ct}}{1 + j\omega C_{dl} R_{ct}} \quad (1.14)$$

Where R_s is the resistance of solution, R_{ct} is the resistance charge transfer and C_{dl} is the double layer capacitance. The C_{dl} capacitance can be calculated using the derivation below (Kustu *et al.*, 2007):

$$C_{dl} = \frac{1}{2\pi f_{max}} \times \frac{1}{R_{ct}} \quad (1.15)$$

Where f_{max} is the maximum frequency at which the Nyquist imaginary component is maximum. Theoretically in corrosion inhibition, an increase of R_{ct} and decrease of C_{dl} with increasing inhibitor concentration will indicate that the inhibitor inhibits the rate of corrosion of metals via charge transfer mechanisms (Perez, 2004; Kustu *et al.*, 2007).

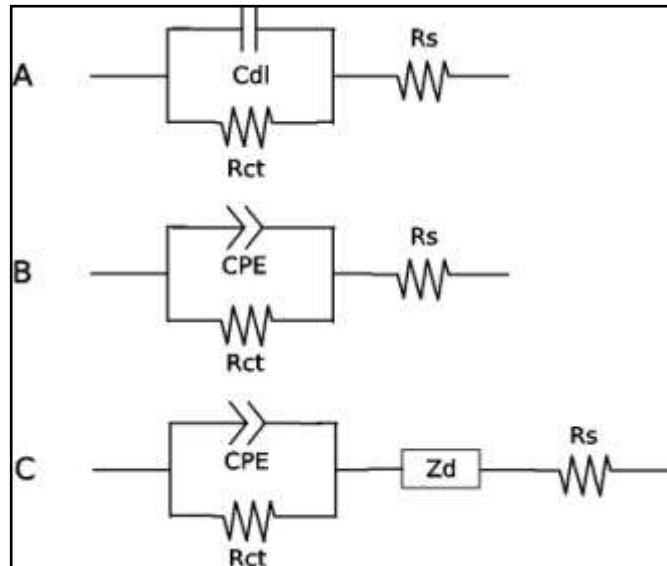


Figure 1.22: Some examples of equivalent circuits used for EIS analysis (C_{dl} : double layer capacitance; CPE: constant phase element; Z_d : diffusion resistant; R_{ct} : charge transfer resistant; R_s : solution resistant).

1.6 Problem statement and motivation

Massive amounts of lignin are produced in Malaysia each year by the pulp and paper industry as by-products of delignification. However, the pulping processes currently used in the paper industry produce degraded lignins that are employed in low-added value utilizations and energy production. To improve the overall effectiveness, one strategy is the biorefinery model in which all components of biomass are fully utilized to produce a wide range of value-added products. Finding the value-added applications of lignin is becoming a mandate for these industries in order to achieve economic and environmental sustainability. In addition, lignin can be considered as a valuable source of antioxidant phenolic compounds (due to high content of diverse functional groups such as phenolic and aliphatic –OH, carbonyls, carboxyls, etc.) that sometimes resulted in positive correlations to corrosion inhibitions of metals and alloys.

Nevertheless, the high non-homogeneity complex structure of lignin with high molecular weight distributions has limited its usage in the industrial sectors. Although this phenolic moiety represents a low and variable fraction of the total lignin, it can strongly affect the reactivity of the polymer. In addition, high hydrophobicity of lignin can limit its capability to be employed in other possible applications. Therefore, the modulation of suitable lignin structures (by considering its solubility, molecular weight, phenolic –OH content) is important so that it can overcome such implications. Obviously, the properties of lignin can be improved by modifying the structure into more suitable structure types.

The primary aim of this study are to undergo the modification of the lignin structure by: i) incorporating organic scavenger (2-naphthol and 1,8-dihydroxyanthraquinone) via combinative treatment and ii) fractionation of lignin structure via ultrafiltration technique. The improved physicochemical properties, solubility and antioxidant activity of modified lignin are expected to act as good corrosion inhibitors. To the best of knowledge, no such research work has been done previously on the lignin structural modifications, correlation between structural characteristic, solubility, antioxidant activity and anticorrosion properties of lignin extracted from oil palm fronds. The enhanced protective properties of the modified lignin lead to an alternative approach for the utilization of these natural waste materials.

1.7 Objectives

It has been demonstrated that lignin extracted from oil palm empty fruit bunches (EFB) are potential corrosion inhibitors of steel. However, the utilization of lignin for corrosion inhibition applications remains a problem because of its high hydrophobicity which limits its capability to act as an efficient corrosion inhibitor. Obviously, the inhibitive action can be improved by modifying the lignin into more soluble lignin. It is therefore the objectives of this study:

- i. To extract lignin from oil palm fronds (OPF) via direct delignification processes and combinative pretreatments.
- ii. To modify the lignin structure through: (a) incorporation of organic scavengers (2-naphthol and 1,8-dihydroxyanthraquinone) during combinative

autohydrolysis treatment and (b) fractionation and purification with an ultrafiltration system.

- iii. To characterize lignin quantitatively and/or qualitatively of its HGS content, phenolic-aliphatic –OH content, molecular structure, dissolution and thermal behavior of the modified and ultrafiltrated lignin.
- iv. To evaluate the antioxidant properties of the modified and ultrafiltrated lignin.
- v. To determine the anticorrosion action of the modified and ultrafiltrated lignin on mild steel in 0.5 M hydrochloric acid (HCl).
- vi. To correlate the inhibition efficiency of lignin inhibitor with its HGS content, phenolic –OH content, molecular weight and antioxidant activity.
- vii. To propose possible inhibition interaction mechanisms by fitting to relevant adsorption models.

CHAPTER TWO

EXPERIMENTAL

The extraction, modification and characterization of lignin have been carried out at the School of Chemical Sciences, Universiti Sains Malaysia and Laboratoire d'Etude et de Recherche sur le MAteriau Bois (LERMAB), Faculte des Sciences et Techniques, Universite de Lorraine, Nancy. The extraction and characterization of lignins extracted from oil palm fronds (Figure 2.1) via direct delignification processes (Kraft, soda and organosolv pulping in 4 L digester) and the anticorrosion tests of all modified and ultrafiltrated lignins on mild steel in 0.5 M hydrochloric acid (HCl) have been carried out at USM. In turn, the extraction and characterization of lignin via combinative pretreatments (dilute sulphuric acid or autohydrolysis followed by ethanol organosolv pulping in 0.6 L digester), modification of lignin structure through incorporation of organic scavengers (2-naphthol and 1,8-dihydroxyanthraquinone) during combinative autohydrolysis treatment and selective fractionation of lignins with ultrafiltration system have been conducted at LERMAB.

2.1 Materials

The oil palm fronds (OPF) were obtained from Valdor Palm Oil Mill near Sungai Bakap plantation (Seberang Prai, Malaysia) in mid 2011. The OPF leaves were removed and the strands were chipped into small pieces.

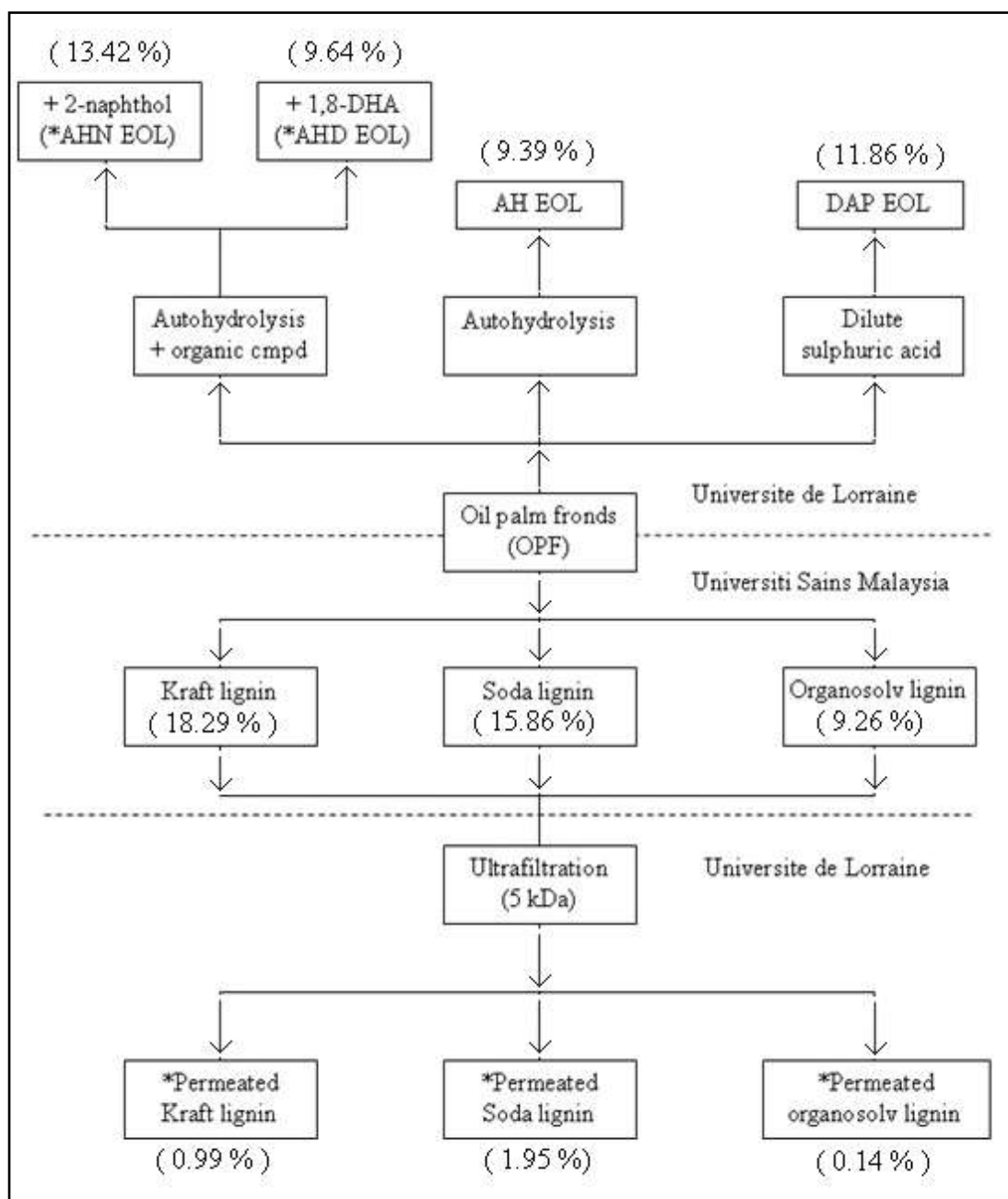


Figure 2.1: An overview of lignin extraction at Universiti Sains Malaysia and Universite de Lorraine with the mass balance, w/w % (*used for corrosion study).

After sun dried for 3 days, the chips were then ground to a 1-3 mm size using Wiley mill and the fiber was further dried in an oven at 50 °C for 24 h. The OPF biomass was first subjected to Soxhlet extraction with ethanol/toluene (2:1, v/v) for 6 h before use. All chemical reagents used in this study were purchased from Sigma Aldrich and VWR (France) and used as received. Dried matter contents were determined using a moisture balance, KERN MRS 120-3 Infra-red moisture analyzer

(drying at 105 °C to constant weight). The effective dry matter content of raw OPF biomass was ~89 %. The severity correlation which describes the severity of the pretreatment as a function of treatment time (t, min) and temperature (T, °C), where $T_{\text{ref}} = 100$ °C was calculated using the formula stated below (Brosse *et al.*, 2010):

$$\text{Log } R_0 = \text{Log } [t \exp(T - T_{\text{ref}})]/14.7 \quad (2.1)$$

$$S_0 = \text{Log } R_0 - \text{pH} \quad (2.2)$$

The pH of the liquor can be employed as a measure of the hydrogen ion concentration under the acidic conditions (dilute sulphuric acid hydrolysis and ethanol organosolv treatment).

2.2 Alkaline lignin extraction

Both Kraft and soda pulping processes were carried out in a 4-L rotary digester. All pulping conditions followed the method outlined by Wanrosli *et al.*, 2007 with slight modifications. For Kraft pulping, a 20 % of active alkali and 30 % of sulfidity with water to fiber ratio of 8:1 was used. The time of maximum cooking temperature (170 °C) was set for 3 h (severity factor: $S_0 = \sim 3.64$). For soda pulping, 30 % of active alkali alone was applied at the same conditions as described above (severity factor: $S_0 = \sim 3.64$). The pressure of both Kraft and soda pulping was around 12-15 bar. The pulp was washed and separated by screening through a sieve and the black liquor was collected. Lignin was precipitated from the concentrated black liquor by acidifying it with 20 % (v/v) sulfuric acid until pH 2 (Mohamad Ibrahim *et al.*,

2011). The precipitated lignins were filtered and washed with pH 2 water. Both lignins were then dried in an oven at 50 °C for 48 h. The purification of both lignins was conducted by extracting it in the soxhlet apparatus for 6 h with n-pentane to remove lipophilic non-lignin matters such as wax and lipids. The precipitate was filtered and washed twice with pH 2 water to remove the excess n-pentane and non-lignin phenolic compounds which may remain after the pulping process. The purified Kraft and soda lignins were then dried in an oven for another 48 h.

2.3 Organosolv lignin extraction

OPF (200 µm particle size, 25 g dry weight biomass) was mixed with water:ethanol (35:65, v/v) and 0.5 % w/w sulphuric acid as a catalyst at 190 °C for 60 min (severity factor: $S_0 = \sim 2.5$), following the method outlined by El Hage *et al.* (2009). The solid to liquid ratio used was 1:8. Treatments were carried out in a 0.6 L stainless steel pressure Parr reactor with a Parr 4842 temperature controller (Parr Instrument Company, Moline, IL). After the reactor was loaded with OPF and cooking liquor, it was heated to the operating temperature which was then maintained throughout the experiment (pressure around 25 bar). The reaction mixture was heated at a rate of 5 °C min⁻¹ with continuous stirring. At the end of the treatment, the free liquid was removed and then the fibrous residue was washed with warm 89 % v/v aqueous ethanol (3 x 50 mL). The liquor was diluted with 3 volumes of water to precipitate the organosolv lignin and the precipitate was then collected by centrifugation at 3500 rpm for 10 min. The resulting organosolv lignin was dried in an oven at 50 °C for 48 h. The purification of lignin was conducted by extracting it in the soxhlet apparatus for 6 h with n-pentane to remove lipophilic non-lignin

matters such as wax, lipids, naphthol and anthraquinone (for effect of organic scavengers) impurities. The purified organosolv lignin was then dried in an oven at 40 °C under atmospheric pressure for another 24 h.

2.4 Pretreatment of OPF

2.4.1 Dilute sulphuric acid pretreatment

The dilute sulphuric acid pretreatment was done according to the method outlined by Brosse *et al.* (2010). OPF was soaked overnight with dilute H₂SO₄ (0.9 %, w/w based on dry matter content, solid to liquid ratio of 1:8) and treated at 170 °C for 2 min (severity factor: $S_0 = \sim 0.73$) in the Parr reactor as described previously. The pretreated OPF was washed thoroughly with water and air dried.

2.4.2 Autohydrolysis pretreatment

OPF sample with 1-3 mm particle size (20 g oven dried matter, raw material or pretreated organic compound) was loaded into a 0.6 L stainless steel pressure Parr reactor with a Parr 4842 temperature controller (Parr Instrument Company, Moline, IL) and was supplemented with an appropriate amount of deionized water to obtain a final solid to liquid ratio of 1:9, taking into account the moisture content of the sample. The mixture was heated at 150 °C with continuous stirring for 8 h (time zero was set when the preset temperature was reached with the heating rate of 5 °C min⁻¹, severity factor: $S_0 = \sim 4.1$). At the end of each reaction, the reactor was cooled and the liquid phase was recovered by filtration through Whatman No. 4 filter paper. The

solid residue was washed with 70 °C water (3 x 50 mL) and a portion of the solid residue and the combined liquid residue were stored in a freezer at -5 °C before analysis.

2.4.3 Pretreatment with organic scavengers

About 20 g (oven dried matter) of OPF were immersed in 100 mL of acetone containing 0.8 g of 2-naphthol or 1,8-dihydroxyanthraquinone at room temperature. After thorough mixing, biomass samples were air-blown to dryness at room temperature followed by autohydrolysis as described above.

2.5 Purification and fractionation of lignin by ultrafiltration unit

The tangential ultrafiltration module used to fractionate the lignins was a Pall Omega Centramate pilot unit equipped with a 1 L reservoir feed with a recirculation pump and a set of Omega cassette equipped with polyethersulfone (PES) membrane cut-off in the interval of 5 kDa manufactured by PALL Corporation, USA. The retentate and permeate were recirculated to the feed tank for 1 h before samples of permeate and retentate were withdrawn. The pressure was measured at the inlet and at the outlet of the membrane tube. As the pressure on the permeate side was atmospheric, the Trans membrane pressure, TMP is the average of the inlet and outlet pressure on the feed side. The experiments were done at the following experimental conditions: TMP: 300 kPa; cross-flow velocity: 5.6 m s^{-1} and temperature: $25 \pm 2 \text{ }^{\circ}\text{C}$.

2.5.1 Fractionation of lignin (Kraft, soda and organosolv lignin) with 5 kDa membrane

Approximately around 2.00 g of dried lignins were weighed and dissolved in 300 mL of mobile phase solvents (0.1 M NaOH for Kraft and soda; 65 % v/v aqueous ethanol for organosolv lignin). The solutions were sonicated for 5 min before gradually filtered. The ultrafiltration system was rinsed 2-3 times with water and 0.1 M NaOH to remove any residues. Blank solution (0.1 M NaOH or 65 % aq. EtOH) was introduced into the ultrafiltration system and the flux rate was measured by controlling pump flow and retentate valve until a stable flux was achieved. Lignin solution was introduced into the ultrafiltration system and the circulation was maintained for 1 h before withdrawal. The permeate solutions were collected until all solution has passed the ultrafiltration membrane. Next, the blank solution was introduced again for flushing purposes for 30 min. All retentate solutions were collected by opening the retentate valve. The permeate and retentate solution of Kraft and soda lignin were next acidified with 20 % v/v H₂SO₄ and then centrifuged for 20 min (4000 rpm) to collect the precipitated lignin. The permeate and retentate solution of organosolv lignin was introduced to the rotary evaporator to evaporate all ethanol. Then the remaining solution was freeze-dried to remove any water impurities. The percentage of permeated lignin fraction recovery (LPR %) was calculated as follows:

$$\text{LPR \%} = \frac{(\text{Total dry weight of lignin after ultrafiltration})}{(\text{Initial weight of lignin before ultrafiltration})} \times 100 \quad (2.3)$$

2.6 Analytical procedures

A KERN MRS 120-3 Infra Red analyser (drying at 105 °C to constant weight) was used for moisture determination. Carbohydrate and lignin contents were measured on extractive-free material, ground to pass a 40-mesh screen, according to the laboratory analytical procedure (LAP) provided by the National Renewable Energy Laboratory (NREL/TP-510-42618) with some modifications. Samples were hydrolyzed with 72 % (w/w) sulphuric acid for 1 h and autoclaved at 120 °C for another 1 h after being diluted to 3 % (w/w) sulphuric acid through the addition of water. The autoclaved samples were filtered, and the dried residue was weighed to obtain the Klason lignin content. Monosaccharide contents in the filtrate were quantified using high-performance anion exchange chromatography with pulsed amperometric detection (HPAEC PAD). The soluble lignin content was determined from absorbance values at 205 nm.

2.7 High-performance anion-exchange chromatography (HPAEC) conditions

Separation and quantification of neutral sugars were performed using Dionex ICS-3000 system consisting of a SP gradient pump, an AS autosampler, an ED electrochemical detector with a gold working electrode, an Ag/AgCl reference electrode and Chromeleon Version 6.8 software (Dionex Corp., USA). A Carbopac PA1 (4 x 250 mm, Dionex) column with a guard column (4 x 50 mm, Dionex) was used as a stationary phase using isocratic conditions with 1 mM sodium hydroxide as eluent. Eluents were prepared by dilution of a 46-48 % NaOH solution (PA

S/4930/05 Fisher Scientific) in ultrapure water. All eluents were degassed before use by flushing with helium for 20 min; subsequently they were kept under constant helium pressure (eluent degassing module, Dionex).

After each run, the column was washed for 10 min with 200 mM NaOH and reequilibrated for 15 min with the starting conditions. Samples were injected through a 25 μ L full loop and separations were performed at 25 °C at a rate of 1 mL min⁻¹. The pulse sequence for pulsed amperometric detection consisted of a potential of +100 mV (0-200 ms), +100 mV integration (200-400 ms), -2000 mV (410-420 ms), +600 mV (430 ms), and -100 mV (440-500 ms).

2.8 Characterization of lignin

2.8.1 Preliminary analysis of lignin

The ash content was determined using the method proposed by Mohamad Ibrahim *et al.*, 2011. The crucible was initially dried at 105 °C until a constant weight was obtained. Next, approximately 500 mg of lignin samples were weighed into the crucible and calcined at 900 °C for 4 h. The ash content of lignin samples was determined by calculating the percentage of sample in the crucible after the burning process has completed. The contents of carbon, hydrogen, nitrogen and sulfur were analyzed using Thermo Finnigan model Eager 300 analyzer. The percentage of oxygen was calculated by subtracting the C, H, N and S contents from 100 %. The percentage of protein was calculated as N (%) x 6.25. The average double bond

equivalent (DBE) was calculated using Equation 2.4, based on the elemental composition ($C_aH_bO_cS_d$) (Robert *et al.*, 1984);

$$DBE = \frac{(2a+2)-b}{2} \quad (2.4)$$

2.8.2 Fourier Transform Infrared (FTIR)

The fourier transform infrared (FTIR) spectrophotometry was carried out in a direct transmittance mode using Perkin Elmer model System 2000 instrument. The region between 4000 and 400 cm^{-1} with a resolution of 4 cm^{-1} and 20 scans was recorded. The samples were prepared according to the potassium bromide technique, in a proportion of 1:100 (200 mg of KBr approximately).

2.8.3 Nuclear Magnetic Resonance Spectroscopy (NMR)

All nuclear magnetic resonance (NMR) spectroscopy experiments were performed on a Bruker Avance-400 spectrometer operating at a frequency of 100.59 MHz for ^1H and ^{13}C . Lignins (150 mg) were dissolved in DMSO d_6 (0.40 mL). ^{13}C NMR spectra were acquired at 50 °C in order to reduce viscosity. Quantitative NMR spectra were acquired using an inverse-gated decoupling (Waltz-16) pulse sequence to avoid Nuclear Overhauser Effect (NOE). Forty thousand scans were collected with a pulse delay of 12 s. ^1H and ^{13}C data were processed offline using XWinNMR processing software.

^{31}P NMR spectra were acquired after derivatizing 25 mg lignin with 2-chloro-4,4,5,5-tetramethyl-1,1,3,2-dioxaphospholane (TMDP) as previously described by Granata and Argyropoulos, (1995). Approximately 25 mg of lignin was added into 400 μL solvent mixture of pyridine: CDCl_3 (1.6/1, v/v) (Aldrich). Then each 150 μL of chromium (III) acetylacetonate (3.6 mg mL^{-1}) and cyclohexanol (4.0 mg mL^{-1}) solution in pyridine/ CDCl_3 was added to the lignin solution. The chromium (III) acetylacetonate served as a relaxation reagent and cyclohexanol as the internal standard. The lignin solution was then vigorously stirred until completely dissolved. Minutes before starting the NMR experiment, approximately 50 μL of TMDP was added to the vial and the solution was transferred into a 5 mm NMR tube. The ^{31}P NMR spectra were recorded with the following acquisition parameters; inverse-gated pulse sequence, 25 s pulse delay, 200 acquisitions, 61.7 ppm sweep width and 30° pulse width ($p1 = 6.5 \text{ usec}$, $p1 = -2.0 \text{ db}$).

^{13}C - ^1H 2D Heteronuclear Single Quantum Correlation (HSQC) and Heteronuclear Multiple Bond Correlation (HMBC) NMR spectra of lignin samples were recorded on a Bruker 500 MHz instrument using standard pulse program.

2.8.4 High performance liquid chromatography (HPLC) of oxidized lignin

Nitrobenzene oxidation was carried out by following the method proposed by Mohamad Ibrahim *et al.* (2008). About 50 mg of dry lignin samples was added into a mixture of 2 M NaOH and 4 mL of nitrobenzene in a steel cap autoclave. Then, the lignin sample was heated to 165°C for 3 h. The solution was cooled to room temperature and the mixture was then transferred to a liquid-liquid extractor for

continuous extraction with chloroform to remove any nitrobenzene reduction product and excess of nitrobenzene. The oxidation mixture was acidified by concentrated HCl to pH 3-4 and further extracted with chloroform. The solvent from the second chloroform solution was removed by using rotary evaporator at 40 °C. The mixture was then dissolved in dichloromethane and made up to 10 mL. This mixture was used as a stock solution for HPLC analysis.

A 0.2 mL of stock solution was pipetted into 25 mL volumetric flask and made up to the mark with acetonitrile-water (1:2, v/v). The resulting sample solution was filtered through a Millipore membrane (pore size 0.45 μm) to remove high molecular weight contaminant. The sample solution (20 μL) was injected into the HPLC system (Shimadzu) equipped with Thermo Hypersil Gold C18 column (particle size 5 μm , 25 mm \times 4.6 mm i.d) to determine phenolic acids and aldehydes content in lignin samples. A mixture of acetonitrile-water (1:8, v/v) containing 1 % acetic acid was used as an eluent with a flow rate of 1 mL min⁻¹. The eluent was monitored with an ultraviolet (UV) detector at 280 nm.

2.8.5 Gel permeation chromatography (GPC)

Lignin samples were subjected to acetylation in order to enhance their solubility in organic solvents, used in gel permeation chromatography (GPC). The acetylation reaction will substitute all the hydroxylic functions into acetyl groups. Lignin (20 mg) was dissolved in a 1:1 acetic anhydride/pyridine mixture (1.00 mL) and stirred for 24 h at room temperature. Ethanol (25.00 mL) was added to the reaction mixture, left for 30 min, and then removed with a rotary evaporator. The addition and

removal of ethanol was repeated several times to ensure complete removal of acetic acid and pyridine from the sample. Afterwards, the acetylated lignin was dissolved in chloroform (2.00 mL) and added drop-wise to diethyl ether (100.00 mL), followed by centrifugation.

The precipitate was washed three times with diethyl ether and dried under vacuum (762 mm of Hg) at 40 °C for 24 h. The number average molecular numbers (M_n) and weight (M_w) of lignin and cellulose were determined after derivatization by GPC with a Dionex Ultimate-3000 HPLC system consisting of an autosampler and a UV detector and using tetrahydrofuran as eluent. Standard polystyrene samples were used to construct a calibration curve. In brief, 1 mg of acetylated lignin samples were dissolved in 1 mL THF and were filtered using 0.45 μ m filter. Then 20 μ L of the filtered solution was injected into the HPLC system. Data were collected and analyzed with Chromeleon software Version 6.8 (Dionex Corp., USA).

2.8.6 Thermal analysis

The thermal behaviors of lignin samples were studied by thermal gravimetric analysis (TGA) using a Perkin Elmer TGA 7 thermogravimetric analyzer. Scans were recorded from 30 to 900 °C with a heating rate of 10 °C min⁻¹ under nitrogen atmosphere. The glass transition temperatures (T_g) were obtained using a Perkin Elmer Pyris 1 differential scanning calorimeter (DSC). The samples were heated from -50 to 200 °C with a heating rate of 10 °C min⁻¹.

2.9 Antioxidant activity

2.9.1 Lignin antioxidant activity by oxygen uptake method

Antioxidant properties of lignins were investigated by evaluating oxygen uptake inhibition during oxidation of methyl linoleate. The induced oxidation by molecular oxygen was performed in a gas-tight borosilicate glass apparatus. Butan-1-ol was used as solvent for lignin dissolution. Temperature was set to 60 °C, initial conditions inside the vessel were as follows; methyl linoleate (Fluka, 99 %) concentration: 0.32 mol L⁻¹; 2,2'-azobisisobutyronitrile (AIBN) (Fluka, 98 %) concentration: 7.2×10^{-3} mol L⁻¹; lignin concentration: 0.2 g L⁻¹; oxygen pressure: 150 Torr. Oxygen uptake was monitored continuously by a pressure transducer (Viatron model 104). Without any additive, oxygen uptake is roughly linear and constitutes the control. In the presence of an antioxidant, oxygen consumption is slower, and the antioxidative capacity (OUI) of extract was estimated by comparing oxygen uptake at a chosen time (3 h), in the presence of this compound (pressure variation ΔP_{sample}) and in the absence of the compound ($\Delta P_{\text{control}}$) according to:

$$\text{OUI (\%)} = (\Delta P_{\text{control}} - \Delta P_{\text{sample}}) / \Delta P_{\text{control}} \times 100 \quad (2.5)$$

This ratio defines antioxidative capacity as an oxygen uptake inhibition index (OUI); it should spread from 0 to 100 %, for poor and strong antioxidants, respectively, and may be negative for prooxidants.

2.9.2 Lignin antioxidant activity by reducing power assay

The reducing power of samples was determined by the method proposed by Gulcin et al. (2003) after a slight modification. Standard syringaldehyde and vanillin (Aldrich) solution ranging from 2.0×10^{-2} mg mL⁻¹ to 0.1 mg mL⁻¹ were prepared. To 1.0 mL of the standard solution, 2.5 mL of 0.2 M phosphate buffer at pH 6.6 (prepared from the addition of 0.2 M Na₂HPO₄ and 0.2 M NaH₂PO₄ (QRec)) and 2.5 mL of 1 % (w/v) potassium ferricyanide, K₃Fe(CN)₆ (Aldrich) solution were added. The mixture was incubated at 50 °C for 20 minutes after which 2.5 mL 10 % (w/v) trichloroacetic acid (Merck) was added. The resultant mixture was centrifuged for 20 minutes at 2500 rpm. The upper layer (2.5 mL) was dispensed and 2.5 mL distilled water and 0.5 mL of 0.1 % (w/v) ferric chloride hexahydrate, FeCl₃6H₂O (Merck) solution were added. The absorbance was measured at 700 nm. The procedure was repeated for lignin samples.

2.10 Dissolution test of lignin

The dissolution test was carried out as follows. Approximately 20 mg sample was added to 50 mL distilled water at 25 °C and agitated constantly at 100 rpm for 6 h. 2 mL solution was withdrawn at predetermined intervals and filtered through a 0.45 µm syringe filter. An equal volume of distilled water was replaced after each withdrawal (Francesco *et al.*, 2009; Lu *et al.*, 2012). After dilution with distilled water, the solution absorbance was measured at 280 nm (Shimadzu UV-2550 Japan). According to the UV linear regression equation, lignin concentration and the percentage of dissolution (D %) was calculated as follows (Lu *et al.*, 2012):

$$A - A_0 = K \times C \times L \quad (2.6)$$

$$D \% = (C_{\max} \times V_{\text{total}}) / m_{\text{initial}} \times 100 \quad (2.7)$$

Where A_0 is the absorption of distilled water, A is the absorption of sample, K is the absorption constant ($21 \text{ L g}^{-1} \text{ cm}^{-1}$), C is the concentration of lignin, C_{\max} is the maximum concentration at 600 min, L is the thickness of quartz cell (cm), V_{total} is the total volume and m_{initial} is the initial mass of lignin.

2.11 Corrosion inhibition studies

Mild steel coupons having chemical composition (wt %) of 0.08 C, 0.01 Si, 1.26 Mn, 0.02 P and remaining Fe were used. The specimens were polished successively using 400, 600 and 800 gritted emery papers. Next, it were degreased with methanol and washed with distilled water before and after each experiment. The solutions were prepared using AR grade hydrochloric acid. Appropriate concentrations of acids were prepared by using distilled water.

2.11.1 Electrochemical measurements

Lignin samples were first dissolved in a small volume of methanol (2 %, v/v) and sonicated for a few seconds to increase solubility. The dissolved lignin samples were next diluted with 0.5 M HCl (AR grade). Various concentrations of inhibitor at 10, 50, 100, 250 and 500 ppm (the maximum concentration was limited to 500 ppm as lignins are difficult to dissolve beyond that concentration) were prepared by diluting

the stock lignin solution. A three electrode cell assembly consists of a mild steel coupon (9 cm x 3 cm x 0.1 cm dimensions with an exposure surface of 3.124 cm²) as a working electrode (WE), platinum rod as a counter electrode (CE) and saturated calomel electrode (SCE) as a reference electrode (RE) immersed in 100 mL of electrolyte. The temperature of the electrolyte was maintained at room temperature (28±2 °C).

The electrochemical impedance spectroscopy (EIS), was carried out using Gamry Reference 600 after the open circuit potential, E_{ocp} has stabilized (30 min) over a frequency range of 100 kHz to 0.1 Hz with a signal amplitude perturbation of 5 mV and scan rate of 1 mVs⁻¹. Next, it was fitted with several sets of circuits using ZSim Demo software to obtain the charge transfer resistance, R_{ct} values. The percentage inhibition efficiency, (IE %) was calculated by the following equation,

$$IE \% = \frac{R_{ct (i)} - R_{ct}}{R_{ct (i)}} \times 100 \quad (2.8)$$

where R_{ct} and $R_{ct (i)}$ are referred as charge transfer resistance without and with the addition of lignin inhibitor, respectively.

Potentiodynamic polarization studies were carried out without and with the addition of lignin solution in 0.5 M HCl solutions at a scan rate of 1 mVs⁻¹. Open circuit potential, E_{ocp} , was measured for 30 minutes to allow stabilization of the steady state potential. The potential range was calculated from the E_{ocp} values obtained (± 250 mV). The percentage inhibition efficiency (IE %) was calculated by using the following equation,

$$IE \% = \frac{I_{corr} - I_{corr(i)}}{I_{corr}} \times 100 \quad (2.9)$$

where I_{corr} and $I_{corr(i)}$ are referred as corrosion current density without and with the addition of lignin inhibitor, respectively. Potentiodynamic polarization curves and other corrosion parameters were produced using Echem Analyst software.

2.11.2 Weight loss measurement

Weight loss of rectangular mild steel specimens of dimension 3 cm x 1.5 cm x 0.1 cm that were immersed in 50 mL of electrolyte with and without the addition of different concentrations of lignin samples and different temperatures (303, 313, 323 and 333 K) was determined after 48 h. The percentage inhibition efficiency (IE %) and the degree of surface coverage θ for different concentrations of lignin (100, 200, 300, 400 and 500 ppm) has been evaluated using the equation:

$$IE \% = \frac{W_0 - W_i}{W_0} \times 100 \quad (2.10)$$

$$\theta = \frac{W_0 - W_i}{W_0} \quad (2.11)$$

where W_0 and W_i are the weight loss values in absence and in presence of lignin inhibitor. The data from the weight loss measurement was used to calculate the corrosion rate, CR ($\text{mg cm}^{-2} \text{ h}^{-1}$) and for determining the activation energy E_a , activated entropy ΔS^* and enthalpy ΔH^* .

2.11.3 Surface analysis

The surface adsorption nature of lignin on mild steel will be further understood by employing potential zero charge (PZC) analysis. The relation between C_{dl} and the electrode potential in the range $E_{corr} \pm 250 \text{ mV}_{SCE}$ for the mild steel electrode in 0.5 M HCl without and with the addition of 500 ppm lignin was studied. The EIS measurements were performed at each potential value in the 10^3 – 10^2 Hz frequency range. At such high frequencies, the electrical double layer capacitor shortcuts the Faradiac impedance. The frequency scan was repeated at various desired potentials.

Surface morphology of corrosion products of mild steel specimens was evaluated by scanning electron microscope/energy dispersive X-Ray spectroscopy, SEM/EDX analysis (Leo Supra 50VP) and X-ray diffraction, XRD patterns (PANalytical X'Pert PRO MRD PW3040). For this purpose, the test specimen that exhibited the highest efficiency of corrosion inhibition from the weight loss measurement was examined together with blank (without inhibitor) at the magnification of 1000 x.

CHAPTER THREE

RESULTS AND DISCUSSION

Four major parts are separated and discussed in this chapter; (1) characterization of lignins extracted from oil palm fronds via direct delignification processes (Kraft, soda and organosolv pulping) and combinative pretreatments (dilute sulphuric acid or autohydrolysis followed by ethanol organosolv pulping), (2) characterization of the modified lignin structure through incorporation of organic scavengers (2-naphthol and 1,8-dihydroxyanthraquinone) during combinative autohydrolysis treatment, (3) the characterization of lignins fractionated with ultrafiltration (UF) system and (4) the anticorrosion action of all resulted lignins (from part 2 and 3) on mild steel in 0.5 M hydrochloric acid (HCl).

3.1 Characterization of oil palm fronds (OPF)

The raw material compositions are summarized in Table 3.1. The composition (% w/w) of the oil palm fronds (OPF) according to TAPPI T203 om-09 and laboratory analytical procedure (LAP) method is cellulose 35.73 ± 1.34 %, hemicelluloses 28.39 ± 1.34 % and Klason lignin 24.62 ± 1.17 % on a dry weight basis. It also contains monosaccharide sugars such as glucose 56.30 ± 3.20 %, xylose 16.80 ± 0.60 %, arabinose 0.90 ± 0.10 %, mannose 0.90 ± 0.001 % and galactose 0.40 ± 0.001 %. These values are compared with the previous findings by Wanrosli *et al.* (2007). The percentage of Klason lignin obtained from this study was slightly higher compared than the previous findings, but the cellulose content and hemicelluloses content were comparable with the previous reports. The higher values of Klason lignin is mainly

due to the higher presence of mineral and siliceous matters which were also included in the Klason lignin calculations. The hemicellulose portion was basically composed of arabinoxylan with a higher proportion of xylose than arabinose. Glucose gives the highest monosaccharide content in OPF followed by xylose, arabinose, mannose and galactose. High sugar content from OPF biomass indicates that it can be a potential biomass resource for the production of biofuels.

Table 3.1: Composition of raw material in OPF.

Components	Composition (% w/w)
Holocellulose	60.39±1.47
Hemicellulose	28.39±1.34
α -cellulose	35.73±1.34
Klason lignin	24.62±1.17
Acid soluble lignin	0.35±0.03
Extractives	1.62±0.15
Ash	3.84±0.46
Moisture	9.10±1.58
Monosaccharide sugars	
Glucose	74.76±3.20
Xylose	22.31±0.60
Arabinose	1.19±0.10
Mannose	1.19±0.001
Galactose	0.53±0.001

3.2 Characterization of lignins extracted from OPF via direct delignification processes

3.2.1 Composition of lignin samples (Kraft, soda and organosolv)

The elemental composition and the respective contents are gathered in Table 3.2. Higher yield of Kraft and soda lignins were observed after delignification process which indicates that alkaline process accelerates the removal of lignin from OPF

biomass. The lower yield of lignin after organosolv process was perhaps due to; i) low severity reaction conditions used and ii) the effect of aqueous ethanol solvent which dissolves small molecular weights of lignin (El Hage *et al.*, 2010; Pan *et al.*, 2005). According to the proximate analysis, it can be seen that the purity of the lignin samples (for Kraft, soda and organosolv) is high since the ash and protein content is low. Previous studies have shown that the content of ash and sugar can be reduced by acid washing after pulping process (El Mansouri and Salvado, 2006). This is clear when comparing the ash content of alkaline lignins (Kraft and soda) to organosolv lignin. The average C₉ formulae calculated from the elemental composition were C₉H_{9.93}O_{4.04}N_{0.07}S_{0.05} for Kraft, C₉H_{9.67}O_{3.34} N_{0.04} for soda and C₉H_{10.51}O_{3.65} N_{0.07} for organosolv lignin.

The sulfur content for Kraft lignin is derived from the hydrosulfide anions during the pulping process whereas the nitrogen content for all lignin samples may be due to the formation of protein-lignin complexes during delignification process (Zhao *et al.*, 2009a). The traces of protein that were still attached to the lignin compound suggest a strong chemical bond that is difficult to be removed even by acid precipitation. The double bond equivalent (DBE) for all lignin samples is related to the degree of condensed lignin and the presence of aromatic ring structure. From the results, it was revealed that the number of DBE for soda lignin was higher compared to Kraft and organosolv lignins due to the dehydration reaction in basic medium of aliphatic chains, leading to the formation of ethylenic bonds (El Mansouri and Salvado, 2006).

Table 3.2: Proximate analysis of Kraft, soda and organosolv lignin from oil palm fronds (% w/w on dry matter).

	Kraft lignin	Soda lignin	Organosolv lignin
Yield (%)	18.29±1.27	15.86±1.17	9.26±1.11
Ash (%)	1.78±0.03	2.16±0.04	2.62±0.15
Moisture (%)	3.59±0.12	2.42±0.08	2.19±0.10
Element (%)			
C	58.22	63.02	60.88
H	5.36	5.61	5.89
N	0.56	0.33	0.54
O	34.92	31.04	32.69
S	0.94	-	-
Protein (%)	3.50	2.06	3.38
Double bond equivalent (DBE)	5.05	5.20	4.80

3.2.2 FTIR analysis

The G/S characteristic from the three different spectra is visible in the region of 1450-780 cm^{-1} as shown in Figure 3.1 and all assignments of the bands are reported in Table 3.3. Both Kraft and soda lignins show a small peak intensity for G bands (1272 and 1033 cm^{-1}) and a moderate absorbance for S bands (1324 and 1125 cm^{-1}) while organosolv lignin shows quite intense G and S bands. It was also observed that for organosolv lignin the absorbance signal of the S unit (1324, 1125 and 833 cm^{-1}) was higher compared to Kraft and soda lignins which suggested the higher syringyl content. It was assumed that different delignification processes would give different absorbance intensity in the FTIR spectra. Theoretically, organosolv pulping which uses an ethanol-water mixture as solvent will release the acetic acid from the hemicelluloses that leads to lignin dissolution. This will promote the acid hydrolysis of lignin generating the phenolic hydroxyl (1365 cm^{-1}) and carbonyl groups (1708 cm^{-1}) in its structure thereby making it more intense than alkaline treated pulping (Tejado *et al.*, 2007).

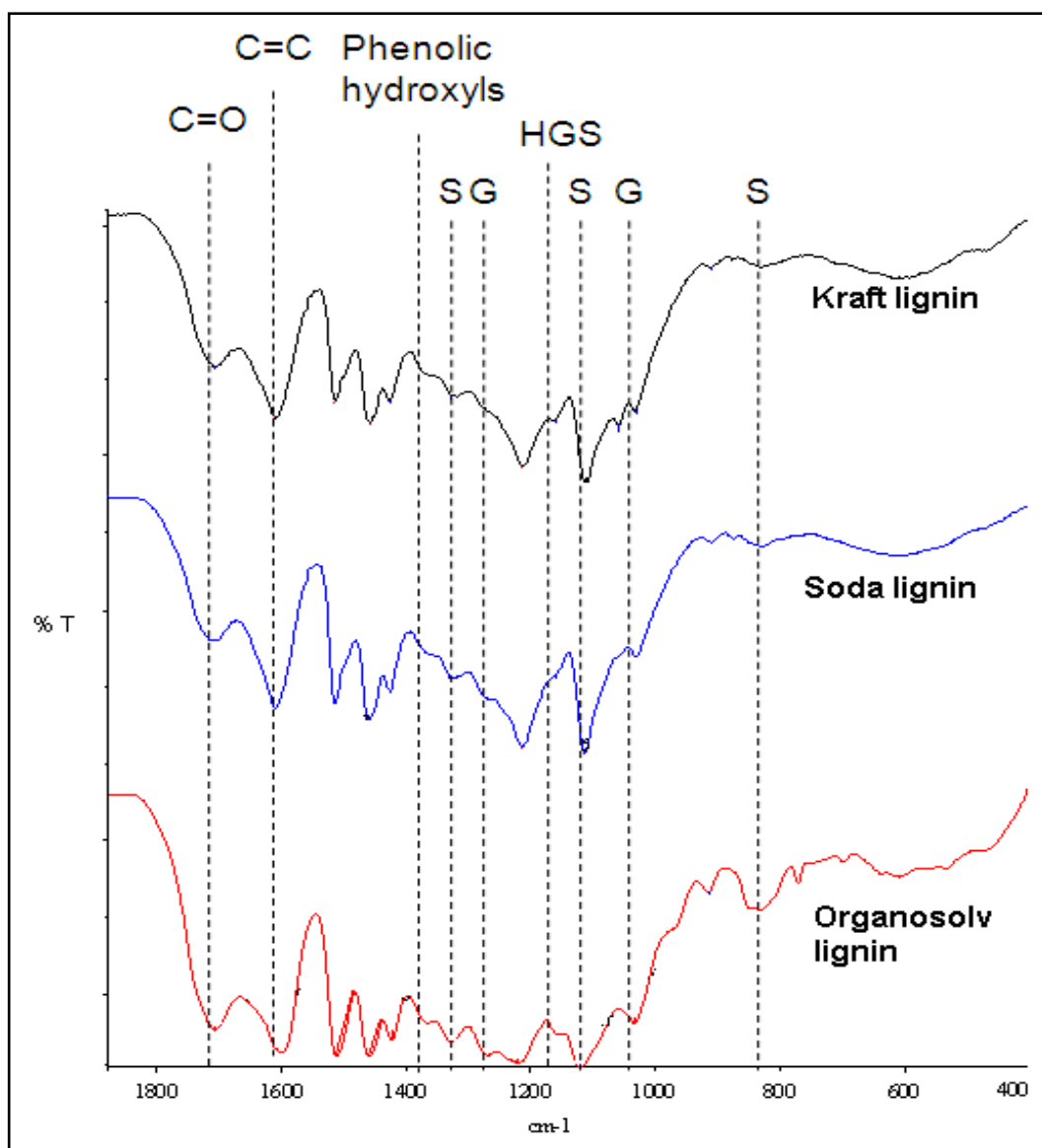


Figure 3.1: FTIR spectra of Kraft, soda and organosolv lignin in the expanded range.

In contrast, the low signal of S units for Kraft and soda lignins compared to that of organosolv lignin was mainly due to demethoxylation that occurred during alkaline pulping process (Nadji *et al.*, 2009). Demethoxylation reactions reported during alkaline pulping is actually an exclusive demethylation reactions, occurred at high severity reaction conditions which converts more S type groups to more stable G type structures (intense signal of G units) within the lignin molecules (Thring *et al.*, 1990b). Typical absorption for HGS lignin can be seen from the absorption signal at 1158 cm^{-1} .

Table 3.3: Assignment of FTIR spectra of lignin from oil palm fronds.

Band (cm ⁻¹)	Assignments	Kraft lignin	Soda lignin	Organosolv lignin
		Band location (cm ⁻¹)		
1460	C-H deformation (asymmetric in -CH ₃ and -CH ₂)	1459	1459	1462
1425	C-C stretching (aromatic skeleton) with C-H in plane deformation	1424	1426	1424
1326	C-O stretching (syringyl)	1325	1331	1328
~1220	C-O(H) + C-O(Ar) (phenolic OH and ether in syringyl and guaiacyl)	1214	1214	1225
1115	Ar-CH in plane deformation (syringyl)	1112	1113	1123
~1030	C-O(H) + C-O(C) (first order aliphatic OH and ether)	1035	1029	1035
915	C-H out of plane (aromatic)	912	912	917
831	C-H out of plane	828	828	834

3.2.3 ¹H, ¹³C and ³¹P NMR spectra

The chemical structure of alkaline lignin and organosolv lignin was studied via ¹H and ¹³C NMR spectrometry. Since alkaline lignins are difficult to dissolve in DMSO, acetylation of lignins was subjected to improve their solubility. Figure 3.2 shows the ¹H NMR spectra of acetylated alkaline (Kraft and soda) and organosolv lignins. The signal at around 2.5 ppm is indicative of protons in DMSO. As shown in Figure 3.2, the integral of signals between 6.0 to 9.0 ppm could be attributed to aromatic -OH protons in syringyl (S) and guaiacyl (G) units while the signals between 0.8 to 1.5 ppm could be attributed to the aliphatic moiety. The methoxyl proton which is related to G and S unit proportion shows an intense signal at around 3.75 ppm.

According to a previous study, acetylation of alkaline lignin produced derivatives that displayed broad proton signals in regions with small interference with other

hydrogen signals. Moreover, the aliphatic and aromatic acetyl groups were slightly shifted, giving rise to separate peaks (Garcia *et al.*, 2009). In our study, acetylated Kraft and soda lignins show higher content of aromatic protons (major depolymerization process) compared to organosolv lignin. This observation was also in good agreement with the FTIR results, where a very broad absorption signals of -OH (see Appendix I) for Kraft and soda lignins were evident as compared to the organosolv lignin. On the other hand, organosolv lignin presents high quantities of methoxyl groups (majority of S units) than Kraft and soda lignins.

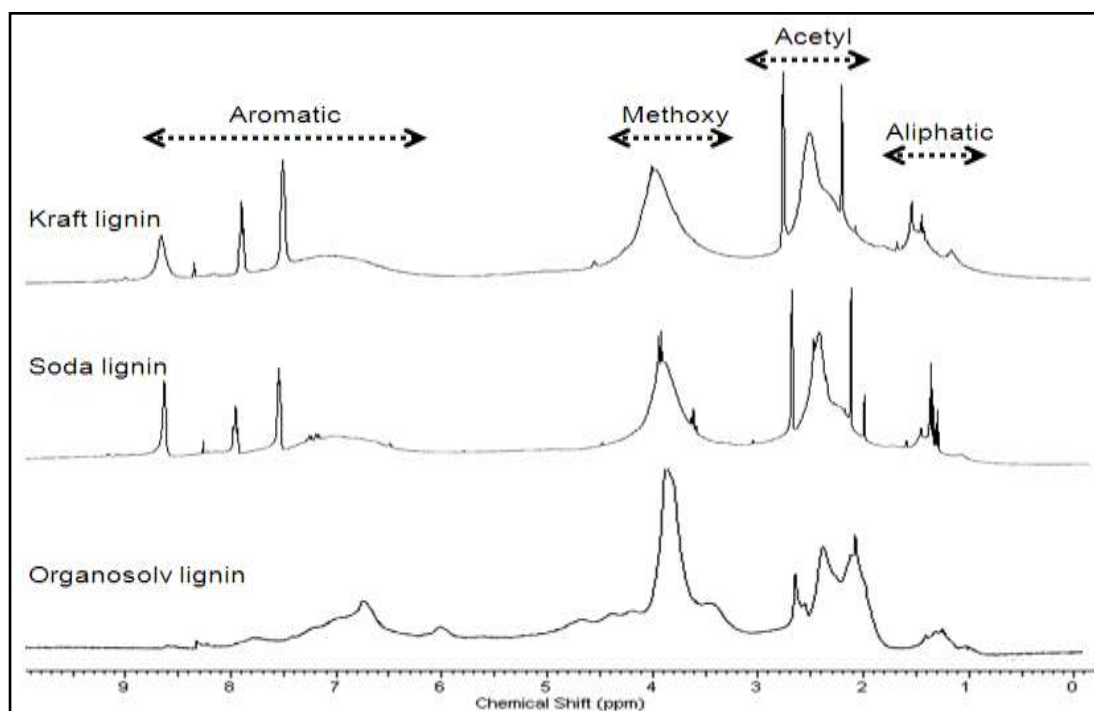


Figure 3.2: ^1H NMR spectra of acetylated alkaline lignin (Kraft and soda) and organosolv lignin from oil palm fronds.

The expanded quantitative ^{13}C NMR spectra of all acetylated lignin samples are given in Figure 3.3B, and their chemical shifts (δ , ppm), values (per Ar) and assignments are listed in Table 3.4 which correspond to lignin substructures (Figure 3.4). The resolution of the ^{13}C NMR spectrum of acetylated organosolv lignin was better than the alkaline lignin (Figure 3.3A). The integral of the 162-102 ppm region was set as

the reference, assuming that it includes six aromatic carbons and 0.12 vinylic carbons. It follows that the integral value divided by 6.12 is equivalent to one aromatic ring (Ar) (Capanema *et al.*, 2004). Guaiacyl (G), syringyl (S) and p-hydroxyphenyl (H) units were clearly observed in the spectra with all assignments given in Figure 3.3B.

Table 3.4: Signal assignment for ^{13}C NMR spectrometry of acetylated alkaline lignin and organosolv lignin from oil palm fronds.

Range (ppm)	Assignment	Amount (per Ar)		
		Kraft	Soda	Organosolv
172-169.6	Primary aliphatic –OH	0.09	0.13	0.26
169.6-168.6	Secondary aliphatic –OH	0.14	0.19	0.23
168.6-166	Phenolic -OH, conjugated COOR	0.49	0.39	0.35
162-148	All C-3 (except A and h-units), C-5 in B , C- α in C , C-6 in D , C-4 in conjugated CO/COOR etherified and h-units			0.95
144.5-142.5	C-3 in A , C-4 in conjugated B _{et} , unknown			0.10
60-59	C- γ in E			0.07
58-54	OMe, C-1 and C- β in D	0.73	0.82	1.16
50-48	C- β in F , A			0.14
Clusters				
125.5-103	“C _{Ar-H} ”			2.22
90-58	Alk-O-			1.68
90-77	Alk-O-Ar, α -O-Alk			0.60
77-65	γ -O-Alk, OH _{sec}			0.53
65-58	-OH _{prim}			0.57

Again, organosolv lignin gives intense signals for S (104 ppm, 138 ppm and 154 ppm) and G (114 ppm, 119 ppm, 135 ppm and 147 ppm) units respectively to the C-2/C6, C-4 and C-3/C5 (for S unit); C-2, C-6, etherified C-1 and non-etherified C-3 (for G unit) carbon position compared to Kraft and soda lignins. Besides, the higher signals for S unit in all lignin samples may suggest that lignin sample from OPF contains more syringal basic unit than the guaiacyl unit. It was reported that these

signals could be identified as GSH lignin (Xu *et al.*, 2006; El Hage *et al.*, 2009; She *et al.*, 2010).

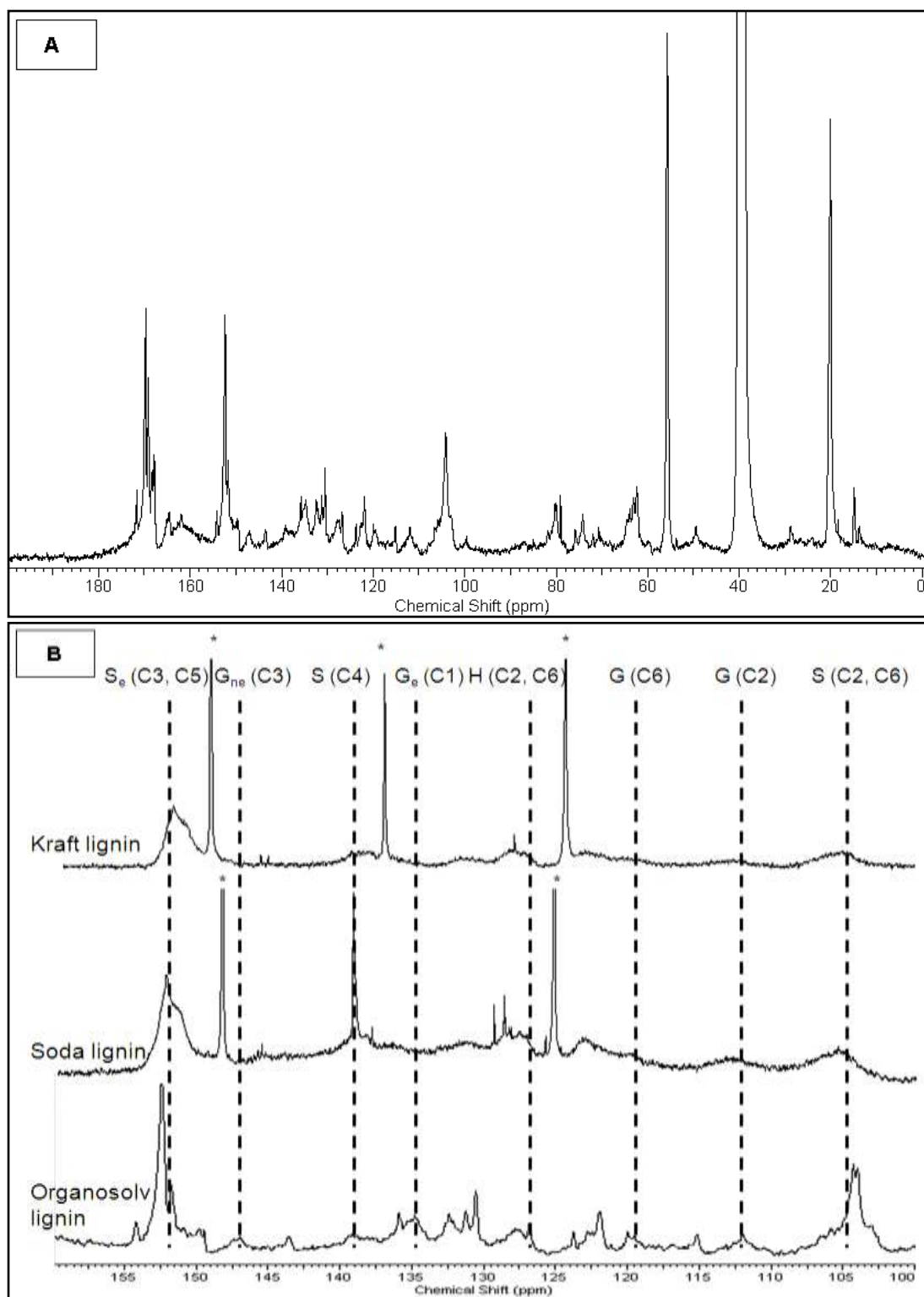


Figure 3.3: ^{13}C NMR spectra of acetylated OPF lignin samples: (A) organosolv lignin and (B) expanded aromatic region.

^{a)} H: p-hydroxyphenyl unit; G: guaiacyl unit; S: syringyl unit; e: etherified; ne: non etherified, *: impurities.



Figure 3.4: Lignin substructures (Capanema *et al.*, 2004).

The ^{13}C NMR of acetylated lignin samples can provide additional information regarding on their hydroxyl groups assignment and amount. The amount of hydroxyl groups based on the integration was calculated in the acetylated lignin samples (Figure 3.5) from the 172-165 ppm region. It was observed that the amount of primary $-\text{OH}$ from organosolv lignin (0.26/Ar) is slightly higher compared to Kraft (0.09/Ar) and soda lignin (0.13/Ar) whereas the amount of secondary $-\text{OH}$ is almost unchanged for Kraft (0.14/Ar), soda (0.19/Ar) and organosolv lignin (0.23/Ar).

There is a good correlation in the amount of primary $-\text{OH}$ groups determined from the integrals at 172-165 ppm and 65-58 ppm (0.57/Ar) for organosolv lignin which justifies the presence of more aliphatic $-\text{OH}$ functional groups in lignin structure. In turn, it was revealed that the higher quantity of phenolic $-\text{OH}$ of Kraft (0.49/Ar) and

soda (0.39/Ar) lignin than organosolv lignin (0.35/Ar) was mainly due to the major cleavage of aryl-ether bonds in OPF biomass during Kraft and soda pulping, resulting in lignin depolymerization and high content of phenolic hydroxyl groups. This observation was significantly correlated with the previous observations in ^1H NMR and FTIR analyses.

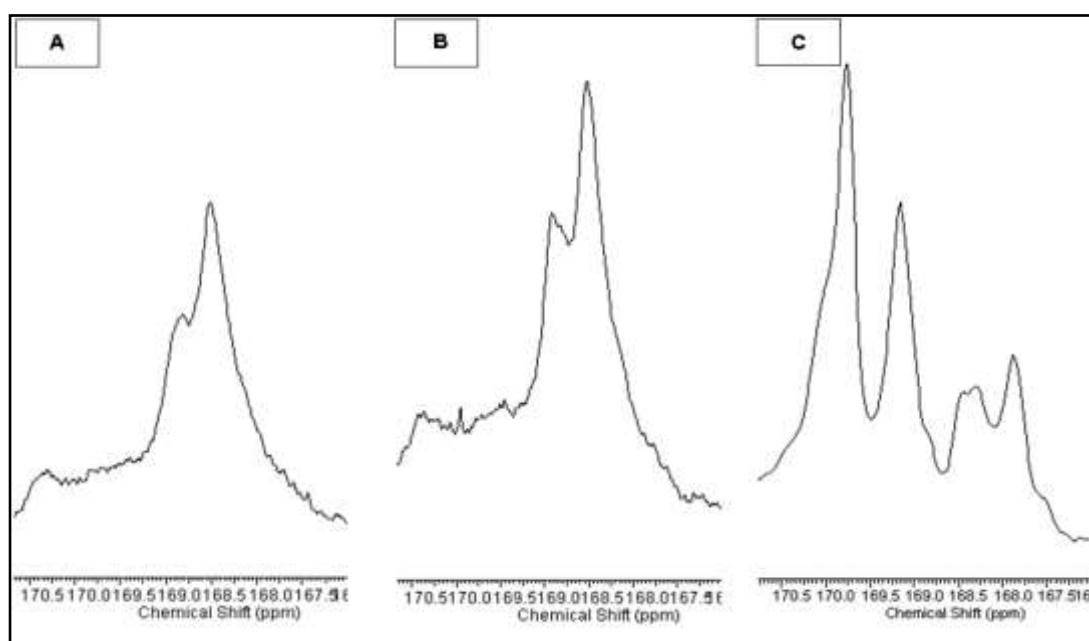


Figure 3.5: ^{13}C NMR spectra of expanded acetyl region for: (A) Kraft; (B) soda and (C) organosolv lignin from OPF.

As a comparison, the ^{31}P NMR studies were done in order to support qualitative assumption on the hydroxyl group content. Data from the quantitative ^{31}P NMR of the three lignin samples (Figure 3.6), obtained following their derivatization with TMDP are presented in Table 3.5. The concentration of each hydroxyl functional group (in mmol g^{-1}) was calculated on the basis of the hydroxyl content of the internal standard cyclohexanol and its integrated peak area (Granata and Argyropoulos, 1995). According to this data, it can be observed that alkaline lignins gave lower concentration of aliphatic $-\text{OH}$ groups and higher concentrations of phenolic $-\text{OH}$ groups (Kraft: 2.20 mmol g^{-1} and soda: 1.66 mmol g^{-1}) compared to

organosolv lignin (1.40 mmol g^{-1}). This phenomenon is mainly due to the extensive depolymerization of lignin during alkaline pulping through the scission of β -O-4 bonds leading to the production of phenolic $-\text{OH}$ groups.

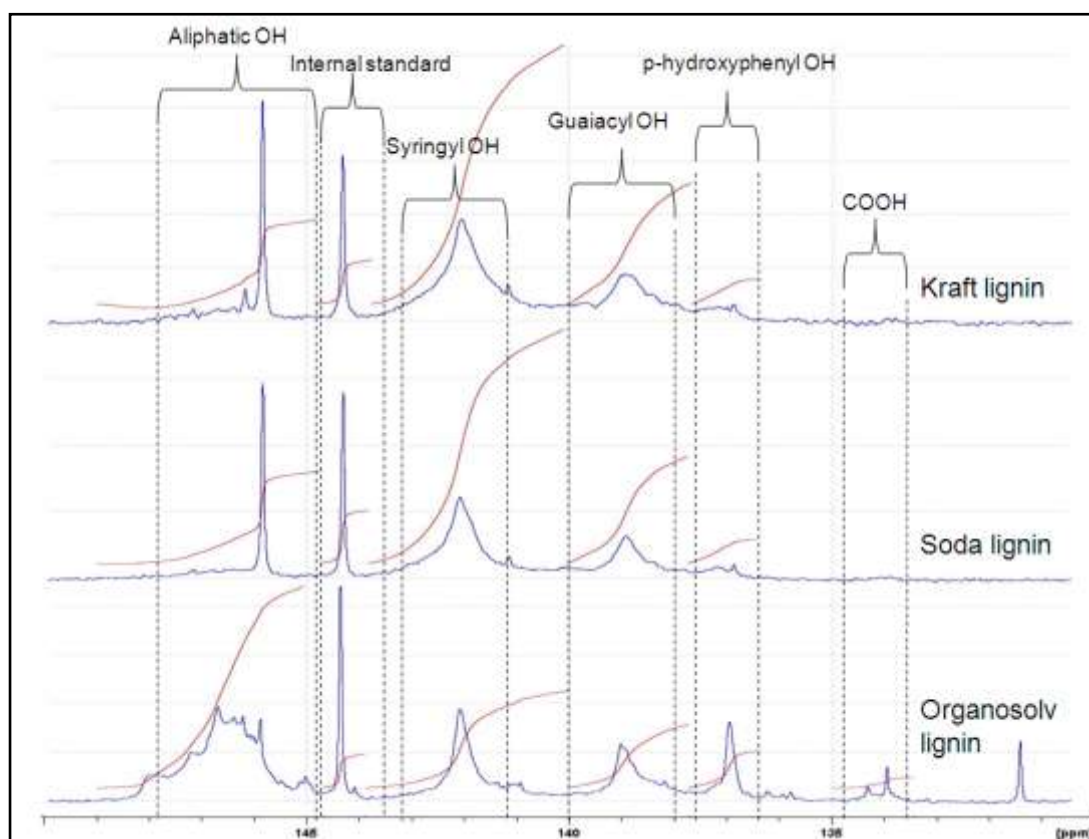


Figure 3.6: ^{31}P NMR spectrum of Kraft, soda and organosolv lignin.

In addition, the reduction of aliphatic $-\text{OH}$ is probably due to the dehydration reactions through acid-catalyzed elimination reaction (El Hage *et al.*, 2009; Obama *et al.*, 2012). The amount of hydroxyl groups based on the integration was calculated in the phosphorylated lignin samples. It was observed that the amount of aliphatic $-\text{OH}$ from organosolv lignin is slightly higher compared to alkaline lignins which justifies the presence of more aliphatic $-\text{OH}$ functional groups in organosolv lignin structure. In turn, it was revealed that the higher quantity of phenolic $-\text{OH}$ of alkaline lignins than organosolv lignin was mainly due to the major cleavage of aryl-

ether bonds in OPF biomass during Kraft and soda pulping, resulting in lignin depolymerization and high content of phenolic –OH groups (in a good agreement with the ^{13}C NMR results). Higher content of phenolic –OH is indeed beneficial for applications such as antioxidant activity and corrosion inhibition. Besides, fine peaks at aliphatic –OH region for Kraft and soda lignin sample could contributed to the presence of more secondary –OH (*erythro* and *threo* at 147 ppm) functional groups than primary –OH at 145 ppm (in complement with the ^{13}C NMR analysis).

Table 3.5: Lignins characterized by ^{31}P NMR.

ppm	Assignments	mmol g $^{-1}$		
		Kraft	Soda	Organosolv
150-145	Aliphatic –OH	0.45	0.42	1.49
144.8	Cyclohexanol (Internal Standard)			
144-140	Syringyl –OH	1.42	1.07	0.69
140-138	Guaiaacyl –OH	0.65	0.48	0.45
138-136	p-hydroxyphenyl –OH	0.13	0.11	0.26
135-133	Carboxylic acid	-	-	0.07

Both techniques provided useful information especially when discussing the hydroxyl group content in the lignin samples. Both ^{13}C and ^{31}P NMR techniques could give an assumption of the total aliphatic –OH (based on their classes; either primary or secondary) and phenolic –OH. Nevertheless, ^{31}P NMR technique may provide better understanding on the amount of HGS phenolic –OH content as compared to ^{13}C NMR technique.

3.2.4 Molecular weight

Molecular weight distribution and average value of lignin samples were evaluated using GPC analysis. From the results, it can be seen that weight-average (M_w) of

soda (1660 g mol^{-1}) and organosolv (1215 g mol^{-1}) lignin were lower than Kraft (2063 g mol^{-1}) lignin. This phenomenon can be explained according to the different lignin compositions. Even though β -O-4 is the most common linkage in all lignin types, there are also some quantities of C-C bonds between the phenylpropanoic units (which involve C5 of aromatic ring). The molecular weight of lignin is related to this assumption (Sjöström, 1981). Guaiacyl-type units are capable of forming this kind of bond, but this is not possible in syringyl-type units as it has both C3 and C5 positions substituted by methoxy groups. As a result, these C-C bonds are not cleaved during the pulping process due to its high stability. Hence, the lignin that contains slightly high guaiacyl-type units is expected to show higher molecular weight (HMW) than those having high contents of syringyl-type units (Tejado *et al.*, 2007).

Besides, repolymerization reactions during alkaline pulping may affect the M_w values of lignin. According to Van de Klashorst (1989), under alkaline conditions some α -hydroxyl groups from quinone methide intermediates form the alkali-stable methylene linkages after they reacted with other lignin fragments. Due to the more severe conditions used in Kraft pulping, high value of lignin molecular weight can be observed. On top of that, previous studies have shown that organosolv pulping process can promote the fragmentation of small molecular weight lignin (El Hage *et al.*, 2010; Pan *et al.*, 2005). Meanwhile, low M_n value for soda lignin is due to the soda pulping process. In this process the hydroxide ions react with the lignin causing the fragmentation of polymer in water/alkali soluble fragment. This corroborates that the cleavage of α and β -O-4 bonds is the predominant process in alkaline medium (El Mansouri and Salvado, 2006; Mohamad Ibrahim *et al.*, 2011).

Low polydispersity of organosolv lignin ($M_w/M_n = 1.17$, $M_n = 1036$) compared to Kraft ($M_w/M_n = 1.89$, $M_n = 1063$) and soda lignins ($M_w/M_n = 2.33$, $M_n = 713$) indicated the high fraction of low molecular weight (LMW) components present in the samples (Alriols *et al.*, 2009). Moreover, the low polydispersity of lignin may cause higher solubility (Gregorova *et al.*, 2005). It has been reported that organosolv lignins could be an appropriate raw material to produce LMW compounds such as vanillin, simple and hydroxylated aromatics, quinines, aldehyde, aliphatic acid and many more (Johnson *et al.*, 2005).

3.2.5 Thermal behavior

3.2.5.1 Thermal gravimetric analysis

The thermal stability of Kraft, soda and organosolv lignins was investigated by thermogravimetric method. DTG (rate of weight loss) and TG (weight loss of substances in relation to the temperature of thermal degradation) curves are presented in Figure 3.7. All lignin thermograms were in accordance with other works in the literature (Sun *et al.*, 2001; Garcia *et al.*, 2009; Alriols *et al.*, 2009; Mohamad Ibrahim *et al.*, 2011). The initial degradation for lignin samples is attributed to the weight loss of water, carbon monoxide, carbon dioxide and other pyrolysis products (Sun *et al.*, 2001). The second degradation around 200 °C indicates the weight loss of hemicelluloses that are attached to the lignin structure (Garcia *et al.*, 2009). Similar phenomenon was also observed in some previous reports showing the presence of hemicellulose as a by-product during the precipitation of lignin (Tejado *et al.*, 2007; Mohamad Ibrahim *et al.*, 2011). The maximum rate of weight loss,

DTG_{max} for Kraft (370 °C), soda (380 °C) and organosolv lignins (350 °C) appeared in the range of 300-400 °C respectively.

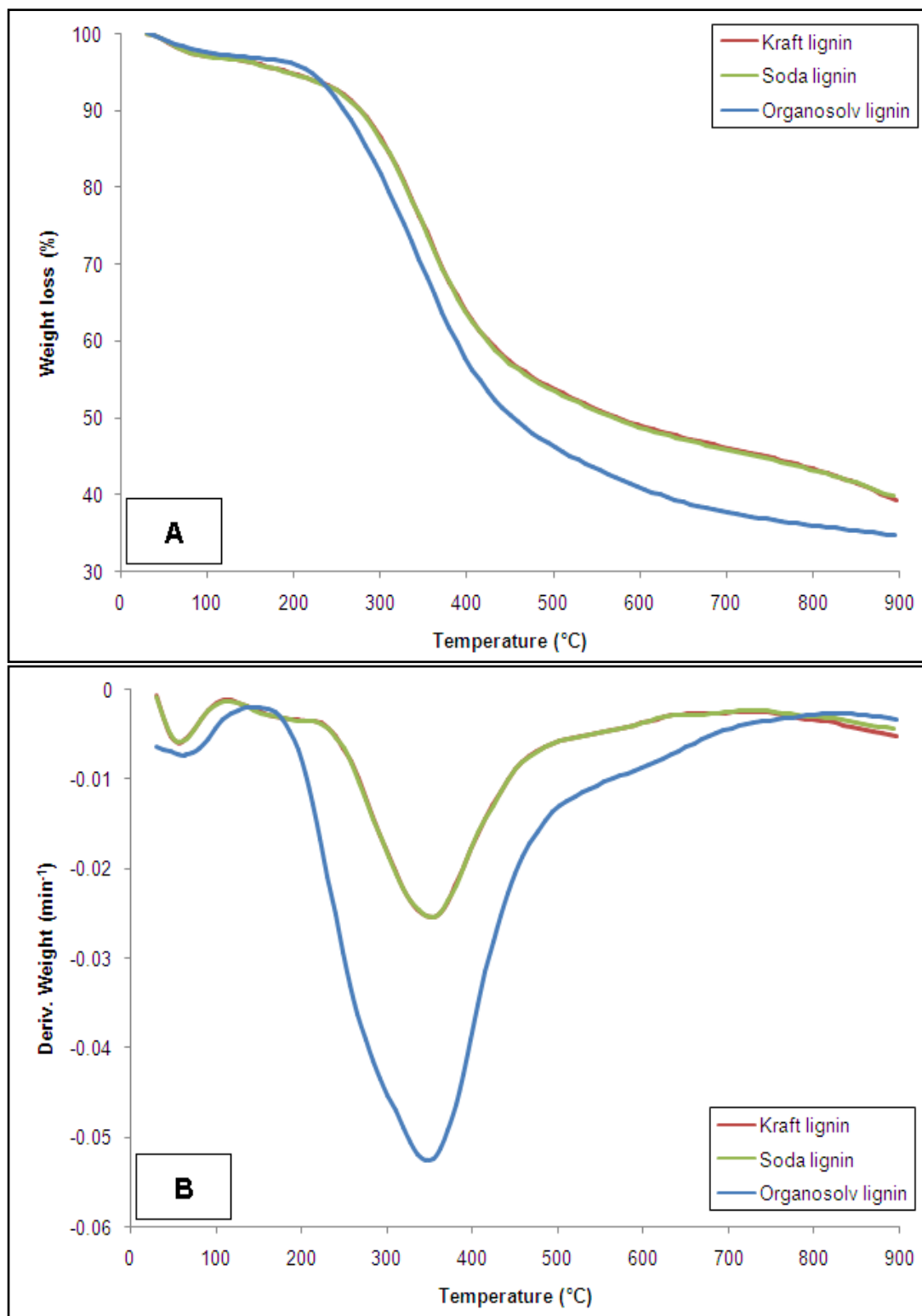


Figure 3.7: (A) TG and (B) DTG curves for Kraft, soda and organosolv lignin.

Degradation of the complex structure of lignin in this temperature region involved fragmentation of inter-unit linkages between phenolic hydroxyl, carbonyl groups and benzylic hydroxyl, releasing monomeric phenols into the vapour phase (Alriols *et al.*, 2009). A broad DTG curve of organosolv lignin is possibly related with the degradation of lignin at lower temperature suggesting that the lignin structure are not so cross linked (contains more β -O-4 linkages) with less C-C interlinked bonds.

Above 400 °C, the lignin samples exhibited a gradual weight loss up to 900 °C, that is related with the degradation or condensation reaction of aromatic rings (Sun *et al.*, 2001) resulting in overall loss of 40 %. These results revealed that all lignin samples are stable at high temperatures which are associated to the high degree of branching and formation of highly condensed aromatic structure of lignin.

3.2.5.2 Differential scanning calorimetry

Glass transition temperature (T_g) was determined by DSC scans after extensive drying of the lignin samples. It was revealed that the value of T_g for soda lignin ($T_g = 81.79$ °C) is higher as compared to Kraft ($T_g = 64.62$ °C) and organosolv ($T_g = 51.65$ °C) lignins. It was suggested that the relation between the molecular weight of lignin samples and the free volume can affect the T_g values. The free volume is the space in a solid or liquid sample that is not occupied by polymer molecules (Young and Lovell, 1991). The T_g can be described by such activation energies through the use of free volume. In theory, the T_g will only appear when the main chain has enough energy to rotate the chain. Initially, the chains in lignin are vibrated when it received energy and the rotation of the lignin chains will create a free volume.

High molecular weight of lignin suggests that it contains few chain ends resulting in low volume mobility, thus more energy is required to rotate the chain (Mohamad Ibrahim *et al.*, 2011). From this theory, we can correlate the T_g values with the molecular weight obtained from alkaline (Kraft and soda) and organosolv lignins by GPC method. A very high molecular weight of alkaline lignins may increase the energy level required to make such rotation. Besides, low M_n and high polydispersity values especially for soda lignin may be associated with such phenomenon. As a result, the T_g value will be increased.

3.2.6 Composition of phenolic acids and aldehydes

Alkaline nitrobenzene oxidation is commonly used for the analysis of lignins. It gives information about the constitutive monomeric composition of the lignin samples. The corresponding chromatograms are shown in Figure 3.8. Syringyl, guaiacyl and p-hydroxyphenyl units are oxidized into corresponding syringic acid (SA), syringaldehyde (S), vanillic acid (VA), vanillin (V), p-hydroxybenzoic acid (PHBA) and p-hydroxybenzaldehyde (PHB). Table 3.6 summarizes the results concerning the analysis of phenolic acids and aldehydes from the lignin fractions, obtained by alkaline nitrobenzene oxidation (all standards linear curves are shown in Appendix IV). All units (H, G and S units) are present in each sample which confirms that the OPF lignin is of HGS type. The predominant oxidation product of lignin was found to be vanillin and syringaldehyde, resulted from the degradation of non-condensed guaiacyl (G) and syringyl (S) units respectively.

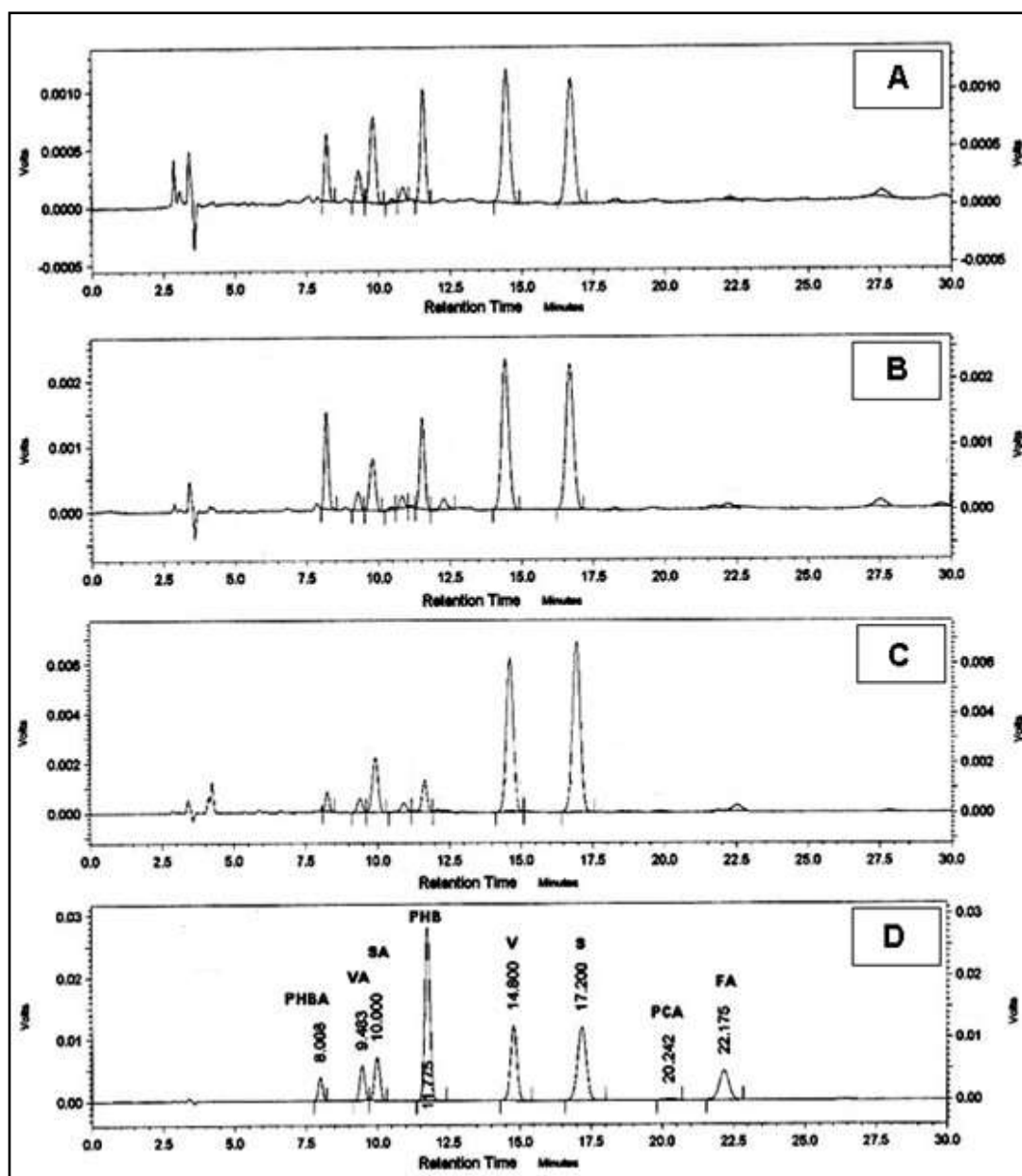


Figure 3.8: HPLC chromatogram of; (A) Kraft, (B) soda, (C) organosolv lignin after nitrobenzene oxidation and (D) mix standards obtained at a flow rate of 1 mL min^{-1} and 280 nm of UV detection.

As shown in Table 3.6, the molar ratios of G (relative total moles of vanillin and vanillic acid), S (relative total moles of syringaldehyde and syringic acid) and H (relative total moles of p-hydroxybenzaldehyde and p-hydroxybenzoic acid) units were found to be 26:51:21 in Kraft, 21:49:30 in soda and 23:67:10 in organosolv lignins. The lignin obtained from organosolv process gives a higher value of syringyl (S) units than lignin obtained from Kraft and soda processes, which implies that the

non-condensed syringal units were more easily degradable than the non-condensed guaiacyl ones during the treatment. Similar observation by Yuen *et al.* (2011), have revealed that lignin obtained by organosolv method gave highest non-condensed syringyl unit compared to lignin obtained by the alkaline method.

Generally, a large ratio of ferulic acid was oxidized to vanillin and most p-coumaric acid was oxidized to p-hydroxybenzaldehyde during alkaline nitrobenzene oxidation (She *et al.*, 2012). Consequently, only small/trace amounts of ferulic acid and p-coumaric acid (PCA) were observed after the quantification. A minimal amount of ferulic acids, FA (0.04 %-0.4 %) in all lignin samples were observed.

Table 3.6: The yield (% dry sample, w/w) of phenolic acids and aldehydes from alkaline nitrobenzene oxidation of lignin samples.

Component	Rt (min)	% Weight (dry basis)		
		Kraft lignin	Soda lignin	Organosolv lignin
p-hydroxybenzoic acid	~8.00	0.44±0.07	1.05±0.12	0.66±0.18
vanillic acid	~9.45	0.13±0.02	0.12±0.001	0.25±0.01
syringic acid	~10.00	0.39±0.02	0.40±0.001	0.84±0.08
p-hydroxybenzaldehyde	~11.77	0.04±0.01	0.07±0.01	0.08±0.01
vanillin	~14.80	0.45±0.001	0.70±0.01	1.59±0.01
syringaldehyde	~17.20	0.74±0.001	1.48±0.02	4.59±0.07
ferulic acid	~22.17	0.04±0.01	0.08±0.02	0.45±0.001
Molar ratio (G:S:H)		26:51:21	21:49:30	23:67:10
S/G ratio		1.96	2.33	2.91

3.2.7 Lignin antioxidant activity by oxygen uptake method

In this study, the antioxidant activity of lignin has been determined by employing oxygen uptake inhibition method. Unlike antiradical tests broadly used in the literature (like DPPH, ABTS etc.), the oxygen uptake inhibition is a realistic model of autoxidation reactions taking place in food and living systems, even though

substrates more complex than methyl linoleate are more representative of specific situations. In addition, previous studies by Poaty *et al.* (2010) and Saha *et al.* (2013) have revealed that the inhibition obtained by oxygen uptake test shows similar trend to that of DPPH assay. The oxygen uptake profile during autoxidation of methyl linoleate is shown in Figure 3.9. By comparing the linear curve of methyl linoleate alone (control), it appears that all lignin samples exhibited antioxidant activity by slowing down the oxidation of methyl linoleate, as shown by the reduced change in pressure of oxygen (ΔPO_2) to that of the control.

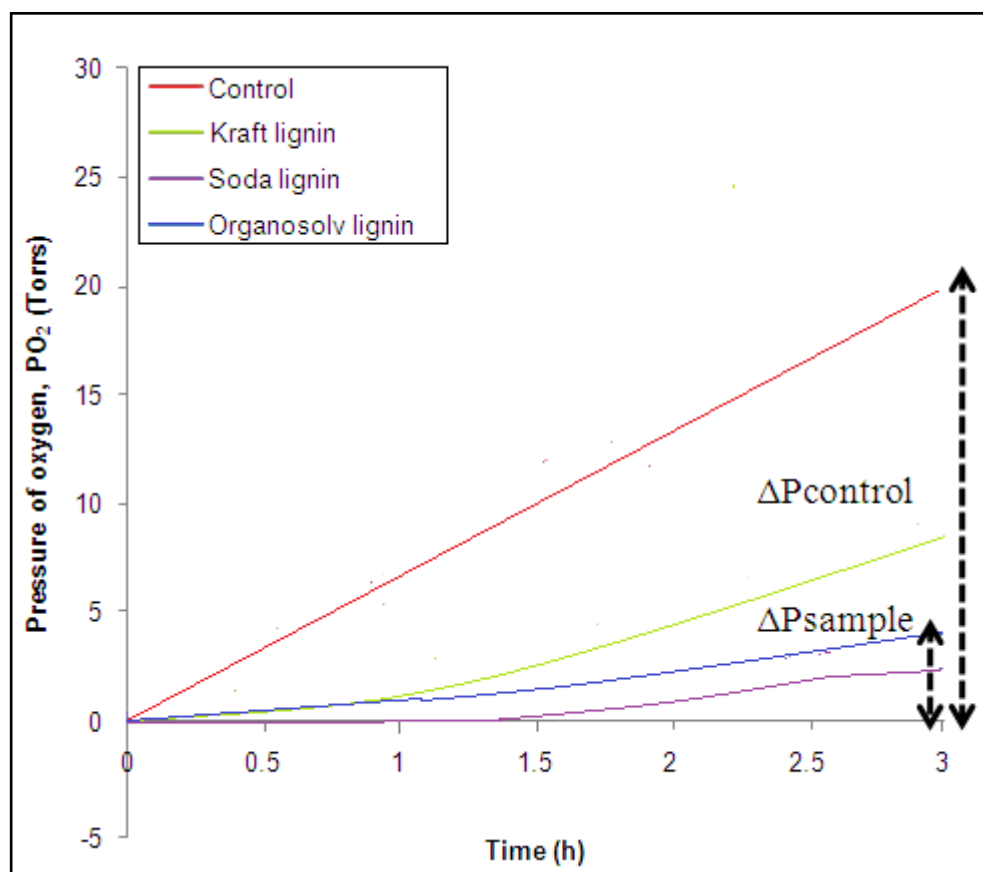


Figure 3.9: Oxygen uptake profile of Kraft, soda and organosolv lignin.

In order to correlate our observation with the previous findings by El Hage *et al.* (2012) (with regards to structure, molecular weight and phenolic $-OH$ content), butanol has been chosen as the corresponding solvent to dissolve lignin samples.

Soda lignin gives the highest inhibition (OUI = 74 %) followed by organosolv (OUI = 60 %) and Kraft lignin (OUI = 55 %). The antioxidant efficiency of lignin has been described to be related with their structure, purity and polydispersity (Pouteau *et al.*, 2003; Pan *et al.*, 2006). Lignin with high molecular weight, low phenolic –OH content and polydispersity value tends to experience poor antioxidant activity (El Hage *et al.*, 2012). However, Pouteau *et al.* (2005) found that low phenolic –OH content can also enhance the antioxidant activity of lignin. Here it was observed that Kraft lignin (with higher phenolic –OH content) experienced lower antioxidant activity than soda and organosolv lignin (with lower phenolic –OH content). This is indeed not in accordance with the previous finding done by El Hage *et al.* (2012). Thus, it might be expected that the phenolic –OH content is not only the factor affecting the antioxidant activity of lignin. Besides, this result is effective only for antioxidant activity of lignin in butanol and since alkaline lignins do not completely dissolve in butanol, the results sometimes could vary.

3.2.8 Lignin antioxidant activity by reducing power assay

Figure 3.10 shows the reducing power of alkaline lignins (Kraft and soda) and organosolv lignin as a function of their concentration. In this assay, the yellow colour of the test solution changes to various shades of green and blue, depending on the reducing power of each lignin. The presence of reducers (i.e. antioxidants) causes the reduction of the Fe^{3+} (ferricyanide) complex to the ferrous complex that has an absorption maximum at 700 nm (Ferreira *et al.*, 2007). As a comparison, reducing power of syringaldehyde and vanillin standard was employed to mimic the reduction ability of syringyl (S) and guaiacyl (G) unit. Increased absorbance of the reaction

mixture indicates increase in reducing power. Higher reducing power of syringaldehyde than vanillin standard revealed that the S unit could facilitate better reduction ability. In this study, the reducing power of lignin increased with concentration to give a plateau at a concentration of 0.08 mg mL^{-1} . The reducing power of soda lignin was better than Kraft and organosolv lignins. Similar trends of antioxidant activity can be observed from this assay to that of the oxygen uptake inhibition (OUI) test where soda lignin gave better inhibition followed by organosolv and Kraft lignin. Again, the antioxidant efficiency of lignin can be explained with regards of its structure, purity and polydispersity.

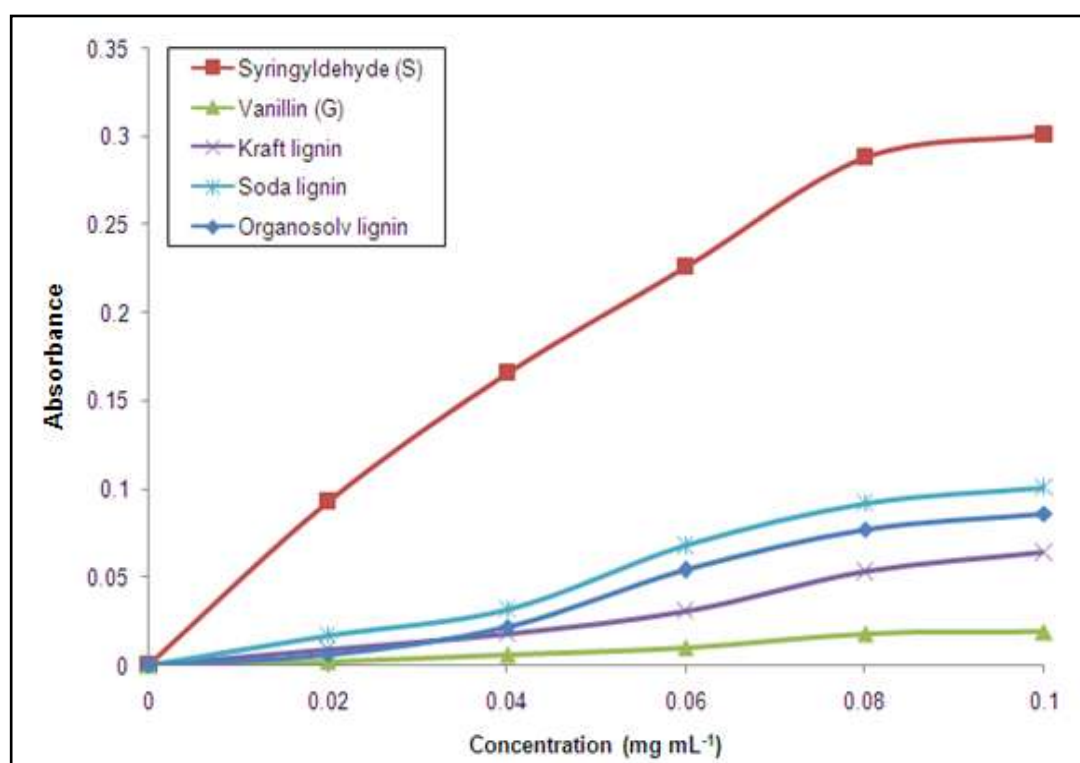


Figure 3.10: Antioxidant profile of Kraft, soda and organosolv lignin by reducing power assay obtained at 700 nm.

3.3 Characterization of lignins extracted from OPF via combinative pretreatment processes (with and without organic scavengers)

3.3.1 Composition of pretreated OPF biomass

The compositions of OPF biomass and solid residue after the prehydrolysis step are given in Table 3.7. According to these data, it can be seen that prehydrolysis treatment of OPF biomass via dilute sulphuric acid and autohydrolysis will produce higher Klason lignin content. These findings were comparable with the previous studies with different biomasses (Brosse *et al.*, 2010; Timilsena *et al.*, 2013a). In contrast, the removal of xylan and arabinan from the degradation of hemicelluloses polysaccharides can be seen for all treated OPF with the highest removal on the autohydrolyzed OPF. Autohydrolyzed OPF in the presence of organic scavengers (2-naphthol and 1,8-dihydroxyanthraquinone) shows higher hemicellulose recovery than normal autohydrolyzed OPF.

Table 3.7: Composition of OPF biomass residues after prehydrolysis.

Prehydrolysis	Solid residue					Aqueous phase			
	Glc	Xyl	Ara	KL ^b	SL ^b	Glc	Xyl	Ara	SL ^b
DAP ^a	63.7	11.8	0.1	30.52	0.23	0.1	0.4	0.4	0.11
AH ^a	57.3	5.4	0.0	36.55	0.20	0.5	5.1	0.3	0.23
AHN ^a	50.4	3.0	0.0	43.80	1.31	0.2	11.9	0.1	0.26
AHD ^a	55.7	4.6	0.0	41.75	1.57	0.1	10.3	0.3	0.25

All experiment data are yields of components per 100 g oven-dried OPF.

^aDAP: dilute sulphuric acid pretreatment; AH: autohydrolysis; AHN: autohydrolysis with 2-naphthol; AHD: autohydrolysis with 1,8-dihydroxyanthraquinone.

^bKL: Klason lignin; SL: soluble lignin.

It was reported previously by El Hage *et al.* (2010) that the addition of organic compounds during autohydrolysis will enhance the hemicellulose recovery yield.

During autohydrolysis, the acetyl groups of xylans are hydrolyzed to acetic acid which decreased the pH of the autohydrolysate and further promotes the autohydrolysis of hemicellulose into water-soluble oligomers (Sabiha-Hanim *et al.*, 2011). Besides, the xylans and arabinans removal were significantly increased with the severity factor (Sabiha-Hanim *et al.*, 2011; Obama *et al.*, 2012; Timilsena *et al.*, 2013a). Small fractions of glucan and soluble lignin recovery from the aqueous residue confirmed that the prehydrolysis process did not affect the total glucan and lignin content inside the biomass.

3.3.2 Composition of lignin samples

In the combinative pretreatment, the OPF biomass was treated first with different types of pretreatment (dilute sulphuric acid prehydrolysis, autohydrolysis and autohydrolysis in the presence of organic scavengers) and then followed by organosolv pulping. Organosolv pulping was chosen as the delignification step because it provides clean fractionation of lignocellulosic feedstocks and the recovery of high-quality lignins (relatively pure, less condensed than other industrial lignins, sulphur free, soluble in organic solvent) are of great interest and are currently a focus of attention (Zhao *et al.*, 2009b). Abbreviations are used in order to identify the types of lignin produced; dilute sulphuric acid treated lignin: DAP EOL, autohydrolyzed lignin: AH EOL, autohydrolyzed with 2-naphthol lignin: AHN EOL and autohydrolyzed with 1,8-dihydroxyanthraquinone lignin: AHD EOL. The elemental composition and the respective contents are gathered in Table 3.8.

Low degree of delignification of all pretreated OPF biomass (lignin extraction yield; AHN EOL: 13.42 % > DAP EOL: 11.86 % > AHD EOL: 9.64 % > AH EOL: 9.36 %) was observed after organosolv treatment compared to that of the total Klason lignin. It can be concluded that ethanol organosolv treatment is not necessarily the best method to give high lignin extractability for the pretreated OPF in this work. Again, the lower yield of lignin after organosolv process was perhaps due to low severity reaction conditions used and the effect of aqueous ethanol solvent which dissolves small molecular weight of lignin (El Hage *et al.*, 2010). The degree of delignification of OPF lignin can be possibly increased by using alkaline pulping method as shown in the previous subchapter.

Table 3.8: Proximate analysis of pretreated organosolv lignin from oil palm fronds (% w/w on dry matter).

	DAP EOL	AH EOL	AHN EOL	AHD EOL
Yield (%)	11.86±0.95	9.39±1.03	13.42±0.71	9.64±0.84
Ash (%)	3.27±0.04	3.97±0.11	2.82±0.02	2.13±0.01
Moisture (%)	3.46±0.12	5.20±0.21	4.12±0.15	5.21±0.17
Element (%)				
C	63.03	64.78	64.90	63.53
H	5.98	6.11	5.82	5.53
N	0.76	0.80	0.68	0.59
O	30.23	28.31	28.60	35.88
Protein (%)	4.75	5.00	4.25	3.69
Double bond equivalent (DBE)	4.86	4.81	5.16	5.29

According to the proximate analysis, the incorporation of organic scavengers (2-naphthol and 1,8-dihydroxyanthraquinone) during autohydrolysis will produce lignin with lower ash and protein content. The average C9 formulae calculated from the elemental composition were DAP EOL: $C_9H_{10.26}N_{0.09}O_{3.24}$, AH EOL: $C_9H_{10.39}N_{0.10}O_{3.01}$, AHN EOL: $C_9H_{9.68}N_{0.08}O_{2.96}$, AHD EOL: $C_9H_{9.42}N_{0.07}O_{3.82}$.

Similar to Kraft, soda and organosolv lignin, all lignins produced in this study gave basic elements like C, H, O and N where the nitrogen content comes from the formation of protein-lignin complexes during delignification process (Zhao *et al.*, 2009a). The number of DBE for both AHN EOL and AHD EOL was higher compared to DAP EOL and AH EOL. This may indicate that the incorporation of organic scavengers (2-naphthol and 1,8-dihydroxyathraquinone) in the lignin structure will increase their number of double bond equivalent, thus justifying the incorporation of the aromatic moieties.

3.3.3 FTIR analysis

The FTIR spectra of different pretreated organosolv lignins are presented in Figure 3.11 and the assignments are given in Table 3.9, which is in accordance with previous reports (Tejado *et al.*, 2007; Mohamad Ibrahim *et al.*, 2011). Similar spectral patterns for all organosolv lignins were observed indicating that the combinative pretreatment processes gave almost similar lignin chemical compositions. Absorption signal at 1160 cm^{-1} which appears in all spectra was assigned to typical HGS lignin. The presence of absorption bands at 1328 cm^{-1} (syringyl), 1219 cm^{-1} (guaiacyl), 1120 cm^{-1} (syringyl) and 1033 cm^{-1} (guaiacyl) supports our hypothesis that organosolv lignin isolated from different pretreated OPF were mainly composed of S and G basic units. Besides, this observation is also in agreement with the absorption band of C-H plane in all positions of H units which appears at 834 cm^{-1} . It was also observed that for all organosolv lignin, the absorbance signal of S unit (1328 and 1120 cm^{-1}) was higher compared to G units (1272 and 1033 cm^{-1}) which suggested the higher syringyl content.

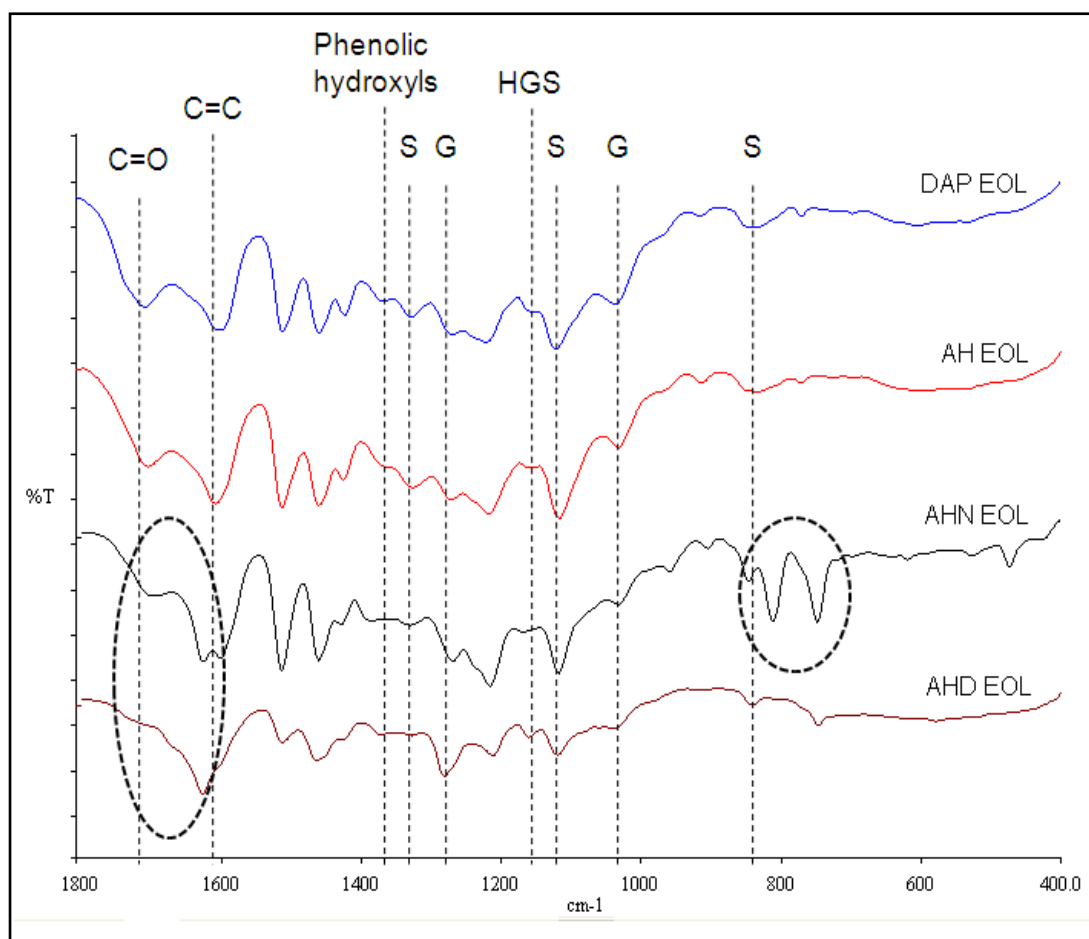


Figure 3.11: Infra red spectra of organosolv OPF lignin after combinative pretreatments. Circle lines indicate region of interest.

* DAP EOL: dilute sulphuric acid prehydrolysis organosolv lignin; AH EOL: autohydrolysis organosolv lignin; AHN EOL: autohydrolysis with 2-naphthol organosolv lignin; AHD EOL: autohydrolysis with 1,8-dihydroxyanthraquinone organosolv lignin.

Based on Figure 3.11, when 2-naphthol was introduced during the autohydrolysis process (AHN EOL), an increasing absorption at around 818 and 750 cm^{-1} can be observed after the organosolv treatment. These bands were indicative of the presence of naphthalene rings substituted in the lignin backbone (Wayman and Lora, 1980; Li and Gellerstadt, 2008). The position C1 of the 2-naphthol molecule was suspected to be involved in the blocking of lignin repolymerization through electrophilic substitution reaction with the carbonium ions generated in the lignin molecule as consequence of the acidic conditions (Norman and Taylor, 1965).

Table 3.9: Organosolv OPF lignins after combinative pretreatments characterized by FTIR.

cm ⁻¹	Assignments	DAP EOL	AH EOL	AHN EOL	AHD EOL
		Band Assignments			
1325-1330	Syringyl ring breathing, C-O stretching	1328	1327	1327	1326
1266-1280	G ring plus C-O stretching	1271	1271	1269	1281
1221-1230	C-C, C-O, C=O stretching ($G_{\text{condensed}} > G_{\text{esterified}}$)	1222	1218	1216	1212
1160	Typical for HGS lignins; C=O in ester groups (conj.)	1158	1159	1161	1160
1120-1128	Typical of S unit; also for secondary alcohol and C=O stretching	1122	1117	1118	1120
1030-1035	Aromatic C-H in plane deformation plus C-O deformation in primary alcohol plus C-H stretching (unconj.)	1037	1033	1033	1033
915-925	C-H out of plane (aromatic ring)	915	914	908	914
834-835	Aromatic C-H out of plane	834	834	847	838

A decrease in the absorption of $1700\text{-}1720\text{ cm}^{-1}$ in the presence of organic scavengers (2-naphthol and 1,8-dihydroxyanthraquinone) may explain the fact that the organic scavenger reduced significantly the number of β -keto (Hibbert ketone) groups by condensing with either their precursor hydroxyl groups or the already formed β -carbonyl groups (Wayman and Lora, 1980). Besides, the reduction was also caused by limitation of the deconstruction on the lateral chain because of the scavenging effect.

3.3.4 ^1H , ^{13}C and ^{31}P NMR

Figures 3.12 and 3.13 show the ^1H NMR spectra of different pretreated organosolv lignins. As a comparison, ethanol organosolv lignin (EOL) was used as a reference in this study. Similar trend of spectra can be observed in Figure 3.12 and 3.13 where their assignments followed almost exactly as what Lundquist (1992) has reported previously. The integral of signals between 6.0 to 8.0 ppm is indicative of aromatic protons in syringyl (S) and guaiacyl (G) units and an intense signal at around 3.75 ppm is attributed to G and S methoxyl proton unit. Meanwhile, the integral of signals between 1.9 to 2.3 ppm is indicative of acetyl group and the signals between 0.8 to 1.5 ppm is attributed to the aliphatic moiety. From this study, there is not much difference in the spectral patterns for organosolv lignins pretreated with dilute sulphuric acid and autohydrolysis.

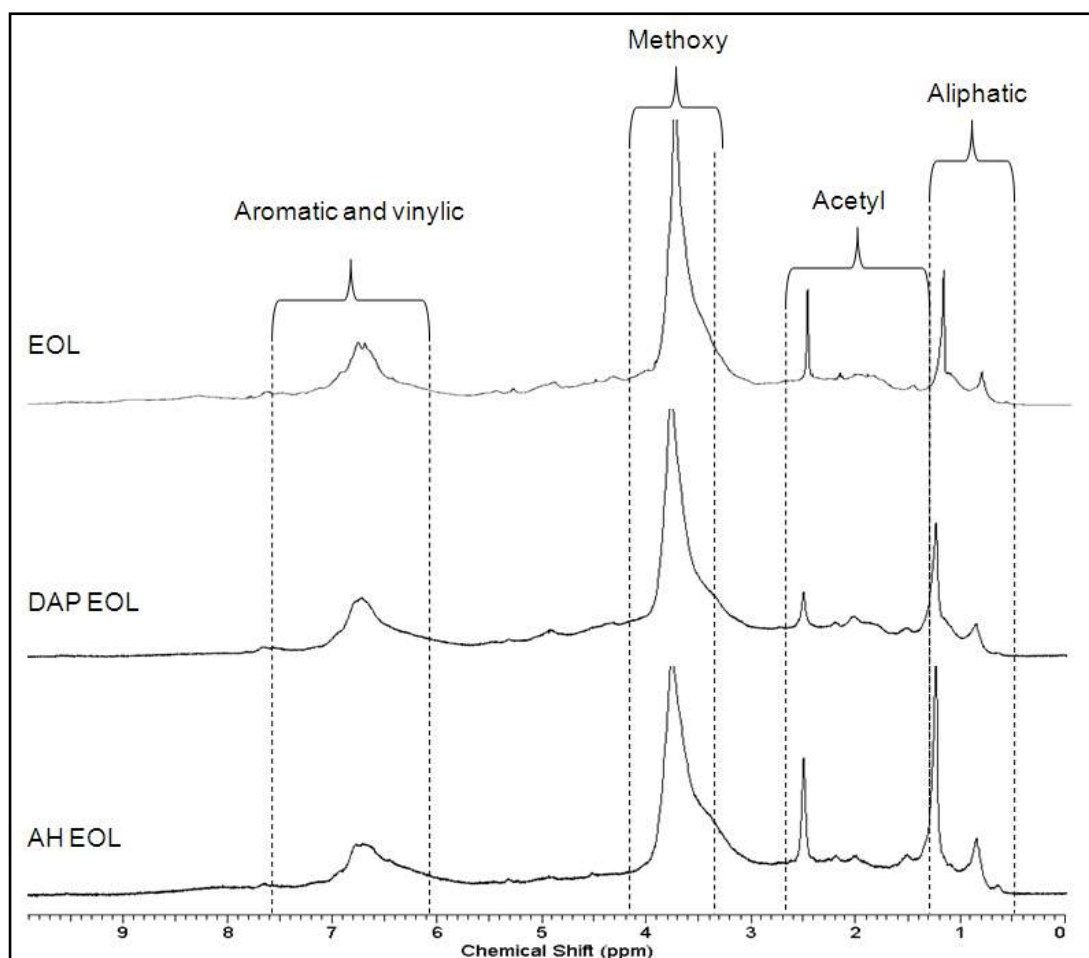


Figure 3.12: ¹H NMR spectra of different pretreated organosolv lignin.

On the other hand, the incorporation of organic scavengers gives some additional peaks especially at the aromatic region. According to Figure 3.13, numerous distinct peaks were observed for AHN EOL and AHD EOL spectra between 6.5 to 8.5 ppm. These peaks were indicative of 2-naphthol and 1,8-dihydroxyanthraquinone structures. Besides, it was shown that the phenolic –OH peak of naphthol (5.19 ppm) at C2 and the phenolic –OH peak of dihydroxyanthraquinone (11.98 ppm) at C3 were greatly reduced. This may suggest the possible bond formation between both organic scavengers with the lignin matrix.

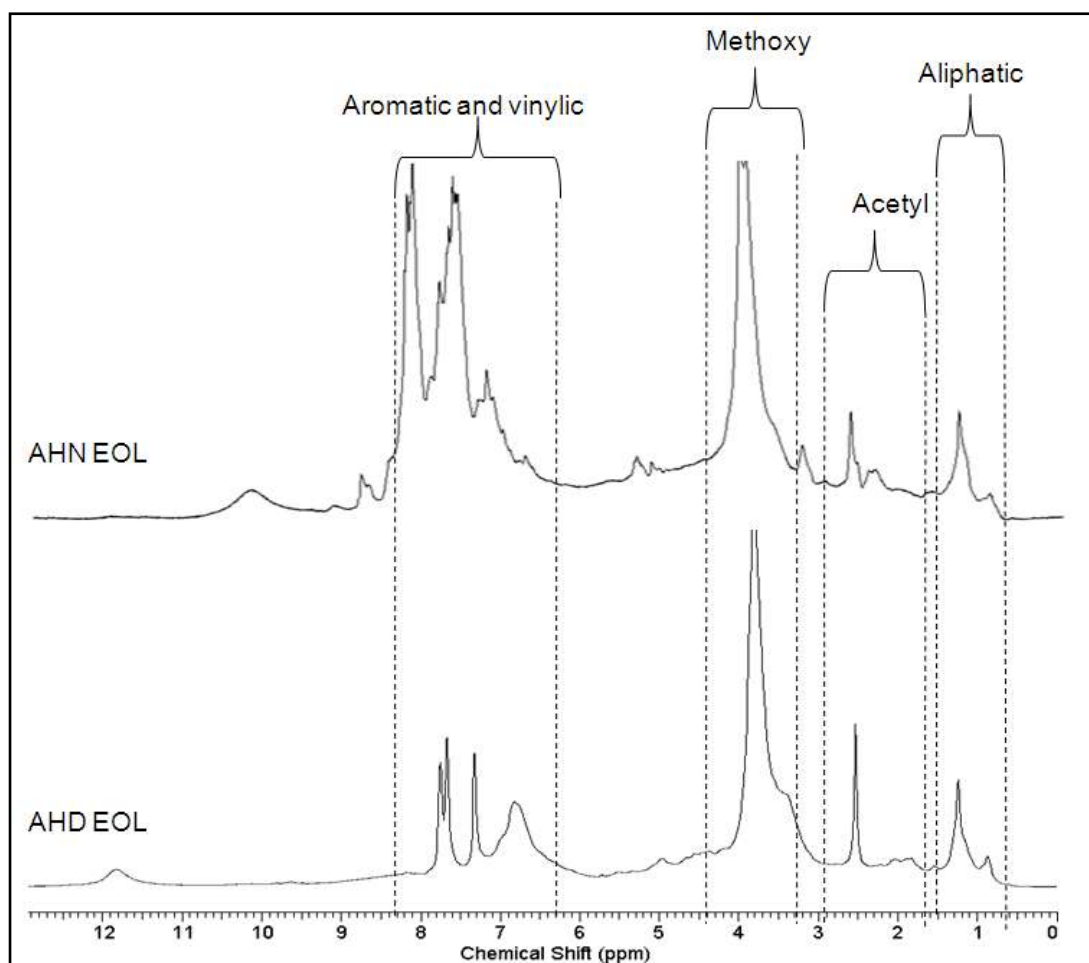


Figure 3.13: ^1H NMR spectra of autohydrolyzed organosolv lignin in the presence of 2-naphthol (AHNEOL) and 1,8-dihydroxyanthraquinone (AHD EOL).

The ^{13}C NMR spectra of all different pretreated organosolv lignins are shown in Figure 3.14. The presence of guaiacyl (G), syringyl (S) and p-hydroxyphenyl (H) units were clearly observed in the spectra with all assignments given in Figure 3.14. As seen in Figure 3.14, all pretreated organosolv lignins gave intense signals for S (104 ppm, 138 ppm and 154 ppm) and G (114 ppm, 119 ppm, 135 ppm and 147 ppm) units respectively to the C2/C6, C4 and C3/C5 (for S unit); C2, C6, etherified C1 and non-etherified C3 (for G unit) carbon positions.

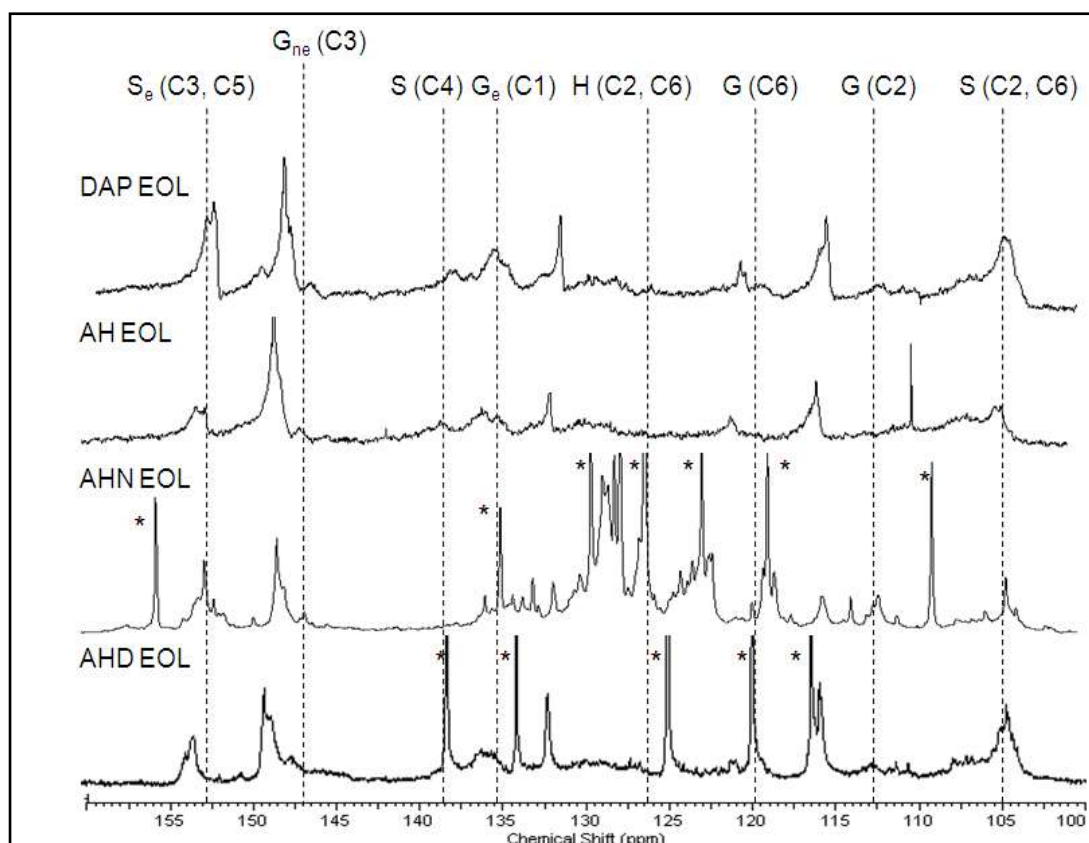


Figure 3.14: ^{13}C NMR spectra of different pretreated organosolv OPF lignin samples in expanded aromatic region. * Chemical shifts of 2-naphthol and 1,8-dihydroxyanthraquinone.

Higher signals for S unit in all pretreated organosolv lignin may suggest that combinative pretreatment processes will produce lignin that contains more syringal basic unit than guaiacyl unit. In addition, numerous distinct peaks were observed for AHN EOL and AHD EOL spectra which are clearly associated with 2-naphthol and 1,8-dihydroxyanthraquinone structures.

Data from the quantitative ^{31}P NMR of the three organosolv lignin samples (Figure 3.15), obtained following their derivatization with TMDP are presented in Table 3.10. According to this data, it can be observed that autohydrolyzed organosolv lignins gave lower concentration of aliphatic $-\text{OH}$ groups and higher concentration of HGS phenolic $-\text{OH}$ groups (AH EOL: 1.67 mmol g^{-1} , AHN EOL: 1.50 mmol g^{-1}

and AHD EOL: 1.49 mmol g⁻¹) compared to dilute sulphuric acid treated organosolv lignin (DAP EOL: 1.14 mmol g⁻¹). This phenomenon is mainly due to the extensive depolymerization of lignin during autohydrolysis through the scission of β -O-4 bonds leading to the production of phenolic –OH groups. Besides, very severe conditions (used during autohydrolysis pretreatment; severity factor: $S_0 = \sim 4.1$) have enhanced the cleavage of α - and β -ether linkages between lignin structural units which later led to the formation of new phenolic –OH when delignification process takes place (Wayman and Lora, 1980; Li and Gellerstadt, 2008).

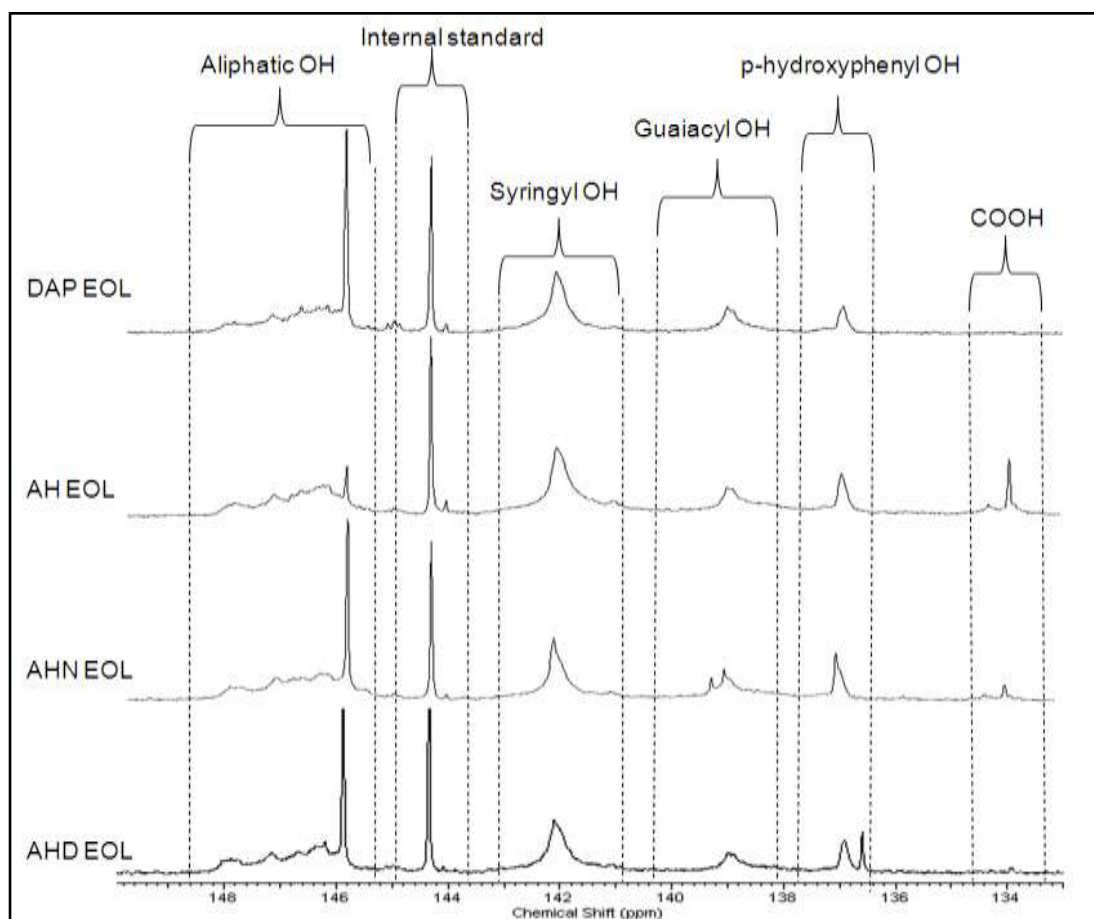


Figure 3.15: ³¹P NMR spectra of different pretreated organosolv OPF lignin samples in expanded region.

The reduction of aliphatic –OH is probably due to the dehydration reactions through acid-catalyzed elimination reaction (El Hage *et al.*, 2009; Obama *et al.*, 2012). More

interestingly, the quantity of p-hydroxyphenyl groups for AHN EOL and AHD EOL were almost similar with the AH EOL lignin which suggests that the production of p-hydroxyphenyl –OH groups and the fractional hydrolysis of p-coumaryl ester residues during autohydrolysis are not disturbed even after the modification process with 2-naphthol and 1,8-dihydroxyanthraquinone. Higher signals for S unit in all pretreated organosolv lignins may suggest that OPF lignin contains more syringal basic unit than guaiacyl unit, as similarly shown in the FTIR spectra.

Table 3.10: Pretreated organosolv lignins characterized by ^{31}P NMR.

ppm	Assignments	mmol g ⁻¹			
		DAP EOL	AH EOL	AHN EOL	AHD EOL
150-145	Aliphatic –OH	1.07	0.92	1.42	1.08
144.8	Cyclohexanol (Internal standard)				
144-140	Syringyl –OH	0.72	0.98	0.79	0.74
140-138	Guaiacyl –OH	0.29	0.45	0.47	0.46
138-136	p-hydroxyphenyl – OH	0.13	0.24	0.24	0.29
135-133	Carboxylic acid	-	0.16	0.05	0.01

3.3.5 HSQC and HMBC NMR

2D NMR is a useful tool for the qualitative and quantitative analysis of lignin structures, due to its well-resolved signals and more detailed diagnostic information on the complex lignin structure. To acquire further information on the structural characterization of modified organosolv lignin, the autohydrolyzed organosolv lignin in the presence of organic compound 2-naphthol and 1,8-dihydroxyanthraquinone were subjected to heteronuclear single quantum correlation, HSQC and heteronuclear multiple bond correlation, HMBC NMR analyses. The main signals in the aromatic region ($\delta_{\text{C}}/\delta_{\text{H}}$ 100-150/6.0-8.0 ppm) of the HSQC NMR spectrum are

shown in Figure 3.16. As previously reported by She *et al.* (2012), the correlation at δ_C/δ_H 103.8/6.69 ppm corresponds to 2/6 position of S units, whereas the correlations for C₂-H₂ (δ_C/δ_H 110.8/6.96 ppm) and C₅-H₅ (δ_C/δ_H 115.5/6.84 ppm) are assigned to G units. Signals for the p-hydroxyphenyl units (H) were identified at δ_C/δ_H 129.7/7.02 ppm. This supports the earlier prediction that the organosolv lignin obtained from different pretreatments could be verified as typical HGS lignin. p-coumarates (pCE 2/6) correlations were also observed in all organosolv lignin samples appearing at δ_C/δ_H 131.2/7.6 ppm. The presence of a naphthalene ring can be detected at around δ_C/δ_H 120-130/7.0-8.0 ppm respectively. This observation is in good agreement with the previous findings (Li and Gellerstedt, 2008). Meanwhile, the presence of an anthraquinone ring can be detected at around δ_C/δ_H 120-140/7.0-8.0 ppm respectively.

The modification of the lignin structure in the presence of 2-naphthol and 1,8-dihydroxyanthraquinone also can be supported by the HMBC analysis. As previously discussed in the infrared spectra, the modification of lignin structure with 2-naphthol is possible either in the C1 or C2 positions (Wayman and Lora, 1980; Li and Gellerstedt, 2008). In this study, an interaction at δ_C/δ_H 79.0/7.09 between C _{β} of lignin matrix to oxygen functional group of naphthol was detected (Figure 3.17A). The correlation of δ_C/δ_H 110/7.09 ppm and 149/7.09 are corresponding to C1 and C2 positions of naphthol as its coupling neighbors. In addition, Figure 3.17B shows a different interaction at correlation of δ_C/δ_H at 135/4.85, suggesting that the bond is formed between C _{α} of lignin matrix to C3 position of naphthol.

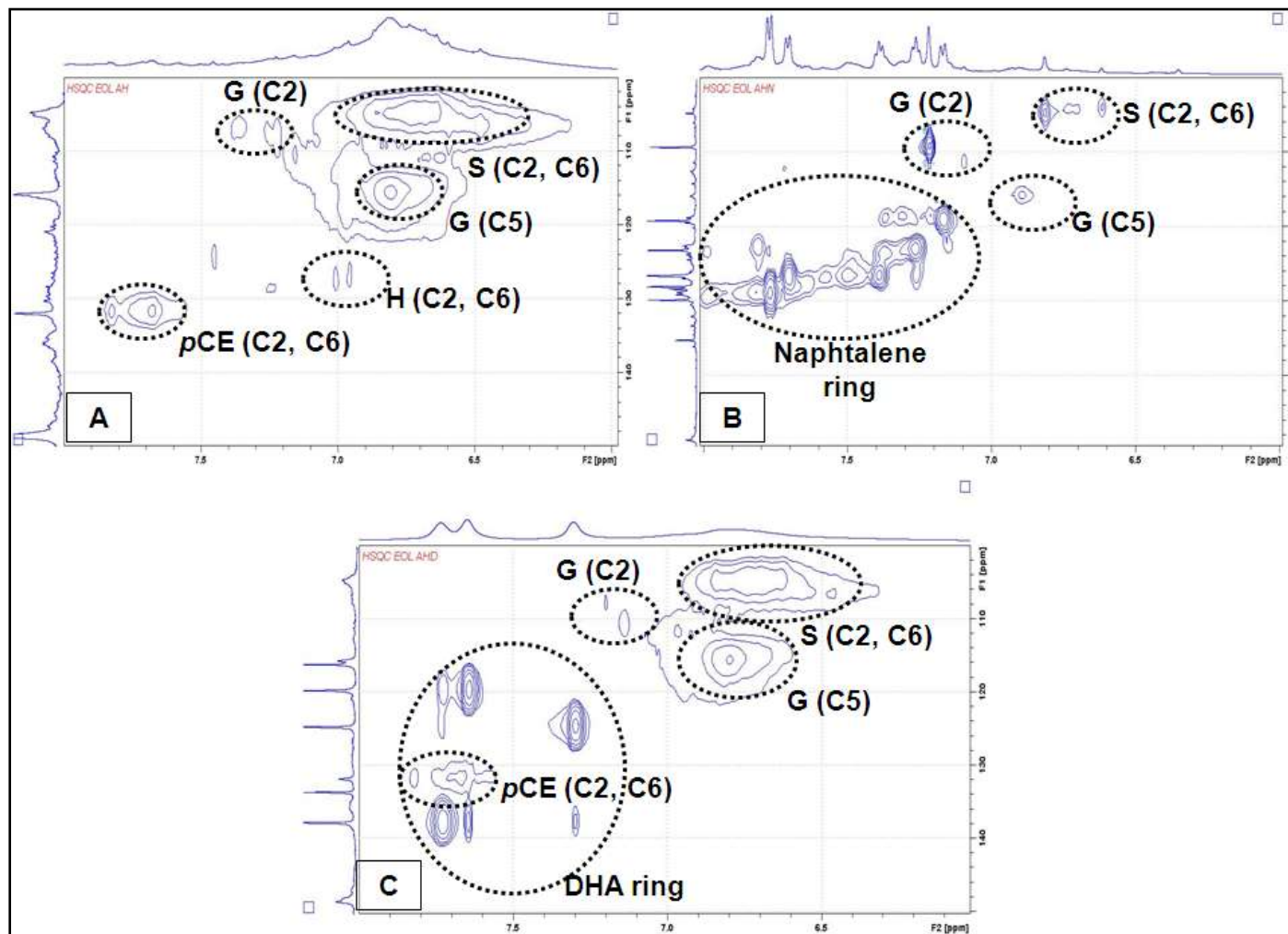


Figure 3.16: 2D-HSQC NMR spectrum of (A) autohydrolyzed; (B) autohydrolyzed with 2-naphthol and (C) autohydrolyzed with 1,8-dihydroxyanthraquinone organosolv lignin..

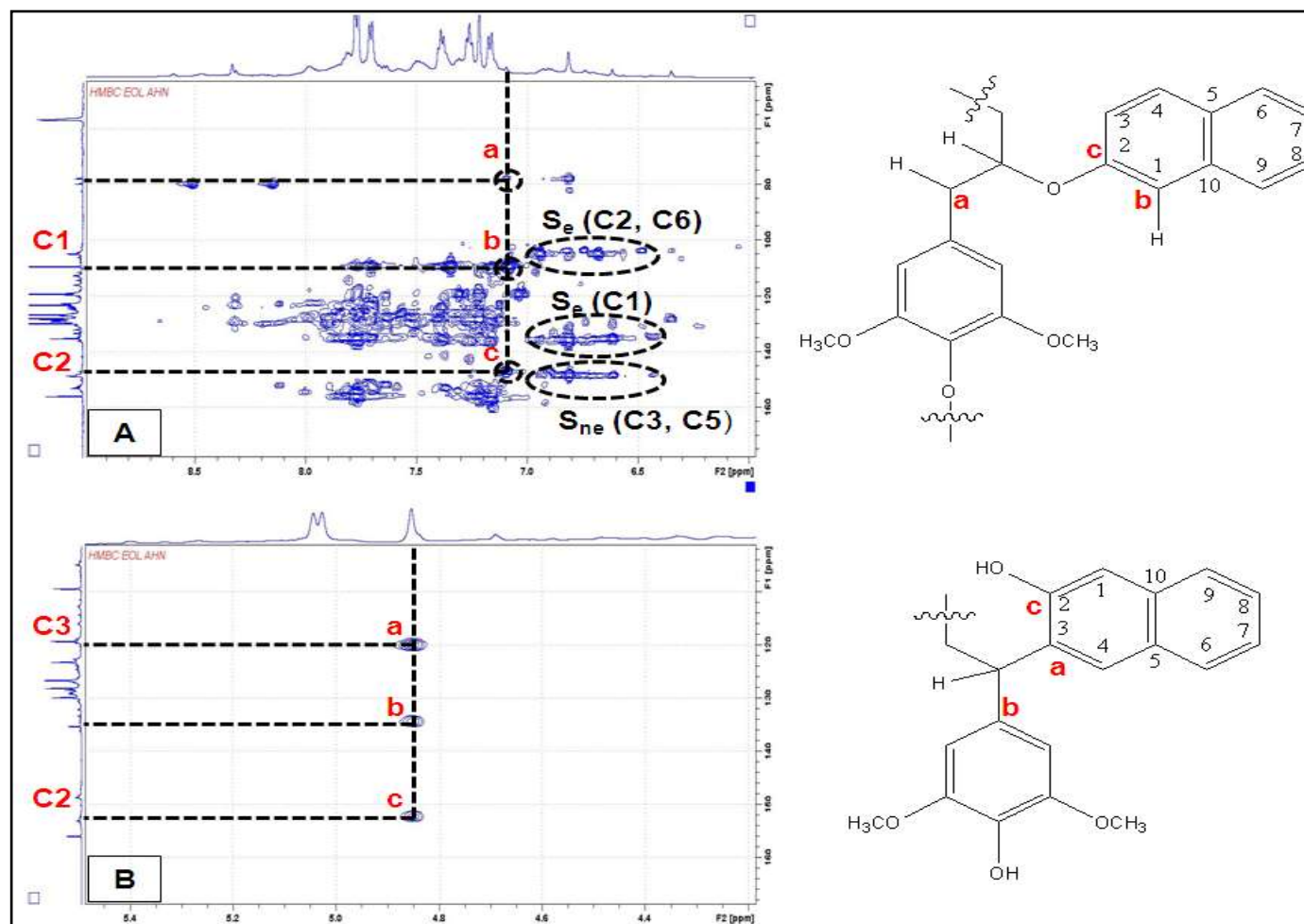


Figure 3.17: 2D-HMBC NMR spectrum at (A) aromatic region; (B) side chain region of autohydrolyzed lignin in presence of 2-naphthol.

In general, the acidic conditions during the prehydrolysis (dilute sulphuric acid or autohydrolysis) and organosolv treatment lead to the formation of carbonium ions by the proton-induced elimination of water from benzylic position. The condensation reactions may occur in the presence of electron-rich carbon atoms such as the C2/C6 present in guaiacyl and syringyl rings leading to repolymerization of the lignin. By introducing organic scavengers like 2-naphthol, the carbonium ion lignin-lignin condensation reaction can be induced respectively through an electrophilic substitution reaction at the C_α position (Wayman and Lora, 1980; Li and Gellerstedt, 2008; Timilsena *et al.*, 2013b). The 2-naphthol can easily undergo substitution at the C2 position because of the more favorable benzenoid structures in the transition state (Li and Gellerstedt, 2008). Therefore, it is proposed that the modification of lignin in the presence of 2-naphthol will form an interaction possibly at C2 and/or C3 position of naphthol.

Previously, the addition of anthraquinone in soda pulping was described to accelerate pulp delignification. Anthraquinone has been shown to operate in a redox cycle: the reducing end groups of carbohydrates dissolved in the pulping liquor reduce the anthraquinone to anthrahydroquinone (Figure 3.18). In the soda pulping conditions, anthrahydroxyquinone then reacts with lignin quinone methides through an addition-elimination reaction and causes the β-aryl ether linkage in the lignin molecule to cleave (Fleming *et al.*, 1978; Blain, 1993). In this study, it was believed that during the autohydrolysis step, 1,8-dihydroxyanthraquinone was reduced in the presence of reducing sugars into the highly nucleophilic 1,8-dihydroxyanthrahydroxyquinone.

The incorporation of 1,8-dihydroxyanthrahydroxyquinone scavenger on the lignin matrixes according the well known mechanism (Blain, 1993) should retard the condensation process (through an electrophilic substitution reaction at the C_α position) and leads to the production of higher phenolic –OH groups. A strong interaction at δ_C/δ_H 162.0/4.5 ppm (Figure 3.19) was detected that indicated a strong correlation of C_α lignin matrix to C3 and/or C6 position of 1,8-dihydroxyanthraquinone. This correlation demonstrates the presence of the anthraquinone structures on the external ring. Organic scavengers like 1,8-dihydroxyanthraquinone, would bind to a lignin quinone methide thus forming a covalently-bonded adduct. The role of anthraquinone here is therefore to induce/scavenge the carbonium ion lignin-lignin condensation reaction through an electrophilic substitution reaction at the C_α position (Lora and Wayman, 1979; Li and Gellerstedt, 2008; Timilsena *et al.*, 2013b). Therefore, it is proposed that the modification of lignin in the presence of 1,8-dihydroxyanthraquinone will form an interaction possibly at C3 and/or C6 of the anthraquinone moiety.

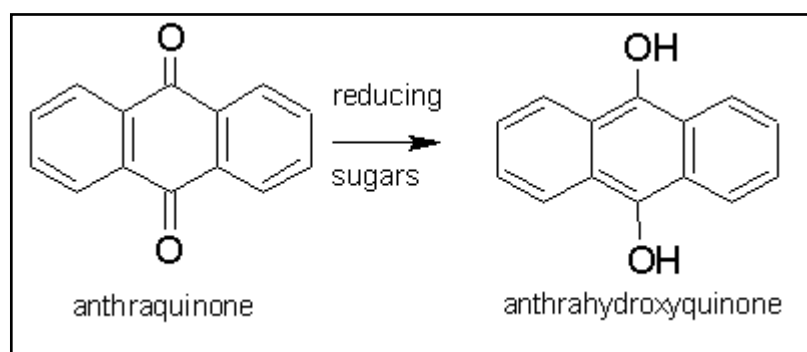


Figure 3.18: Anthraquinone/ anthrahydroxyquinone redox cycle in presence of reducing sugar.

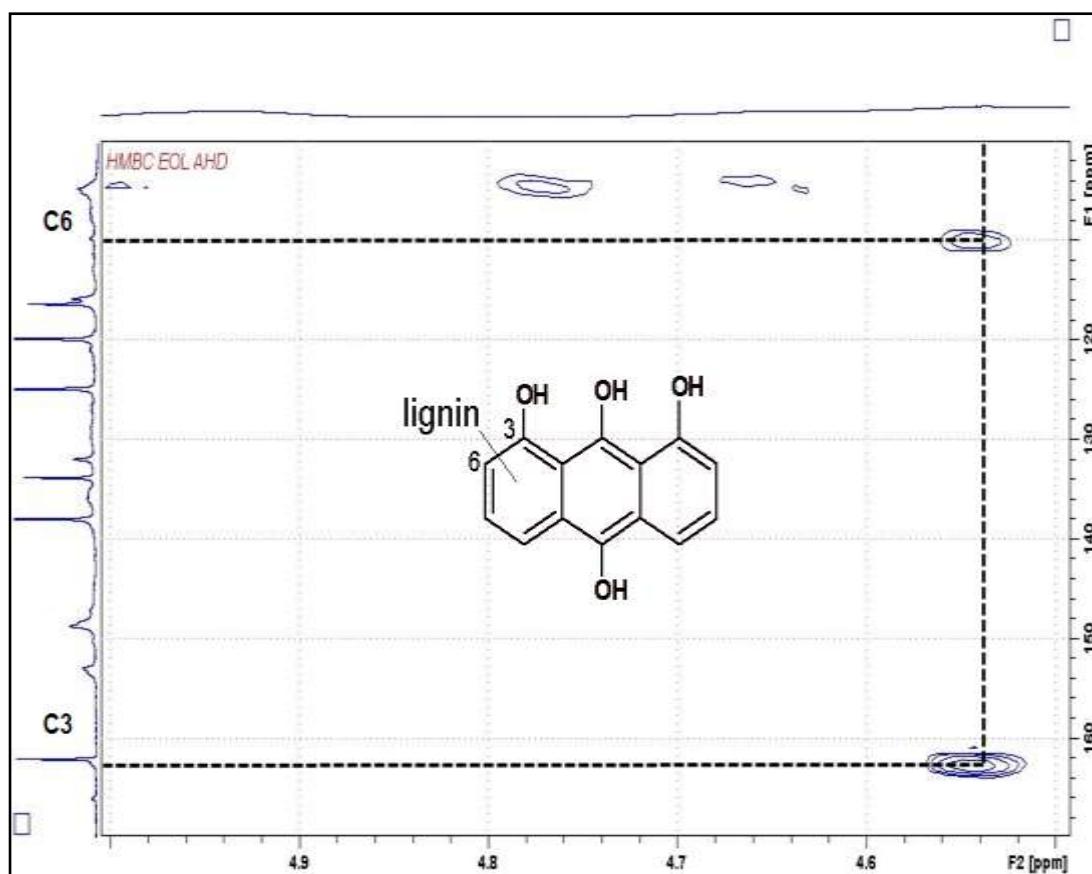


Figure 3.19: 2D-HMBC NMR spectrum at side chain region of lignin with 1,8-dihydroxyanthraquinone. (Inset: Structure of 1,8-dihydroxyanthraquinone).

3.3.6 Molecular weight

The weight average (M_w) and number average (M_n) molecular weight of all organosolv lignins are shown in Table 3.11. As for comparison, the M_w and M_n values of untreated OPF organosolv lignin (EOL) extracted at LERMAB is also included in the table. From the results, it can be seen that weight-average (M_w) of autohydrolyzed pretreated (AH EOL: 3330 g mol^{-1} ; AHN EOL: 3093 g mol^{-1} and AHD EOL: 3624 g mol^{-1}) organosolv lignins were lower than dilute sulphuric acid organosolv lignin (DAP EOL: 4098 g mol^{-1}) and untreated organosolv lignin (EOL: 5151 g mol^{-1}). This shows that autohydrolysis pretreatment facilitates the extensive

cleavage of inter-unit bonds in lignin during the organosolv treatment, producing smaller fragments of lignin with low molecular weight.

Besides, low molecular weight of lignin will increase its solubility in some organic solvents (Alriols *et al.*, 2009). The deconstruction of lignin is associated with the repolymerization reactions through the formation of new C-C bonding. As a result, the repolymerization of lignin during this process will decrease the degree of delignification that produces undesirable effects to the properties and reactivity of lignin (Li and Gellerstedt, 2008; El Hage *et al.*, 2010). Based on this theory, it can be assumed that the fraction of the repolymerized lignin which occurred during the single-step organosolv treatment will produce a very high molecular weight of lignin after delignification process.

Table 3.11: GPC results of weight-average (M_w), number-average (M_n) and polydispersity (PD) of different pretreated organosolv lignin from oil palm fronds.

	Untreated EOL	DAP EOL	AH EOL	AHN EOL	AHD EOL
M_w (g mol ⁻¹)	5151	4098	3330	3093	3624
M_n (g mol ⁻¹)	2373	1881	1661	1647	1888
M_w/M_n (polydispersity)	2.17	2.18	2.01	1.88	1.92

On the other hand, very low polydispersity (PD) values especially for lignin extracted from autohydrolysis treated OPF biomass (AH EOL: PD 2.01; AHN EOL: PD 1.88 and AHD EOL: PD 1.92) than to lignin extracted from dilute sulphuric acid treated OPF and untreated organosolv lignin (DAP EOL: PD 2.18 and EOL: PD 2.17) were observed. Low polydispersity of organosolv lignin indicated the high fraction of low molecular weight (LMW) components present in the samples (Alriols *et al.*, 2009). In addition, a low polydispersity value also contributes to the

uniformity of overall packing structures of lignin. Lignins with high fraction of low molecular weight are suitable for condensates with phenol formaldehyde because they are more reactive than those with high molecular weight molecules (Pizzi, 1994). Therefore, it can be concluded that combined processes such as autohydrolysis of OPF biomass can produce smaller fragments of lignin (by producing smaller M_w and polydispersity value) and at the same time increases its ability to be used in various applications like adhesives, antioxidants and paints.

3.3.7 Thermal behavior

3.3.7.1 Thermal gravimetric analysis

The results obtained by thermal analysis (Figure 3.20) showed that the TG (weight loss of lignin in relation to the temperature of thermal degradation) and DTG (rate of weight loss) curves gave three different degradation steps: (1) that is mainly attributed to weight loss of water; (2) weight loss of hemicelluloses at around 200 °C and (3) degradation of lignin complex structure at around 300-400 °C. This observation is in good agreement with previous findings (Mohamad Ibrahim *et al.*, 2011). A slight decrease of maximum rate of weight loss, DTG_{max} for AHD EOL (300 °C) than for DAP EOL (360 °C), AH EOL (350 °C) and AHN EOL (350 °C) which appeared at low temperature suggested the presence of hemicellulose-lignin complexes in the compound. According to Toledano *et al.* (2010a), the decomposition temperature that appears between hemicellulose (~200 °C) and lignin (~350 °C) was found to an intermediate product. A broad lignin degradation curve was observed for AHN EOL and AHD EOL lignin sample at lower temperature may

suggest that the lignin structure are less cross-linked (contains more lignin-naphthalene/lignin-anthraquinone linkages) compared to C-C interlinked bonds.

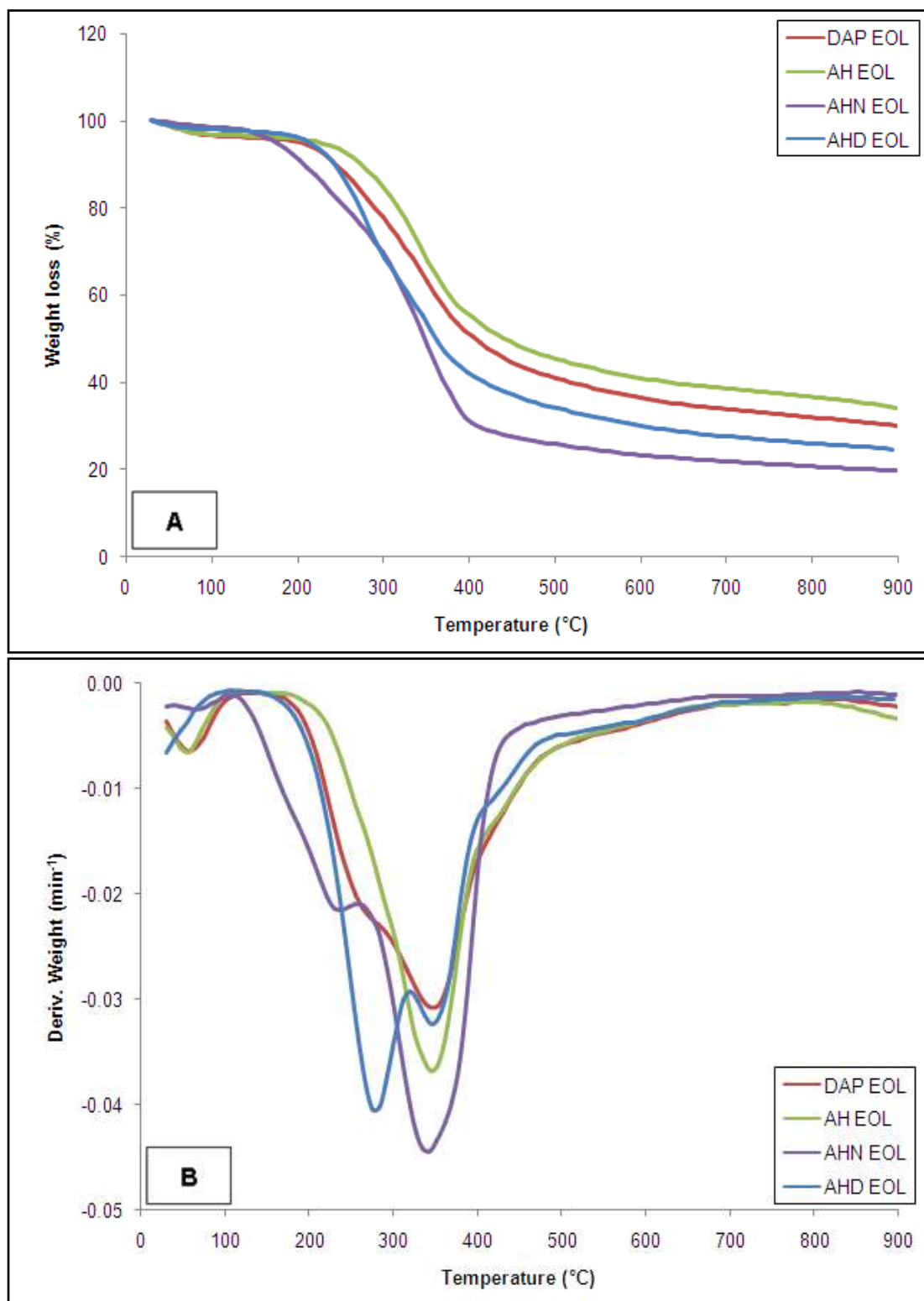


Figure 3.20: (A) TG and (B) DTG curves for different pretreated organosolv lignin.

3.3.7.2 Differential scanning calorimetry

In order to further characterize the different treated organosolv lignins, differential scanning calorimetry (DSC) at heating rate of $10\text{ }^{\circ}\text{C min}^{-1}$ was performed. It was observed that the values of glass transition (T_g) of all treated organosolv lignins increased in the following order: AHN EOL (T_g : $42.53\text{ }^{\circ}\text{C}$) < AHD EOL (T_g : $49.71\text{ }^{\circ}\text{C}$) < AH EOL (T_g : $64.67\text{ }^{\circ}\text{C}$) < DAP EOL (T_g : $71.52\text{ }^{\circ}\text{C}$). The lower T_g value of AHN EOL lignin is essentially due to the increase in the free volume of the lignin molecules as the naphthalene substituent binds to the carbonium ion intermediates under acidic conditions during prehydrolysis of OPF biomass. In contrast, the higher T_g value for DAP EOL lignin is mainly caused by limited free volume of lignin molecule as a result of repolymerization. A good correlation between the T_g values with M_w , M_n and polydispersity values obtained from GPC analysis were observed indicating that higher molecular weight of lignin may increase the energy level required to make chain rotation.

3.3.8 Composition of phenolic acids and aldehydes

Alkaline nitrobenzene oxidation was again used for the analysis of different pretreated organosolv lignins. The corresponding chromatograms are shown in Figure 3.21 and Table 3.12 summarizes the results concerning the analysis of phenolic acids and aldehydes from the lignin fractions, obtained by alkaline nitrobenzene oxidation (all standards linear curve are shown in Appendix IV). All units (H, G and S units) are present in each sample which confirms that the OPF lignin is of HGS type. Similar to alkaline (Kraft and soda) lignin, the predominant

oxidation products of pretreated organosolv lignins were found to be vanillin and syringaldehyde, resulted from the degradation of non-condensed guaiacyl (G) and syringyl (S) units respectively.

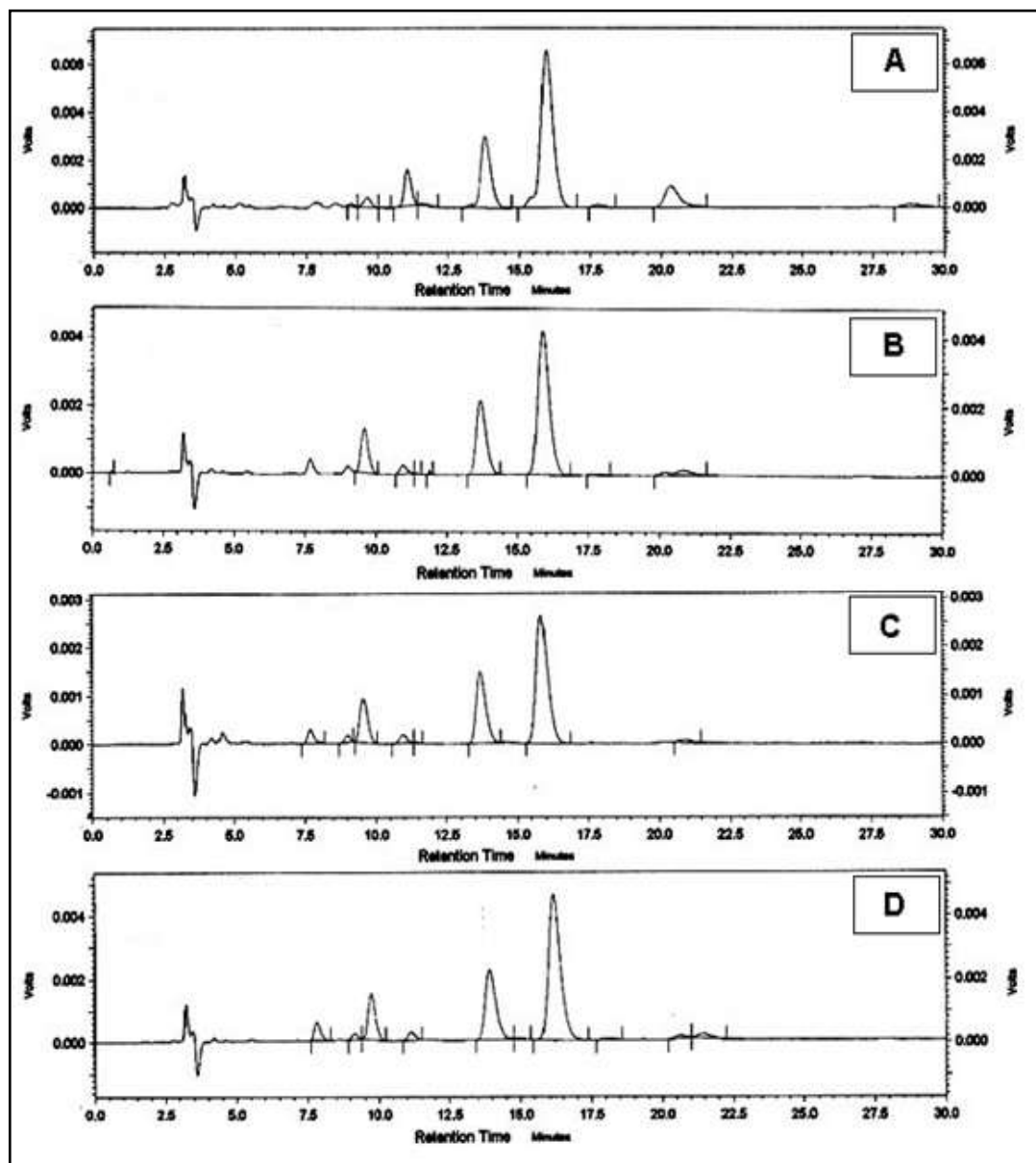


Figure 3.21: HPLC chromatogram of; (A) DAP EOL, (B) AH EOL, (C) AHN EOL and (D) AHD EOL organosolv lignins obtained at a flow rate of 1 mL min^{-1} and 280 nm of UV detection.

The molar ratios of G (relative total moles of vanillin and vanillic acid), S (relative total moles of syringaldehyde and syringic acid) and H (relative total moles of p-hydroxybenzaldehyde and p-hydroxybenzoic acid) units were found to be 17:77:5 in DAP EOL, 15:77:8 in AH EOL, 17:75:8 in AHN EOL and 17:76:7 in AHD EOL lignins. The uniform HGS ratios of all pretreated organosolv lignins may suggest that the prehydrolysis treatment may not affect the HGS ratios even after delignification with organosolv pulping process.

Table 3.12: The yield (% dry sample, w/w) of phenolic acids and aldehydes from alkaline nitrobenzene oxidation of different pretreated organosolv lignin samples.

Component	% Weight (dry basis)			
	DAP EOL	AH EOL	AHN EOL	AHD EOL
p-hydroxybenzoic acid	0.23±0.08	0.46±0.02	0.31±0.01	0.32±0.07
vanillic acid	0.07±0.02	0.09±0.01	0.07±0.01	0.11±0.01
syringic acid	0.15±0.11	0.69±0.01	0.51±0.01	0.79±0.02
p-hydroxybenzaldehyde	0.13±0.02	0.004±0.001	0.008±0.001	0.008±0.001
vanillin	1.06±0.11	0.87±0.02	0.63±0.01	0.69±0.01
syringaldehyde	4.87±1.72	4.11±0.09	2.52±0.03	2.77±0.12
ferulic acid	1.41±0.15	0.21±0.04	0.07±0.02	0.14±0.01
Molar ratio (G:S:H)	17:77:5	15:77:8	17:75:8	17:76:7
S/G ratio	4.53	5.13	4.41	4.47

*Retention time (Rt, min) appears similar as listed in subchapter 3.2.6 where p-hydroxybenzoic acid = 8.00 min; vanillic acid = 9.48 min; syringic acid = 10.00 min; p-hydroxybenzaldehyde = 11.77 min; vanillin = 14.80 min; syringaldehyde = 17.20 min and ferulic acid = 22.17 min.

As indicated in subchapter 3.2.6, the lignin obtained from organosolv process always gives a higher value of syringyl (S) units, which implies that the non-condensed syringal units were more easily degradable than the non-condensed guaiacyl ones during the treatment. Although aldehydes are the dominant product, other phenolic acids also can be detected from the nitrobenzene oxidation. From Table 3.12, it is observed that autohydrolyzed organosolv lignins (AH EOL, AHN EOL and AHD

EOL) produce lower aromatic aldehydes (namely syringaldehyde and p-hydroxybenzaldehyde) with high phenolic acids than organosolv lignin pretreated with dilute sulphuric acid, DAP EOL.

According to Wayman and Chua (1979), the decrease of aromatic aldehydes from autohydrolyzed lignin was attributed mainly to condensation reactions that involve the formation new C-C bonds. These will produce lignin structures which are much less amenable to oxidize the phenolic acids. Besides, the low yield of aromatic aldehydes can also be attributed to the physicochemical incorporation of other materials (Klemola and Nyman, 1966), in this case carbohydrate degradation products and organic scavengers (2-naphthol and 1,8-dihydroxyanthraquinone). It is highly suspected that these reaction intermediates participate in lignin condensation reaction and later result in the formation of new C-C bonds and affect the condensed nature of organosolv lignin. The S/G ratio of AH EOL lignin was observed to be higher than others. During autohydrolysis, lignin and non-lignin degradation products form prominent reactive intermediates. It was postulated that the reactive intermediates were Hibbert ketones, p-hydroxybenzoic acids, syringic acids, vanillic acids, furfural and their precursors (Klemola and Nyman, 1966; Klemola, 1968). The increase of S/G ratio was due to the chemical reaction between remaining non-condensed guaiacyl with the reactive intermediates that result in new C-C bonds and consequently contribute to the increase in S/G ratio (Wayman and Chua, 1979).

3.3.9 Lignin antioxidant activity by oxygen uptake method

The oxygen uptake profile during autoxidation of methyl linoleate is shown in Figure 3.22. By comparing the linear curve of methyl linoleate alone (control), it appears that all different pretreated organosolv lignin samples exhibited antioxidant activity by slowing down the oxidation of methyl linoleate. Lignins recovered at higher severity level (AH EOL, OUI: 81 %; AHN EOL, OUI: 77 % and AHD EOL, OUI: 78 %) seems to be more efficient than DAP EOL lignin (OUI: 73 %). As reproducibility of OUI is 5% (El Hage *et al.*, 2012), from Figure 3.22, autohydrolyzed organosolv lignins (AH EOL, AHN EOL and AHD EOL) seems to have a better antioxidant activity than dilute sulphuric acid treated organosolv lignin, DAP EOL and untreated organosolv lignin (refer to subchapter 3.2.7).

The assessment of autohydrolysis pretreatment has greatly increased the antioxidant activity of organosolv lignins. Besides, positive correlations between the OUI values to the total HGS phenolic –OH content (refer to subchapter 3.3.4) was observed. As seen from previous analysis with ^{31}P NMR, autohydrolyzed organosolv lignin showed a very high phenolic hydroxyl content (AH EOL_{phenolic –OH}: 1.67 mmol g⁻¹; AHN EOL_{phenolic –OH}: 1.50 mmol g⁻¹ and AHD EOL_{phenolic –OH}: 1.49 mmol g⁻¹) compared to dilute sulphuric acid treated (DAP EOL_{phenolic –OH}: 1.14 mmol g⁻¹) and untreated organosolv lignin (EOL_{phenolic –OH}: 1.35 mmol g⁻¹). Very severe conditions (used during autohydrolysis pretreatment) have enhanced the cleavage of α - and β -ether linkages between lignin structural units which later led to the formation of new phenolic –OH when delignification process takes place (Pan *et al.*, 2006). Thus the

process generates more phenolic –OH than aliphatic –OH. Hence, it seems that the OUI % increases with the increase of the phenolic –OH content of lignin.

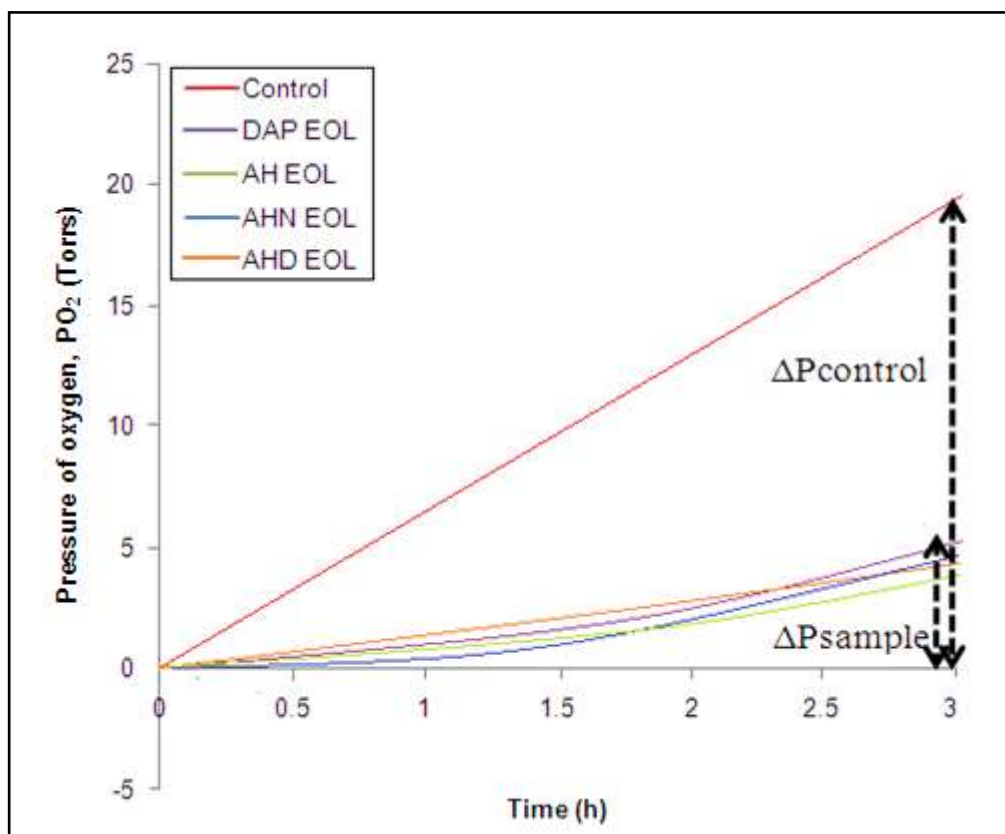


Figure 3.22: Oxygen uptake profile of different pretreated organosolv lignins.

The radical scavenging ability of phenolic lignin compounds depends not only on the withdrawal of hydrogen atom but also on the stability of radical formed (Pan *et al.*, 2006). *Ortho*-methoxyl substitution (which was exhibited in S and G units) might provide resonance stabilization to the incipient phenoxyl radical that can increase the antioxidant activity (Barclay *et al.*, 1997; Nadji *et al.*, 2009). Therefore the antioxidant activity of lignin should increase with the free phenolic –OH and *ortho*-methoxyl S and G group content, through the stability of radical formed. Besides, lignin with high molecular weight and polydispersity values tend to experience poor

antioxidant activity (El Hage *et al.*, 2012). It was also observed that modified organosolv lignins that possess low molecular weight (AHN EOL_{MW}: 3093 g mol⁻¹ and AHD EOL_{MW}: 3624 g mol⁻¹) tends to experience high antioxidant activity than unmodified organosolv lignin (EOL_{MW}: 5151 g mol⁻¹). This observation is consistent with the previous report regarding the effect of molecular weight of lignin on antioxidant activity (Pan *et al.*, 2006; El Hage *et al.*, 2012). The low molecular weight lignin resulted from the inter-unit bonds cleavage in lignin structure is also accompanied by an increment of phenolic –OH and decrease of aliphatic –OH.

3.3.10 Lignin antioxidant activity by reducing power assay

Figure 3.23 shows the reducing power of different pretreated and untreated (EOL) organosolv lignins as a function of their concentration. In this study, the reducing power of organosolv lignins has increased with concentration. All pretreated organosolv lignins show better reducing power than untreated organosolv lignin. In addition the reducing power of lignin incorporated with 1,8-dihydroxyanthraquinone (AHD EOL) was observed to be better than lignin incorporated with 2-naphthol (AHN EOL) and unmodified organosolv lignin (EOL). Even though both modified lignin possess higher S unit content (that might also give better antioxidant activity through the resonance stabilization of *ortho*-methoxyl substitution), it is observed that the reducing power ability of the modified lignin mainly relies on the properties of the organic scavengers used. A previous study has reported that the reducing power of some chemical compounds might be due to their hydrogen-donating ability (Shimada *et al.*, 1992). Hence, the higher reducing power of AHD EOL is probably due to the presence of more electronegative organic scavenger of 1,8-

dihydroxyanthraquinone on the lignin moiety. Therefore, the AHD EOL lignin might contain higher amounts of reductants, which are able to reduce Fe^{3+} ion into Fe^{2+} ions. The better antioxidant property exhibited by the modified lignin would indeed be beneficial for the inhibition of mild steel corrosion.

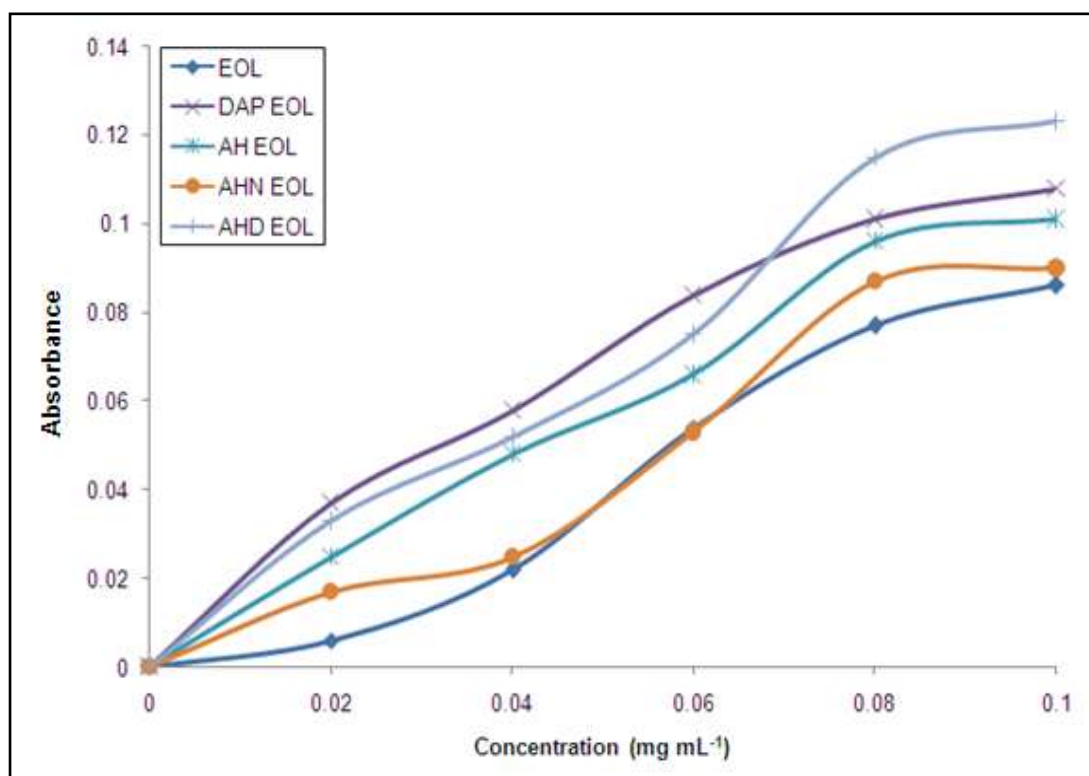


Figure 3.23: Antioxidant profile of different pretreated and untreated organosolv lignins by reducing power assay obtained at 700 nm.

3.4 Characterization of OPF lignins fractionated by ultrafiltration technique

The resulted permeates and retentates of three different types of lignins (Kraft, soda and organosolv) after passing through 5 kDa ultrafiltration membrane were collected and characterized in order to determine their physicochemical properties. The flow flux for each sample was maintained at around 9 mL min⁻¹ for Kraft and soda lignin and 0.30 mL min⁻¹ for organosolv lignin. It was found that the highest recovery of permeated lignin fraction (LFR %, w/w) was obtained by soda lignin followed by

Kraft and organosolv lignin ($LFR_{\text{soda}}: 12.29 \pm 0.54 \% > LFR_{\text{Kraft}}: 5.41 \pm 2.04 \% > LFR_{\text{organosolv}}: 1.48 \pm 0.15 \%$). Unexpectedly, the LFR value of all lignin samples shows unclear trend with their average molecular weight, M_w (refer to subchapter 3.2.4). Indeed, Kraft lignin shows low permeate yield due to the higher average molecular weight ($M_{w\text{Kraft}}: 2063 \text{ g mol}^{-1}$) than soda lignin ($M_{w\text{soda}}: 1660 \text{ g mol}^{-1}$). Higher M_w of Kraft lignin makes it difficult to pass through smaller membrane cut-off (5 kDa). In contrast, organosolv lignin gives lower permeate yield even though it has a low M_w value ($M_{w\text{organosolv}}: 1215 \text{ g mol}^{-1}$). Lower permeate yield for organosolv lignin could be explained by its low chemical affinity with the relatively high hydrophilic polyethersulfone membrane and also by the use of aqueous ethanol as mobile phase. In addition, during organosolv pulping the lignin was extracted from the raw material, which produced different sizes and shapes of lignin fragments (Toledano, 2012). Besides, it should be understood that the ultrafiltration method produces not only product fractionation but also product concentration. Hence, all retentates presented high lignin concentration. Since all permeates could possess low molecular weight (LMW) of lignin, it was further characterized and subjected for the next study.

3.4.1 FTIR analysis

The FTIR spectra of the obtained ultrafiltration fractions are shown in Figure 3.24. In this study, the following structure signals were detected; aromatic phenylpropane vibrations ($1600, 1515 \text{ and } 1427 \text{ cm}^{-1}$), aromatic and aliphatic $-\text{OH}$ groups stretching ($3400 \text{ and } 1033 \text{ cm}^{-1}$), C-H in methyl and methylene bonds ($2923, 2850 \text{ and } 1462 \text{ cm}^{-1}$).

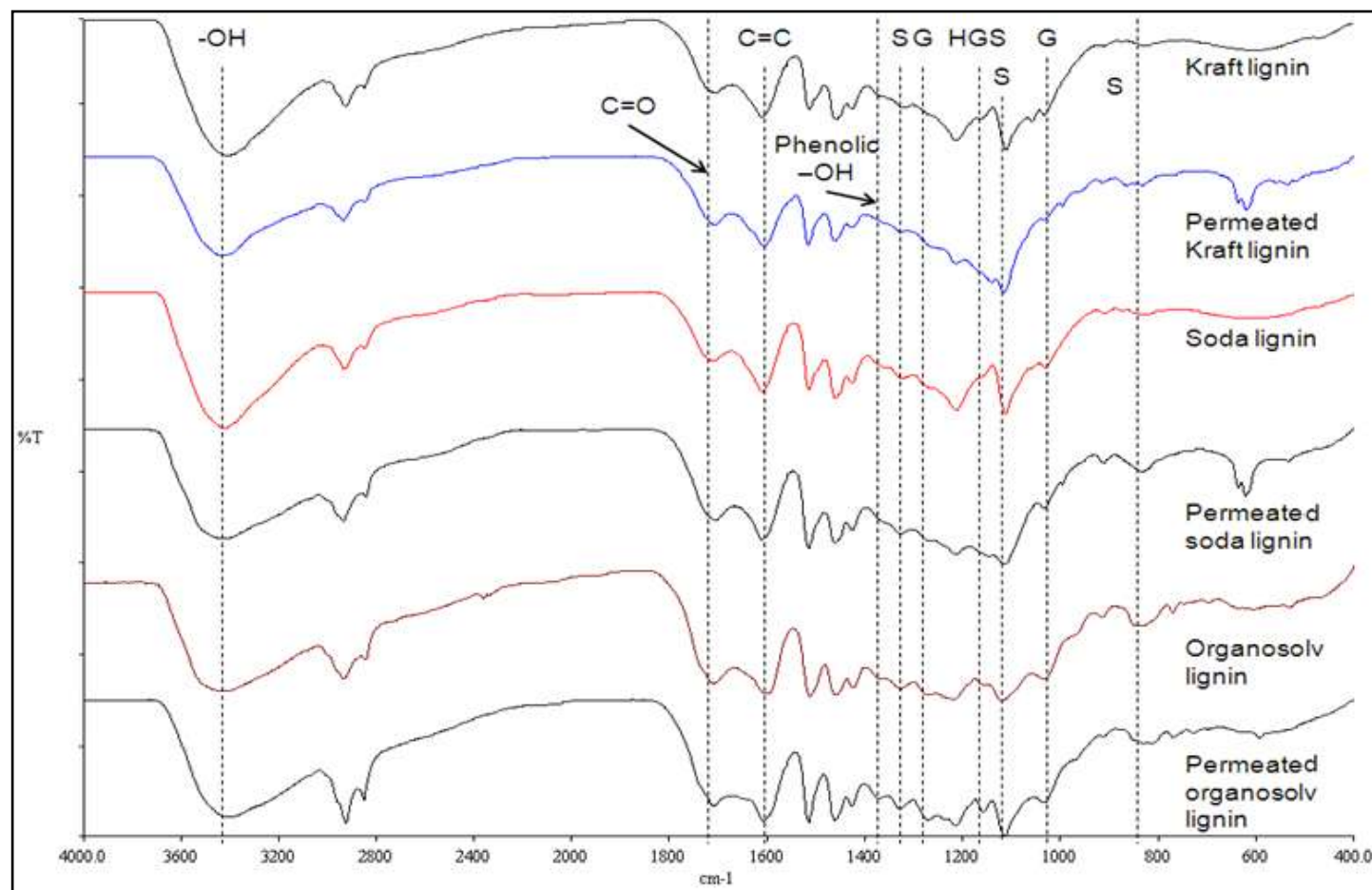


Figure 3.24: FTIR spectra of lignin obtained before and after ultrafiltration (5 kDa) of Kraft, soda and organosolv solutions.

The signals for C=O stretching in unconjugated ketone and conjugated carboxylic groups (1706 cm^{-1}), C-O-C bridges (1217 cm^{-1}) and aromatic C-H out-of-plane deformation (833 cm^{-1}) were also observed. This result is in good agreement with previous studies with different types and fractions of lignin after ultrafiltration (Alriols *et al.*, 2010; Garcia *et al.*, 2010; Toledano *et al.*, 2010a; Toledano *et al.*, 2010b). A small band at 620 cm^{-1} which was detected for both Kraft and soda lignin fractions was attributed to hemicelluloses and silicates. This suggested that lignin fractions obtained through acid precipitation contains hemicelluloses contamination. It was believed that suspended lignin drags the hemicellulose and lignin-carbohydrate complex (LCC) when precipitation occurred (Toledano *et al.*, 2010b). Organosolv lignin fraction showed higher intensities in aliphatic/aromatic -OH groups and C-H bands as compared to organosolv lignin before the ultrafiltration process. Meanwhile soda lignin fraction showed intensified peak at 1700 cm^{-1} which is attributed to C=O conjugated aromatic bonds (Hibbert ketones) presented in quinonic structures.

Besides these typical lignin structure bands, signals that are associated with syringyl (S) and guaiacyl (G) were also detected. The S-type aromatic C-H in-plane and out-of-plane deformations were observed at 1116 and 833 cm^{-1} while breathing S ring with C-O stretching gave a signal at 1327 cm^{-1} . In addition, breathing G ring with C-O stretching (1265 cm^{-1}), G-type aromatic C-H in-plane and out-of-plane bending (1033 cm^{-1}) were found respectively. It was noticed that the S-bands intensity of all lignin fractions were higher than the G-bands. According to Alriols *et al.* (2010), the intensity of signal was dependant on the lignin fraction cut off. Lignin with higher percentages of G units will produce lignin fraction with high molecular weight

through the formation of C5 bonds. In the case of S units, it is impossible to form C5 bonds as they have C5 position substituted by the methoxy groups. Therefore, the low membrane cut-off used in this study (5 kDa) will produce lignin fraction with higher S-band intensity (low molecular weight) and this observation is in good agreement with study done by Alriols *et al.* (2010).

3.4.2 ^{31}P NMR

The quantitative ^{31}P NMR values after derivatization with TMDP and their corresponding spectra of the resulted lignin fraction samples are shown in Table 3.13 and Figure 3.25. From this data, it can be seen that the organosolv lignin fraction produce highest aliphatic –OH content (due to a lower dehydration/degradation of lateral chains produced after organosolv treatment) as compared to Kraft and soda lignin fractions. The sharp peak observed at 147 ppm for both Kraft and soda lignin fractions could corresponds to secondary (*erythro* and *threo*) aliphatic –OH, while the peak at 145.8 ppm for organosolv lignin fraction was assigned to primary aliphatic –OH groups. This is in good agreement to previous analysis that organosolv lignin gave higher primary aliphatic –OH content whereas alkaline lignins (Kraft and soda) have more secondary aliphatic –OH than primary aliphatic –OH (refer to subchapter 3.2.3).

In addition, some increment of the total HGS phenolic –OH content than the crude was observed for soda (1.84 mmol g⁻¹) and organosolv (1.52 mmol g⁻¹) lignin fractions. However, the total HGS phenolic –OH content for Kraft (1.75 mmol g⁻¹) lignin fraction shows some reduction. According to Garcia *et al.* (2010), the

molecular weight of crude lignin may reflect the total phenolic content in the lignin fractions.

Table 3.13: Permeate lignin fractions characterized by ^{31}P NMR.

ppm	Assignments	mmol g ⁻¹		
		Permeated Kraft	Permeated Soda	Permeated Organosolv
150-145	Aliphatic –OH	0.77	0.69	0.89
144.8	Cyclohexanol (Internal Standard)			
144-140	Syringyl –OH	1.10	1.21	0.99
140-138	Guaiacyl –OH	0.58	0.47	0.44
138-136	p-hydroxyphenyl –OH	0.07	0.16	0.08
135-133	Carboxylic acid	-	-	-

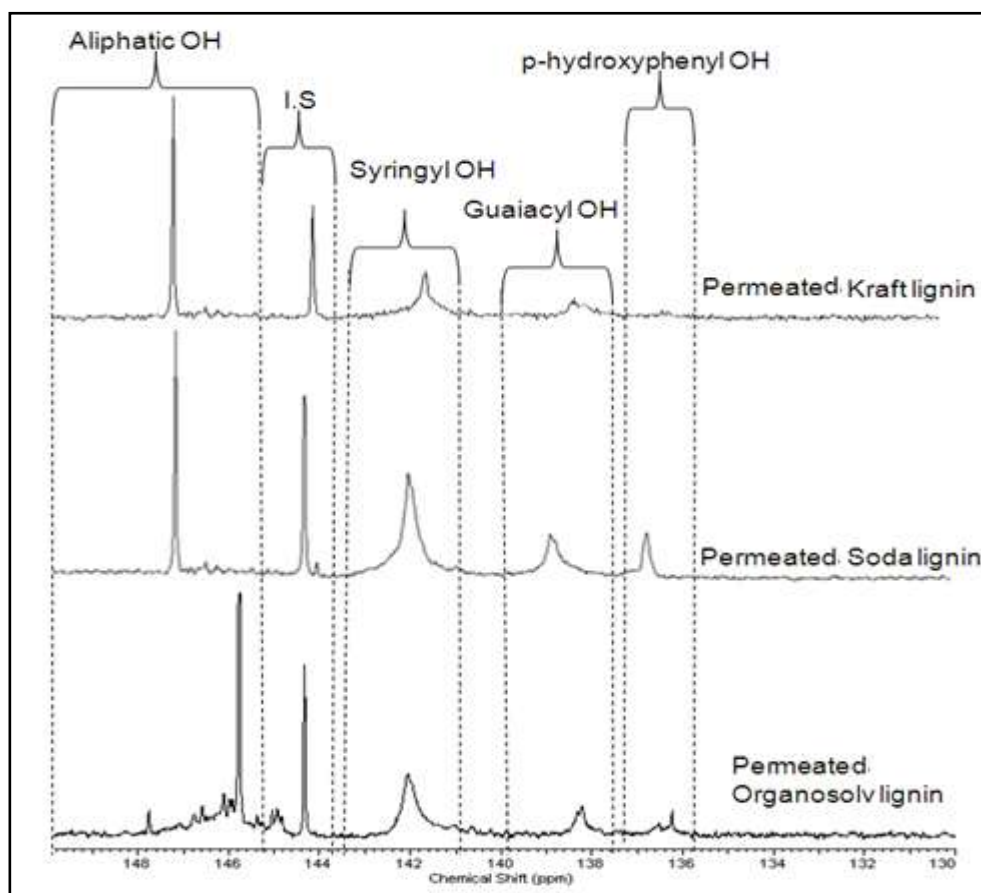


Figure 3.25: ^{31}P NMR spectra of OPF lignin fractions after ultrafiltration (5 kDa) in expanded region.

Higher M_w value of crude lignin will give lignin fractions with lower total phenolic content. Perhaps that is why crude Kraft lignin (M_w : 2063 g mol⁻¹) produces lignin fraction with low total phenolic content. Hence, the amount of phenolic content of lignin fractions through the utilization of low ultrafiltration membrane cut-off will strongly rely on their crude molecular weight.

3.4.3 Molecular weight

Gel permeation chromatography (GPC) was carried out to obtain the distributions of molecular weight of different acetylated lignin fractions obtained by ultrafiltration. The average molecular weight (M_w), number average (M_n) and polydispersity ($PD = M_w/M_n$) of lignin fractions are shown in Table 3.14. Clearly, it can be seen that the molecular weight distributions of lignin fractions were significantly decreased after the ultrafiltration process. The ultrafiltration technique also produced lignin fractions with low polydispersity. The low PD values indicated high fraction of lignin with low molecular weight (LMW) (Toledano *et al.*, 2010b).

As explained earlier, the low PD values were due to the possibility of forming C-C bonds that is mainly related to the aromatic C5 ring structures in G-type and S-type units. It was believed that G-type units are able to form this kind of bonds and it not possible for S-type units due to the presence of methoxy functional groups at both C3 and C5 position. Thus, lignins that are mostly composed of G units tend to show higher M_w (Glasser *et al.*, 1993; Toledano *et al.*, 2010a; Garcia *et al.*, 2010). This is in agreement with the ³¹P NMR study where Kraft lignin fraction gave higher guaiacyl –OH content compared to soda and organosolv lignin fractions.

Table 3.14: GPC results of weight-average (M_w), number-average (M_n) and polydispersity (PD) of OPF lignin fractions after ultrafiltration.

	Permeated Kraft lignin	Permeated Soda lignin	Permeated Organosolv lignin
M_w (g mol ⁻¹)	1394	955	848
M_n (g mol ⁻¹)	1064	837	823
M_w/M_n (polydispersity)	1.31	1.14	1.03

Generally, the reactivity of lignins with high fractions of low molecular weight, LMW molecules are higher than the one with high molecular weight, HMW (Pizzi, 1994). High fractions of LMW are suitable to be used as a component of phenol-formaldehyde resins or an extender due to their high reactivity (Benar *et al.*, 1999; Goncalves and Benar, 2001; El Mansouri and Salvado, 2006).

3.4.4 Thermal behavior

3.4.4.1 Thermal gravimetric analysis

In order to study the decomposition of organic polymers, the thermogravimetric analysis (TGA) was carried out for the ultrafiltrated fractions. The TG curves (Figure 3.26) show three major steps during sample degradation and as similarly reported by several authors (Alriols *et al.*, 2010; Garcia *et al.*, 2010; Mohamad Ibrahim *et al.*, 2011). Similar to other lignin thermograms, the first one corresponded to water evaporation (observed around 90 °C) and the second one was related to the degradation of hemicelluloses (at around 200 to 300 °C), which are present in the lignin samples. These degradation peaks were more pronounced for the alkaline lignin fractions (Kraft and soda permeates) which entail small hemicellulose

impurity content (as observed in the FTIR spectra). The third step was related to the degradation of lignin, which occurred progressively from 200 up to 400 °C.

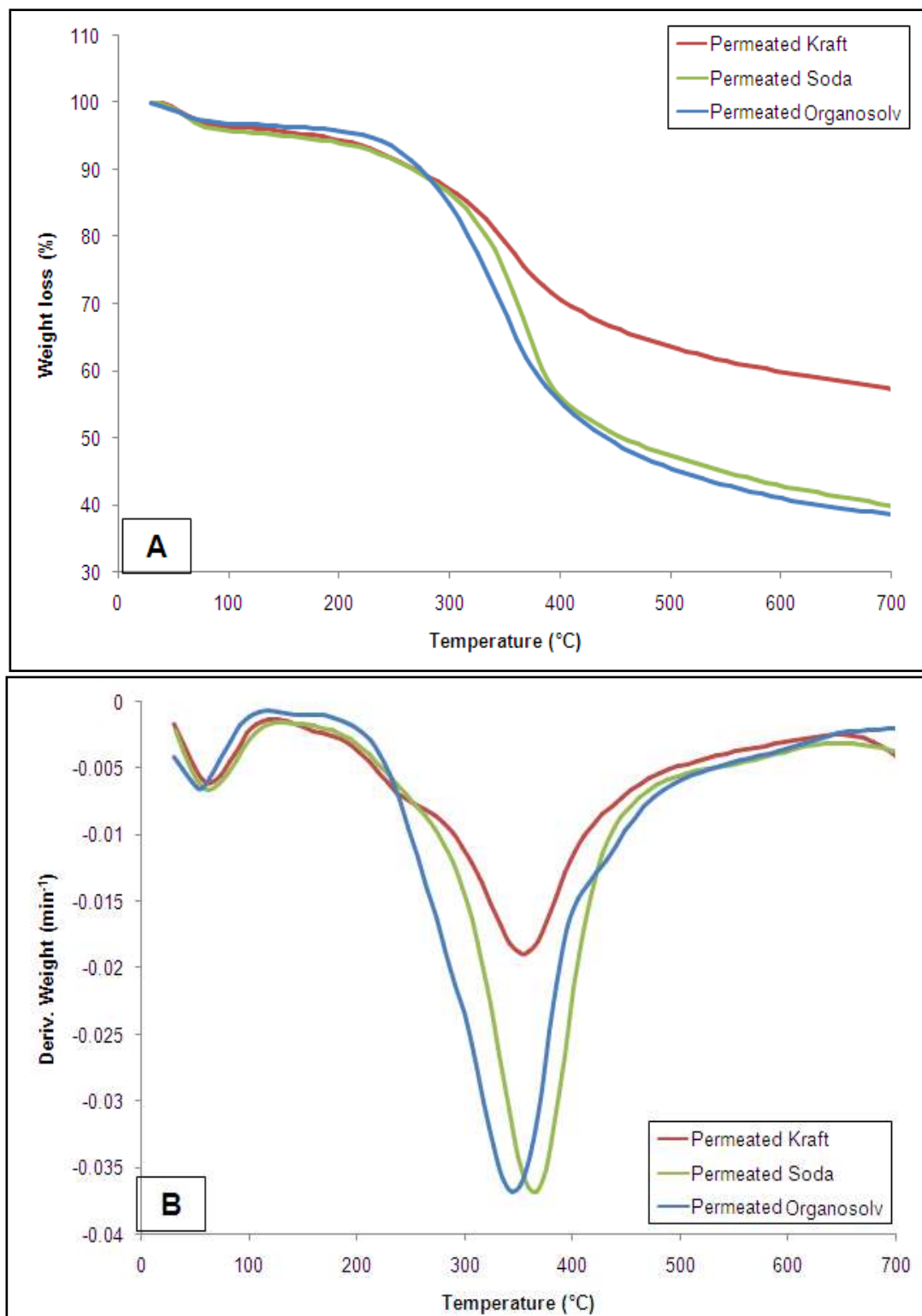


Figure 3.26: (A) TG and (B) DTG curves for OPF lignin fractions after ultrafiltration (5 kDa).

In some cases, wide degradation peaks suggested the presence of hemicellulose-lignin complexes. This phenomenon was observable to that of organosolv lignin fraction. The lower DTG temperature obtained for organosolv lignin fraction (DTG_{max}: 340 °C) than Kraft and soda lignin fractions (DTG_{max}: 380 °C) was due to the less recondensed structure (less C-C bonds with more β-O-4 linkages) of organosolv lignin. Besides, this could also due to the decomposition temperature of hemicellulose-lignin intermediate (Toledano *et al.*, 2010b). It was believed that the maximum weight loss rate depended strongly on the lignin structure, particularly their functional groups and linkages formed.

Additionally, the residue obtained after the thermal degradation was also related to the lignin molecule structural complexity and their grade of linkages. High percentage of residue will imply high thermal stability of the sample (Dominguez *et al.*, 2008). However, high residue percentage could also indicate the presence of inorganic matter in the lignin samples (Garcia *et al.*, 2010). In this analysis, it was found that Kraft lignin fraction shows high residue value (50-60 %) due to the use of sodium salts (sodium hydroxide and sodium sulfide) during crude delignification.

3.4.4.2 Differential scanning calorimetry

The thermal behavior of lignin fractions were further analyzed with differential scanning calorimetry (DSC) to study the thermal effect associated with physical and/or chemical changes. The obtained organosolv lignin fraction presented a lower glass transition (T_g: 49.39 °C) value than alkaline lignin fractions (Kraft T_g: 51.58 °C; Soda T_g: 55.28 °C). It was reported previously by other authors (Feldman and

Banu, 1997; Lora and Glasser, 2002; Alriols *et al.*, 2010) that the T_g values of alkaline lignins (Kraft and soda) were higher than for organosolv ones. Besides, it can be seen that the ultrafiltration lignin fractions T_g increases with the lignin molecular weight. This confirms that the fractionation process has a great influence on the obtained lignin molecular weight (Randhir *et al.*, 2004; Lora, 2008).

This observation is also in concordance with the results obtained by other techniques (FTIR, ^{31}P NMR and GPC) where the relation between lignin molecular weight and the S and G groups content was established. Fractionation of lignin using low membrane cut-off (5 kDa) will produce small molecular weight fractions with lower G content (units that contribute to the formation of C-C bonds) and low T_g value.

3.4.5 Lignin antioxidant activity by oxygen uptake method

The results of the antioxidant activity of different lignin fractions obtained by the oxygen uptake inhibition (OUI) method are shown in Figure 3.27. In this study, it was found that fractionation of lignin samples through the ultrafiltration system improved their antioxidant activity compared to the crude lignins (refer to subchapter 3.2.7). Soda lignin fraction shows higher OUI value followed by Kraft and organosolv lignin fractions ($\text{OUI}_{\text{Soda}}: 83 \% > \text{OUI}_{\text{Kraft}}: 79 \% > \text{OUI}_{\text{Organosolv}}: 77 \%$). As previously discussed, the performance of the lignin antioxidant activity could be dependent on their phenolic $-\text{OH}$ content. It can be noticed from ^{31}P NMR analysis that Soda lignin fraction has higher HGS phenolic $-\text{OH}$ (1.84 mmol g^{-1}) content than Kraft (1.75 mmol g^{-1}) and organosolv (1.51 mmol g^{-1}) fractions. Thus a good correlation between lignin phenolic $-\text{OH}$ content with their OUI value affirmed that

membrane technology is a suitable process for the production of high antioxidant capacity.

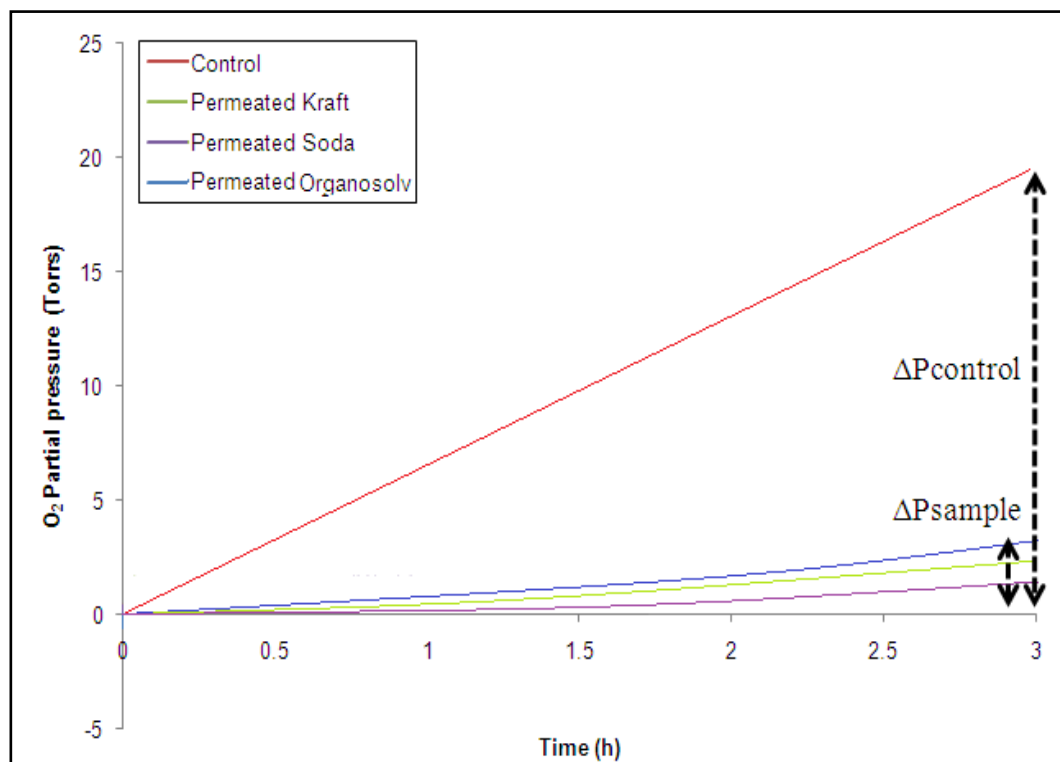


Figure 3.27: Oxygen uptake profile of different lignin fractions after ultrafiltration (5 kDa).

Another factor that strongly affected the radical scavenging activity of lignin was the heterogeneity and purity (Dizhbite *et al.*, 2004). The presence of hemicellulose components could diminish the antioxidant capacity of lignin samples; due to the formation of hydrogen bondings between carbohydrates and lignin phenolic –OH groups that later interfere with the antioxidant properties (Garcia *et al.*, 2010). It was proposed from the TGA analysis that organosolv lignin fraction could contain higher carbohydrate contamination (hemicellulose-lignin complexes) than other lignin fractions. Thus, this could corroborate the low antioxidant capacity of organosolv lignin fraction as observed from the OUI value. Besides, high S-type units in both

soda and Kraft lignin fractions can also contribute to a better antioxidant activity. As mentioned earlier, the *ortho*-methoxyl substitution exhibited in S might provide resonance stabilization to the incipient phenoxyl radical that can increase the antioxidant activity (Barclay *et al.*, 1997; Nadji *et al.*, 2009). Therefore the antioxidant activity of lignin fraction should increase with the free phenolic –OH and *ortho*-methoxyl content, through the stability of the radical formed.

3.4.6 Lignin antioxidant activity by reducing power assay

In Figure 3.28, dependence of the reducing power of lignin fractions on its concentration was observed and reached a plateau at 0.08 mg L⁻¹. The reducing power of all ultrafiltrated lignins was higher than the crude lignin ones (refer to Figure 3.10). In addition, similar trends of antioxidant capacity through lignin reducing power and oxygen uptake inhibition method were seen. Soda lignin fraction gives better reducing power ability compared to Kraft and organosolv lignin fractions. The improvement of lignin reducing power ability was again related to their phenolic –OH and S unit content, as discussed earlier in subchapter 3.4.5.

As seen in Figure 3.28, lignin reducing power ability increased and behaved almost similar to standard S (syringaldehyde) unit. Thus, this confirms that lignin samples with high S unit content would probably improve the antioxidant ability. It could be affirmed that fractionation of lignin by ultrafiltration method produced high phenolic –OH content and better antioxidant activity. All these properties are useful for various applications especially as a corrosion inhibitor.

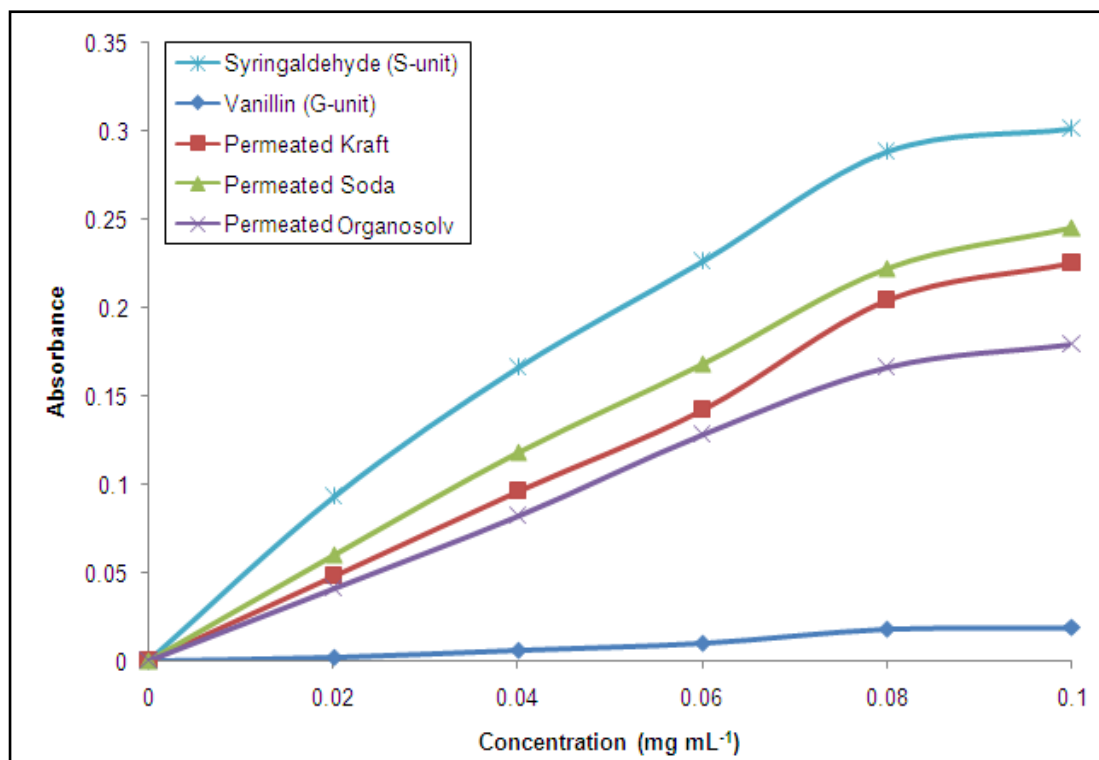


Figure 3.28: Antioxidant profile of different lignin fractions by reducing power assay obtained at 700 nm.

3.5 Corrosion inhibition studies of modified (AHN EOL and AHD EOL) and ultrafiltrated (Kraft, soda and organosolv fractions) OPF lignins in 0.5 M HCl

The corrosion inhibition studies of lignins were carried out. In this study, modified (autohydrolyzed organosolv lignin incorporated with 2-naphthol (AHN EOL) and 1,8-dihydroxyanthraquinone (AHD EOL)) and ultrafiltrated (Kraft, soda and organosolv fractions) lignins were chosen to be evaluated for their inhibition properties towards the corrosion of mild steel in 0.5 M hydrochloric acid (HCl) solutions. The improved properties of modified and ultrafiltrated lignins (in terms of phenolic –OH content, low molecular weight and antioxidant activity) are expected to affect the corrosion inhibition efficiency (*IE*).

3.5.1 Preliminary dissolution test of lignins

One of the most important aspects in corrosion inhibition studies is to determine the solubility of each inhibitor in the tested electrolyte; particularly in aqueous medium, as water and oxygen play important roles in corrosion processes. Therefore, it can be assumed that the solubility of the inhibitor could influence the corrosion inhibition process. Also, to complement the characterization work, the dissolution test of lignin is needed to correlate the lignin solubility with their improved properties (higher phenolic –OH content, small molecular fractions and better antioxidant activity). The dissolution profile of modified (AHN EOL and AHD EOL) and ultrafiltrated (Kraft, soda and organosolv) lignin are presented in Figure 3.29.

In Figure 3.29A, it can be seen that the modified lignin and the unmodified organosolv lignin exhibited different dissolution curves but all showed increased dissolution with time. The results show that about 22.14 % of AHD EOL lignin, but only 2.87 % of unmodified organosolv lignin (EOL) and 2.07 % (w/w) of AHN EOL, have dissolved at 600 min. The solubility of AHD EOL lignin was 7.71 times higher than the solubility of EOL. Better solubility of lignin was obtained when 1,8-dihydroxyanthraquinone was incorporated into the lignin structure. This is due to the fact that 1,8-dihydroxyanthraquinone contains more polar hydroxyl functional groups than 2-naphthol, thus increases the hydrophilicity of lignin and consequently promotes dissolution in water.

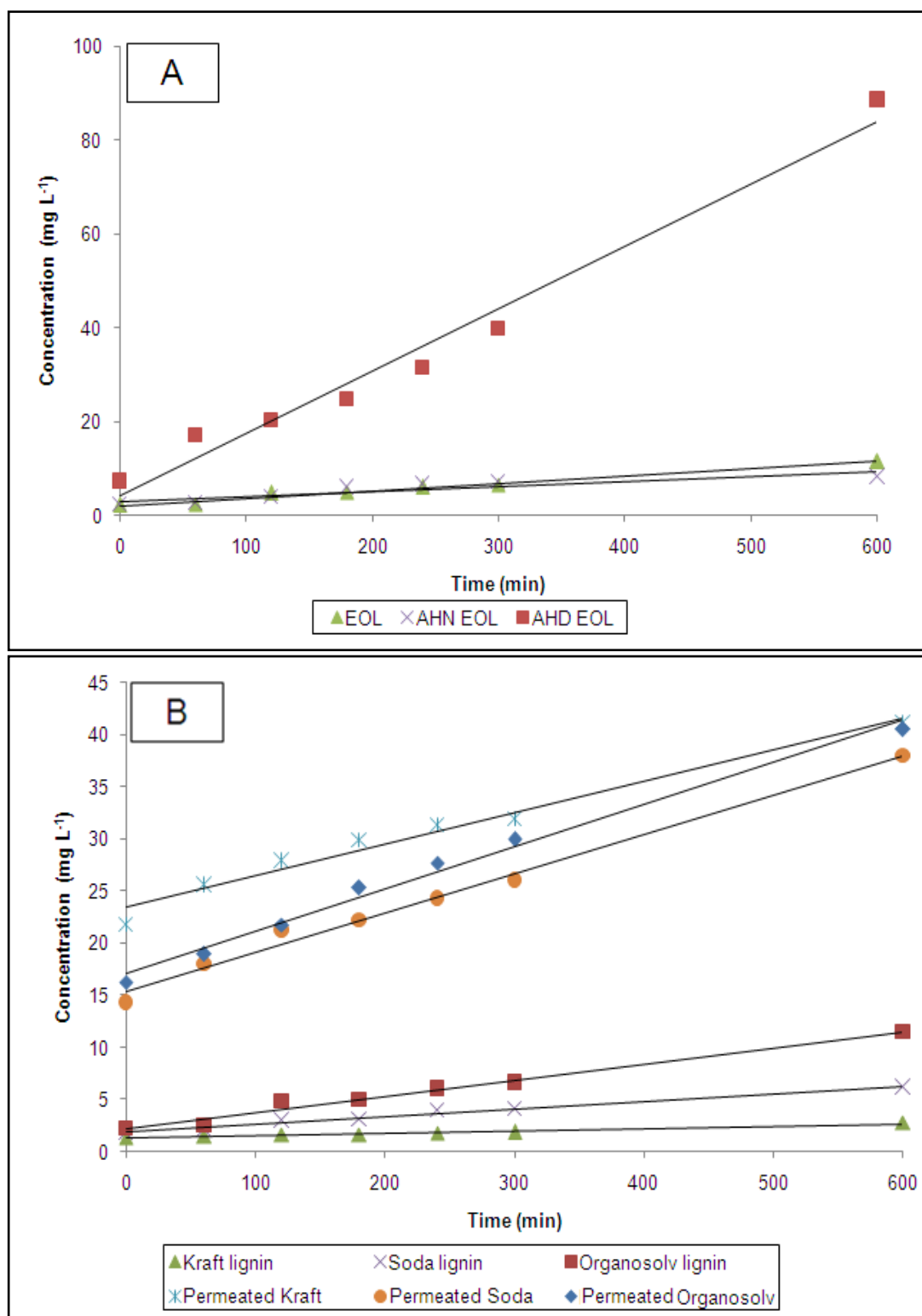


Figure 3.29: Dissolution profiles of modified, ultrafiltrated and crude lignins.

In addition, Figure 3.29B shows that the dissolution of all lignin fractions (after ultrafiltration) was greater compared to the crude lignins (D_{Kraft} : 0.69 %; D_{Soda} : 1.57 % and $D_{\text{Organosolv}}$: 2.07 %). Kraft lignin fraction presented the highest percentage of dissolution and followed by organosolv and soda lignin fractions ($D_{\text{PermeateKraft}}$: 10.27 % > $D_{\text{PermeateOrganosolv}}$: 10.11 % > $D_{\text{PermeateSoda}}$: 9.49 %). Better dissolution properties of all lignin fractions can be rationalized by two major factors; 1) low molecular weight/polydispersity (due to the uniformity of the overall packing structures) (Alriols *et al.*, 2009) and 2) higher phenolic content (more polar structures), which promotes better hydrogen bonding with water molecules. Therefore, it can be affirmed that modification (with more polar organic scavenger) and fractionation of lignin could substantially improve their hydrophilicity and applicability as corrosion inhibitors.

3.5.2 Electrochemical measurements of the mild steel corrosion in 0.5 M HCl solution

3.5.2.1 Electrochemical impedance spectroscopy (EIS)

The corrosion of mild steel in 0.5 M HCl solution in the presence of modified (AHN EOL and AHD EOL) and ultrafiltrated (Kraft, soda and organosolv) lignin samples were investigated by the electrochemical impedance spectroscopy, EIS at room temperature after an exposure period of 30 min. An addition of 2 % (v/v) methanol was required to obtain maximum solubility of lignin samples. Tables 3.15 and 3.16 list the impedance parameters (charge-transfer resistance, R_{ct} ; constant phase element, CPE, exponential value of CPE, n and percentage inhibition efficiency, IE

%) of the Nyquist plots of the modified and ultrafiltrated lignins at different concentrations.

Table 3.15: Electrochemical impedance parameters for mild steel in 0.5 M HCl solution in the absence and presence of AHN EOL and AHD EOL lignin at 303 K.

Concentration (ppm)	R_{ct} ($\Omega \text{ cm}^2$)	CPE ($\mu\text{F cm}^{-2}$)	n	IE (%)
0.5 M HCl	61.59	211	0.7149	-
10 ppm AHN EOL	68.41	181	0.7899	9.97
50 ppm AHN EOL	71.16	179	0.8336	13.45
100 ppm AHN EOL	87.58	167	0.8412	29.68
250 ppm AHN EOL	119.00	159	0.8610	48.24
500 ppm AHN EOL	383.00	144	0.8650	83.92
10 ppm AHD EOL	63.02	182	0.7573	2.27
50 ppm AHD EOL	85.77	168	0.7789	28.19
100 ppm AHD EOL	100.30	152	0.8400	38.59
250 ppm AHD EOL	319.90	146	0.8470	80.75
500 ppm AHD EOL	632.30	110	0.8476	90.26

Table 3.16: Electrochemical impedance parameters for mild steel in 0.5 M HCl solution in the absence and presence of different ultrafiltrated lignin fractions (5 kDa) at 303 K.

Concentration (ppm)	R_{ct} ($\Omega \text{ cm}^2$)	CPE ($\mu\text{F cm}^{-2}$)	n	IE (%)
0.5 M HCl	61.59	211	0.7149	-
10 ppm P.Kraft lignin	111.50	184	0.8119	44.76
50 ppm P.Kraft lignin	164.00	161	0.8142	62.45
100 ppm P.Kraft lignin	212.80	134	0.8152	71.06
250 ppm P.Kraft lignin	310.50	112	0.8188	80.16
500 ppm P.Kraft lignin	331.40	109	0.8119	81.42
10 ppm P.Soda lignin	82.85	179	0.8084	25.66
50 ppm P.Soda lignin	86.61	178	0.8100	28.89
100 ppm P.Soda lignin	131.00	167	0.8184	52.98
250 ppm P.Soda lignin	208.20	139	0.8428	70.42
500 ppm P.Soda lignin	482.00	93	0.8457	87.22
10 ppm P.Organosolv lignin	53.50	205	0.8146	-15.12
50 ppm P.Organosolv lignin	76.65	201	0.8205	19.65
100 ppm P.Organosolv lignin	85.20	193	0.8340	27.71
250 ppm P.Organosolv lignin	188.30	187	0.8384	67.29
500 ppm P.Organosolv lignin	376.80	158	0.8495	83.65

Meanwhile, the Nyquist plots for mild steel obtained at the interface in the absence and presence of modified and ultrafiltrated lignins at different concentrations are given in Figure 3.30 and 3.31, respectively. The impedance diagram obtained shows only one depressed semi-circle (at higher frequency) whereby the size increases as the inhibitor concentrations increased, indicating that the corrosion is mainly a charge transfer process (Aljourani *et al.*, 2009), and the formed inhibitive film (Chauhan and Gunasekaran, 2007; Satapathy *et al.*, 2009) was strengthened by the addition of modified and ultrafiltrated lignin molecules that increased the resistivity of the mild steel surface. The depressed semi-circle is a characteristic of solid electrodes and it often refers to the frequency dispersion which arises due to the roughness and other non-homogeneities of the surface (Bentiss *et al.*, 2005; Hassan *et al.*, 2007; Ahamad *et al.*, 2010).

It is worth noting that the change in the concentration of modified and ultrafiltrated lignins did not alter the shape of the impedance curves, suggesting that a similar mechanism of corrosion process is involved. The direct network of charge transfer and double layer capacitance ($R_{cr}-C_{dl}$) was said to give a poor estimation of inhibition system (Satapathy *et al.*, 2009). Therefore the constant phase element, CPE (Figure 3.32) is introduced in the equivalent circuit instead of a pure double layer capacitor to give a more accurate fit (Noor and Al-Moubaraki, 2008). The CPE, which is considered as the surface irregularity of the electrode, causes a greater depression in the Nyquist semi-circle where the metal/solution interface acts as a capacitor with the irregular surface (Hassan *et al.*, 2007; Ashassi-Sorkhabi *et al.*, 2008; Satapathy *et al.*, 2009).

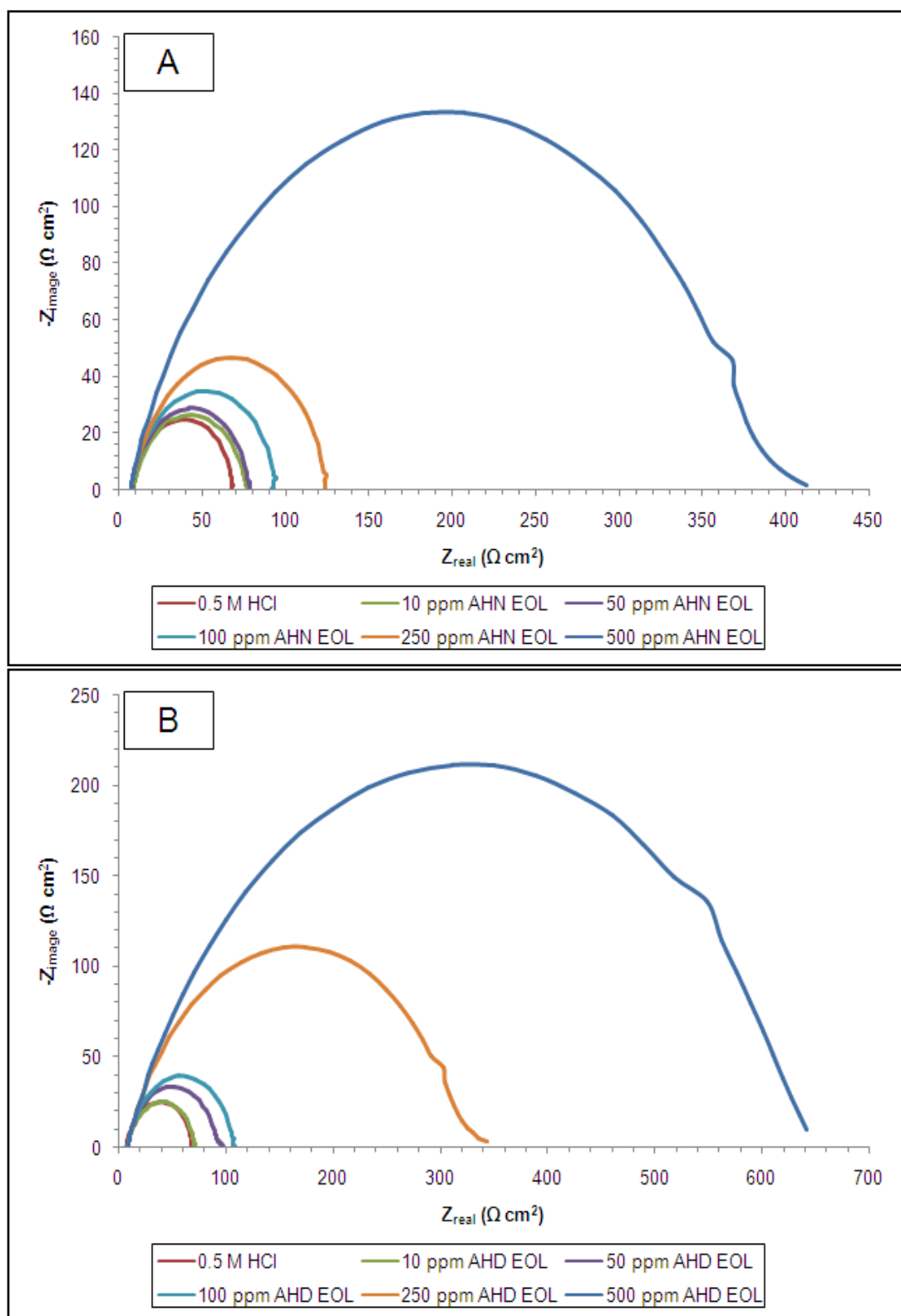


Figure 3.30: Nyquist plot of mild steel in 0.5 M HCl solution in absence and presence of; (A) AHN EOL and (B) AHD EOL lignin at 303 K.

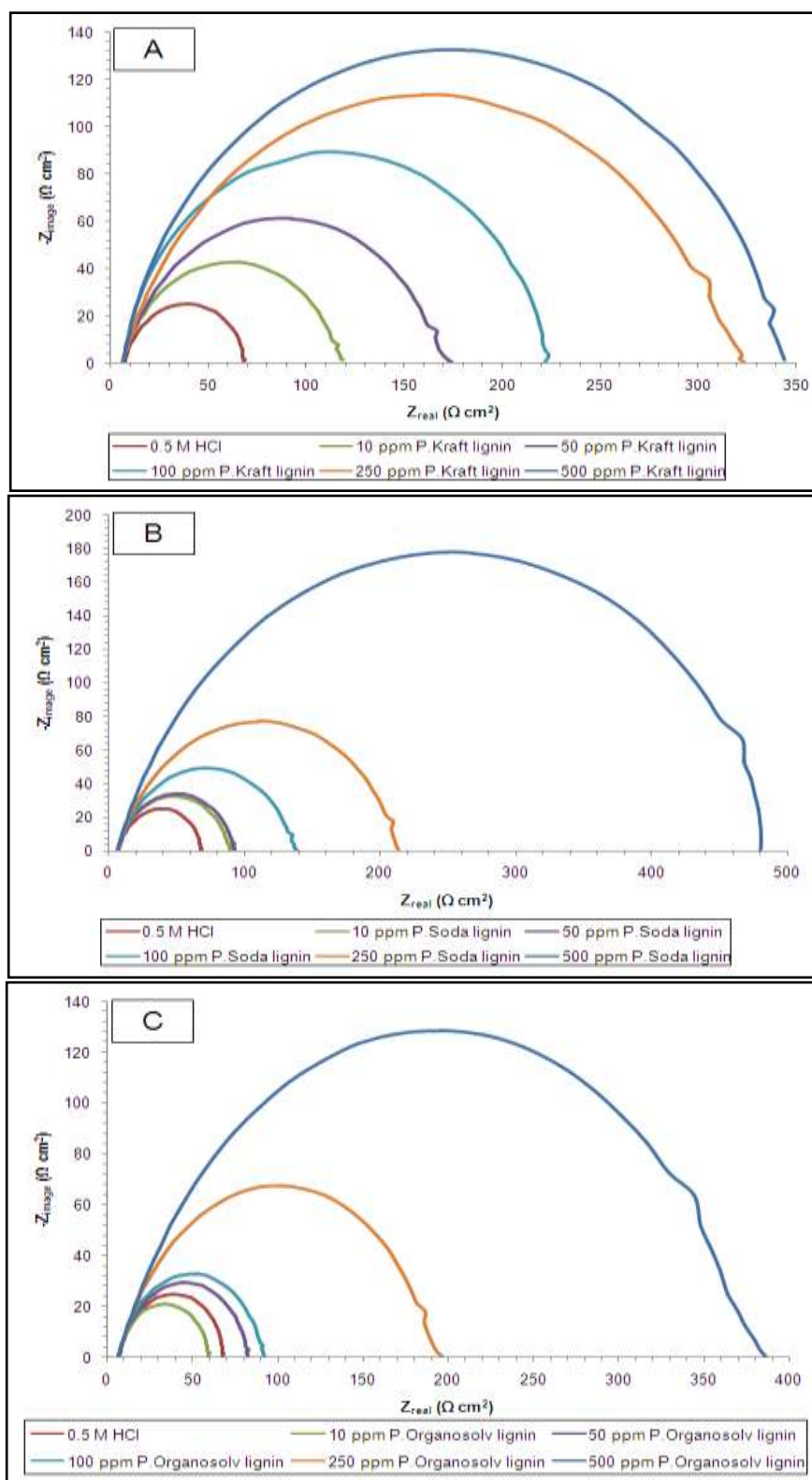


Figure 3.31: Nyquist plot of mild steel in 0.5 M HCl solution in absence and presence of; (A) Kraft, (B) Soda and (C) Organosolv lignin fractions at 303 K.

The impedance of the CPE is expressed as:

$$Z_{\text{CPE}} = \frac{1}{Y_0(j\omega)^n} \quad (3.1)$$

where Y_0 is the magnitude of the CPE, j is the imaginary unit, ω is the angular frequency ($\omega = 2\pi f$, where f is the AC frequency) and n is the CPE exponent (phase shift). From Table 3.15 and 3.16, the extrapolation of Nyquist plots with the corresponding Randles-CPE circuit model gives better data fitting. It can be noted that the corrosion of mild steel was significantly decreased (with the increase of R_{ct} values) after addition of lignin inhibitors. The addition of the lignin inhibitors increased the R_{ct} and decreased the CPE values, hence ensuring the highest corrosion inhibition efficiency at maximum concentration of 500 ppm ($IE_{\text{AHD EOL}}: 90.26 \% > IE_{\text{P.Soda}}: 87.22 \% > IE_{\text{AHN EOL}}: 83.92 \% > IE_{\text{P.Organosolv}}: 83.65 \% > IE_{\text{P.Kraft}}: 81.42 \%$).

According to other authors (Babic-Samardzija *et al.*, 2005; Abdel-Gaber *et al.*, 2006) the R_{ct} values is inversely proportional to the corrosion rate of metals. This shows that the addition of the modified and ultrafiltrated lignins will slow down the corrosion rate of mild steel in acidic solution. Additionally, the increased R_{ct} values with inhibitor concentration could suggest that more inhibitor molecules were adsorbed on the metal surface, hence leading to higher surface coverage (Ashassi-Sorkhabi *et al.*, 2008).

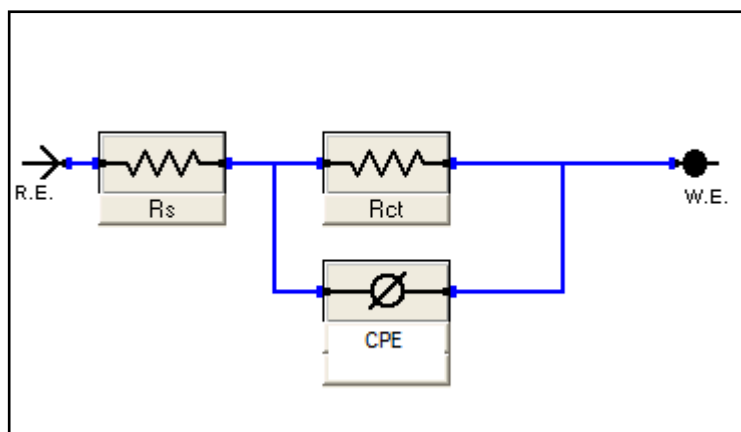


Figure 3.32: The electrical equivalent circuit of Randles-CPE for EIS measurement.

Meanwhile, the decrease of CPE was probably due to the reduction in the local dielectric constant and/or by the increase in the electrical double layer thickness (Stanly-Jacob and Parameswaran, 2010). The inhibitive film formed is increasing with increasing inhibitor concentration as more inhibitor molecules could adsorb on the metal surface (Yildiz *et al.*, 2014). Hence, lower CPE values were obtained. In this experiment, it was also observed that as the CPE decreased the n values increased with the addition of modified and ultrafiltrated lignin inhibitors. The increment was probably due to the reduction of surface inhomogeneity encountered during the adsorption of inhibitor molecules (Satapathy *et al.*, 2009); in this case modified and ultrafiltrated lignin.

Modified autohydrolyzed organosolv lignin through the incorporation of 1,8-dihydroxyanthraquinone (AHD EOL) and ultrafiltrated soda lignin fraction have shown higher R_{ct} value compared to the rest of lignin samples. This observation could be due to the fact that both AHD EOL and soda lignin fraction have higher phenolic $-OH$ content and solubility, that led to the increase of the antioxidant (as

evidenced by oxygen uptake and reducing power assays) and corrosion inhibition activities. As a consequence, higher IE values were obtained.

3.5.2.2 Potentiodynamic polarization measurement

Potentiodynamic polarization experiments were performed in order to understand the kinetics of the cathodic and anodic reactions. The polarization curves in the absence and presence of modified (AHN EOL and AHD EOL) and ultrafiltrated (Kraft, soda and organosolv) lignin in 0.5 M HCl solutions are shown in Figure 3.33 and 3.34, respectively. The respective electrochemical corrosion parameters such as the corrosion potential (E_{corr}), cathodic and anodic Tafel slopes (β_c and β_a) and corrosion current density (I_{corr}) obtained from the extrapolation of the Tafel polarization curves are given in Tables 3.17 (modified lignin) and 3.18 (ultrafiltrated lignin). It is illustrated from the data that the addition of modified and ultrafiltrated lignins decreased the corrosion current density (I_{corr}) through the inhibition of anodic mild steel dissolution and cathodic hydrogen evolution reactions.

The decrease of the current density values was due to the adsorption of the inhibitor on the mild steel/acid solution interface (Bahrami *et al.*, 2010; Ahamad *et al.*, 2010). It was reported by all authors (Wang *et al.*, 1995; Wu *et al.*, 1998; Bahrami *et al.*, 2010) that the presence of phenylic ring in the inhibitor molecules (having higher electron density) could merely block the mild steel redox reactions, resulting in low current density values. Additionally, both anodic and cathodic current densities (I_{corr}) were decreased (as the concentration of lignin inhibitors was increased), suggesting that the inhibitors suppressed both anodic and cathodic corrosion reactions.

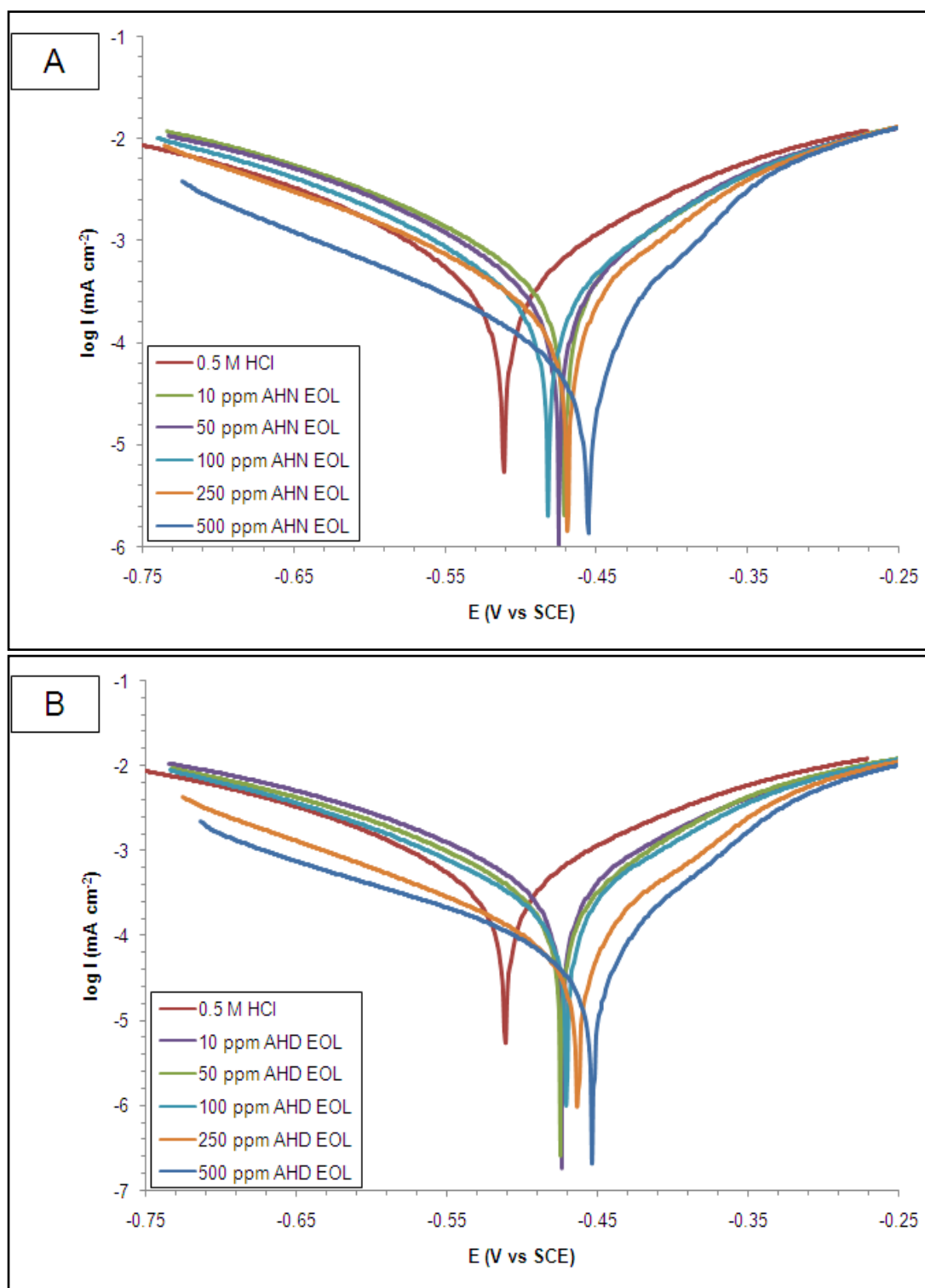


Figure 3.33: Tafel curves of mild steel in 0.5 M HCl solution in absence and presence of; (A) AHN EOL and (B) AHD EOL lignin at 303 K.

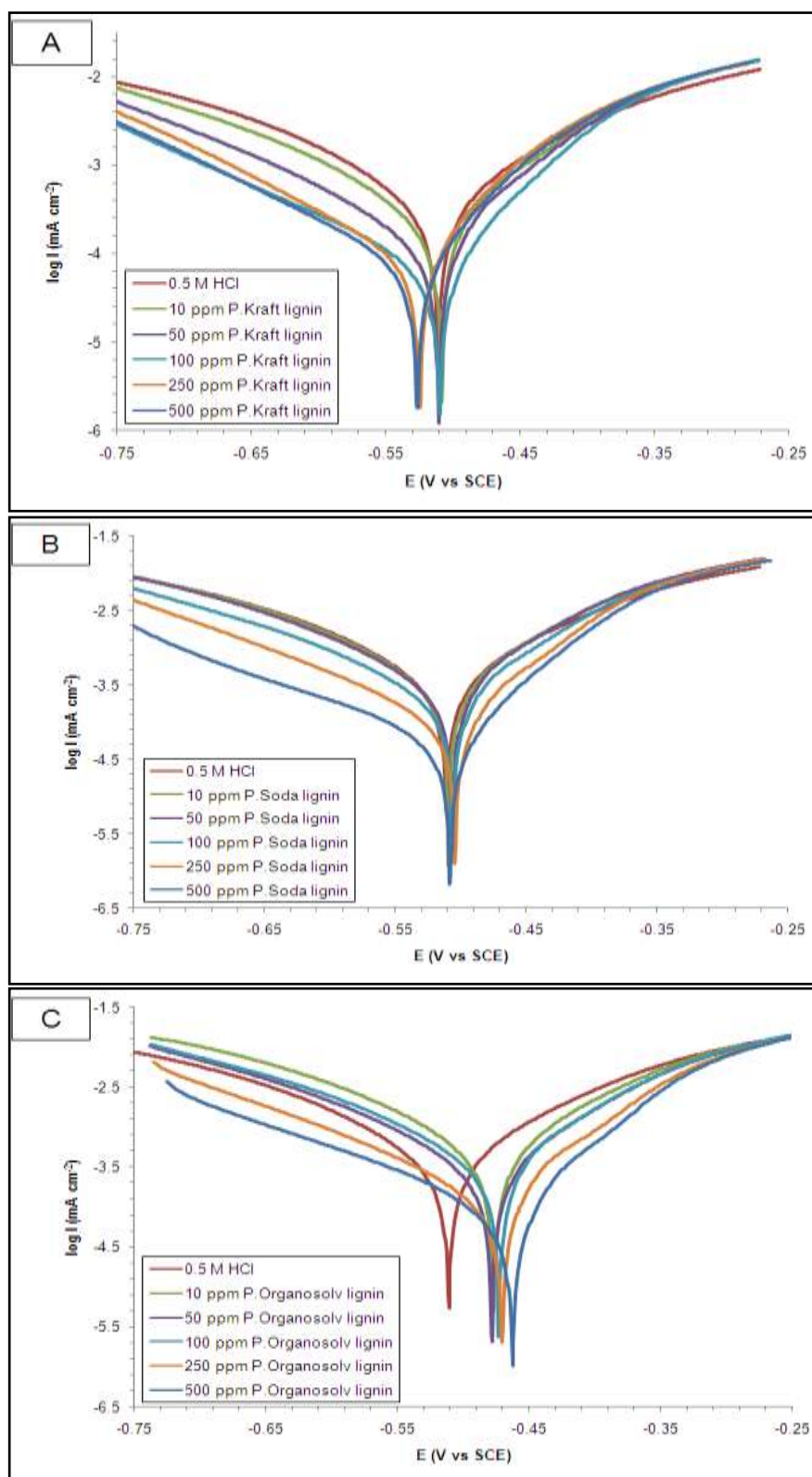


Figure 3.34: Tafel curves of mild steel in 0.5 M HCl solution in absence and presence of; (A) Kraft, (B) Soda and (C) Organosolv lignin fractions at 303 K.

Table 3.17: Electrochemical polarization parameters for mild steel in 0.5 M HCl solution in the absence and presence of AHN EOL and AHD EOL lignin at 303 K.

Concentration (ppm)	E_{corr} (mV)	I_{corr} (mA cm ⁻²)	β_a (mV decade ⁻¹)	$-\beta_c$ (mV decade ⁻¹)	IE (%)	CR (mm y ⁻¹)
0.5 M HCl	-511	1.1200	245	616	-	13.24
10 ppm AHN EOL	-470	0.9180	33	37	18.04	10.85
50 ppm AHN EOL	-475	0.7361	22	24	34.28	8.70
100 ppm AHN EOL	-482	0.5334	27	49	52.38	6.31
250 ppm AHN EOL	-469	0.4393	29	39	60.77	5.19
500 ppm AHN EOL	-456	0.1787	23	33	84.04	2.11
10 ppm AHD EOL	-475	0.7073	29	32	36.85	8.36
50 ppm AHD EOL	-474	0.5519	19	21	50.72	6.53
100 ppm AHD EOL	-471	0.4301	21	25	61.59	5.09
250 ppm AHD EOL	-464	0.2448	20	26	78.14	2.89
500 ppm AHD EOL	-454	0.1124	22	28	89.96	1.33

Table 3.18: Electrochemical polarization parameters for mild steel in 0.5 M HCl solution in the absence and presence of different ultrafiltrated lignin fractions (5 kDa) at 303 K.

Concentration (ppm)	E_{corr} (mV)	I_{corr} (mA cm ⁻²)	β_a (mV decade ⁻¹)	$-\beta_c$ (mV decade ⁻¹)	IE (%)	CR (mm y ⁻¹)
0.5 M HCl	-511	1.1200	245	616	-	13.24
10 ppm P.Kraft lignin	-509	0.7891	32	35	29.54	9.33
50 ppm P.Kraft lignin	-511	0.3145	24	30	71.92	3.72
100 ppm P.Kraft lignin	-510	0.2973	34	58	73.45	3.52
250 ppm P.Kraft lignin	-525	0.2544	86	59	77.29	3.01
500 ppm P.Kraft lignin	-527	0.2116	115	37	81.11	2.50
10 ppm P.Soda lignin	-509	0.8331	40	55	25.62	9.85
50 ppm P.Soda lignin	-507	0.8247	41	53	26.37	9.75
100 ppm P.Soda lignin	-507	0.7490	55	104	33.13	8.86
250 ppm P.Soda lignin	-504	0.3153	100	26	71.85	3.73
500 ppm P.Soda lignin	-508	0.1371	26	32	87.76	1.62
10 ppm P.Organosolv lignin	-477	1.5434	31	100	-37.80	18.24
50 ppm P.Organosolv lignin	-479	0.9861	34	47	11.96	11.66
100 ppm P.Organosolv lignin	-473	0.8915	62	107	20.40	10.54
250 ppm P.Organosolv lignin	-471	0.3175	33	32	71.65	3.75
500 ppm P.Organosolv lignin	-463	0.1799	24	36	83.94	2.13

The decrease of the current density of lignin in comparison with 0.5 M HCl (blank) for both anodic and cathodic sites may suggest the mixed type of corrosion inhibition behavior with a predominant decrease at the anodic (for AHN EOL, AHD EOL and organosolv lignin fraction) and cathodic (Kraft and soda lignin fractions) site. This is supported by the large change in the anodic Tafel slope (β_a) and cathodic Tafel slope (β_c) values from that of the blank in the presence of modified and ultrafiltrated lignins in 0.5 M HCl solution.

As the concentration of the inhibitor increased, the linearity of the Tafel region disappeared (due to the slow diffusion of Fe and H⁺ ions at both anodic and cathodic branches) that gave larger I_{corr} values than the actual values (Raja *et al.*, 2013). Therefore, it is difficult to estimate the I_{corr} values since the calculation depends on the marked curvature of the experimental polarization curves and the calculated linear curves. Hence, the estimation of the I_{corr} values was carried out several times to obtain an average value. In addition, different immersion durations of the EIS (short-period of immersion) than polarization (long-period of immersion) might also contribute to the difference of the IE values between the two measurements. As a result, the IE % values obtained from the polarization and EIS measurements might vary even though they show similar trends. In this study, the maximum inhibition for all lignin inhibitor was obtained at the maximum concentration of 500 ppm ($IE_{AHD\ EOL}$: 89.96 % > $IE_{P.Soda}$: 87.76 % > $IE_{AHN\ EOL}$: 84.04 % > $IE_{P.Organosolv}$: 83.94 % > $IE_{P.Kraft}$: 81.11 %). This result was in good agreement with the EIS measurement which has been discussed earlier. It is interesting to note that even though Kraft lignin fraction at 500 ppm shows lower IE % value compared to others, it still gives better inhibitive protection (up till 70 %) at lower concentrations especially from 50

ppm onwards. In contrast, organosolv lignin fraction gave poor inhibitive action at lower concentrations (from 10 to 100 ppm). This phenomenon could be rationalized by their phenolic –OH content and dissolution ability. It can be assumed that higher degree of dissolution and phenolic –OH content posses by Kraft lignin fraction (as compared to that of organosolv lignin fraction) improved its inhibitive action at lower concentrations.

The presence of modified and ultrafiltrated lignin inhibitors also resulted in a slight shift of the corrosion current potential (E_{corr}) towards the noble and/or active region from its origin (blank). In general, the displacement of $E_{corr} > 85$ mV was associated to cathodic or anodic type inhibition and if the displacement of $E_{corr} < 85$ mV it can be assumed that it behaved as mixed type inhibitor (Riggs Jr., 1973; Ferreira *et al.*, 2004; Satapathy *et al.*, 2009; Ahamad *et al.*, 2010). The maximum displacement of E_{corr} for modified and ultrafiltrated lignins was around 3-57 mV, which indicates that the inhibitor acts as a mixed type inhibitor with predomination at anodic (for AHN EOL, AHD EOL and organosolv lignin fraction) and cathodic (Kraft and soda lignin fractions) sites. According to Ashassi-Sorkhabi *et al.* (2008), most of organic compounds (either synthetic or natural) were mixed type inhibitors that could affect both anodic and cathodic reactions. The corrosion rate (CR) of mild steel can be determined by employing the following formula:

$$CR \text{ (mm y}^{-1}\text{)} = \frac{0.13 \times I_{corr} \times M_{ew}}{\rho} \times 0.0254 \quad (3.2)$$

where M_{ew} is the equivalent molar weight of mild steel (27.93 g eq⁻¹) and ρ is the density of mild steel (7.8 g cm⁻³). The general unit for CR is millimeters per year

(mm y⁻¹). Based on the results, the corrosion rate of mild steel was significantly reduced upon addition of the modified and ultrafiltrated lignins. Similar trends of *CR* and *IE* % were observed where the lowest *CR* value was attained for AHD EOL at 500 ppm ($CR_{\text{AHD EOL}}: 1.33 \text{ mm y}^{-1} < CR_{\text{P.Soda}}: 1.62 \text{ mm y}^{-1} < CR_{\text{AHN EOL}}: 2.11 \text{ mm y}^{-1} < CR_{\text{P.Organosolv}}: 2.13 \text{ mm y}^{-1} < CR_{\text{P.Kraft}}: 2.50 \text{ mm y}^{-1}$). Therefore it can be concluded that AHD EOL lignin performed better than other types of lignin.

3.5.3 Weight loss measurement

The inhibition efficiency of modified and ultrafiltrated lignins towards the corrosion of mild steel in 0.5 M HCl solution was also studied using weight loss measurement. Table 3.19 and 3.20 summarize corrosion inhibition efficiency of modified and ultrafiltrated lignins, respectively after 48 hours of immersion at ~303 K. The corrosion rate (*CR*) of the mild steel can be calculated using the following formula:

$$CR \text{ (mm y}^{-1}\text{)} = 87.6 \times \frac{W_L}{\rho A t} \quad (3.3)$$

where W_L is the weight loss (in mg), ρ is the density of mild steel (7.8 g cm⁻³), A is the area of mild steel sample (4.5 cm²) and t is the time of immersion (48 h). The general unit for the corrosion rate is millimeters per year (mm y⁻¹).

Table 3.19: The inhibition efficiency of mild steel in 0.5 M HCl solution in the absence and presence of AHN EOL and AHD EOL lignin at 303 K.

Concentration (ppm)	W_L (g)	IE (%)	CR (mm y ⁻¹)
0.5 M HCl	0.1861±0.0191	-	9.67
10 ppm AHN EOL	0.1346±0.0028	27.65	6.99
50 ppm AHN EOL	0.0978±0.0082	47.43	5.08
100 ppm AHN EOL	0.0749±0.0045	59.76	3.89
250 ppm AHN EOL	0.0333±0.0021	82.10	1.73
500 ppm AHN EOL	0.0154±0.0007	91.69	0.80
10 ppm AHD EOL	0.1548±0.0198	16.77	8.05
50 ppm AHD EOL	0.0498±0.0117	73.23	2.59
100 ppm AHD EOL	0.0308±0.0027	83.45	1.60
250 ppm AHD EOL	0.0127±0.0006	93.17	0.66
500 ppm AHD EOL	0.0084±0.0003	95.51	0.43

Table 3.20: The inhibition efficiency of mild steel in 0.5 M HCl solution in the absence and presence of different ultrafiltrated lignin fractions (5 kDa) at 303 K.

Concentration (ppm)	W_L (g)	IE (%)	CR (mm y ⁻¹)
0.5 M HCl	0.1861±0.0191	-	9.67
10 ppm P.Kraft lignin	0.1489±0.0115	19.99	7.74
50 ppm P.Kraft lignin	0.0579±0.0017	68.88	3.01
100 ppm P.Kraft lignin	0.0442±0.0023	76.24	2.29
250 ppm P.Kraft lignin	0.0312±0.0007	83.20	1.62
500 ppm P.Kraft lignin	0.0217±0.0003	88.34	1.13
10 ppm P.Soda lignin	0.1581±0.0086	15.02	8.22
50 ppm P.Soda lignin	0.0891±0.0032	52.14	4.63
100 ppm P.Soda lignin	0.0808±0.0064	56.57	4.20
250 ppm P.Soda lignin	0.0424±0.0014	77.21	2.20
500 ppm P.Soda lignin	0.0127±0.0002	93.09	0.67
10 ppm P.Organosolv lignin	0.1898±0.0071	-1.98	9.87
50 ppm P.Organosolv lignin	0.1728±0.0004	7.12	8.98
100 ppm P.Organosolv lignin	0.1306±0.0015	29.80	6.79
250 ppm P.Organosolv lignin	0.0515±0.0081	72.51	2.66
500 ppm P.Organosolv lignin	0.0213±0.0002	88.56	1.11

From this experiment, it was observed that the highest IE % value for modified and ultrafiltrated lignin inhibitors was attained at the maximum concentration of 500

ppm. Similar to EIS and potentiodynamic polarization measurements, AHD EOL lignin inhibitor showed the highest inhibitive action of more than 90 % as compared to other lignin inhibitors ($IE_{\text{AHD EOL}}: 95.51 \% > IE_{\text{P.Soda}}: 93.09 \% > IE_{\text{AHN EOL}}: 91.69 \% > IE_{\text{P.Organosolv}}: 88.56 \% > IE_{\text{P.Kraft}}: 88.34 \%$). In addition, Figure 3.35 indicated that all lignin inhibitors are ‘concentration-dependent’ as the IE value increases with the increase in the concentration of lignin inhibitors and obtained a plateau at 250 ppm. This could be attributed to the increase in adsorption of the inhibitor at the metal/solution interface (Obot and Obi-Egbedi, 2010; Issaadi *et al.*, 2011).

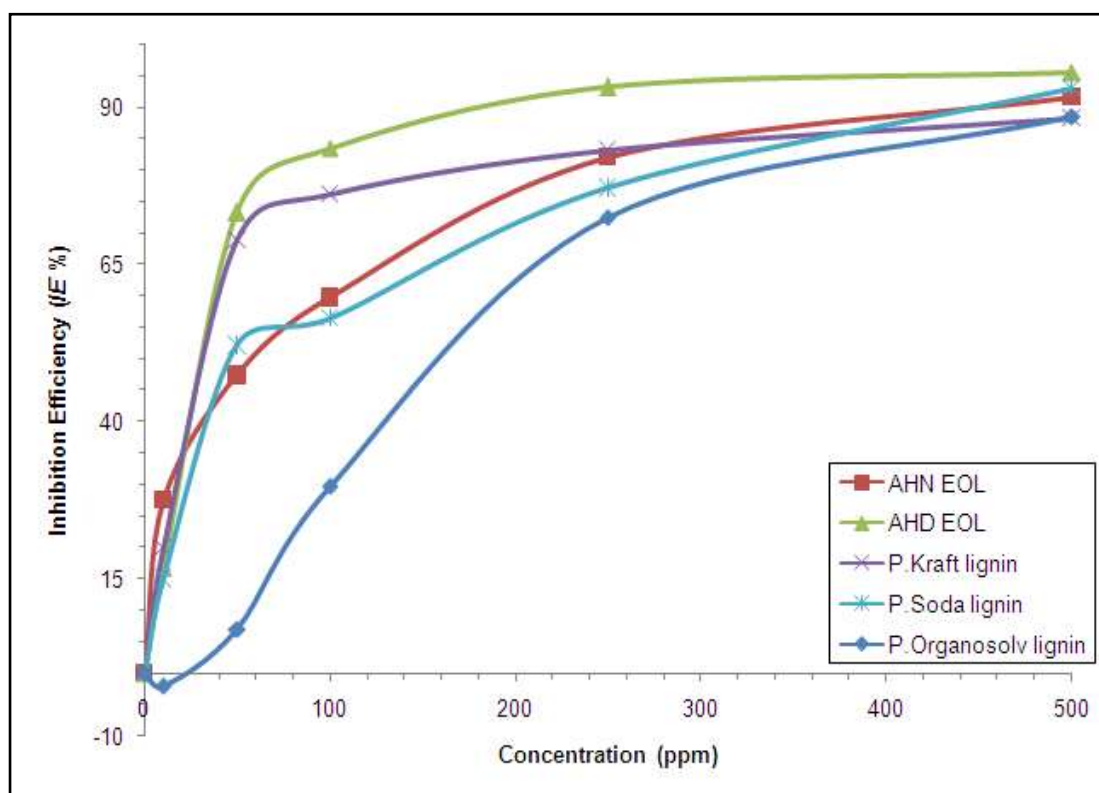


Figure 3.35: The correlation of inhibition efficiency with concentration for all lignin inhibitors at 303 K.

From this study, it can be concluded that all lignin inhibitors gave satisfactory inhibitions on the corrosion of mild steel in 0.5 M HCl solution. Improved properties (solubility, phenolic –OH content, molecular weight and size) of lignin established

via incorporation of organic scavengers and/or membrane fractionation technology have provided better antioxidant activity and inhibition efficiency. The thermodynamic and adsorption behaviors of lignin inhibitor with respect to their inhibitive mechanism will be discussed in the next subchapter.

3.5.3.1 Thermodynamics of corrosion process

In order to understand more about the performance of the modified and ultrafiltrated lignins with the nature of adsorption and activation processes, the effect of temperature was studied. For this purpose, the weight loss measurements were employed at various temperatures (303-333 K) for 48 hours of immersion. From the Arrhenius plots obtained, the activation energy (E_a) can be calculated and thus it can provide further explanations on the mechanism of the inhibitive process (Ansari and Quraishi, 2014). In order to calculate the activation thermodynamic parameters of the corrosion reaction such as activation energy E_a , activated entropy, ΔS^* and enthalpy, ΔH^* , the Arrhenius equation (Eqs. 3.4) and its alternative formulation called the transition state equation (Eqs. 3.5) were employed (Bouklah *et al.*, 2006; de Souza and Spinelli, 2009):

$$CR = K \exp\left(\frac{-E_a}{RT}\right) \quad (3.4)$$

$$CR = \frac{RT}{Nh} \exp\left(\frac{\Delta S^*}{RT}\right) \exp\left(\frac{-\Delta H^*}{RT}\right) \quad (3.5)$$

where CR is the corrosion rate (in $\text{mg cm}^{-2} \text{ h}^{-1}$), T is the absolute temperature, K is a constant and R is the universal gas constant ($8.3142 \text{ J K}^{-1} \text{ mol}^{-1}$), h is Plank's

constant (6.626×10^{-34} J s) and N is Avogadro's number (6.023×10^{23} mol⁻¹). Plotting the natural logarithm of the corrosion rate versus $1/T$, the activation energy can be calculated from the slope ($-E_a/R$). Figure 3.36 and 3.37 shows the variations of the logarithm of the corrosion rate with the presence and absence of the modified and ultrafiltrated lignin inhibitor, respectively with the reciprocal of absolute temperature.

As the lignin inhibitor was added into the solution, the IE of mild steel values decreased slightly (poor inhibitive action at the higher temperature) with increasing temperatures (refer to Appendix VI), probably due to the desorption of inhibitor from the mild steel surface (Cheng *et al.*, 2007). The E_a values in the presence of lignin inhibitors were observed to be higher than those in 0.5 M HCl solution (Tables 3.21 and 3.22) and were not concentration dependent. This suggests that the energy barrier for the corrosion reaction increases with the addition of lignin inhibitors. In addition, the values of the activation energy that were around ~ 20 to ~ 60 kJ mol⁻¹ can be suggested to obey the physical adsorption (physisorption) mechanism (Orobite and Oforka, 2004). High values of activation energy will lower the corrosion rate or lower the corrosion current density. This indicates that the charge transfer in oxidation-reduction processes will become less dense and hence it will lower the corrosion rate (Wahyuningrum *et al.*, 2008).

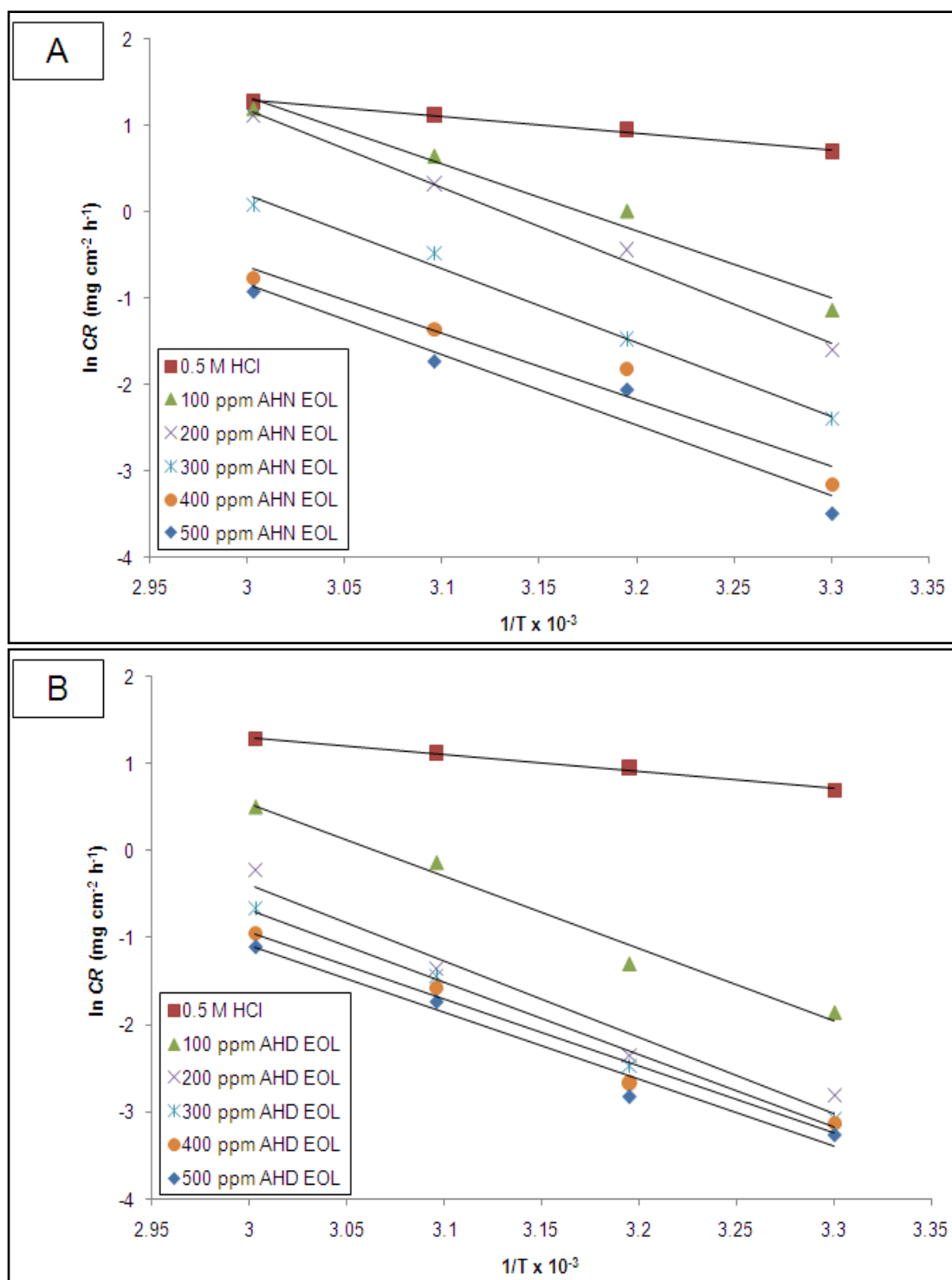


Figure 3.36: Transition-state plots of the corrosion rate (CR) of mild steel in 0.5 M HCl solution in absence and presence of; (A) AHN EOL and (B) AHD EOL lignin.

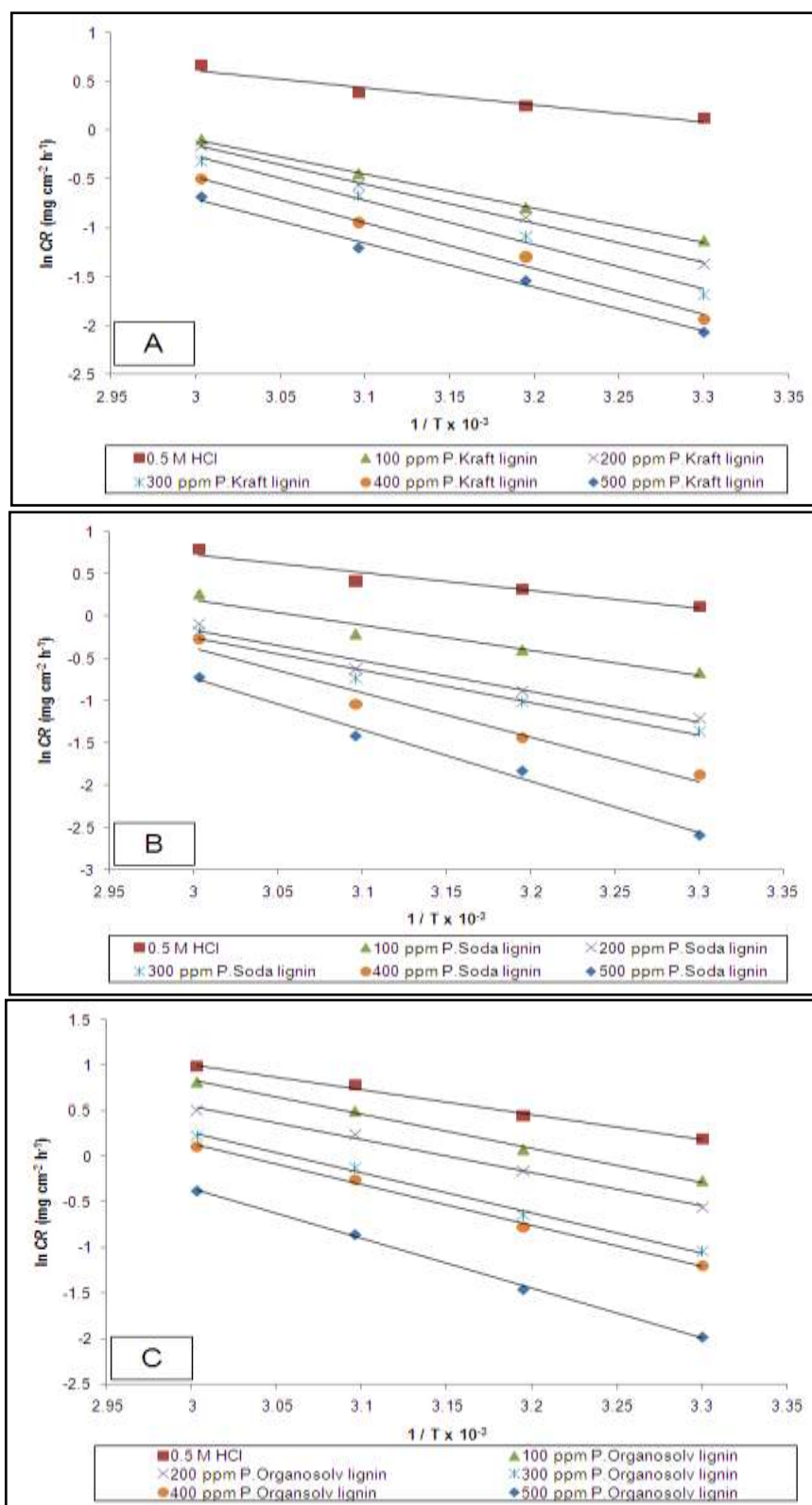


Figure 3.37: Transition-state plots of the corrosion rate (CR) of mild steel in 0.5 M HCl solution in absence and presence of; (A) Kraft, (B) Soda and (C) Organosolv lignin fractions.

Table 3.21: Activation parameters for mild steel dissolution in 0.5 M HCl solution in the absence and presence of AHN EOL and AHD EOL lignin.

Concentration (ppm)	E_a (kJ mol ⁻¹)	ΔH^* (kJ mol ⁻¹)	ΔS^* (J mol ⁻¹ K ⁻¹)
0.5 M HCl	15.89	13.26	-195.26
100 ppm AHN EOL	44.33	41.69	-129.72
200 ppm AHN EOL	54.91	52.27	-109.21
300 ppm AHN EOL	50.77	48.12	-113.91
400 ppm AHN EOL	44.20	41.56	-126.43
500 ppm AHN EOL	47.52	44.88	-118.19
100 ppm AHD EOL	48.96	46.33	-114.40
200 ppm AHD EOL	52.99	50.35	-107.99
300 ppm AHD EOL	49.01	46.38	-115.38
400 ppm AHD EOL	43.83	41.18	-127.09
500 ppm AHD EOL	43.50	40.86	-132.33

Table 3.22: Activation parameters for mild steel dissolution in 0.5 M HCl solution in the absence and presence of different ultrafiltrated lignin fractions (5 kDa).

Concentration (ppm)	E_a (kJ mol ⁻¹)	ΔH^* (kJ mol ⁻¹)	ΔS^* (J mol ⁻¹ K ⁻¹)
0.5 M HCl	14.60	11.97	-204.79
100 ppm P.Kraft lignin	29.08	26.44	-167.30
200 ppm P.Kraft lignin	33.37	30.73	-154.86
300 ppm P.Kraft lignin	37.90	35.27	-142.17
400 ppm P.Kraft lignin	39.08	36.45	-142.43
500 ppm P.Kraft lignin	37.60	34.96	-146.75
100 ppm P.Soda lignin	24.76	22.12	-177.94
200 ppm P.Soda lignin	30.06	27.42	-164.89
300 ppm P.Soda lignin	31.73	29.09	-160.72
400 ppm P.Soda lignin	43.43	40.79	-126.62
500 ppm P.Soda lignin	50.62	47.98	-107.99
100 ppm P.Organosolv lignin	30.90	28.26	-154.14
200 ppm P.Organosolv lignin	30.19	27.55	-158.60
300 ppm P.Organosolv lignin	36.23	33.59	-142.94
400 ppm P.Organosolv lignin	37.38	34.74	-140.47
500 ppm P.Organosolv lignin	45.49	42.85	-120.25

Additionally, a plot of $\ln CR/T$ against $1/T$ gives a straight line with a slope value of $(\Delta H^*/R)$ and an intercept of $[\ln (R/Nh) + (\Delta S^*/R)]$ as shown in Figures 3.38 and 3.39.

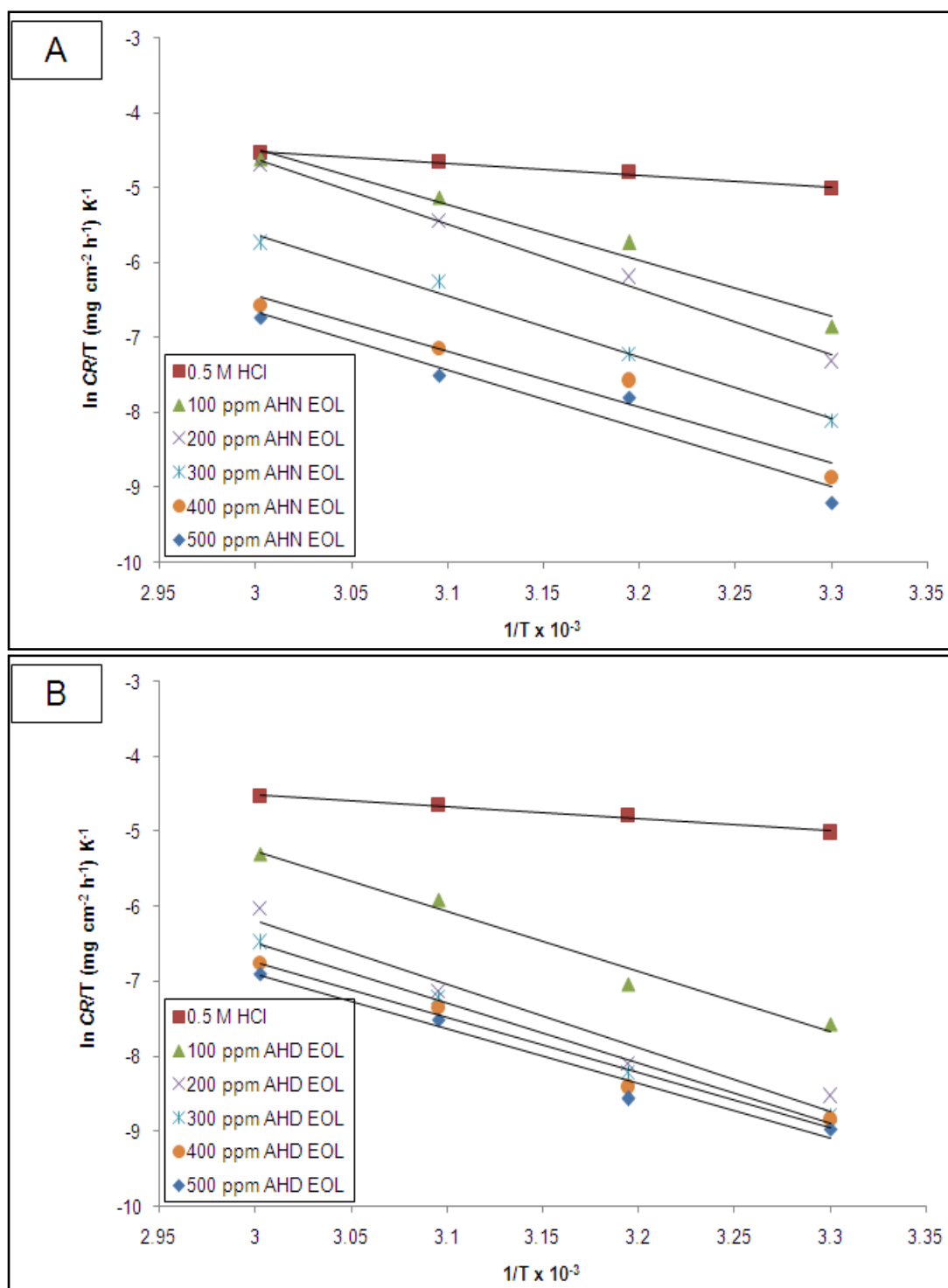


Figure 3.38: Modified Arrhenius plots of the corrosion rate (CR/T) of mild steel in 0.5 M HCl solution in absence and presence of; (A) AHN EOL and (B) AHD EOL lignin.

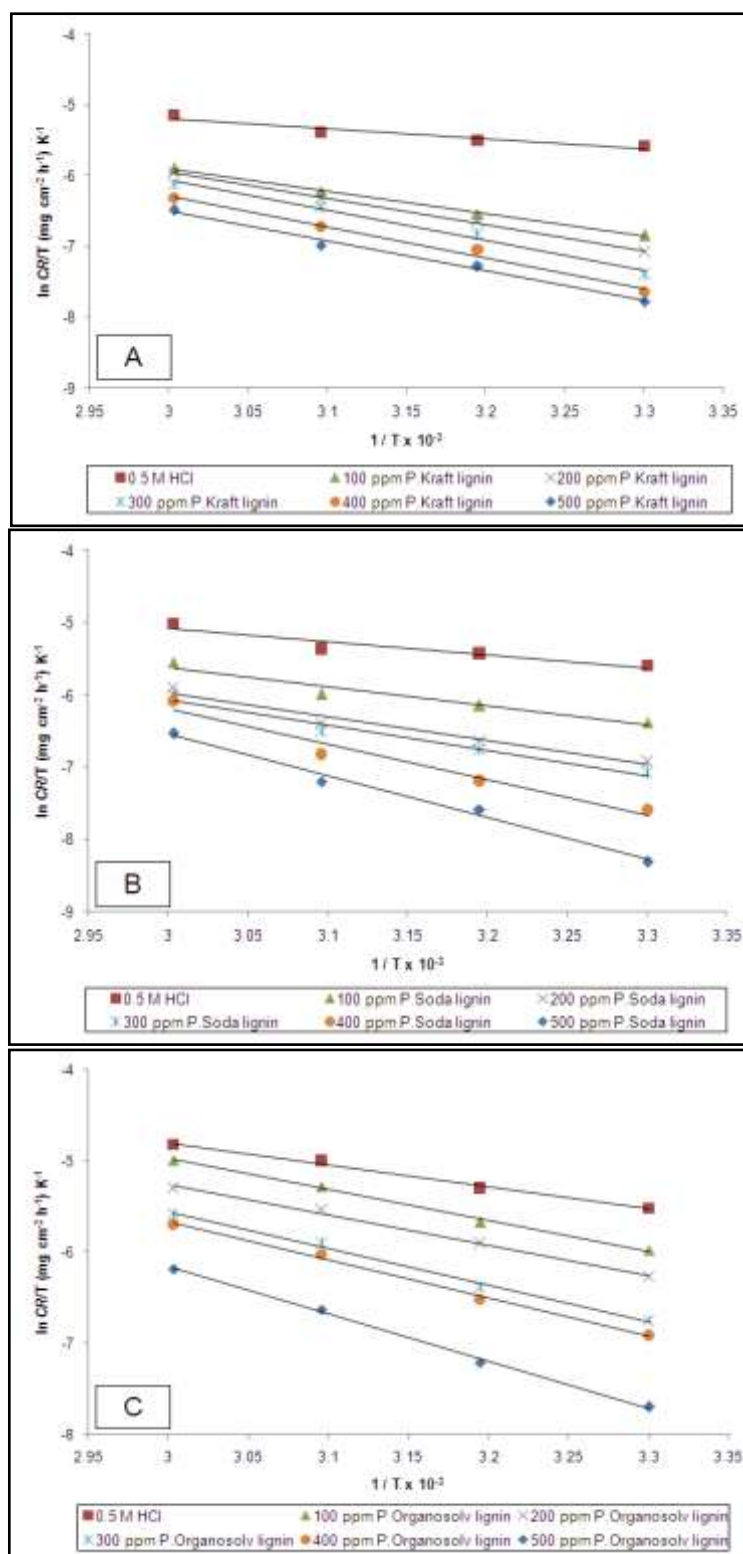
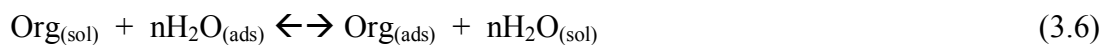


Figure 3.39: Modified Arrhenius plots of the corrosion rate (CR/T) of mild steel in 0.5 M HCl solution in absence and presence of; (A) Kraft, (B) Soda and (C) Organosolv lignin fractions.

Positive values of the activated enthalpy, ΔH^* mean that the process is an endothermic process and it reflects that the mild steel dissolution was slow (it requires more energy to achieve activated state) in the presence of inhibitor (Bouklah *et al.*, 2006; Fouda and Mahfouz, 2009; Ansari and Quraishi, 2014). The increase of ΔS^* value (more positive) in the presence of inhibitors indicates that the metal dissolution system passes from orderly arrangement to a more random arrangement (Morad and El-Dean, 2006; Wahyuningrum *et al.*, 2008). Perhaps this might be due to the adsorption of organic inhibitor molecules that later could be regarded as a quasi-substitution process between the organic inhibitor molecules in the aqueous phase and water molecules at the mild steel surface (Sahin *et al.*, 2002). In addition, the adsorption of organic inhibitor was accompanied by the desorption of water molecules from the metal surface thus increasing the solvent entropy of activation (Ateya *et al.*, 1984).

3.5.3.2 Adsorption studies

It is known that the adsorption of the inhibitors on the metal surface is an essential step in the corrosion inhibition mechanism. The adsorption process of inhibitor is a displacement reaction where the adsorbed water molecule is being removed from the surface of the metal (Cheng *et al.*, 2007):



$\text{Org}_{(\text{sol})}$ and $\text{Org}_{(\text{ads})}$ are the organic molecules in the aqueous solution that are adsorbed onto the metal surface. $\text{H}_2\text{O}_{(\text{ads})}$ is the water molecule on the metal surface

in which n is the coefficient that represents water molecules being replaced by a unit of inhibitor. In order to obtain an effective adsorption of an inhibitor on the metal surface, the interaction force between metal and inhibitor must be greater than the interaction force of metal and water molecules (Sastri *et al.*, 2007). Therefore, to establish the adsorption mode, the fraction of the surface coverage, θ was calculated from Eqs. (2.11). Next, the data were tested graphically by fitting them with Temkin (Appendix VII) and Langmuir adsorption isotherms to obtain the best adsorption fit. It was found that the data obtained best fitted the Langmuir adsorption isotherm. The Langmuir adsorption isotherm is given by;

$$\frac{C}{\theta} = \frac{1}{K_{ads}} + C \quad (3.7)$$

where θ is the surface coverage, K_{ads} is the adsorption-desorption equilibrium constant and C is the concentration of inhibitor (in g L⁻¹). The corresponding plots are shown in Figure 3.40 and the adsorption parameters are presented in Tables 3.23 and 3.24. A good linearity ($R^2 = 0.992 - 0.999$) as observed in the Langmuir adsorption isotherm can be explained by the assumption of a monolayer adsorption of the inhibitor onto the mild steel surface (Cheng *et al.*, 2007; Wahyuningrum *et al.*, 2008; Ahamad *et al.*, 2010).

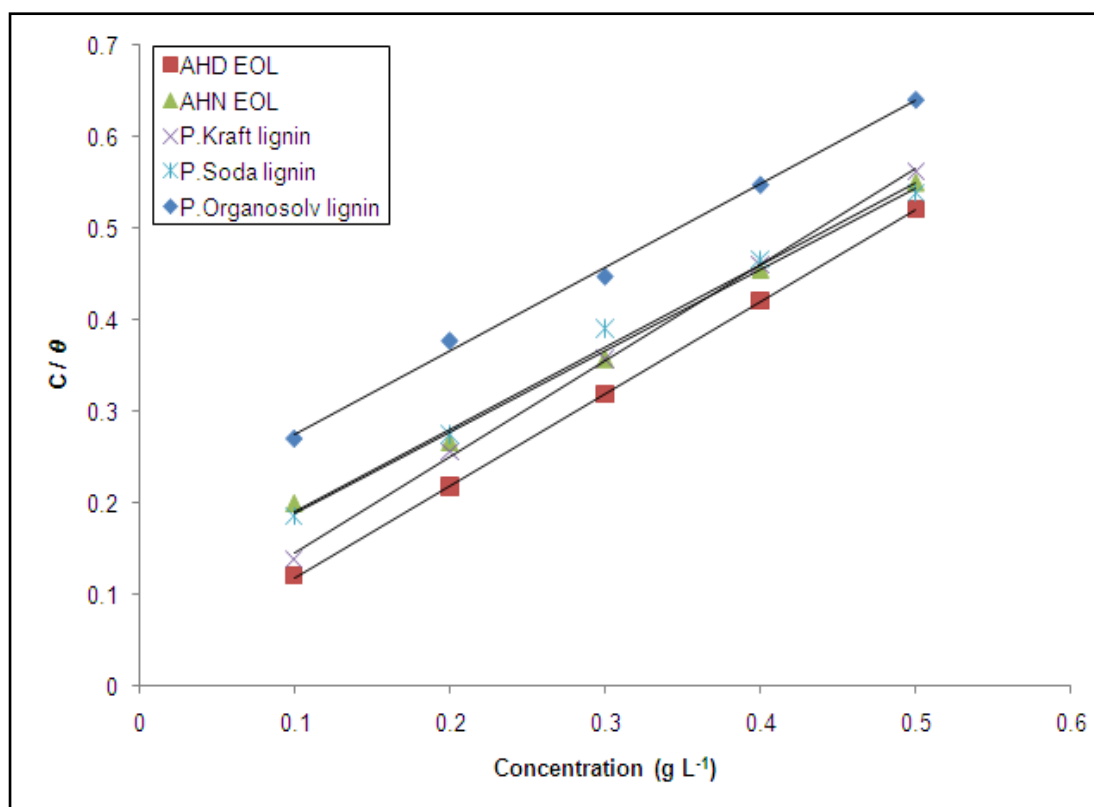


Figure 3.40: Langmuir adsorption plot of mild steel after 48 h of immersion in 0.5 M HCl solution in absence and presence of lignin inhibitors at 303 K.

Table 3.23: Adsorption parameters for mild steel in 0.5 M HCl by weight loss measurement in the absence and presence of AHN EOL and AHD EOL lignin at 303 K.

Concentration (ppm)	θ	R^2	K_{ads} (L g ⁻¹)	ΔG°_{ads} (kJ mol ⁻¹)
0.5 M HCl	-			
100 ppm AHN EOL	0.50			
200 ppm AHN EOL	0.75			
300 ppm AHN EOL	0.84	0.995	10.10	-23.23
400 ppm AHN EOL	0.88			
500 ppm AHN EOL	0.91			
100 ppm AHD EOL	0.83			
200 ppm AHD EOL	0.92			
300 ppm AHD EOL	0.94	0.999	55.56	-27.52
400 ppm AHD EOL	0.95			
500 ppm AHD EOL	0.96			

Table 3.24: Adsorption parameters for mild steel in 0.5 M HCl by weight loss measurement in the absence and presence of different ultrafiltrated lignin fractions at 303 K.

Concentration (ppm)	θ	R^2	K_{ads} (L g ⁻¹)	ΔG°_{ads} (kJ mol ⁻¹)
0.5 M HCl	-			
100 ppm P.Kraft lignin	0.72			
200 ppm P.Kraft lignin	0.78			
300 ppm P.Kraft lignin	0.84	0.999	25.00	-25.51
400 ppm P.Kraft lignin	0.87			
500 ppm P.Kraft lignin	0.89			
100 ppm P.Soda lignin	0.54			
200 ppm P.Soda lignin	0.73			
300 ppm P.Soda lignin	0.77	0.992	9.62	-23.11
400 ppm P.Soda lignin	0.86			
500 ppm P.Soda lignin	0.93			
100 ppm P.Organosolv lignin	0.37			
200 ppm P.Organosolv lignin	0.53			
300 ppm P.Organosolv lignin	0.67	0.997	5.46	-21.68
400 ppm P.Organosolv lignin	0.73			
500 ppm P.Organosolv lignin	0.78			

The values of K_{ads} obtained from the Langmuir adsorption isotherm can be correlated with the Gibbs free energy of adsorption ΔG°_{ads} by the following equation:

$$\Delta G^\circ_{ads} = -RT \ln(K_{ads} \times A) \quad (3.8)$$

Where A is the molar concentration of water (55.5 M or 1000 g L⁻¹), R is the universal gas constant (8.3142 J K⁻¹ mol⁻¹) and T is the temperature in Kelvin, (303 K).

The negative value of ΔG°_{ads} indicates that the inhibitor, in this case the modified lignin were spontaneously adsorbed onto the mild steel surface and later became a

stable adsorptive layer (Ansari and Quraishi, 2014). It is well known that values of ΔG_{ads}° around -20 kJ mol^{-1} or less negative are often associated with the physisorption phenomenon where the electrostatic interactions between the charged molecule and the charged metal are evident, while those around -40 kJ mol^{-1} or more negative are associated with the chemisorption phenomenon, suggesting the sharing or transfer of organic molecules electrons with/to the metal surface (Popova *et al.*, 2003; Bouklah *et al.*, 2006; Ahamad *et al.* 2010; Ansari and Quraishi, 2014).

Hence, it was assumed that lignin inhibitors were mainly physically (ΔG_{ads}° : $21.68 - 27.52 \text{ kJ mol}^{-1}$) adsorbed onto the mild steel surface. The adsorption is enhanced by the presence of the increased number of electrons of oxygen donor atoms and delocalized π electrons (through modification and fractionation process) in the lignin structures that create electrostatic adsorption with the mild steel surface. As a result, stable protective films are formed on the mild steel surface, thus decreasing the metal dissolution. In addition, AHD EOL shows higher K_{ads} (55.56 L g^{-1}) value compared to rest of lignin inhibitors. According to Ahamad *et al.* (2010), higher value of K_{ads} indicates that stronger adsorption layer was formed, hence increases the inhibitive action.

3.5.4 Surface analysis

In the HCl solution, one can assume that Cl^- anions are first adsorbed onto the positively charged metal surface;



In this way, it is likely that the protonated inhibitor molecules that are formed in acidic media are adsorbed through electrostatic interactions with the negatively charged metal surface where Cl^- anions form an interconnecting bridge between the positively charged metal surface and protonated inhibitors. To justify this assumption, the measurement of the potential zero charge (PZC) may help in determining the type of adsorption that occurs at the metal surface when an inhibitor is added. The EIS measurement offers a good method in order to determine the PZC of metals (Hassan *et al.*, 2007; Solmaz *et al.*, 2008). Figure 3.41 shows the relation between the C_{dl} and the electrode potential for the mild steel electrode in 0.5 M HCl without and with the addition of 500 ppm modified and ultrafiltrated lignin.

The corresponding PZC and the Antropov ‘rational’ corrosion potential, E_r values are shown in Table 3.25. When the difference of $E_r = E_{\text{corr}} - \text{PZC}$ is negative, the working electrode surface has a net negative charge and the adsorption of cations is favored. Conversely, the adsorption of anions is favored when E_r becomes positive. The different charges of metal surfaces under different corrosion conditions might be considered as one of the reasons for the selective action of inhibitors (Keles *et al.*, 2008).

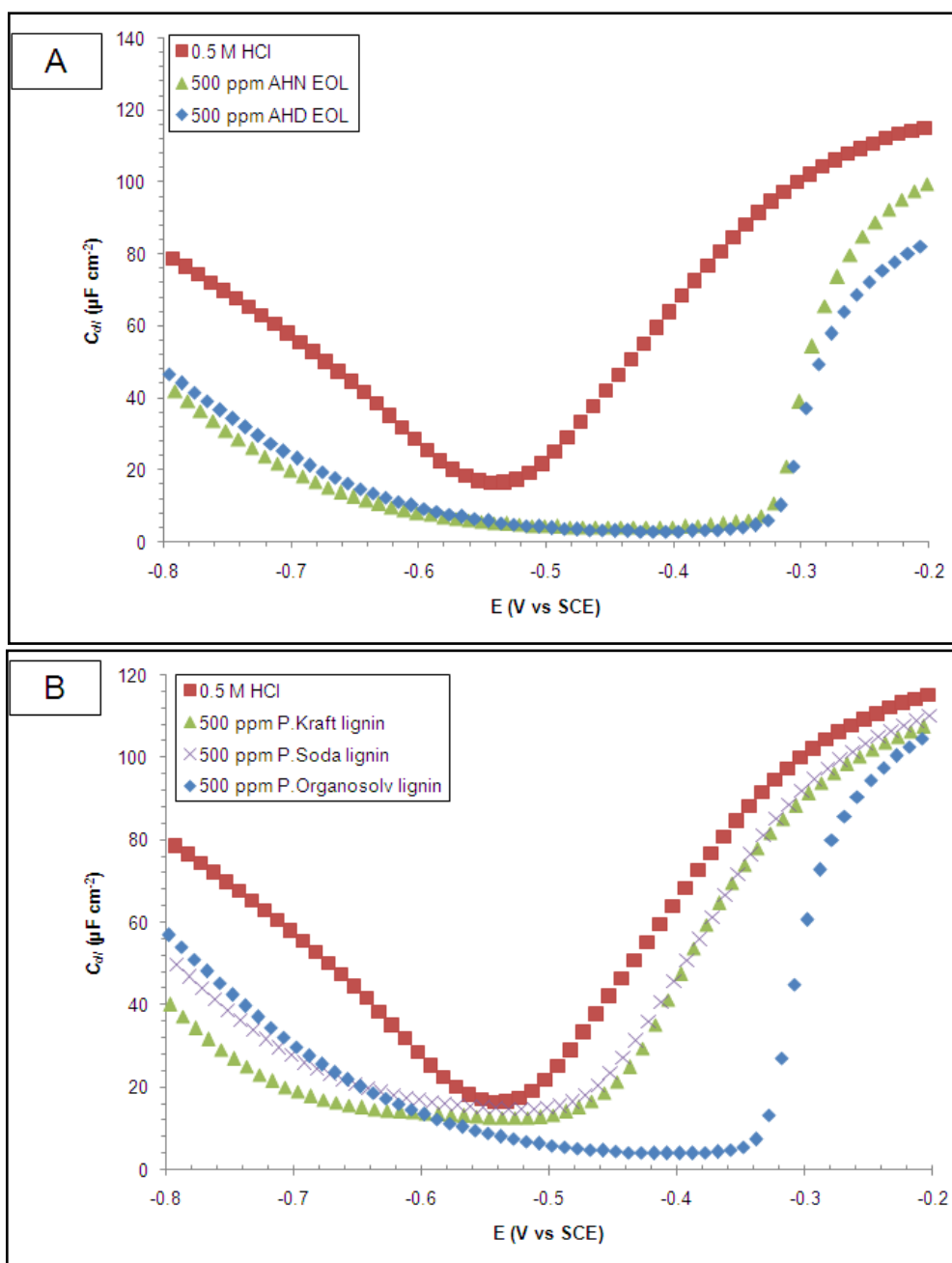


Figure 3.41: Relation between C_{dl} and the applied potential on a mild steel electrode in 0.5 M HCl without and with; (A) modified and (B) ultrafiltrated lignin inhibitors.

In the presence of the optimum concentration of 500 ppm lignin inhibitors in 0.5 M HCl solution, the conductivity seems to be lower than it is in free acid solution. A positive value of E_r as observed for the blank solution has indicated that the positively charged mild steel will specifically be adsorbed by chloride ions (anions). The adsorption of negatively charged chloride ions on the mild steel surface creates

an excess of negative charge on the surface, thus leading to the adsorption of cations (protonated inhibitors; details on subchapter 3.5.5) (Solmaz *et al.*, 2008; Moretti *et al.*, 2013).

Table 3.25: Values of E_r for the mild steel electrode in 0.5 M HCl for studied inhibitors.

Sample	f_{max} (Hz)	E_{corr} (mV)	PZC (mV)	E_r (mV)
0.5 M HCl	125	-511	-543	+32
500 ppm AHN EOL	100	-456	-441	-15
500 ppm AHD EOL	63	-454	-415	-39
500 ppm P.Kraft lignin	158	-527	-506	-21
500 ppm P.Soda lignin	100	-508	-481	-27
500 ppm P.Organosolv lignin	65	-463	-408	-55

When lignin inhibitors were added to 0.5 M HCl solution, their molecules (with its positive center, namely the protonated hydroxyl group) would electrostatically be adsorbed at the oxide/solution interface through Van der Waals attraction force because of the excess negative charge (due to the adsorbed layer of the Cl^- anions) at this interface at the corrosion potential. The adsorption of lignin molecules impedes further adsorption of the aggressive Cl^- anions. Thus, the mild steel electrode is protected against corrosion. It is not surprising to understand why the PZC is shifted positively, resulting in negative values of E_r in the presence of modified and ultrafiltrated lignins.

The surface analyses of mild steel plates using the scanning electron microscope/energy dispersive X-ray spectroscopy (SEM/EDX) and X-ray diffraction (XRD) are shown in Figure 3.42 (for modified lignin) and Figure 3.43 (for ultrafiltrated lignin).

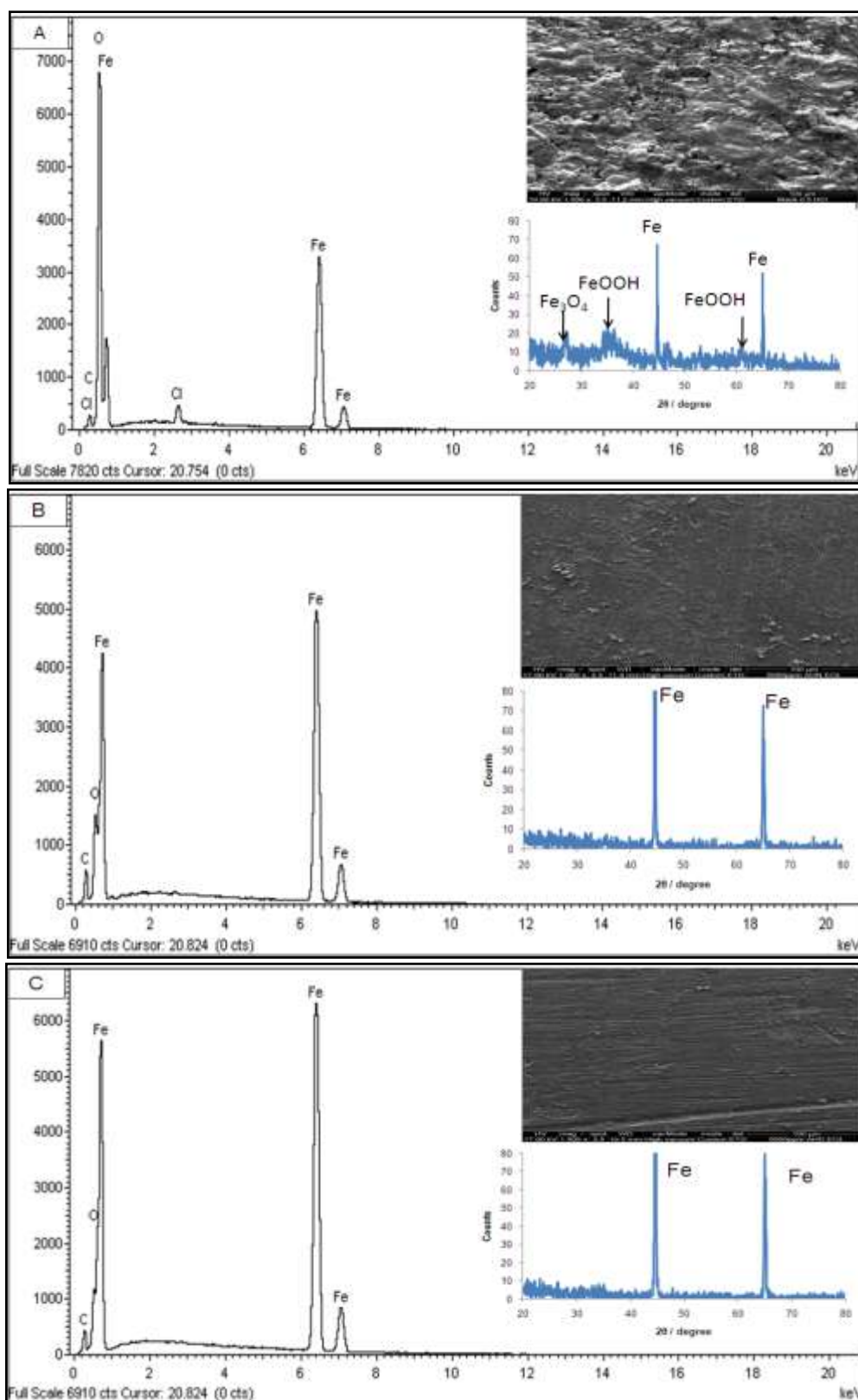


Figure 3.42: SEM (top right) micrograph, XRD (below right) and EDX spectra of mild steel after 48 h of immersion in 0.5 M HCl solution in; (A) absence and presence of (B) AHN EOL and (C) AHD EOL lignin at 303 K and magnification 1000 x.

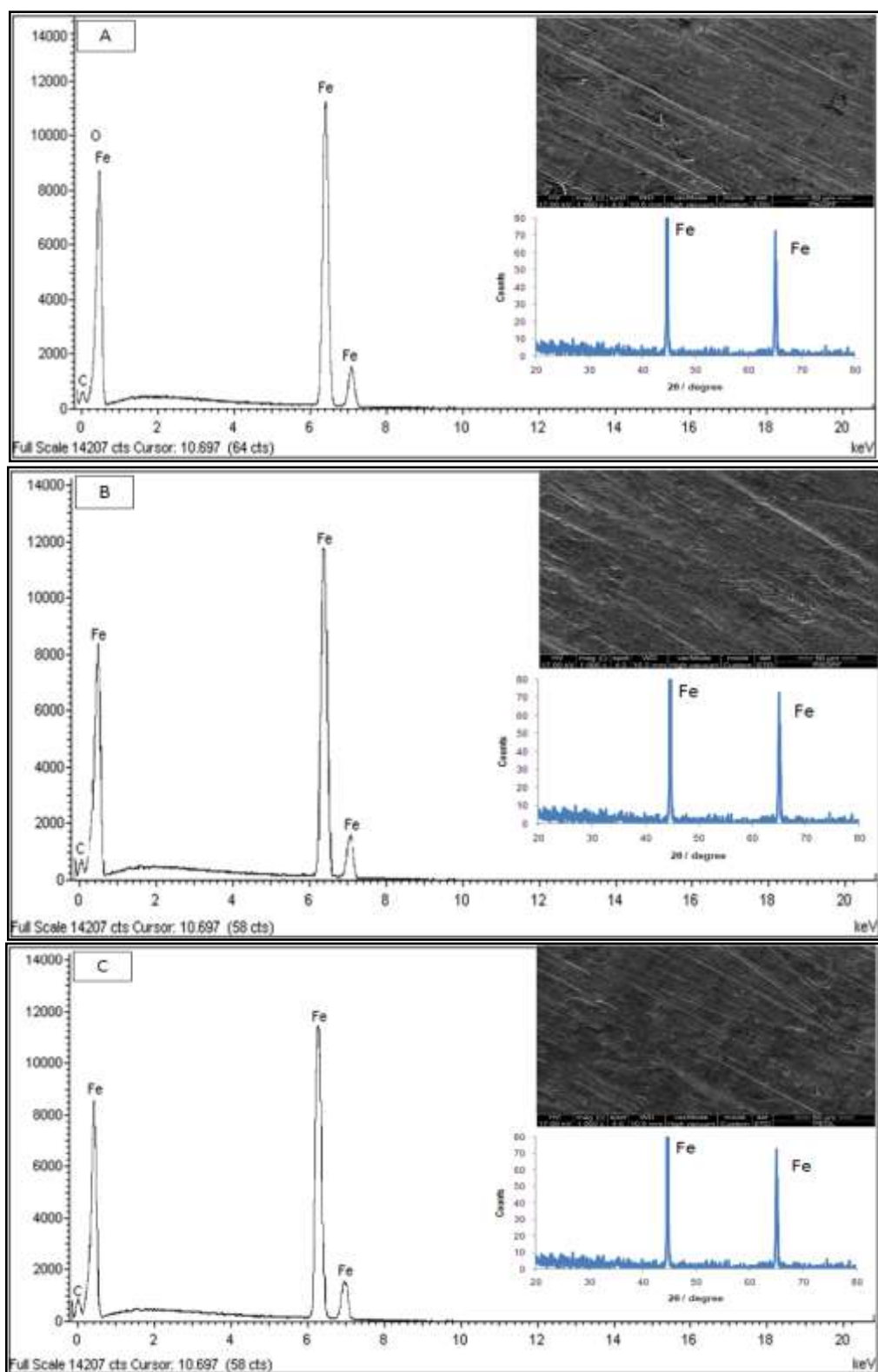


Figure 3.43: SEM (top right) micrograph, XRD (below right) and EDX spectra of mild steel after 48 h of immersion in 0.5 M HCl solution in presence of; (A) Kraft, (B) soda and (C) organosolv lignin fractions at 303 K and magnification 1000 x.

Table 3.26: Percentage atomic contents of elements obtained from EDX spectra.

Mild steel samples	Element (% atomic)			
	Fe	C	O	Cl
Polished	97.05	2.13	0.82	-
0.5 M HCl	60.27	2.68	35.39	1.66
500 ppm AHN EOL	68.53	6.74	24.73	-
500 ppm AHD EOL	75.35	4.35	20.30	-
500 ppm P.Kraft lignin	64.45	4.66	30.89	-
500 ppm P.Soda lignin	73.10	5.14	21.76	-
500 ppm P.Organosolv lignin	65.69	6.34	27.98	-

Obviously, the surface morphology of the mild steel plates in the presence of modified and ultrafiltrated lignin inhibitors were significantly improved as compared to that in the blank (0.5 M HCl). Smoother surfaces (Figure 3.42B-C & Figure 3.43A-C) were observed in the inhibited mild steel surface whilst a rough surface was noticed for mild steel immersed in 0.5 M HCl solution (Figure 3.42A). This indicates that the modified and ultrafiltrated lignin inhibitors hinders further dissolution of iron, resulting in the reduced rate of corrosion of mild steel in 0.5 M HCl solution. Meanwhile, the EDX spectra of mild steel plate in 0.5 M HCl show high atomic percentage of oxygen (Table 3.26) which confirms the formation of corrosion products (such as ferric hydroxide, $\text{Fe}(\text{OH})_3$ and oxyhydroxides, FeOOH) due to the further oxidation of adsorptive ferrous chloride, $(\text{FeCl})_{\text{ads}}$. In the presence of lignin inhibitors, the EDX spectra show lower intensity of oxygen atom but high iron content, indicating that the inhibitors have slowed down the dissolution of iron and protected the mild steel surface from the formation of corrosion products.

The X-ray diffraction patterns of the surface of the mild steel specimens immersed in various test solutions are given in Figures 3.42 and 3.43. As observed in the figure, the peaks at $2\theta = 28^\circ$, 35.4° and 61.5° can be assigned to various oxides/oxyhydroxides of iron and the peaks due to iron appeared at $2\theta = 44.6^\circ$ and

65.4° (Abboud *et al.*, 2012). In the absence of the inhibitor, the surface of the mild steel plate contains magnetite (Fe_3O_4) and lepidocrocite ($\gamma\text{-FeOOH}$). Upon immersion in the modified lignin inhibitors, several lepidocrocite peaks have diminished as well as reduced in favor of the formation of a thin protective film, thus impeding further the corrosion process.

3.5.5 Correlation between modified lignin properties and the mild steel corrosion inhibition and their possible mechanisms

The modification (via the incorporation of organic scavengers; 2-naphthol and 1,8-dihydroxyanthraquinone during the autohydrolysis pretreatment) and fractionation (via ultrafiltration membrane method) of lignin structures has tremendously altered both physical and chemical properties of the lignin (Figure 3.44). Higher phenolic – OH content (especially the S-unit content) with smaller fragments of lignin structures (low average molecular weight and T_g value) was produced leading to a good antioxidant activity (as observed from the oxygen uptake inhibition and reducing power assay) with better solubility. Indeed, a positive correlation between the modified lignin structures, antioxidant activity and the corrosion inhibitive action has been obtained in this study. All tested lignin samples exhibited good inhibitive properties towards the corrosion of mild steel in 0.5 M HCl solution. AHD EOL shows ideal lignin properties with a better corrosion inhibition action than other lignin samples due to the fact that 1,8-dihydroxyanthraquinone scavenger induced higher polarity (increase solubility) and hydrogen donating ability (better reducing power).

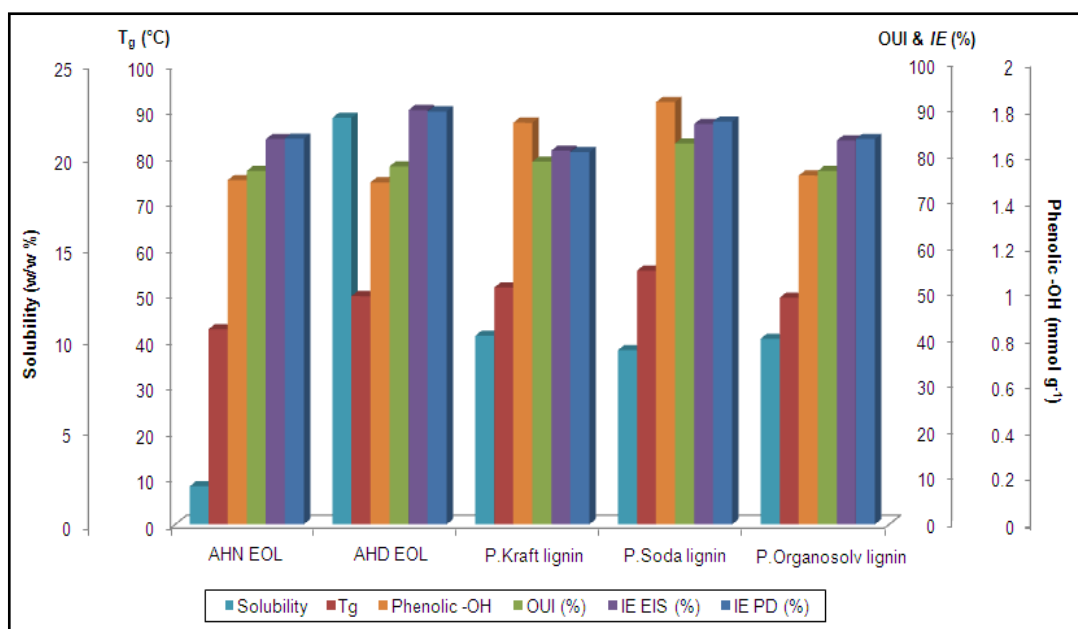


Figure 3.44: Influence of the diverse parameters studied on the inhibition efficiency of the analyzed lignins at the concentration of 500 ppm.

Both EIS and polarization measurements (predominant anodic inhibition: AHN EOL, AHD EOL and organosolv lignin fraction; predominant cathodic inhibition: Kraft and soda lignin fraction) have revealed that all lignin inhibitors gave the highest percentage of inhibition efficiency (% IE) up to 80-90 %. The inhibition efficiency of modified and ultrafiltrated lignin obtained from this study was comparable with other previous lignin derivatives used as corrosion inhibitors (Vargin *et al.*, 2006; Ren *et al.*, 2008; Abu-Dalo *et al.*, 2013). The adsorption and PZC studies suggested that the adsorption of mild steel in the presence of modified and ultrafiltrated lignins are enhanced through the Van der Waals interaction (ΔG_{ads}° obtained close to physisorption phenomenon) between the smaller lignin molecules that are more uniform (as observed from GPC analysis) and which possess high number of protonated hydroxyl donor atoms, with the mild steel surface. Thus possible inhibition mechanism could be similar to the mechanism shown in Figure 3.45.

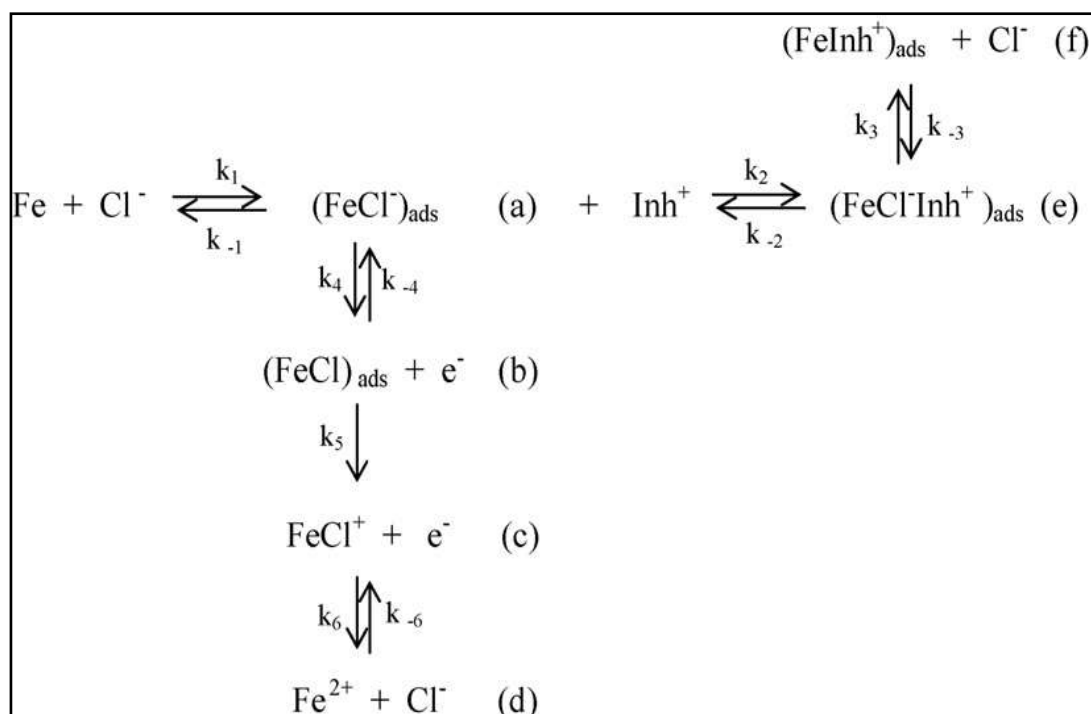


Figure 3.45: Corrosion inhibition reaction pathway of mild steel (Solmaz *et al.*, 2008).

As observed in the PZC studies (refer to previous subchapter 3.5.4), in the absence of lignin inhibitors, the anodic dissolution reaction of mild steel follows the pathway (a→d) (Yurt *et al.*, 2004). The positive excess charge (+32 mV) of mild steel in 0.5 M HCl allows the adsorption of Cl^- ions. The adsorption of negatively charged Cl^- ions on mild steel surface creates an excess of positive charge in the solution (Solmaz *et al.*, 2008). Protonated inhibitor molecules (in this case modified and ultrafiltrated lignins) could adsorb on the mild steel surface; through Cl^- ions that forms an interconnecting bridge between the positively charged mild steel and the protonated inhibitors (Tang *et al.*, 2006). According to Solmaz *et al.* (2008), the reaction mechanism is changed and proceeded to form $(\text{FeInh}^+)_{\text{ads}}$ (a→f). The electrostatic interaction of inhibitor molecules (via adsorbed Cl^- ions) on the mild steel surface has decreased the excess positive charge in the solution. In order to follow the reaction pathway from (a) to (f), the k_3 rate constant must be bigger than k_2 as well as k_4 .

Additionally, the cathodic hydrogen evolution reaction can be described as follows:



The protonated lignin inhibitor molecules could also be adsorbed at the cathodic sites to compete with the hydrogen ions that will later be reduced to hydrogen gas. This assumption is also supported by the result of potentiodynamic polarization measurements which suggested a mixed type inhibition, with predominance either at anodic (for AHN EOL, AHD EOL and organosolv lignin fraction) or cathodic (Kraft and soda lignin fractions) sites. In addition the $\Delta G_{\text{ads}}^\circ$ values indicated that both physical and chemical adsorptions are possible (values between -20 and -40 kJ mol⁻¹). The physical and chemical adsorption of modified and ultrafiltrated lignin molecules on the mild steel surface could be rationalized by the following ways (Figure 3.46); i) electrostatic interaction of protonated inhibitor with the adsorbed Cl⁻ ions, ii) donor acceptor interactions between π electrons to d-orbitals of iron and iii) interaction between lone pairs electron of heteroatoms (S, O and/or N) to d-orbitals of iron. The formation of a protective film on the mild steel surface has reduced the localized attack that could lead to the formation of corrosion products.

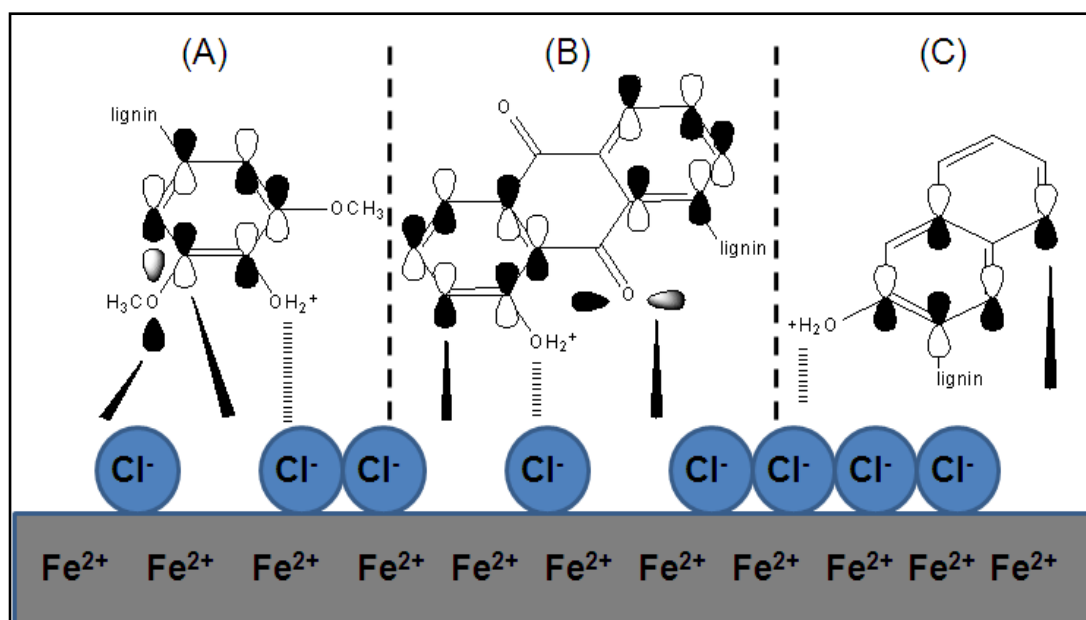


Figure 3.46: Schematic adsorption and inhibition interaction mechanism of lignin molecules at; (A) syringyl unit, (B) 1,8-dihydroxyanthraquinone and (C) 2-naphthol sites on mild steel in 0.5 M HCl.

CHAPTER FOUR

CONCLUSION AND FUTURE RESEARCH RECOMMENDATIONS

The treatment of oil palm fronds (OPF) with alkaline and organic alcoholic solution is practically suitable for the isolation of lignins. The differences with regards to the spectral characteristics and analytical results among the lignin samples are related to the delignification processes. FTIR, ^1H and ^{13}C NMR spectra of Kraft, soda and organosolv lignin samples were classified as HGS lignin since Kraft and soda lignin samples comprised mainly of phenolic $-\text{OH}$ while organosolv lignin comprised mainly of primary and secondary aliphatic $-\text{OH}$ functional groups. High molecular weight of Kraft lignin (as compared to soda and organosolv lignin) was influenced by the repolymerization reaction during the alkaline pulping process. Quantification of phenolic acids and aldehydes in OPF using alkaline nitrobenzene oxidation has revealed that non-condensed syringyl (S) units were more favorable to be degraded compared with the non-condensed guaiacyl (G) units. From this study, it was shown that alkaline pulping method (Kraft and soda) gave higher phenolic $-\text{OH}$ and molecular weight to that of the organosolv method. Higher amounts of phenolics, molecular weight and thermal decomposition temperature of the OPF lignin may suggest that it could potentially serve as better and green phenolic substitutes for various applications.

In order to improve the lignin extractability and properties, combinative pretreatments (dilute sulphuric acid and/or autohydrolysis with organosolv delignification step) was done. The physicochemical characterization shows that the combinative pretreatment processes gave almost similar lignin chemical

compositions (mainly the HGS subunit content) with the direct delignification process. It was successfully proven that different pretreatment processes can influence several properties of extracted lignin, mainly its molecular weight distribution, phenolic –OH content and thermal stability. It was observed that the combined autohydrolysis with organosolv process gave lower concentration of aliphatic –OH groups and higher concentration of HGS phenolic –OH groups. This phenomenon is mainly due to the extensive depolymerization (at higher severity) of lignin during autohydrolysis through the scission of β -O-4 bonds leading to the production of phenolic –OH groups. At the same time, the repolymerization of lignin decreased the degree of delignification, resulting in undesirable effects on the properties and reactivity of lignin. This phenomenon relevant only to a relatively minor part of the lignin since the combinative treatment extracted small percentage of the total lignin.

The complexity of lignin structures might affect the properties of lignin. In addition, high hydrophobicity of organosolv lignin can limit its capability to be employed in other possible applications. Therefore, the modulation of suitable lignin structures (by considering its solubility, molecular weight, phenolic content) is important so that it can overcome such limitations. Obviously, the properties of lignin can be improved by modifying its structure. It was revealed that the modification of the lignin structures by the incorporation of organic scavengers (2-naphthol and 1,8-dihydroxyanthraquinone) during the autohydrolysis pretreatment could substantially improve the lignin recovery. The HMBC NMR study proposed that the modification of lignin in the presence of 2-naphthol gave rise to an interaction possibly at C2 and/or C3 position of naphthol while the presence of 1,8-dihydroxyanthraquinone

will form an interaction possibly at C3 and/or C6 of the anthraquinone moiety. Modified lignin fractions with higher phenolic –OH content but low molecular weight, polydispersity as well as aliphatic –OH content resulted in higher values of antioxidant activity (as observed from oxygen uptake inhibition and reducing power assay) and better solubility.

Alternatively, modification of lignin structure can also be done by using fractionation technique. In fact, fractionation of lignin via ultrafiltration technique is one of a proper way to obtain smaller fractions of lignin (with low molecular weight). Lignin samples resulting from the direct delignification processes (Kraft, soda and organosolv) were subjected to the ultrafiltration system using smaller membrane cut-off (5 kDa). Improved physicochemical properties of ultrafiltrated lignins were observed where smaller fragments of lignin with higher phenolic –OH content (especially the phenolic S units) were produced from this method. In addition, the second major finding was that the oxygen uptake inhibition of ultrafiltrated lignins seems be dependent on the increased free phenolic –OH and *ortho*-methoxyl content, through the stabilization of the radical formed. Besides, the reducing power assay has also revealed that lignin samples with high S unit content could probably improve the antioxidant ability.

The corrosion inhibitive properties of the resulted lignin from these two modification methods towards the corrosion of mild steel were tested. Preliminary dissolution tests proved that both modification methods produced lignin with better solubility. The improved solubility of lignin translates into better corrosion inhibitors. It was observed that the higher solubility of AHD EOL lignin was because it contains more

polar hydroxyl functional groups (from the incorporation of 1,8-dihydroxyanthraquinone) thus increase the hydrophilicity of lignin that promotes dissolution in water. Both modified and ultrafiltrated lignins have exhibited good corrosion inhibition properties for mild steel in 0.5 M HCl solution. The best percentage of inhibition efficiency (% *IE*) was attained at the concentration of 500 ppm for all lignin inhibitors (with AHD EOL act as the most efficient corrosion inhibitor than others) but decreased with the increase in temperature as observed from the weight loss measurement.

Potentialdynamic polarization measurements demonstrate that modified and ultrafiltrated lignins act as mixed-type inhibitors with predominant anodic (for AHN EOL, AHD EOL and organosolv lignin fraction) and cathodic (Kraft and soda lignin fractions) effectiveness. The adsorption of lignin molecules on the mild steel surface was found to fit the Langmuir adsorption isotherm best. The free energy of adsorption ΔG°_{ads} , indicates that the process was spontaneous and the inhibitors were physically adsorbed (physisorption) onto the mild steel surface. The surface analysis shows that there was a significant surface improvement (with large reduction of corrosion products evidenced by EDX and XRD analysis) in the presence of lignin inhibitors, indicating that a temporary protective film was formed on the mild steel surface. The increased inhibition efficiency were associated with the improved properties of modified lignins namely the smaller and compact structure (low molecular weight, high phenolic –OH content with better solubility) of lignin.

In this study, it was shown that both modification techniques (incorporation of organic scavengers and ultrafiltration) produce smaller lignin fragments with

improved properties. Positive results from corrosion inhibition study revealed that both modification techniques will produce lignin with good inhibitive properties. Nevertheless, the incorporation of organic scavengers can be said as the best method to modify the lignin structure since it gave good extraction yield (refer to mass balance in Figure 2.1), better solubility, inexpensive (only small amount of organic scavengers required, ~ 4 % wt) and high % *IE* values. In contrast, modification of lignin structure via ultrafiltration membrane gave very low percentage of recovery, time consuming (since the flow flux small) and costly (requires more solvent and the price of ultrafiltration membrane is expensive) even though it gave better solubility and good corrosion inhibition efficiencies. These assumptions are important for upscaling purposes especially in the industry.

In order to have better understanding and improvements on the various processes and techniques in this work, further studies can be possibly carried out in the future. The isolation of lignin from oil palm fronds using various kinds of combined delignification and/or valorization processes (such as microwave assisted extraction, steam explosion or enzymatic hydrolysis) in order to give better lignin extractability and properties can be carried out. Besides, the incorporation of lignin with other types of organic scavenger compounds (such as aniline or amine derivatives and phenolic compounds) can be also studied to obtain better dissolution and antioxidant properties of lignin. For instance, the fractionation of lignin molecules using different types of ultrafiltration membrane cut-off (300, 150, 50, 15 and 10 kDa) or materials (ceramic, polysulfone, polypropylene, nylon 6, PTFE, PVC and acrylic copolymer) would be more interesting to study with. Modulation of proposed structure of lignin

can be studied by employing modeling technique, so that it will give more precise information on their possible chemical interactions.

The improved properties of modified lignin molecules and their correlation with corrosion inhibition efficiencies (especially to the phenolic –OH content and antioxidant activity) can be also linked with possible chemical assays such as total phenolic content, ABTS and DPPH. Apart from that, the corrosion inhibition studies of lignin inhibitors can also be done for other metals (like stainless steel, carbon steel, aluminum, copper and zinc alloys) and employing recent techniques such as scanning electrochemical microscopy (SECM), electron probe microanalyzer (EPMA) and electrochemical noise (EN). These perhaps would broaden the applicability of lignin corrosion inhibitors. In the same time, the inhibitive action of lignin inhibitors in different types of corrosive media at various concentration ranges would also give beneficial information for corrosion scientist.

REFERENCES

- Abboud, Y., Hammouti, B., Abourriche, A., Ihssane, B., Bennamara, A., Charrouf, M., Al-Deyab, S.S. (2012). 2-(o-Hydroxyphenyl)Benzimidazole as new corrosion inhibitor for mild steel in hydrochloric acid solution. *International Journal of Electrochemical Science* 7, 2543-2551.
- Abdel-Gaber, A.M., Abd-El-Nabey, B.A., Sidahmed, I.M., El-Zayady, A.M., Saadawy, M. (2006). Inhibitive action of some plant extracts on the corrosion of steel in acidic media. *Corrosion Science* 48, 2765-2779.
- Abdul Khalil, H.P.S., Nurul Fazita, M.R., Bhat, A.H., Jawaid, M., Nik Fuad, N.A. (2010). Development and material properties of new hybrid plywood from oil palm biomass, *Materials & Design* 31, 417-424.
- Abdullah, N., Sulaiman, F., Gerhauser, H. (2011). Characterization of oil palm empty fruit bunches for fuel application. *Journal of Physical Science* 22 (1), 1-24.
- Abu-Dalo, M.A., Al-Rawashdeh, N.A.F., Ababneh, A. (2013). Evaluating the performance of sulfonated Kraft lignin agent as corrosion inhibitor for iron-based materials in water distribution system. *Desalination* 313, 105-114.
- Ahamad, I., Prasad, R., Quraishi, M.A. (2010). Adsorption and inhibitive properties of some new Mannich bases of Isatin derivatives on corrosion of mild steel in acidic media, *Corrosion Science* 52, 1472-1481.
- Ahmad, Z. (2006). *Principles of Corrosion Engineering and Corrosion Control*. Oxford: Elsevier, pp. 1-7, 635-641.
- Aljourani, J., Raeissi, K., Golozar, M.A. (2009). Benzimidazole and its derivatives as corrosion inhibitors for mild steel in 1 M HCl solution. *Corrosion Science* 51, 1836-1843.
- Allwar, Md Noor, A.B., Mohd Nawi, M.A. (2008). Textural Characteristics of Activated Carbons Prepared from Oil Palm Shells Activated with ZnCl_2 and Pyrolysis Under Nitrogen and Carbon Dioxide. *Journal of Physical Science* 19(2), 93-104.
- Alriols, M.G., Tejado, A., Blanco, M., Mondragon, I., Labidi, J. (2009). Agricultural palm oil tree residues as raw material for cellulose, lignin and hemicelluloses production by ethylene glycol pulping process. *Chemical Engineering Journal* 148, 106-114.
- Alriols, M.G., Garcia, A., Llano-ponte, R., Labidi, J. (2010). Combined organosolv and ultrafiltration lignocellulosic biorefinery process. *Chemical Engineering Journal* 157, 113-120.

- Ammalahti, E., Brunow, G., Bardet, M., Robert, D., Kipelainen, I.J. (1998). Identification of side-chain structures in a poplar lignin using three-dimensional HMQC-HOHAHA NMR spectroscopy. *Journal of Agricultural and Food Chemistry* 46, 5113-5117.
- Ansari, K.R. and Quraishi, M.A. (2014). Bis-Schiff bases of isatin as new and environmentally benign corrosion inhibitor for mild steel. *Journal of Industrial and Engineering Chemistry* 20, 2819-2829.
- Araujo, J.D.P. (2008). Production of vanillin from lignin present in the Kraft black liquor of the pulp and paper industry. PhD thesis, Porto: University of Porto, Portugal.
- Asan, A., Soylu, S., Kiyak, T., Yıldırım, F., Oztas, S. G., Ancin, N., Kabasakaloglu, M. (2006). Investigation on some Schiff bases as corrosion inhibitors for mild steel. *Corrosion Science* 48, 3933–3944.
- Ashassi-Sorkhabi, H., Seifzadeh, D., Hosseini, M. G. (2008). EN, EIS and polarization studies to evaluate the inhibition effect of 3H-phenothiazin-3-one, 7-dimethylamin on mild steel corrosion in 1 M HCl solution. *Corrosion Science* 50, 3363–3370.
- Ateya, B., El-Anadouli, B.E., El-Nizamy, F.M. (1984). The adsorption of thiourea on mild steel. *Corrosion Science* 24, 509-515.
- Babic-Samardzija, K., Lupu, C., Hackerman, N., Barron, A. R., and Luttge, A. (2005). Inhibitive Properties and Surface Morphology of a Group of Heterocyclic Diazoles as Inhibitors for Acidic Iron Corrosion. *Langmuir* 21, 12187.
- Bahrami, M. J., Hosseini, S. M. A., Pilvar, P. (2010). Experimental and theoretical investigation of organic compounds as inhibitors for mild steel corrosion in sulfuric acid medium. *Corrosion Science* 52, 2793-2803.
- Baker, R.W. (2000). *Membrane technology and applications*. Hoboken, New Jersey: John Wiley and Sons.
- Barclay, L.R.C., Xi, F., Norris, J.Q. (1997). Antioxidant properties of phenolic lignin model compounds. *Journal of Wood Chemistry and Technology* 17 (1-2), 73-90.
- Behpour, M., Ghoreishi, S. M., Salavati-Niasari, M., Ebrahimi, B. (2008). Evaluating two new synthesized S–N Schiff bases on the corrosion of copper in 15% hydrochloric acid. *Materials Chemistry and Physics* 107, 153-157.
- Belgacem, M.N., Blayo, A., Gandini, A. (2003). Organosolv lignin as a filler in inks, varnishes and paints. *Industrial Crops and Products* 18, 145–153.

- Benar, P., Goncalves, A.R., Mandelli, D., Schuchardt, U. (1999). Eucalyptus organosolv lignins: study of the hydroxymethylation and use in resols. *Bioresource Technology* 68, 11-16.
- Bendahou, M., Benabdellah, M., Hammouti, B. (2006). A study of rosemary oil as a green corrosion inhibitor for steel in 2 M H₃PO₄. *Pigment & Resin Technology* 35/2, 95–100.
- Bengaly, K., Liang, J.B., Jelan, Z.A., Ho, Y.W., Ong, H.K. (2010). Utilization of steam-processed oil palm (*Elaeis guineensis*) frond by ruminants in Malaysia: Investigations for nitrogen supplementation. *African Journal of Agricultural Resources* 5(16), 2131-2136.
- Bentiss, F., Lebrini, M., Lagrenee, M. (2005). Thermodynamic characterization of metal dissolution and inhibitor adsorption processes in mild steel/2,5-bis(n-thienyl)-1,3,4-thiadiazoles/hydrochloric acid system. *Corrosion Science* 47, 2915–2931.
- Blain, T.J. (1993). Anthraquinone Pulping: Fifteen Years Later. *TAPPI* 76 (3), 137-146.
- Boeriu, C.G., Bravo, D., Gosselink, R.J.A., Van Dam, J.E.G. (2004). Characterisation of structure-dependent functional properties of lignin with infrared spectroscopy. *Industrial Crops and Products* 20, 205-218.
- Bouklah, M., Benchat, N., Hammouti, B., Aouriti, A., Kertit, S. (2006). Thermodynamic characterisation of steel corrosion and inhibitor adsorption of pyridazine compound in 0.5 M H₂SO₄. *Materials Letters* 60, 1901-1905.
- Bouyanzer, A., Hammouti, B., Majidi, L., (2006). Pennyroyal oil from *Mentha pulegium* as corrosion inhibitor for steel in 1 M HCl. *Materials Letters* 60, 2840-2843.
- Brosse, N., El Hage, R., Sannigrahi, P., Ragauskas, A. (2010). Dilute sulphuric acid and ethanol organosolv pretreatment of *Miscanthus x Giganteus*. *Cellulose Chemistry and Technology* 44 (1-3), 71-78.
- Brosse, N., Mohamad Ibrahim, M.N., Abdul Rahim, A. (2011). Biomass to Bioethanol: Initiatives of the future for lignin. *ISRN Material Science* 461482, 1-10.
- Brosse, N., Dufour, A., Meng, X., Sun, Q., Ragauskas, A. (2012). *Miscanthus*: a fast-growing crop for biofuels and chemical production. *Biofuels Bioproducts and Biorefining*, 1-19. In Press, DOI: 10.1002/bbb.1353.
- Brunow, G. (2001) Methods to Reveal the Structure of Lignin. In: M. Hofrichter, A. Steinbüchel, (Eds.) *Biopolymers. Volume 1. Lignin, Humic Substances and Coal*, Vol. 1, Berlin: Wiley-VCH Verlag GmbH, p. 106.

- Burton, G.W., Doba, T., Gabe, E., Hughes, L., Lee, F.L., Prasad, L., Ingold, K.U. (1985). Autoxidation of biological molecules. Maximizing the antioxidant activity of phenols. *Journal of American Chemical Society* 107 (24), 7035-7065.
- Camarero, S., Bocchini, P., Galletti, G.C., Martinez, A.T. (1999). Pyrolysis-gas chromatography/Mass spectrometry analysis of phenolic and etherified units in natural and industrial lignins. *Rapid Communication in Mass Spectroscopy* 13, 630-636.
- Capanema, E.A., Balakshin, M.Y., Kadla, J.F. (2004). A comprehensive approach for quantitative lignin characterization by NMR spectroscopy. *Journal of Agricultural and Food Chemistry* 52, 1850-1860.
- Chandel, A.K., Singh, O.V., Rao, L.V. (2010). *Biotechnological Applications of Hemicellulosic Derived Sugars: State-of-the-Art*. Sustainable Biotechnology, Berlin: Springer-Verlag, pp. 63-81.
- Chauhan, L. R. and Gunasekaran, G. (2007). Corrosion inhibition of mild steel by plant extract in dilute HCl medium. *Corrosion Science* 49, 1143–1161.
- Cheng, S., Chen, S., Liu, T., Chang, X., Yin, Y. (2007). Carboxymethylchitosan as an ecofriendly inhibitor for mild steel in 1 M HCl. *Materials Letters* 61, 3276-3280.
- Chenier, P. J. (2002). *Survey of Industrial Chemistry* (3rd Edition). Berlin: Springer-Verlag.
- Clasen, C. and Kulicke, W.M. (2011). Determination of viscoelastic and rheo-optical material functions of water-soluble cellulose derivative. *Progress in Polymer Science* 26, 1839-1937.
- Cleveland, C. J. (2004). *Encyclopedia of Energy*. Volumes 1-6, Amsterdam: Elsevier B.V.
- Dahlan, I. (2000). Oil palm frond, a feed for herbivores. *Asian Australasian Journal of Animal Sciences* 13, 300-303.
- Davis, J. R. (2000). *Corrosion: Understanding The Basic*, ASM International. Ohio: The Materials Information Society, pp. 1-14.
- de Souza, F. S. and Spinelli, A. (2009). Caffeic acid as a green corrosion inhibitor for mild steel. *Corrosion Science* 51, 642–649.
- de Vrije, T., de Hass, G.G., Tan, G.B., Keijsers, E.R.P., Claaseen, P.A.M. (2002). Pretreatment of Miscanthus for hydrogen production by Thermotoga elfii. *International Journal of Hydrogen Energy* 27, 1381-1390.
- Dence, C.W. and Lin, S.Y. (1992). *Methods in lignin chemistry*. Berlin: Springer-Verlag, pp. 3-17.

- Dizhbite, T., Telysheva, G., Jurkjane, V., Viesturs, U. (2004). Characterization of radical scavenging activity of lignin-natural antioxidants. *Bioresource Technology* 95 (3), 309-317.
- Dominguez, J.C., Oliet, M., Alonso, M.V., Gilarranz, M.A., Rodriguez, F. (2008). Thermal stability and pyrolysis kinetics of organosolv lignins obtained from *Eucalyptus globulus*. *Industrial Crops and Products* 27, 150-156.
- Dominguez-Benetton, X., Sevda, S., Vanbroekhoven, K., Pant, D. (2012). The accurate use of impedance analysis for the study of microbial electrochemical systems, *Chemical Society Reviews* 41, 7228-7246.
- Duff, S.J.B. and Murray, W.D. (1996). Bioconversion of forest products industry waste cellulosic to fuel ethanol: a review. *Bioresource Technology* 55, 1-33.
- Elaeis guineensis, (2014). Wikipedia. Available via URL.
http://www.en.wikipedia.org/wiki/Elaeis_guineensis, (accessed January 2014).
- El-Etre, A. Y. (2006). Khillah extract as inhibitor for acid corrosion of SX 316 steel. *Applied Surface Science* 252, 8521–8525.
- El-Etre, A. Y. (2007). Inhibition of acid corrosion of carbon steel using aqueous extract of olive leaves. *Journal of Colloid and Interface Science* 314, 578–583.
- El Hage, R., Brosse, N., Chrusciel, L., Sanchez, C., Sannigrahi, P., Ragauskas, A. (2009). Characterization of milled wood lignin and ethanol organosolv lignin from miscanthus. *Polymer Degradation and Stability* 94, 1632-1638.
- El Hage, R., Chrusciel, L., Desharnais, L., Brosse, N. (2010). Effect of autohydrolysis of *Miscanthus x giganteus* on lignin structure and organosolv delignification. *Bioresource Technology* 101, 9321-9329.
- El Hage, R., Perrin, D., Brosse, N. (2012). Effect of pre-treatment severity on the antioxidant properties of ethanol organosolv *Miscanthus x giganteus* lignin. *Natural Resources* 3, 29-34.
- El Mansouri, N.E. and Salvado, J. (2006). Structural characterization of technical lignins for the production of adhesives: application to lignosulfonate, kraft, soda-anthraquinone, organosolv and ethanol process lignins. *Industrial Crops and Products* 24, 8-16.
- Eloualja, H., Perrin, D., Martin, R. (1995). Kinetic study of the thermal oxidation of all trans- β -carotene and evidence of its antioxidant properties. *New Journal of Chemistry* 19 (11), 863-872.
- European Union Directive 2009/28/EC.

- FAO. (2009). FAOSTAT online statistical service. Food and Agriculture Organization of the United Nations, Rome, Italy. Available via URL. <http://faostat.fao.org/> (accessed February 2014).
- Feldman, D. and Banu, D. (1997). Contribution to the study of rigid PVC polyblends with different lignins. *Journal of Applied Polymer Science* 66(9), 1731-1744.
- Ferreira, E. S., Giancomelli, C., Giancomelli, F. C., Spinelli, A. (2004). Evaluation of the inhibitor effect of l-ascorbic acid on the corrosion of mild steel. *Materials Chemistry and Physics* 83, 129-134.
- Field, C.B., Behrenfeld, M.J., Randerson, J.T., Falkowski, P. (1998). Primary Production of the Biosphere: Integrating Terrestrial and Oceanic Components. *Science* 281 (5374), 237–240.
- Fitzherbert, E.B., Struebig, M.J., Morel, A., Danielsen, F., Brühl, C.A., Donald, P.F., Phalan, B. (2008). How will oil palm expansion affect biodiversity? *Trends in Ecology and Evolution* 23 (10), 539-545.
- Fleming, B.I., Kubes, G.J., Macleod, J.M., Bolker, H.I. (1978). Soda Pulping with Anthraquinone. *TAPPI* 61 (6), 43-46.
- Fontana, M. G. (1986). *Corrosion Engineering, 3rd Edition*. New York: McGraw-Hill Book Company.
- Fouda, A. S. and Mahfouz, H. (2009). Inhibition of corrosion of α -brass (Cu-Zn, 67/33) in HNO_3 solutions by some arylazo indole derivatives. *Journal of Chilian Chemical Society* 54 (3), 302-308.
- Francesco, L., Chiara, S., Guido, E., Francesca, M., Giaime, M., Anna Maria, F. (2009). Diclorfenec nanosuspension: Influence of preparation procedure and crystal form on drug dissolution behavior. *International Journal of Pharmacognosy* 373, 124–132.
- Garcia, A., Toledano, A., Serrano, L., Egues, I., Gonzales, M., Marinn, F., Labidi, J. (2009). Characterization of lignins obtained by selective precipitation. *Separation and Purification Technology* 68, 193-198.
- Garcia, A., Toledano, A., Andres, M.A., Labidi, J. (2010). Study of the antioxidant capacity of Miscanthus sinensis lignins. *Process Biochemistry* 45, 935-940.
- Garrote, G., Dominguez, H., Parajo, J.C. (1999). Mild autohydrolysis: an environmentally friendly technology for xylooligosaccharide production wood. *Journal of Chemical Technology and Biotechnology* 74 (11), 1101-1109.
- Gierer, J. (1980). Chemical aspect of kraft pulping. *Wood Science and Technology* 14, 241-266.

- Glasser, W.G., Dave, V., Frazier, C.E. (1993). Molecular weight distribution of semi-commercial lignin derivatives. *Journal of Wood Chemistry and Technology* 13 (4), 545-559.
- Goh, C.S., Lee, K.T., Bhatia, S. (2010a). Hot compressed water pretreatment of oil palm fronds to glucose recovery for production of second generation bio-ethanol. *Bioresource Technology* 101, 7362-7367.
- Goh, C.S., Tan, H.T., Lee, K.T., Mohamed, A.R. (2010b). Optimizing ethanolic hot compressed water (EHCW) cooking as a pretreatment to glucose recovery for the production of fuel ethanol from oil palm fronds (OPF). *Fuel Processing Technology* 91, 1146-1151.
- Goncalves, A.R. and Benar, P. (2001). Hydroxymethylation and oxidation of organosolv lignins and utilization of the products. *Bioresource Technology* 79, 103-111.
- Gosselink, R.J.A. (2011). Lignin as a renewable aromatic resource for the chemical industry. PhD thesis, Wageningen: Wageningen University, Netherland.
- Granata, A. and Argyropoulos, D.S. (1995). 2-chloro-4,4,5,5-tetramethyl-1,3,2-dioxaphospholane, a reagent for the accurate determination of the uncondensed and condensed phenolic moieties in lignins. *Journal of Agricultural Food Chemistry* 43, 1538-1544.
- Gregorova, A., Cibulkova, Z., Kosikova, B., Simon, P. (2005). Stabilization effect of lignin in polypropylene and recycled polypropylene. *Polymer Degradation and Stability* 89, 553-558.
- Groysman, A. (2010). *Corrosion for Everybody*. New York: Springer, pp. 10, 152, 223-224.
- Gulcin, I., Oktay, M., Kirecci, E., Kufrevioglu, O.I. (2003). Screening of antioxidant and antimicrobial activities of anise (*Pimpinella anisum* L.) seed extracts. *Food Chemistry* 83, 371-382.
- Hasanov, R., Sadıkoğlu, M., Bilgiç, S. (2007). Electrochemical and quantum chemical studies of some Schiff bases on the corrosion of steel in H₂SO₄ solution. *Applied Surface Science* 253, 3913–3921.
- Hassan, H.H., Abdelghani, E., Amin, M.A. (2007). Inhibition of mild steel corrosion in hydrochloric acid solution by triazole derivatives. Part I: Polarization and EIS studies. *Electrochimica Acta* 52, 6359–6366.
- Henriksson, G., Li, G., Zhang, L., Lindström, M.E. (2010) Lignin Utilization. In: Crocker, M. (Ed.). *Thermochemical Conversion of Biomass to Liquid Fuels and Chemicals*, Royal Society of Chemistry. pp. 223-262.

- Holladay, J.E., Bozell, J.J., White, J.F., Johnson, D. (2007) Top value added chemicals from biomass, volume II – results of screening for potential candidates from biorefinery lignin. Pacific Northwest National Laboratory and the National Renewable Energy Laboratory. *US Department of Energy* DE-ACOS-76RL01830.
- Holtmam, K.M., Chang, H.M., Jameel, H., Kadla, J.F. (2003). Comparison of modified DFRC and thioacidolysis. *Journal of Agricultural and Food Chemistry* 51, 3535-3540.
- Holton, H.H. (1977). Delignification of lignocellulosic materials with an alkaline pulping liquor containing a alder adduct of benzoquinone or naphthquinone, *US Patent* 4,036,681.
- Issaadi, S., Douadi, T., Zouaoui, A., Chafa, S., Khan, M. A., Bouet, G. (2011). Novel thiophene symmetrical Schiff bases compounds as corrosion inhibitor for mild steel in acidic media. *Corrosion Science* 53, 1484-1488.
- Johnson, D.K., Bozell, J., Holladay, J.E., White, J.F. (2005). Use of lignin in the biorefinery. *Proceeding of the International Lignin Institute 7th Forum*, Barcelona. 31-34.
- Kamide, K. (2005). *Cellulose and cellulose derivatives: molecular characterization and its applications*. Amsterdam: Elsevier B.V., p. 150.
- Kawamoto, H., Mohamed, W.Z., Mohd Shukur, N.I., Mohd Ali, M.S., Ismail, Y., Oshio, S. (2001). Palatability, digestibility and voluntary intake of processed oil palm fronds in cattle. *Jarq-Japan Agricultural Research Quarterly* 35(3), 195-200.
- Keles, H., Keles, M., Dehri, I., Serindag, O. (2008). Adsorption and inhibitive properties of aminobiphenyl and its Schiff base on mild steel corrosion in 0.5 M HCl medium. *Colloid Surface A: Physicochemical Engineering Aspects* 320, 142-143.
- Kirk-Othmer Encyclopedia. (2005). *Encyclopedia of Chemical Technology*. 5th Edition, Hoboken, New Jersey: John Wiley and Sons.
- Klemola, A., Nyman, G. A. (1966). Steam hydrolysis of birchwood: The effect hydrolysis on the hemicellulose, cellulose, and on the lignin of birchwood. *Paperi ja Puu* 48, 595-603.
- Klemola, A. (1968). Steam hydrolysis of birchwood. Part III: Investigation of low-molecular aromatic degradation products. *Suom Kemistil B* 41, 83-98.
- Koh, L.P. and Ghazoul, J. (2008). Biofuels, biodiversity and people: understanding the conflicts and finding opportunities. *Biololgy Conservation* 141, 2450-2460.

- Kringstad, K.P. and Roland, M. (1983). ^{13}C -NMR Spectra of Kraft lignin. *Holzforschung* 37, 237-244.
- Kruger, J. (2001), *Electrochemistry of Corrosion, Electrochemistry Encyclopedia*, Baltimore: The Johns Hopkins University, pp. 1-13.
- Kubo, S. and Kadla, J.F. (2004). Poly(ethylene oxide)/organosolv lignin blends: relationship between thermal properties, chemical structure, and blend behavior. *Macromolecules* 37, 6904–6911.
- Kustu, C., Emregul, K. C., Atakol, O. (2007). Schiff bases of increasing complexity as mild steel corrosion inhibitors in 2 M HCl. *Corrosion Science* 49, 2800–2814.
- Lester, R.B. (2006). *Plan B 2.0 Rescuing a Planet Under Stress and a Civilization in Trouble*. New York: WW Norton & Co., Earth Policy Institute.
- Li, S. and Lundquist, K. (2000). Cleavage of arylglycerol beta-aryl ethers under neutral and acidic conditions. *Nordic Pulp and Paper Research Journal* 15, 292-299.
- Li, J. and Gellerstedt, G. (2008). Improved lignin properties and reactivity by modifications in the autohydrolysis process of aspen wood. *Industrial Crops and Products* 27, 175-181.
- Liu, P. (2002). Improvement of bio-oil stability in wood pyrolysis. PhD thesis, Birmingham: Aston University, UK.
- Loh, Y.F., Paridah, M.T., Hoong, Y.B., Bakar, E.S., Anis, M., Hamdan, H. (2011). Resistance of phenolic-treated oil palm stem plywood against subterranean termites and white rot decay. *International Biodeterioration & Biodegradation* 65, 14-17.
- Lora, J.H. and Wayman, M. (1979). Delignification of hardwoods by autohydrolysis and extraction. *TAPPI* 61, 47-50.
- Lora, J.H. and Glasser, W.G.J. (2002). Recent industrial applications of lignin – a sustainable alternative to non-renewable materials. *Journal of Polymer and the Environment* 10, 39-48.
- Lora, J.H. (2008). Industrial commercial lignins: sources, properties and applications. In: Belgacem, M.N., Gandini, A. (Eds.) *Monomers, polymers and composites from renewable resources*. Oxford: Elsevier, pp. 225-241.
- Lu, Q., Zhu, M., Zu, Y., Liu, W., Yang, L., Zhang, Y., Zhao, X., Zhang, X., Zhang, X., Li, W. (2012). Comparative antioxidant activity of nanoscale lignin prepared by a supercritical antisolvent (SAS) process with non-nanoscale lignin. *Food Chemistry* 135, 63-67.

- Lundquist, K. (1992). ^1H NMR spectral studies of lignins. *Nordic Pulp and Paper Research Journal* 1, 4-16.
- Marcus, P. and Mansfeld, F. (2006). *Analytical Method in Corrosion Science and Engineering*, Florida: Taylor and Francis Group, pp. 466-472.
- Matsushita, Y., Imai, M., Iwatsuki, A., Fukushima, K. (2008). The relationship between surface tension and the industrial performance of water-soluble polymers prepared from acid hydrolysis lignin, a saccharification by-product from woody materials. *Bioresource Technology* 99, 3024-3028.
- Mohamad Ibrahim, M.N. and Azian, H. (2005). Extracting soda lignin from the black liquor of oil palm empty fruit bunch. *Jurnal Teknologi*, 42(C), 11–20.
- Mohamad Ibrahim, M.N., Yusof, N.N.M., Saleh, N.M., Coswald, S.S., Sollehuddin, S. (2008). Separation of vanillin from oil palm empty fruit bunch lignin. *Clean* 36(3), 287-291.
- Mohamad Ibrahim, M.N., Zakaria, N., Sipaut, C.S., Sulaiman, O., Hashim, R. (2011). Chemical and thermal properties of lignin from oil palm biomass as a substitute for phenol formaldehyde resin production. *Carbohydrate Polymers* 86, 112-119.
- Mohan, D., Pittman, C.U., Steele, P.H. (2006). Single, binary and multi-component adsorption of copper and cadmium from aqueous solutions on Kraft lignin – a biosorbent. *Journal of Colloid and Interface Science* 297, 489-504.
- Morad, M.S. and Kamal El-Dean, A.M. (2006). 2,2'-dithiobis(3-cyano-4,6-dimethylpyridine): A new class of acid corrosion inhibitors for mild steel. *Corrosion Science* 48, 3398-3412.
- Moretti, G., Guidi, F., Fabris, F. (2013). Corrosion inhibition of mild steel in 0.5 M HCl by 2-butyl-hexahydropyrrolo[1,2-b][1,2]oxazole. *Corrosion Science* 76, 206-218.
- Morgan, J. J. and Stumm, W. (1981). *Aquatic Chemistry*, 2nd Edition. New York: Wiley, p 235.
- Mosier, N., Wyman, C., Dale, B., Elander, R., Lee, Y.Y., Holtzapple, M., Ladisch, M. (2005). Features of promising technologies for pretreatment of lignocellulosic biomass. *Bioresource Technology* 96, 673-686.
- Mulder, M. (1991). *Basic principles of membrane technology*. New York: Kluwer Academic Publisher.
- Mussatto, S.I., Fernandes, M., Roberto, I.C. (2007). Lignin recovery from brewer's spent grain black liquor. *Carbohydrate Polymers* 70, 218-223.

- Mussatto, S.I. and Teixeira, J.A. (2010). Lignocellulose as raw material in fermentation processes. In: Mendez-Vilas, A. (Ed.) Current Research, Technology and Education Topics in Applied Microbiology and Microbial Biotechnology, *FORMATEX*, pp. 897-907.
- NACE. (2002). Corrosion index. Available via URL.
<http://events.nace.org/publicaffairs/cocorrindex.asp>
- Nada, A.M.A, Yousef, M.A, Shaffei, K.A., & Salah, A.M. (1998). Infrared Spectroscopy of some treated lignins. *Polymer Degradation and Stability* 62(1), 157-163.
- Nadji, H., Diouf, P.N., Benaboura, A., Bedard, Y., Riedl, B., Stevanovic, T. (2009). Comparative study of lignins isolated from Alfa grass (*Stipa tenacissima* L.). *Bioresource Technology* 100, 3585-3592.
- Noor, E.A. and Al-Moubaraki, A.H. (2008). Thermodynamic study of metal corrosion and inhibitor adsorption processes in mild steel/1-methyl-4[4'(-X)-styryl pyridinium iodides/hydrochloric acid systems. *Materials Chemistry and Physics* 110, 145–154.
- Norman, R.O.C. and Taylor, R. (1965). *Electrophilic substitution in benzenoid compounds*. New York: Elsevier.
- Norul Izani, M.A., Paridah, M.T., Mohd Nor, M.Y., Anwar, U.M.K. (2013). Properties of medium-density fibreboard (MDF) made from treated empty fruit bunch of oil palm. *Journal of Tropical Forest Science* 25 (2), 175–183.
- Obama, P., Ricochon, G., Munuglia, L., Brosse, N. (2012). Combination of enzymatic hydrolysis and ethanol organosolv pretreatments: Effect on lignin structures, delignification yields and cellulose-to-glucose conversion. *Bioresource Technology* 112, 156-163.
- Obot, I. B., Obi-Egbedi, N. O., Umoren, S. A. (2009). Adsorption characteristics and corrosion inhibitive properties of clotrimazole for aluminium corrosion in hydrochloric acid. *International Journal of Electrochemical Science* 4, 863-877.
- Obot, I.B. and Obi-Egbedi, N.O. (2010). 2,3-Diphenylbenzoquinoxaline: A new corrosion inhibitor for mild steel in sulphuric acid. *Corrosion Science* 52, 282-285.
- Oguzie, E. E. (2007). Corrosion inhibition of aluminium in acidic and alkaline media by *Sansevieria trifasciata* extract. *Corrosion Science* 49, 1527–1539.
- Oil palm biomass, (2011). Available via URL.
<http://www.bfdic.com/en/Features/Features/79.html>, (accessed August 2011).

- Okafor, P. C. and Ebenso, E. E. (2007). Inhibitive action of *Carica papaya* extracts on the corrosion of mild steel in acidic media and their adsorption characteristics. *Pigment & Resin Technology* 36/3, 134–140.
- Önnerud, H. and Gellerstedt, G. (2003). Inhomogeneities in chemical structure of hard-wood lignins. *Holzforschung* 57, 255-265.
- Onuorah, E.O. (2005). Properties of fiberboards made from oil palm (*Elaeis guineensis*) stem and/or mix tropical hardwood sawmill residues. *Journal of Tropical Forest Science* 17(4), 497-507.
- Orubite, K. O. and Oforka, N. C. (2004). Inhibition of the corrosion of mild steel in hydrochloric acid solutions by the extracts of leaves of *Nypa fruticans* Wurmb. *Materials Letters* 58, 1768– 1772.
- Pan, X., Arato, C., Gilkes, N., Gregg, D., Mabey, W., Pye, K., Xiao, Z., Zhang, X., Saddler, J. (2005). Biorefining of softwoods using ethanol organosolv pulping: Preliminary evaluation of process streams for manufacture of fuel-grade ethanol and co-products. *Biotechnology and Bioengineering* 90 (4), 473-481.
- Pan, X.J., Kadla, J.F., Ehara, K., Gilkes, N., Sadler, J.N. (2006). Organosolv ethanol lignin from hybrid poplar as a radical scavenger: Relationship between lignin structure extraction conditions and antioxidant activity. *Journal of Agricultural and Food Chemistry* 54 (16), 5806-5813.
- Patel, D.P. and Varshney, A.K. (1989). The effect of presoaking and prehydrolysis on the organosolv delignification of bagasse. *Indian Journal of Technology* 27 (6), 285-288.
- Perez, N. (2004), *Electrochemistry and Corrosion Science*. New York: Kluwer Academic Publishers, pp. 72-85, 97-105.
- Pizzi, A. (1994). *Advanced Wood Adhesives Technology*. New York: Marcel Dekker, pp. 219-241.
- Poaty, B., Dumarcay, S., Gerardin, P., Perrin, D. (2010). Modification of grape seed and wood tannins to lipophilic antioxidant derivatives. *Industrial Crops and Products* 31, 509-515.
- Popova, A., Sokolova, E., Raicheva, S., Christov, M. (2003). AC and DC study of the temperature effect on mild steel corrosion in acid media in the presence of benzimidazole derivatives. *Corrosion Science* 45, 33–58.
- Pouteau, C., Dole, P., Cathala, B., Averous, L., Boquillon, N. (2003). Antioxidant properties of lignin in polypropylene. *Polymer Degradation and Stability* 81 (1), 9-18.

- Pouteau, C., Cathala, B., Dole, P., Kurek, B., Monties, B. (2005). Structural modification of kraft lignin after acid treatment: characterization of the apolar extracts and influence on the antioxidant properties in polypropylene. *Industrial Crops and Products* 21, 101-108.
- Ragauskas, A., Williams, C., Davison, B., Britovsek, G., Cairney, J., Eckert, C., Frederick, W., Hallett, J., Leak, D., Liotta, C., Mielenz, J., Murphy, R., Templer, R., Tschaplinski, T. (2006). The path forward for biofuels and biomaterials. *Science* 311, 484-489.
- Rahman, S.H., Choudhury, J.P., Ahmad, A.L., & Kamaruddin, A.H. (2007). Optimization studies on acid hydrolysis of oil palm empty fruit bunch fiber for production of xylose. *Bioresource Technology*, 98, 554-559.
- Rahman M. M. and Yusof A. M. (2011). Preparation and Modification of Activated Carbon from Oil Palm Shell and its Adsorption Capacity through Speciation of Chromium. *Research Journal of Chemistry and Environment* 15 (4), 49-51.
- Raja, P.B., Qureshi, A.K., Rahim, A.A., Osman, H., Awang, K. (2013). Neolamarckia cadamba alkaloids as eco-friendly corrosion inhibitors for mild steel in 1 M HCl media. *Corrosion Science* 69, 292-301.
- Randhir, R., Lin, Y.T., Shetty, K. (2004). Stimulation of phenolics, antioxidant and antimicrobial activities in dark germinated mung bean sprouts in response to peptide and phytochemical elicitors. *Process Biochemistry* 39, 637-646.
- Rasat, M.S.M., Wahab, R., Sulaiman, O., Mokhtar, J., Mohamed, A., Tabet, T.A., Khalid I. (2011). Properties of composite boards from oil palm frond agricultural waste. *BioResources* 6(4), 4389-4403.
- Ren, Y., Luo, Y., Zhang, K., Zhu, G., Tan, X. (2008). Lignin terpolymer for corrosion inhibition of mild steel in 10 % hydrochloric acid medium. *Corrosion Science* 50, 3147-3153.
- Revie, R. W. and Uhlig, H. H. (2008). *Corrosion and Corrosion Control: An Introduction to Corrosion Science and Engineering, 4th Edition*. New Jersey: John Wiley and Sons, pp. 303, 75-77.
- Riggs Jr., O. L. (1973). *Corrosion Inhibitors, 2nd Edition*. Texas: C. C. Nathan.
- Roberge, P. R. (2008). *Corrosion Engineering Principles and Practice*. New York: McGraw Hill, p 19.
- Robert, D.R., Michel, B., Gellerstedt, G., Lindfors, L. (1984). Structural changes in lignin during kraft cooking. Part 3. On the structure of dissolved lignins. *Journal of Wood Chemistry and Technology* 4, 239-263.

- Rohella, R.S., Sahoo, N., Paul, S.C., Choudhury, S. Chakravortty, V. (1996). Thermal studies on isolated and purified lignin. *Thermochimica Acta* 287, 131-138.
- Rozman, H.D., Kumar, R.N., Abdul Khalil, H.P.S., Abusamah, A., Lim, P.P., Ismail, H. (1997). Preparation and properties of oil palm frond composite based on methacrylic silane and glycidyl methacrylate. *European Polymer Journal* 33(3), 225-230.
- Saari, N., Hashim, R., Sulaiman, O., Hiziroglu, S., Sato, M., Sugimoto, T. (2014). Properties of steam treated binderless particleboard made from oil palm trunks. *Composites Part B: Engineering* 56, 344-349.
- Sabiha-Hanim, S., Noor, M.A.M., Rosma, A. (2011). Effect of autohydrolysis and enzymatic treatment on oil palm (*Elaeis guineensis* Jacq.) frond fibres for xylose and xylooligosaccharides production. *Bioresource Technology* 102, 1234-1239.
- Saha, J.B.T., Abia, D., Dumarcay, S., Ndikontar, M.K., Gerardin, P., Noah, J.N., Perrin, D. (2013). Antioxidant activities, total phenolic contents and chemical compositions of extracts from four Cameroonian woods: Padouk (*Pterocarpus soyauxii* Taubb), tali (*Erythrophleum suaveolens*), moabi (*Baillonella toxisperma*), and movingui (*Distermonanthus benthamianus*). *Industrial Crops and Products* 41. 71-77.
- Sahin, M., Bilgic, S., Yilmaz, H. (2002). The inhibition effects of some cyclic nitrogen compounds on the corrosion of the steel in NaCl mediums. *Applied Surface Science* 195, 1-7.
- Salamatinia, B., Kamaruddin, A.H., Abdullah, A.Z. (2010). Regeneration of reuse of spent NaOH-treated oil palm frond for copper and zinc removal from wastewater. *Chemical Engineering Journal* 156, 141-145.
- Samuel, R., Cao, S., Das, B.K., Hu, F., Pu, Y., Ragauskas, A.J. (2013). Investigation of the fate of poplar lignin during autohydrolysis pretreatment to understand the biomass recalcitrance. *RSC Advances* 3 (16), 5305-5309.
- Sannigrahi, P., Pu, Y., Ragauskas, A. (2010). Cellulosic biorefineries - unleashing lignin opportunities. *Current Opinion in Environmental Sustainability* 2, 383-393.
- Sarkar, N., Ghosh, S.K., Bannerjee, S., Aikat, K. (2012). Bioethanol production from agricultural wastes: An overview. *Renewable Energy* 37, 19-27.
- Sastri, V. S., Ghali, E., Elboujdaini, M. (2007). *Corrosion Prevention and Protection (Practical Solutions)*. England: John Wiley and Sons, pp. 80-84.
- Satapathy, A.K., Gunasekaran, G., Sahoo, S.C., Amit, K., Rodrigues, P.V. (2009). Corrosion inhibition by *Justicia gendarussa* plant extract in hydrochloric acid solution. *Corrosion Science* 51, 2848-2856.

- Schweitzer, P.A. (2007). *Corrosion of Linings and Coatings, Cathodic and Inhibition Protection and Corrosion Monitoring*. Florida: Taylor & Francis Group, pp. 55-67, 537-538.
- Sena-Martins, G., Almeida-Vara, E., Duarte, J.C. (2008). Eco-friendly new products form enzymatically modified industrial lignins. *Industrial Crops and Products* 27, 189-195.
- She, D., Xu, F., Geng, Z., Sun, R., Jones, G.L., Baird, M.S. (2010). Physicochemical characterization of extracted lignin from sweet sorghum stem. *Industrial Crops and Products* 32, 21-28.
- She, D., Nie, X.N., Xu, F., Geng, Z.C., Jia, H.T., Jones, G.L., Baird, M.S. (2012). Physico-chemical characterization of different alcohol-soluble lignins from rice straw. *Cellulose Chemistry and Technology* 46 (3-4), 207-219.
- Sheir, L. L, Jarman, R. A., Burstein, G. T. (1994). *Corrosion: Metal and Environment reactions, 3rd Edition*. London: Butterworth-Heinemann, p 3:4.
- Sherif, E. M. and Park, S. M. (2006). 2-amino-5-ethyl-1,3,4-thiadiazole as a corrosion inhibitor for copper in 3 % NaCl solution. *Corrosion Science* 48, 4065-4079.
- Shimada, K., Fujikawa, K., Yahara, K., Nakamura, T. (1992). Antioxidative properties of xanthan on the autoxidation of soybean oil in cyclodextrin emulsion. *Journal of Agricultural and Food Chemistry* 40, 945–948.
- Sims, R. (2003). *Biomass and resources bioenergy options for a cleaner environment in developed and developing countries*. London: Elsevier Science, pp. 184-198.
- Singley, J. F., Beaudet, B. A., Markey, P. H., DeBerry, D. W., Kidwell, J. R., Mallsh, D. A. (1985). *Corrosion Prevention and Control in Water Treatment and Supply Systems*. New Jersey: Noyes Publication, pp. 51-57.
- Sjöström, E. (1981). *Wood polysaccharides: Wood Chemistry, Fundamentals and Applications*. New York: Academic Press.
- Solmaz, R., Kardas, G., Yazici, B., Erbil, M. (2008). Adsorption and corrosion inhibitive properties of 2-amino-5-mercapto-1,3,4-thiadiazole on mild steel in hydrochloric acid media. *Colloid Surface A: Physicochemical Engineering Aspects* 312, 15-16.
- Spiridon, I. and Popa, V.I. (2008). Hemicelluloses: Major sources, properties and applications. In: Belgacem, M.N. and Gandini, A. (Eds.) *Monomers, polymers and composites from renewable resources*. Amsterdam: Elsevier B.V., pp. 289-304.

- Stanly-Jacob, K. and Parameswaran, G. (2010). Corrosion inhibition of mild steel in hydrochloric acid solution by Schiff base furoin thiosemicarbazone. *Corrosion Science* 52, 224-228.
- Stupnisek-Lisac, E., Gazivoda, A., Madzarac, M. (2002). Evaluation of non-toxic corrosion inhibitors for copper in sulphuric acid. *Electrochimica Acta* 47, 4189-4194.
- Sun, R.C., Tomkinson, J., Bolton, J. (1999). Effects of precipitation pH on the physicochemical properties of the lignins isolated from the black liquor of oil palm empty fruit bunch fibre pulping. *Polymer Degradation and Stability* 63 (2), 195-200.
- Sun, R.C., Lu, Q., Sun, X.F. (2001). Physico-chemical and thermal characterization of lignins from *Caligonum monogoliacum* and *Tamarix* sp. *Polymer Degradation and Stability* 72, 229-238.
- Sun, Y. and Cheng, J. (2002). Hydrolysis of lignocellulosic materials for ethanol production: A review. *Bioresource Technology* 83, 1-11.
- Talati, J. D., Desai, M. N., Shah, N. K. (2005). *meta*-Substituted aniline-*N*-salicylidenes as corrosion inhibitors of zinc in sulphuric acid. *Materials Chemistry and Physics* 93, 54-64.
- Tamura, H. (2008). The role of rusts in corrosion and corrosion protection of iron and steel, *Corrosion Science* 50, 1872-1883.
- Tang, L., Li, X., Li, L., Mu, G., Liu, G. (2006). The effect of 1-(2-pyridylazo)-2-naphthol on the corrosion of cold rolled steel in acidic media: Part 2: Inhibitive action of 0.5 M sulfuric acid. *Materials Chemistry and Physics* 97, 301-307.
- Tejado, A., Pena, C., Labidi, J., Echeverria, J.M., Mondragon, I.I. (2007). Physicochemical characterization of lignins from different sources for use in phenol-formaldehyde resin synthesis. *Bioresource Technology* 98, 1655-1663.
- Thring, R. Chornet, E., Qverend, R. (1990a). Recovery of a solvolytic lignin: effects of spent liquor/acid volume ratio, acid concentration and temperature. *Biomass* 23, 289-305.
- Thring, R.W., Chornet, E., Bouchard, J., Vidal, P.F., Overend, R.P., (1990b). Characterization of lignin residues derived from the alkaline hydrolysis of glycol lignin. *Canadian Journal of Chemistry* 68, 82-89.
- Thring, R.W., Vanderlaan, M.N., Griffin, S.L. (1996). Fractionation of Alcell lignin by sequential solvent extraction. *Journal of Wood Chemistry and Technology* 16 (2), 139-154.

- Timilsena, Y.P. (2012). Effect of different pretreatment methods in combination with the organosolv delignification process and enzymatic hydrolysability of three feedstocks in correlation with lignin structure. M.Eng thesis, Pathumthani: Asian Institute of Technology, Thailand.
- Timilsena, Y.P., Abeywickrama, C.J., Rakshit, S.K., Brosse, N. (2013a). Effect of different pretreatments on delignification pattern and enzymatic hydrolysability of miscanthus, oil palm biomass and typha grass. *Bioresource Technology* 135, 82-88.
- Timilsena, Y.P., Audu, I.G., Rakshit, S.K., Brosse, N. (2013b). Impact of the lignin structure of three lignocellulosic feedstocks on their organosolv delignification. Effect of carbonium ion scavengers. *Biomass and Bioenergy* 52, 151-158.
- Toledano, A., Garcia, A., Mondragon, I., Labidi, J. (2010a). Lignin separation and fractionation by ultrafiltration. *Separation and Purification Technology* 71, 38-43.
- Toledano, A., Serrano, L., Garcia, A., Mondragon, I., Labidi, J. (2010b). Comparative study of lignin fractionation by ultrafiltration and selective precipitation. *Chemical Engineering Journal* 157, 93-99.
- Toledano, A. (2012). Lignin extraction, purification and depolymerization study. PhD thesis. Pais Vasco: Universidad del Pais Vasco, Spain.
- Uhlig, H. H. (1985). *Corrosion and Corrosion Control*, 3rd Edition. New York: John Willey and Sons.
- UNEP. (2011). Oil palm plantations: threats and opportunities for tropical ecosystems. In: UNEP Global Environmental Alert Service (GEAS). Available via URL. <http://www.unep.org/geas>, 1-8, (accessed February 2014).
- Urgatondo, V., Mitjans, M., Vinardell, M.P. (2009). Applicability of lignin from different sources as antioxidants based on the protective effects on lipid peroxidation induced by oxygen radicals. *Industrial Crops and Products* 30 (2), 184-187.
- Uri, N. (1961). Physico-chemical aspects of autoxidation. In: Lundberg, W.O. (Ed.), *Autoxidation and antioxidants*. New York: Inter-Science Publisher, pp. 55-106.
- Valek, L. and Martinez, S. (2007). Copper corrosion inhibition by Azadirachta indica leaves extract in 0.5 M sulphuric acid. *Materials Letters* 61, 148-151.
- Van de Klashorst, G.H. (1989). Lignin-formaldehyde wood adhesives. In: Pizzi, A. (Ed.), *Wood Adhesives Chemistry and Technology*. New York: Marcel Dekker, pp. 155-190.

- Vargin, M.Y., Trashin, S.A., Karyakin, A. (2006). Corrosion protection of steel by electropolymerized lignins. *Electrochemistry Communications* 8, 60-64.
- Volk, T.A., Abrahamson, L.P., White, E.H., Neuhauser, E., Gray, E., Demeter, C., Lindsey, C., Jarnefeld, J., Aneshansley, D.J., Pellerin, R., Edick, S. (2000). Developing a Willow Biomass Crop Enterprise for Bioenergy and Bioproducts in the United States. *Proceedings of Bioenergy 2000*, North East Regional Biomass Program, OCLC 45275154.
- Wahyuningrum, D., Achmad, S., Syah, Y. M., Buchari, Bundjali, B., Ariwahjoedi, B. (2008). The correlation between structure and corrosion inhibition activity of 4,5-diphenyl-1-vinylimidazole derivative compounds towards mild steel in 1 % NaCl solution. *International Journal of Electrochemical Science* 3, 154-166.
- Walch, E., Zemmann, A., Schinner, F., Bonn, G., Bobleter, O. (1992). Enzymatic saccharification of hemicellulose obtained from hydrothermally pretreated sugar cane bagasse and beech bark. *Bioresource Technology* 39, 173-177.
- Wallberg, O., Jonsson, A.S., Wimmerstedt, R. (2003). Ultrafiltration of kraft black liquor with a ceramic membrane. *Desalination* 156, 145-153.
- Wan Adnan, W.E.A. (2012). Corrosion inhibition of mild steel by Xylopia Ferruginea leaf and bark extracts in 1 M HCl solution. M.Sc thesis, Penang: Universiti Sains Malaysia, Malaysia.
- Wanasundara, U.N. and Shahidi, F. (1994). Stabilization of canola oil with flavonoid. *Food Chemistry* 50 (4), 393-396.
- Wang, J., Cao, C., Chen, J., Zhang, M., Ye, G., Lin, H. (1995). Anodic desorption of inhibitors I. The phenomenon of anodic desorption of inhibitors. *Journal of China Society of Corrosion Protection* 15, 241-248.
- Wanrosli, W.D., Law, K.N., Zainuddin, Z., Asro, R. (2004). Effect of pulping variables on the characteristics of oil-palm frond-fiber. *Bioresource Technology* 93, 233-240.
- Wanrosli, W.D., Zainuddin, Z., Roslan, S. (2005). Upgrading the recycled paper with oil palm fiber soda pulp. *Industrial Crops and Products* 21, 325-329.
- Wanrosli, W.D., Zainuddin, Z., Law, K.N., Asro, R. (2007). Pulp from oil palm fronds by chemical processes. *Industrial Crops and Products* 25, 89-94.
- Wayman, M. and Lora, J.H. (1978). Aspen autohydrolysis. The effect of 2-naphthol and other aromatic compounds. *TAPPI* 61 (6), 55-57.
- Wayman, M. and Chua, M.G.S. (1979). Characterization of autohydrolysis aspen (P. tremuloides) lignins. Part 2. Alkaline nitrobenzene oxidation studies of extracted autohydrolysis lignin. *Can. J. Chem.* 57, 2599-2602.

- Wayman, M. and Lora, J.H. (1980). Simulated autohydrolysis of Aspen milled wood lignin in the presence of aromatic additives: Structural modifications. *Journal of Applied Polymer Science* 25, 2187-2194.
- Wu, T. X., Li, Z. J., Zhao, J. C. (1998). A facile method for the synthesis of 4-amino-5-hydrocarbon 2,4-dihydro-3h-1,2,4-triazole-3-thion Schiff bases. *Chemical Journal of China University* 19, 1617–1625.
- Xu, F., Sun, J.X., Sun, R.C., Fowler, P., Baird, M.S. (2006). Comparative study of organosolv lignins from wheat straw. *Industrial Crops and Products* 23, 180–193.
- Yang, D., Qiu, X., Zhou, M., Lou, H. (2007). Properties of sodium lignosulfonate as dispersant of coal water slurry. *Energy Conversion and Management* 48, 2433-2438.
- Yildiz, R., Doner, A., Dogan, T., Dehri, I. (2014). Experimental studies of 2-pyridinecarbonitrile as corrosion inhibitor for mild steel in hydrochloric acid solution. *Corrosion Science* 82, 125-132.
- Young, R.J. and Lovell, P.A. (1991). *Introduction to polymers (2nd ed.)*. London: Chapman and Hall.
- Yuan, T.Q., He, J., Xu, F., Sun, R.C. (2009). Fractionation and physicochemical analysis of degraded lignins from the black liquor of Eucalytup pellita KP-AQ pulping. *Polymer Degradation and Stability* 94, 1142-1150.
- Yuen, T.Q., Sun, S., Xu, F., Sun, R.C. (2011). Isolation and physico-chemical characterization of lignins from ultrasound irradiated fast-growing poplar wood. *BioResources* 6(1), 414-433.
- Yurt, A., Balaban, A., Ustun Kandemir, S., Bereket, G., Erk, B. (2004). Investigation on some Schiff bases as HCl corrosion inhibitors for carbon steel. *Materials Chemistry and Physics* 85, 420-426.
- Zahari, M.A.K.M., Zakaria, M.R., Ariffin, H., Mokhtar, M.N., Salihon, J., Shirai, Y., Hassan, M.A. (2012). Renewable sugars from oil palm frond juice as an alternative novel fermentation feedstock for value-added products. *Bioresource Technology* 110, 566-571.
- Zakzeski, J., Bruijninx, P.C.A, Jongerius, A.L., Weckhuysen, B.M. (2010). The catalytic valorization of lignin for the production of renewable chemicals. *Chemical Reviews* 110 (6), 3552-3599.
- Zhang, Y.H.P. (2008). Reviving the carbohydrate economy via multi-product lignocelluloses biorefineries. *Journal of Industrial Microbiology and Biotechnology* 35 (5), 367-375.

- Zhang, B., Wang, L., Shahbazi, A., Diallo, O., Whitmore, A. (2011). Dilute sulfuric acid pretreatment of cattails for cellulose conversion. *Bioresource Technology* 102, 9308-9312.
- Zhao, X.B., Dai, L., Liu, D. (2009a). Characterization and comparison of acetosolv and milox lignin isolated from crofton weed stem. *Journal of Applied Polymer Science* 114, 1295-1302.
- Zhao, X., Cheng, K., Liu, D. (2009b). Organosolv pre-treatment of lignocellulosic biomass for enzymatic hydrolysis. *Applied Microbiology and Biotechnology* 82, 815-27.
- Zheng, Y., Pan, Z., Zhang, R. (2009). Overview of biomass pretreatment for cellulosic ethanol production. *International Journal of Agricultural and Biological Engineering* 2 (3), 51-68.

LIST OF PUBLICATIONS, PRESENTATIONS AND AWARDS

Publications:

1) Physicochemical characterization of alkaline and ethanol organosolv lignins from oil palm (*Elaeis guineensis*) fronds as phenol substitutes for green material applications, (**M. Hazwan Hussin**, Afidah Abdul Rahim, Mohamad Nasir Mohamad Ibrahim, Nicolas Brosse), *Industrial Crops and Products*, (2013) 29, 23-32, Impact Factor: 3.208, Elsevier, Q1.

2) Investigation on the structure and antioxidant properties of modified lignin obtained by different combinative processes of oil palm fronds (OPF) biomass, (**M. Hazwan Hussin**, Afidah Abdul Rahim, Mohamad Nasir Mohamad Ibrahim, Mehdi Yemloul, Dominique Perrin, Nicolas Brosse), *Industrial Crops and Products* (2014) 52, 544-551, Impact Factor: 3.208, Elsevier, Q1.

3) Impact of catalytic oil palm fronds (OPF) pulping on organosolv lignin properties, (**M. Hazwan Hussin**, Afidah Abdul Rahim, Mohamad Nasir Mohamad Ibrahim, Mehdi Yemloul, Dominique Perrin, Nicolas Brosse), *Polymer Degradation and Stability* (2014) 109, 33-39, Impact Factor: 2.77, Elsevier, Q1.

4) Antioxidant and anticorrosive properties of oil palm frond lignins extracted with different techniques, (**M. Hazwan Hussin**, Affaizza Mohd Shah, Afidah Abdul Rahim, Mohamad Nasir Mohamad Ibrahim, Nicolas Brosse), *Annals of Forest Science* (2014), Article online, DOI: 10.1007/s13595-014-0405-1, Impact Factor: 1.63, Springer, Q1.

5) Improved corrosion inhibition of mild steel by chemically modified lignin polymers, (**M. Hazwan Hussin**, Afidah Abdul Rahim, Mohamad Nasir Mohamad Ibrahim, Nicolas Brosse), *Materials Chemistry and Physics*, Under review, Impact Factor: 2.1, Elsevier. Q1.

6) Enhanced properties of oil palm fronds (OPF) lignin via ultrafiltration fractionation technique, (**M. Hazwan Hussin**, Afidah Abdul Rahim, Mohamad Nasir Mohamad Ibrahim, Dominique Perrin, Nicolas Brosse), *Industrial Crops and Products*, Under review, Impact Factor: 3.208, Elsevier. Q1.

Proceedings:

Valorisation de co-produits de l'industrie de l'huile de palme pour la production de retardateurs de corrosion des métaux, (**M. Hazwan Hussin**, Affaizza Mohd Shah, Afidah Abdul Rahim, Mohamad Nasir Mohamad Ibrahim, Nicolas Brosse), *Seminaires Ecole Doctoral RP2E 2013*, Faculte des Sciences, 17th January 2013, Nancy, France.

Presentations:

1) Poster presentation entitles “The potential of oil palm biomass waste as mild steel corrosion inhibitor in acidic solution”, 2nd International Symposium of Sciences 2012, Organized by School of Biological Sciences, USM, 29th-31st August 2012, Penang.

2) Oral and poster presentation entitles “The extraction of lignin from Malaysian oil palm fronds and its application for as corrosion inhibitor”, USM-Universite de Lorraine Colloquium 2012, Faculte des Sciences, 12th-15th November 2012, Nancy, France.

3) Poster presentation entitles “Valorisation de co-produits de l'industrie de l'huile de palme pour la production de retardateurs de corrosion des métaux’, Seminaire Ecole Doctoral RP2E 2013, Faculte des Sciences, 17th January 2013, Nancy, France.

4) Oral presentation entitles “Extraction and characterization of lignin from oil palm fronds by different treatment and its corrosion inhibition ability”, Seminaire LERMAB, Faculte des Sciences, 27th May 2013, Nancy, France.

5) Oral presentation entitles “Extraction and characterization of lignin biopolymers from Malaysian oil palm fronds (OPF) and its possible material applications”, Malaysian Polymer International Conference 2013 (MPIC 2013), Hotel Equatorial Bangi, 24-25th September 2013, Bangi, Kuala Lumpur.

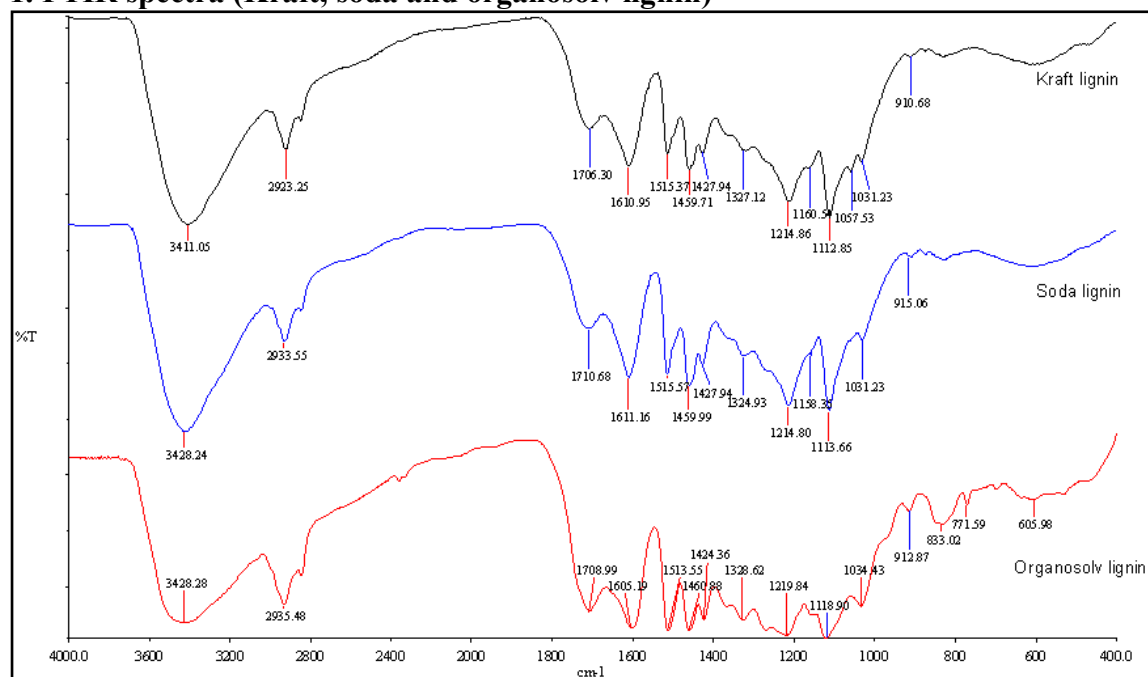
Awards:

- 1) Best Postgraduate Research Award (PhD – Natural Sciences), Majlis Persada Kencana 2014, Dewan Budaya, Universiti Sains Malaysia.
- 2) Prestigious External Award (Postgraduate Research Grant – Government of France), Majlis Persada Kencana 2014, Dewan Budaya, Universiti Sains Malaysia.

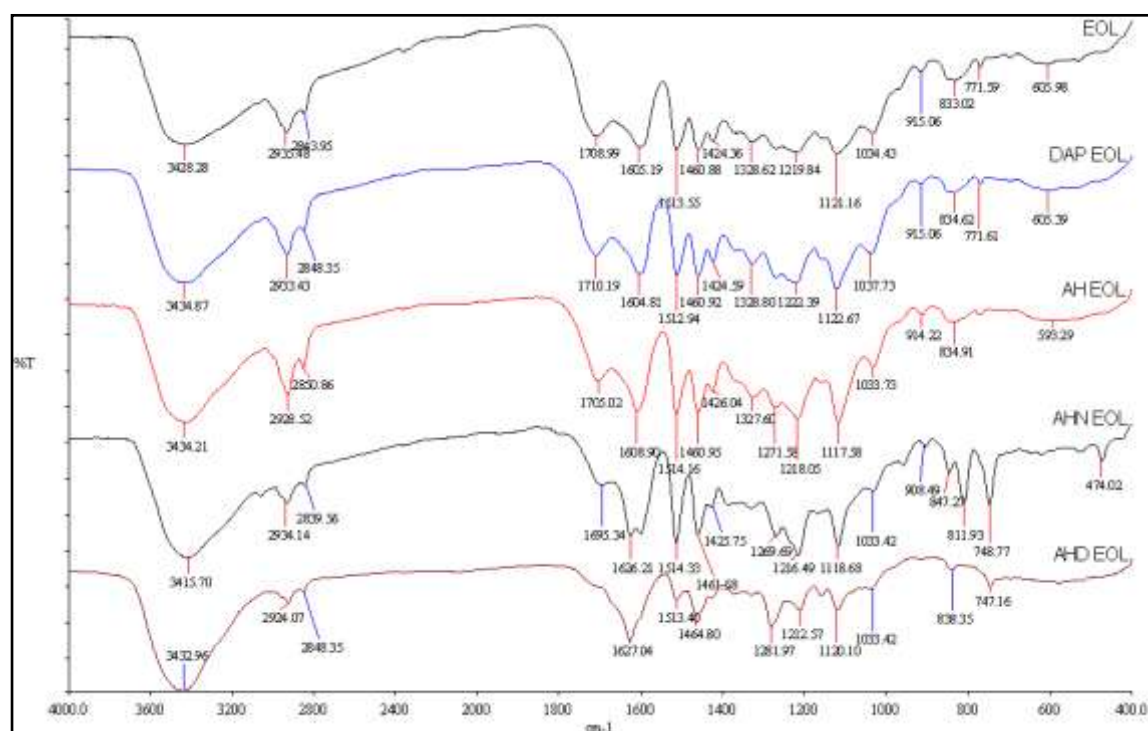
APPENDICES

APPENDIX I: FTIR spectra of lignin samples

1. FTIR spectra (Kraft, soda and organosolv lignin)

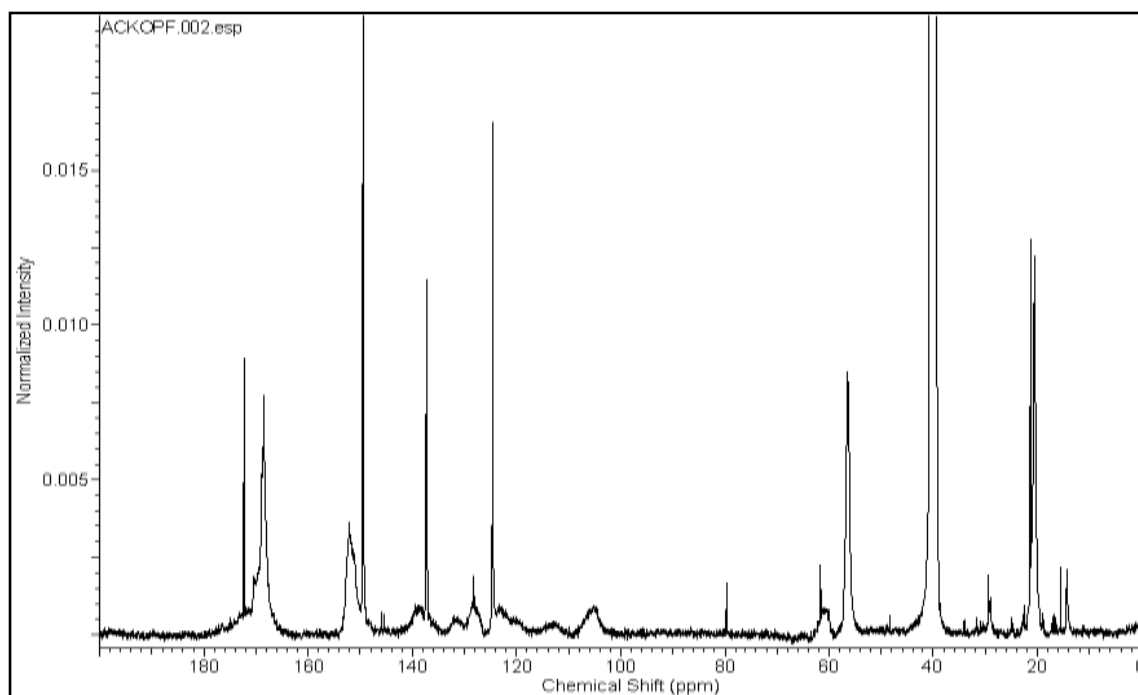


2. FTIR spectra (Organosolv lignin, DAP EOL, AH EOL, AHN EOL, AHD EOL)

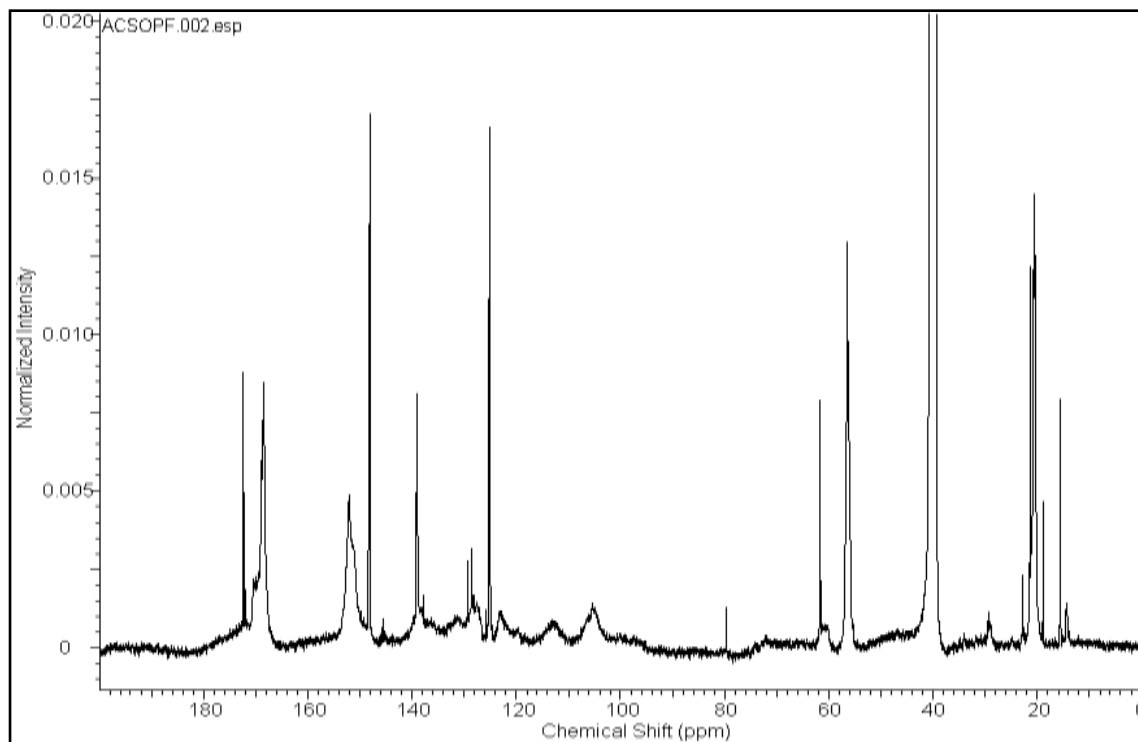


APPENDIX II: ^{13}C NMR spectra of lignin samples

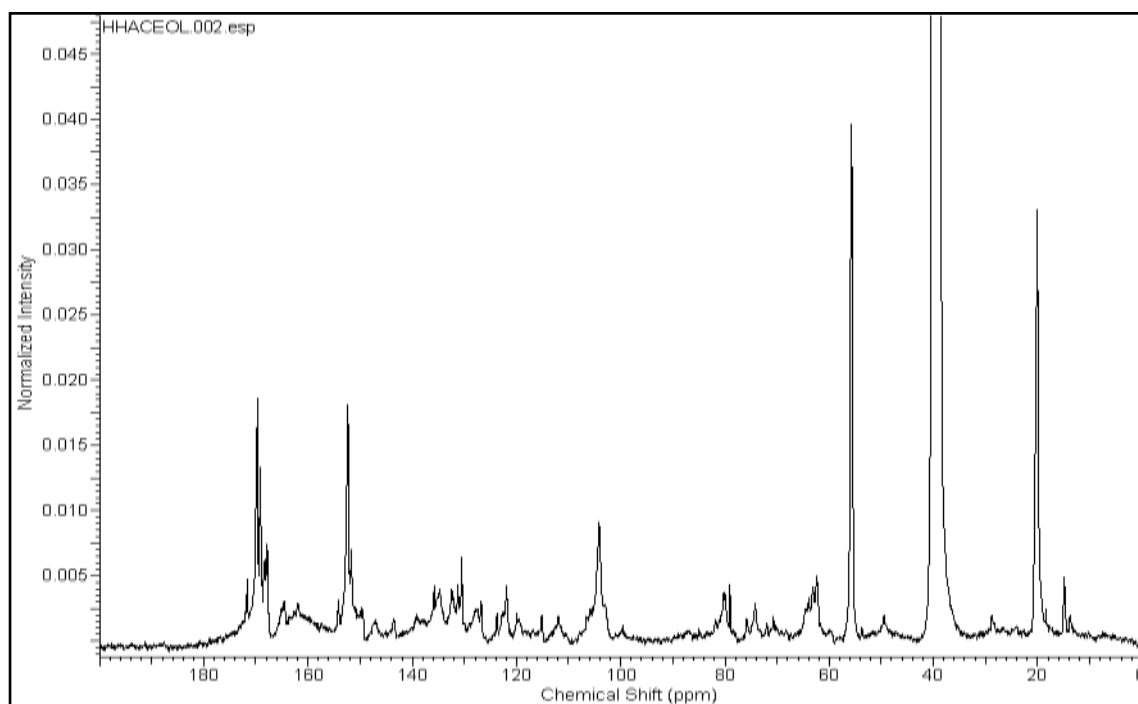
1. ^{13}C NMR spectrum of acetylated Kraft lignin



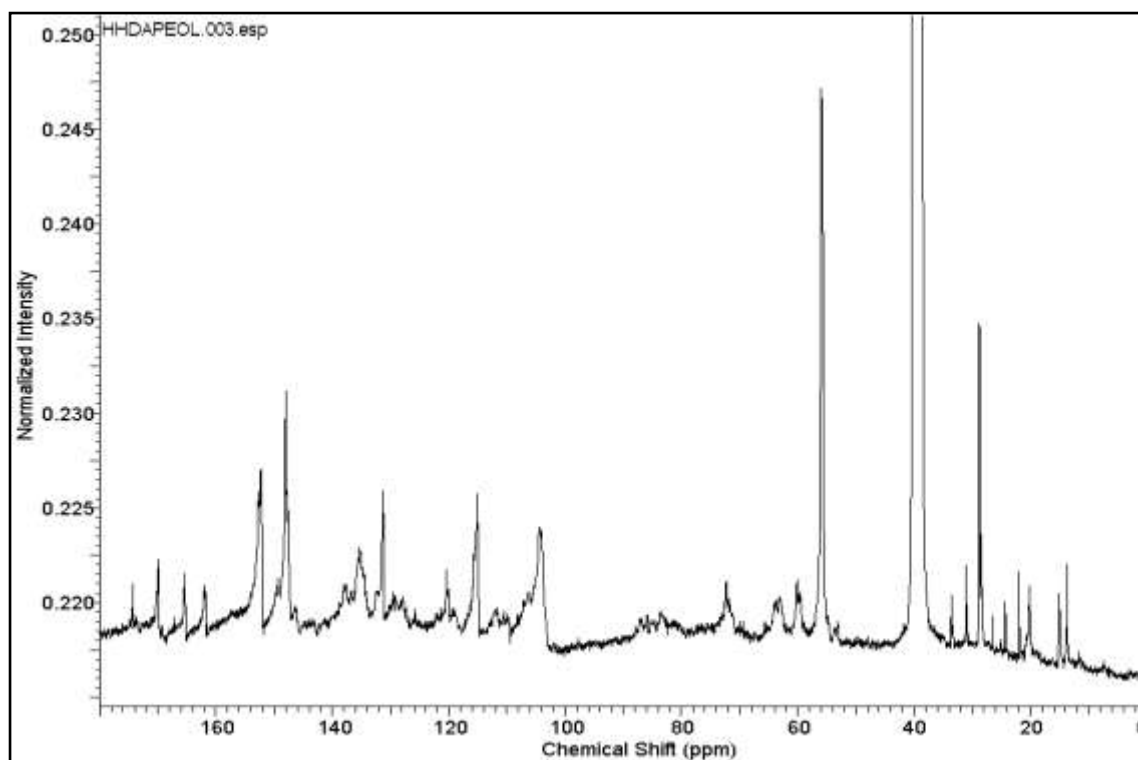
2. ^{13}C NMR spectrum of acetylated soda lignin



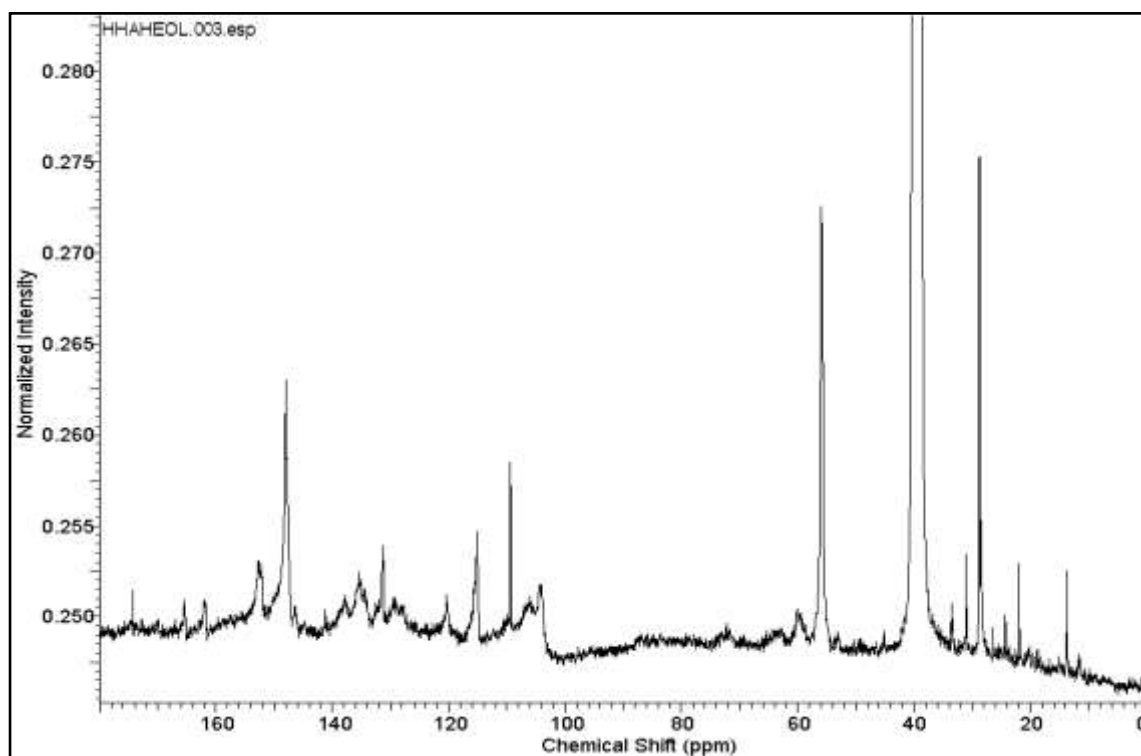
3. ^{13}C NMR spectrum of acetylated organosolv lignin



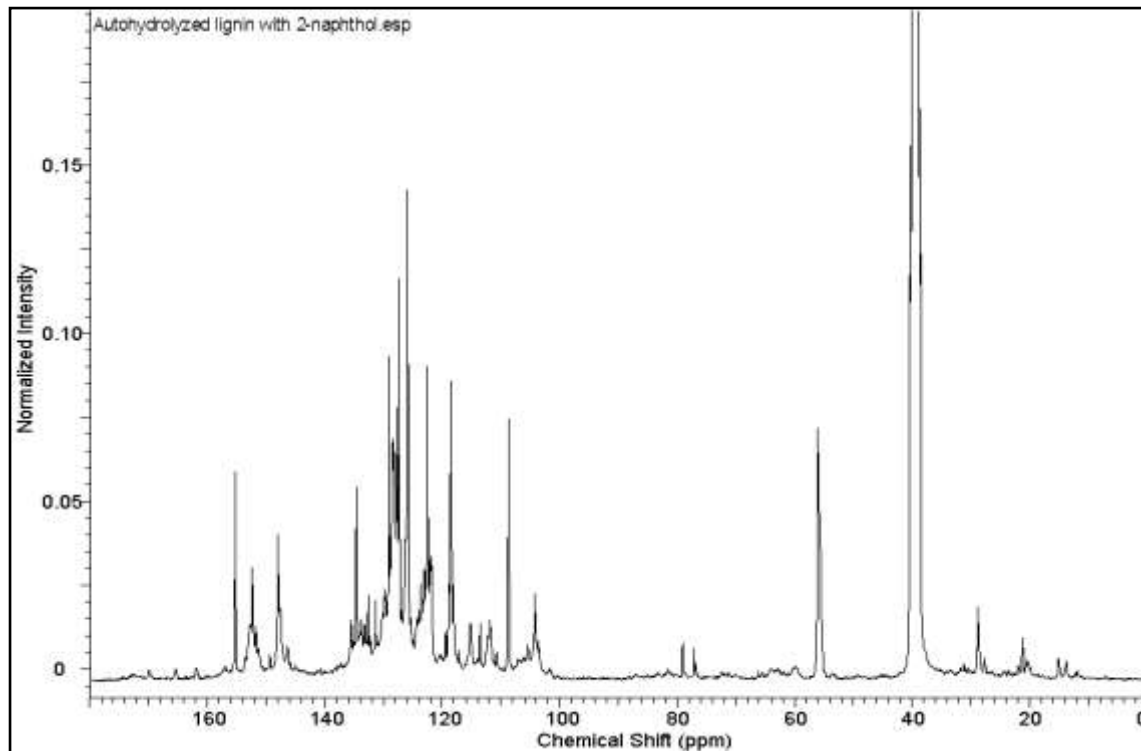
4. ^{13}C NMR spectrum of DAP EOL lignin



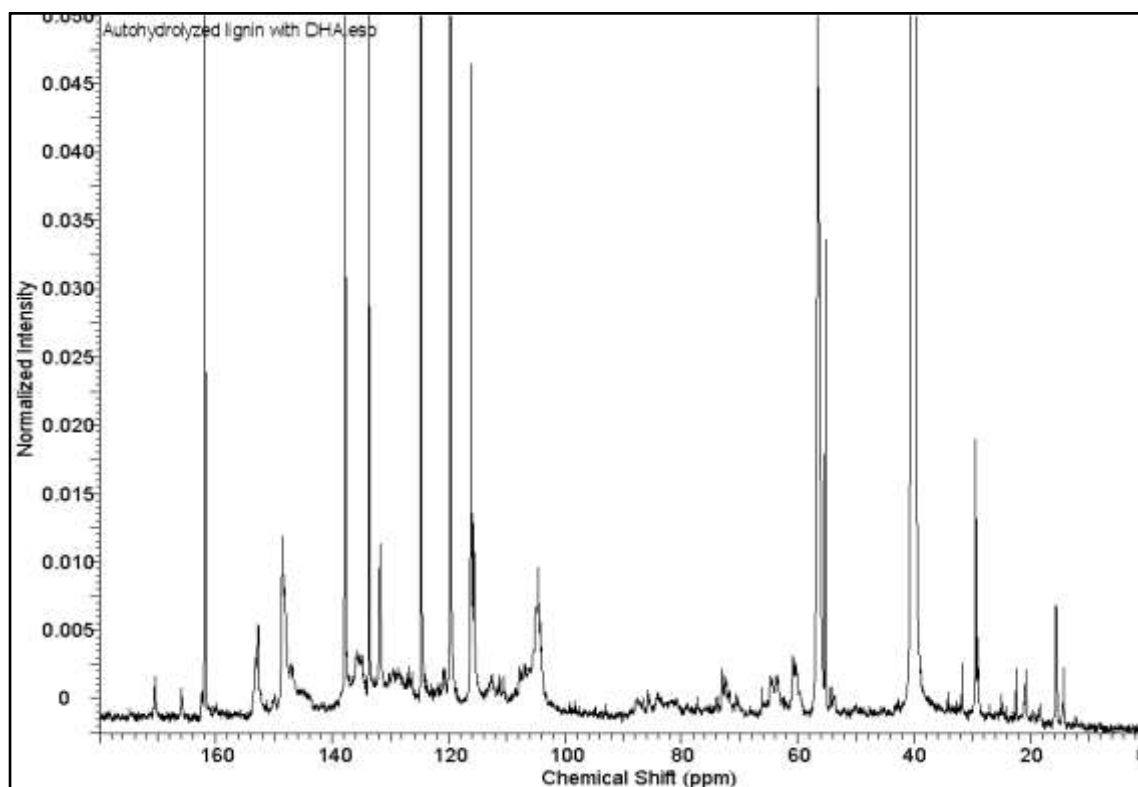
5. ^{13}C NMR spectrum of AH EOL lignin



6. ^{13}C NMR spectrum of AHN EOL lignin



7. ^{13}C NMR spectrum of AHD EOL lignin



^{31}P NMR

Quantitative estimation of the various hydroxyl functional groups were made by employing the calculation outlined:

- The signal area of the cyclohexanol derivatized with TMDP which was due to 6.01×10^{-4} g of cyclohexanol, was intergrated and clibrated to 1.0.
- Because of this molecule contains one hydroxyl group and posses molecular weight of $100.16 \text{ g mol}^{-1}$, then the number of moles of hydroxyl groups present in the internal standard was;

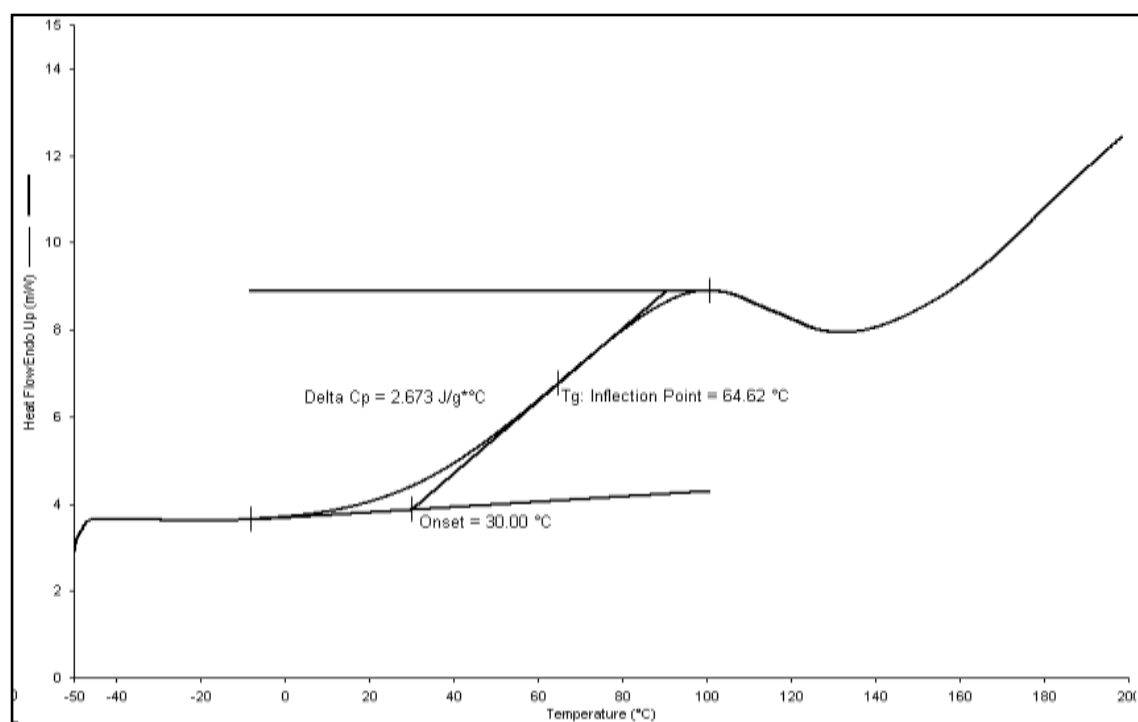
$$6.01 \times 10^{-4} \text{ g} / 100.16 \text{ g mol}^{-1} = 5.9994 \times 10^{-6} \text{ mol}$$

- Because of the integration region of the internal standard was calibrated to 1.0, then each unit area in the spectrum is equal to 5.9994×10^{-6} moles of hydroxyl groups.
- For example, if the lignin sample weighed 25.28 mg and the integration of the carboxylic acid region equaled to 1.859, then;

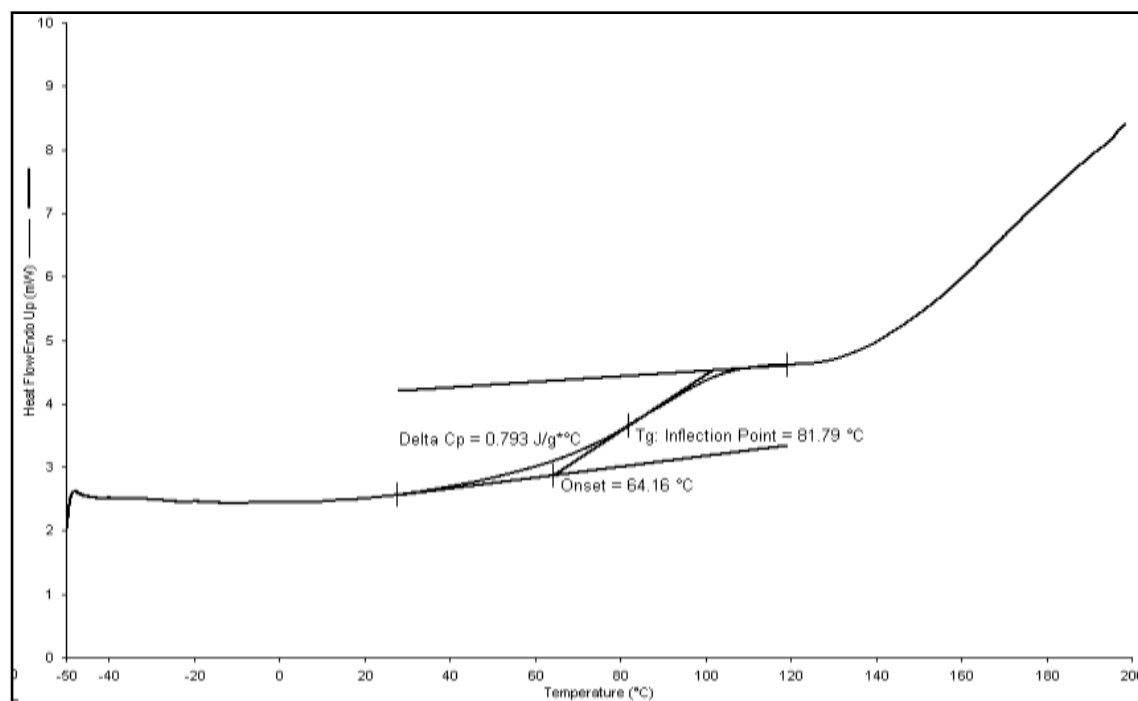
$$(1.859 \times 5.9994 \times 10^{-6} \text{ mol}) / (0.2528 \text{ g}) \times 1000 = 0.44 \text{ mmol g}^{-1} \text{ lignin}$$

APPENDIX III: DSC thermograms of lignin samples

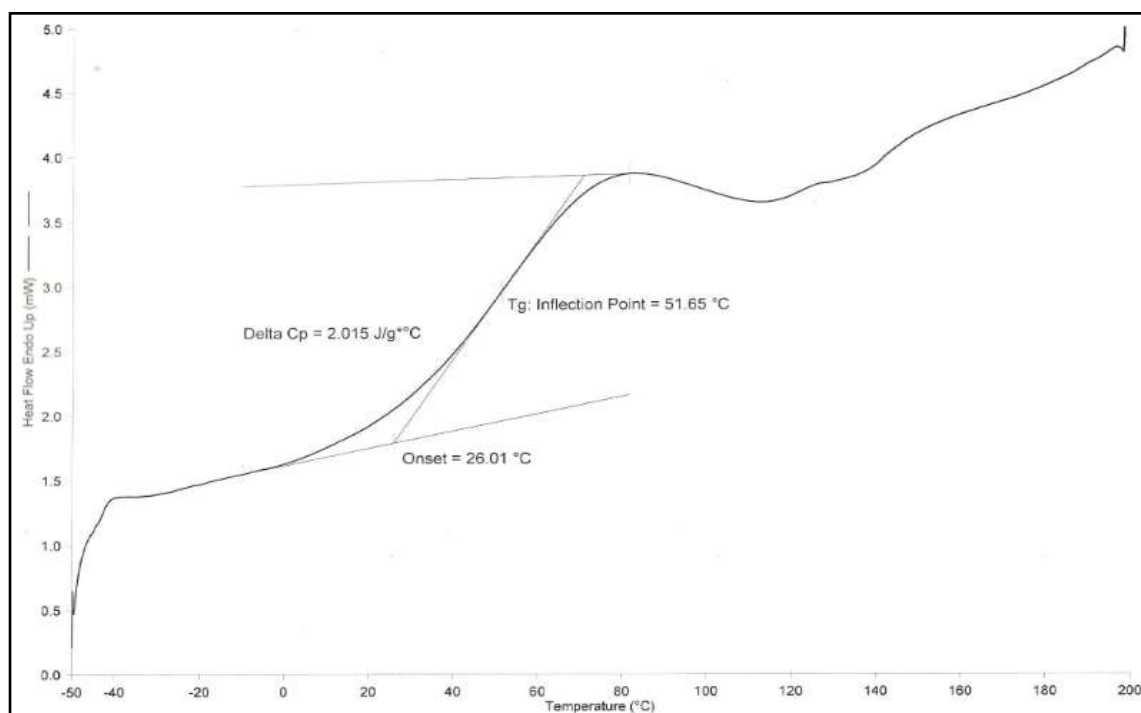
1. DSC thermogram of Kraft lignin



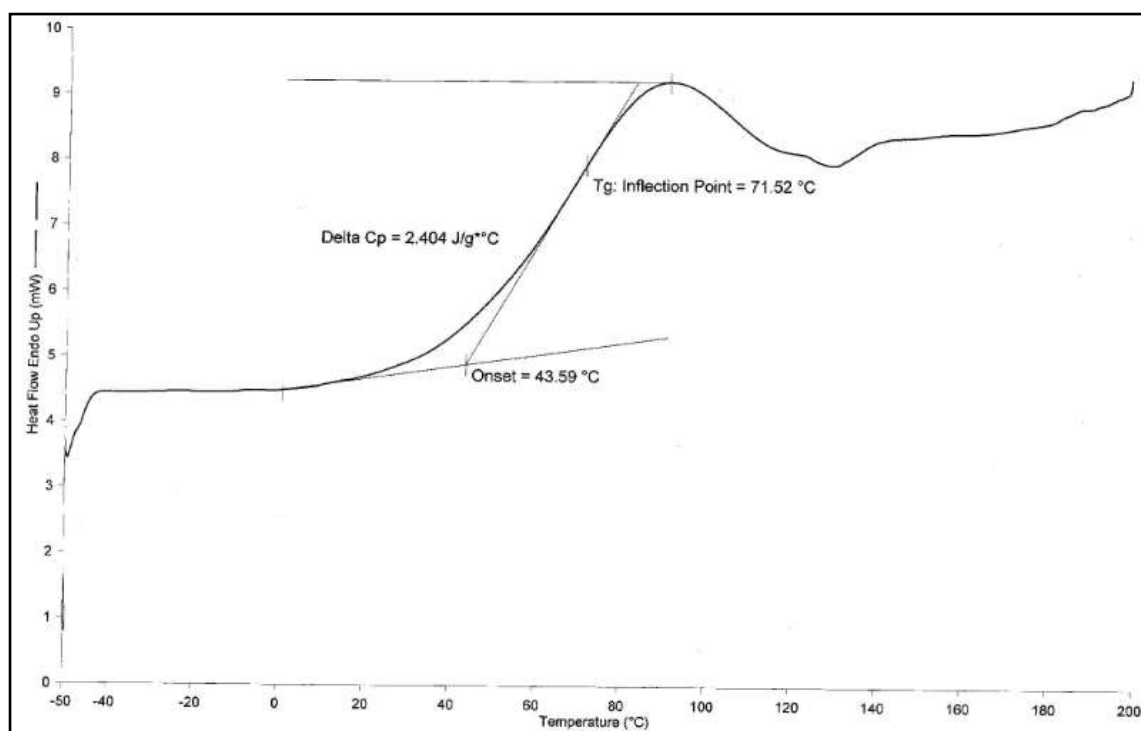
2. DSC thermogram of soda lignin



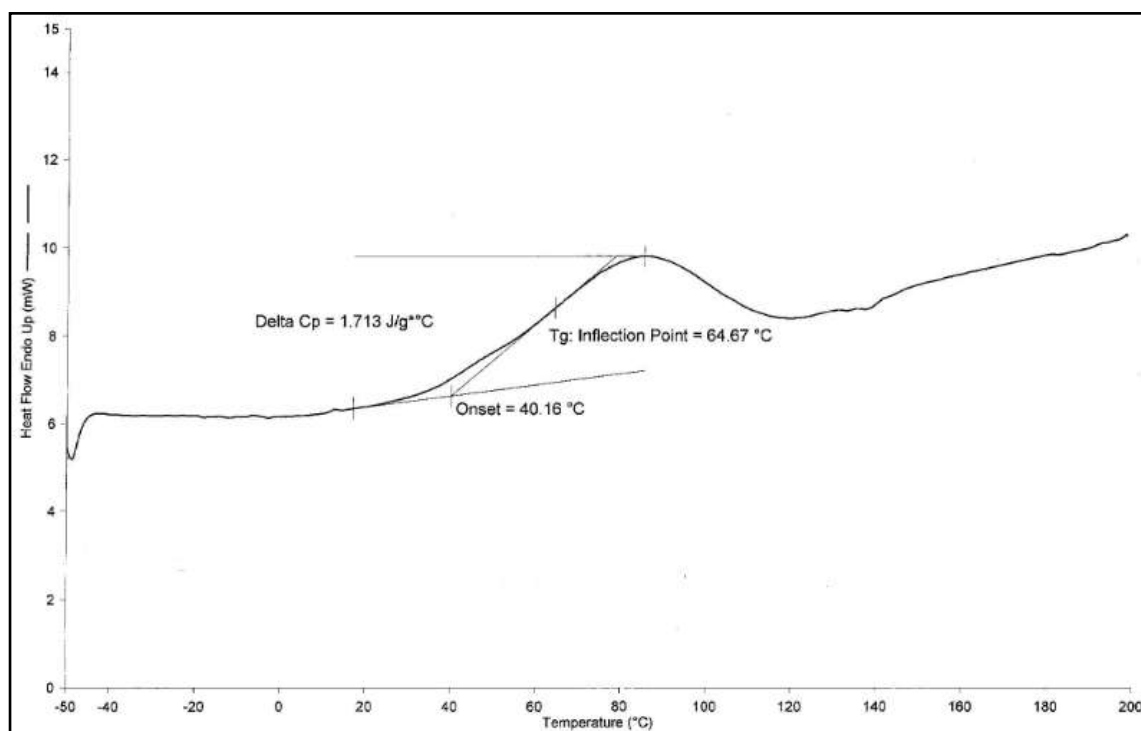
3. DSC thermogram of organosolv lignin



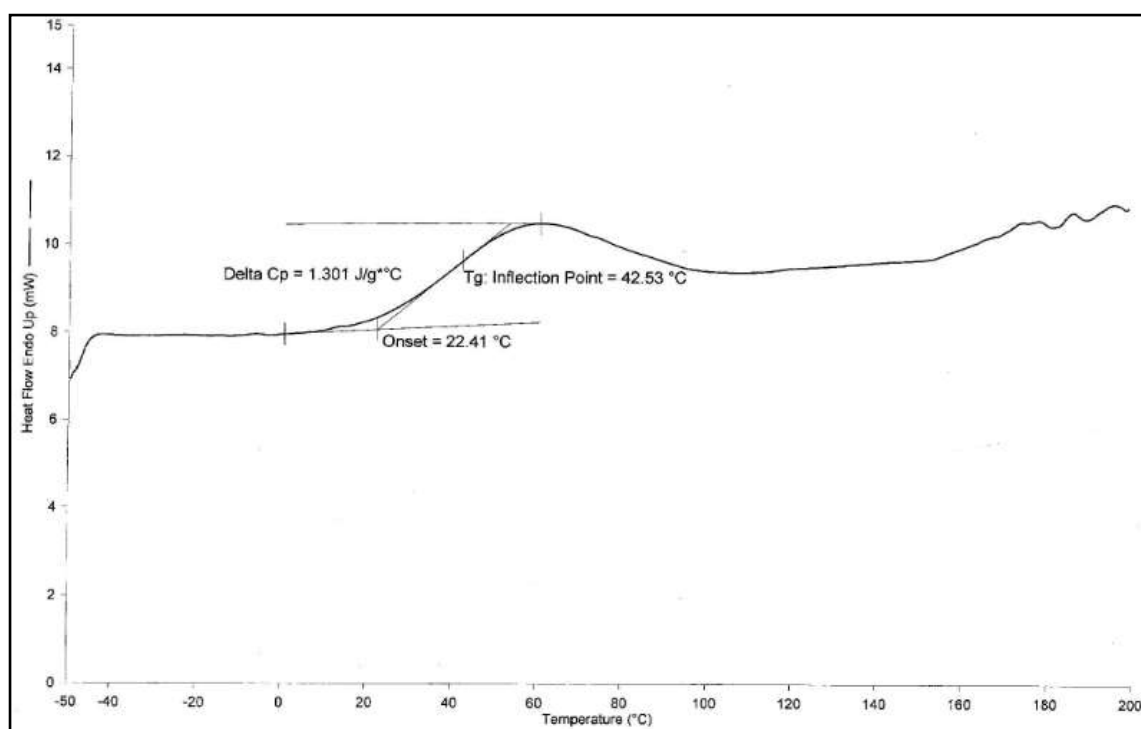
4. DSC thermogram of DAP EOL lignin



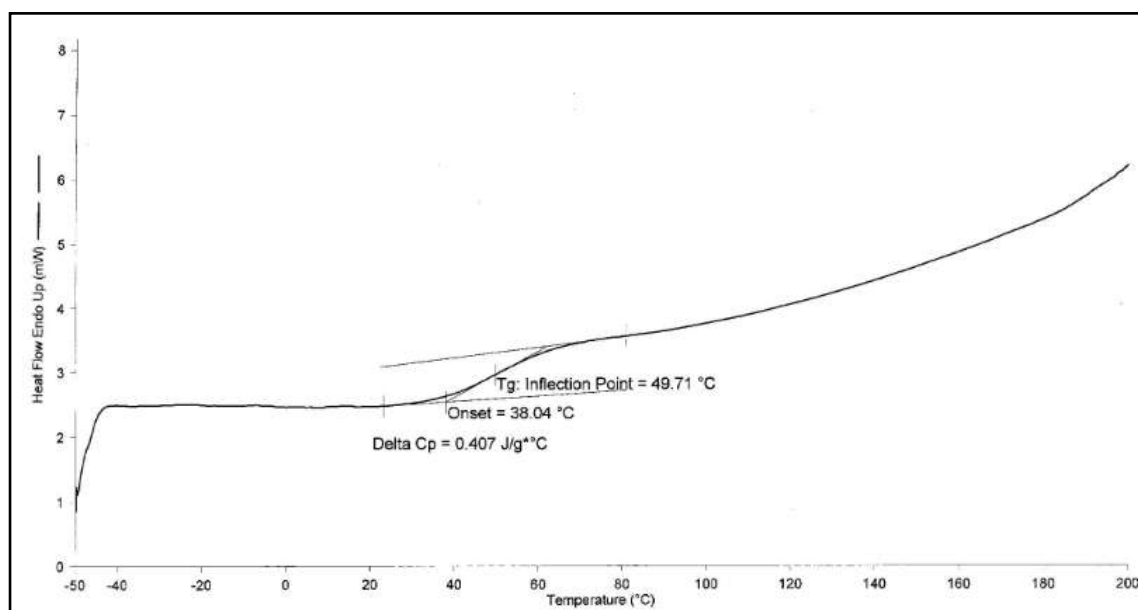
5. DSC thermogram of AH EOL lignin



6. DSC thermogram of AHN EOL lignin

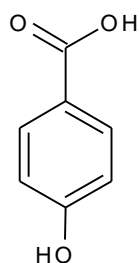


7. DSC thermogram of AHD EOL lignin

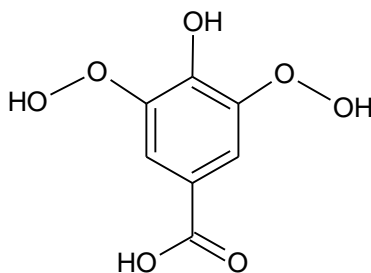


APPENDIX IV: Calibration curves of all standards obtained from HPLC

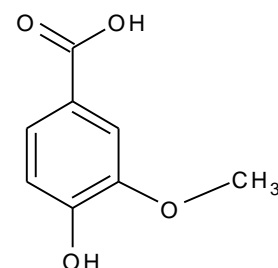
1. Chemical structure of phenolic acids and aldehydes



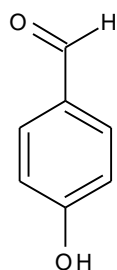
p-hydroxybenzoic acid



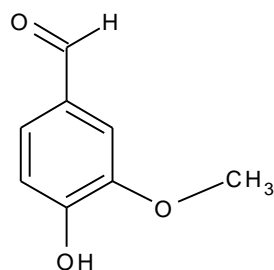
Syringic acid



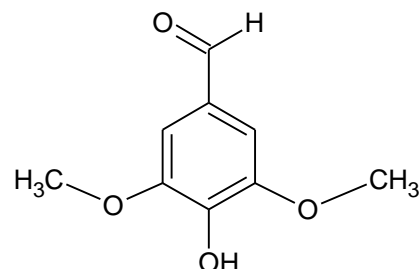
Vanillic acid



p-hydroxybenzaldehyde

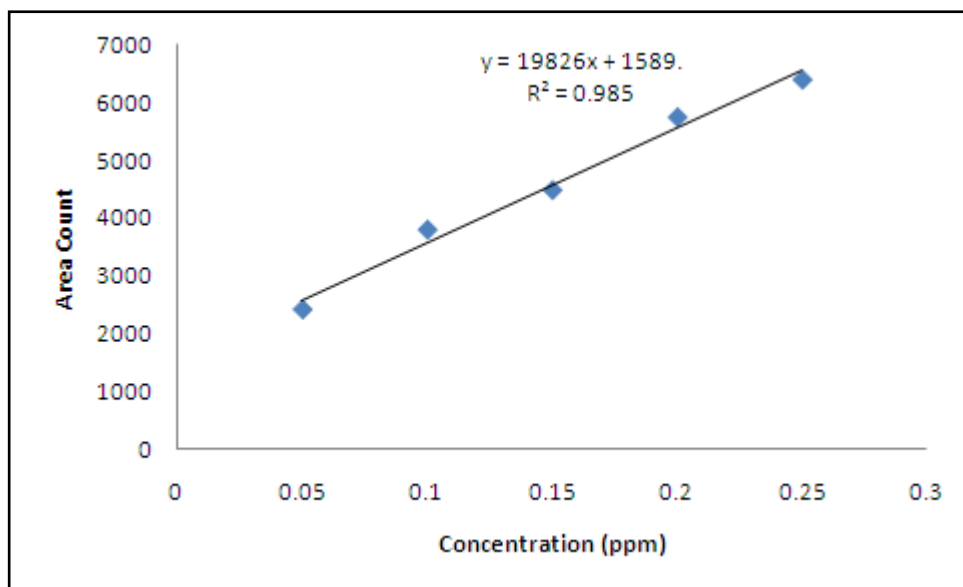


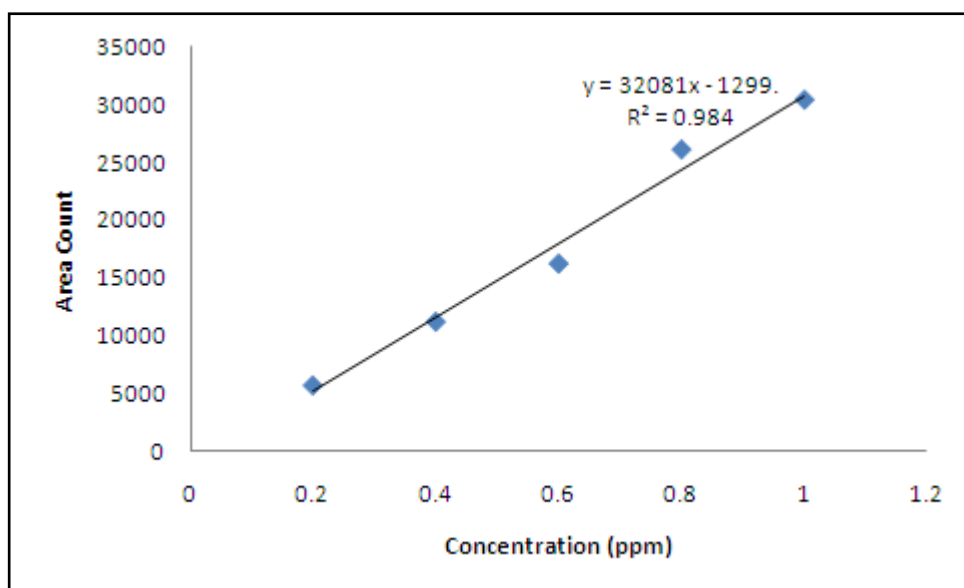
Vanillin



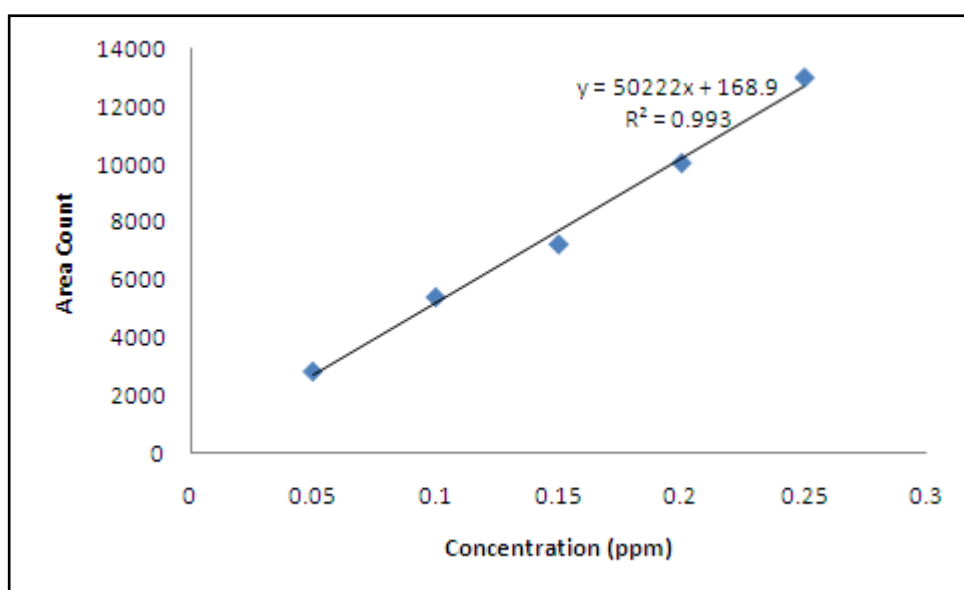
Syringaldehyde

2. Calibration curve of standard p-hydroxybenzoic acid

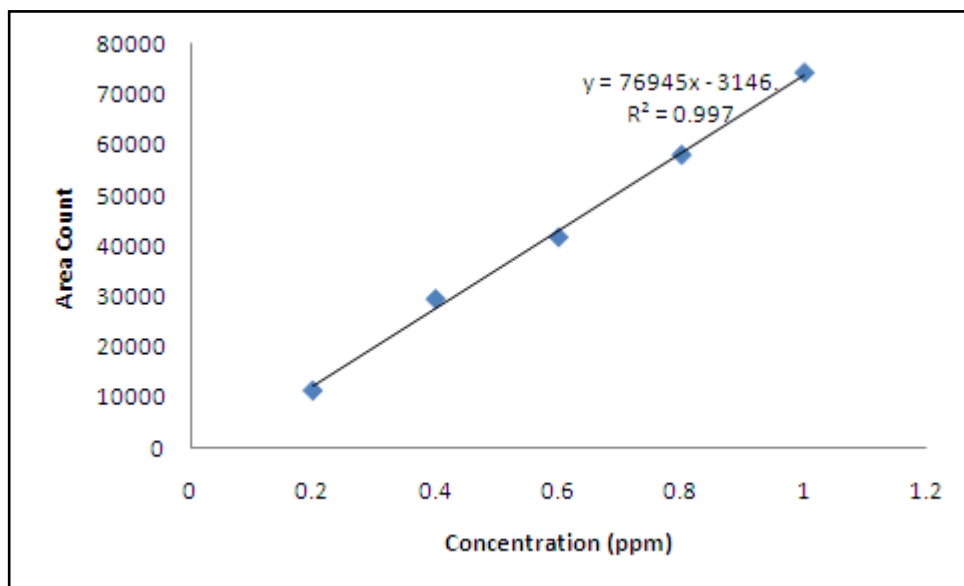
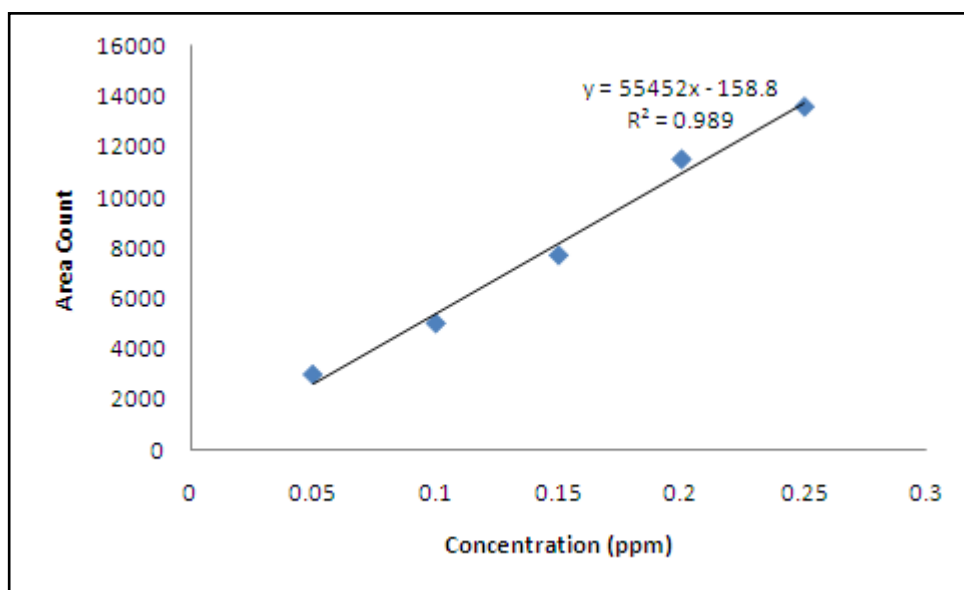




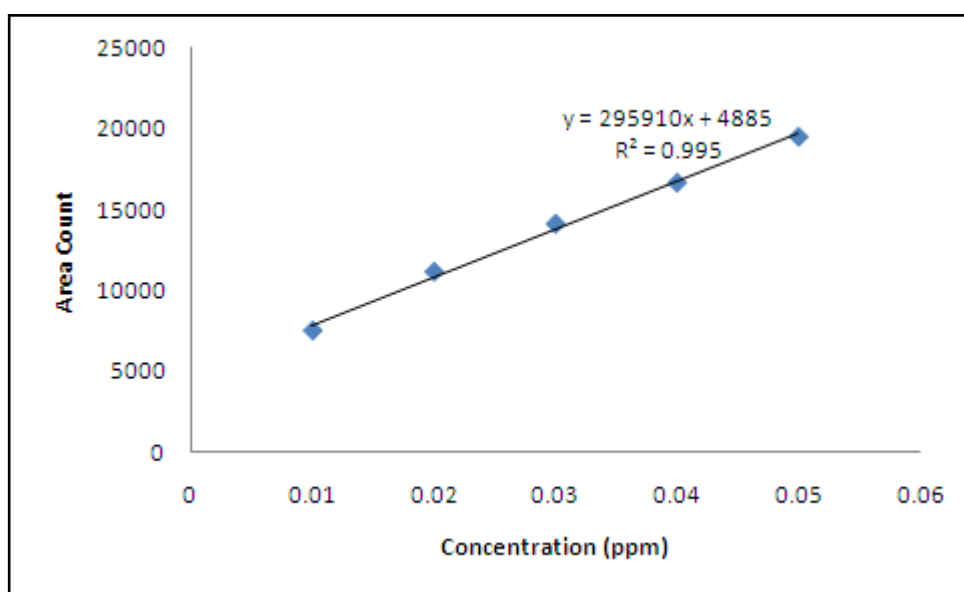
3. Calibration curve of standard vanillic acid



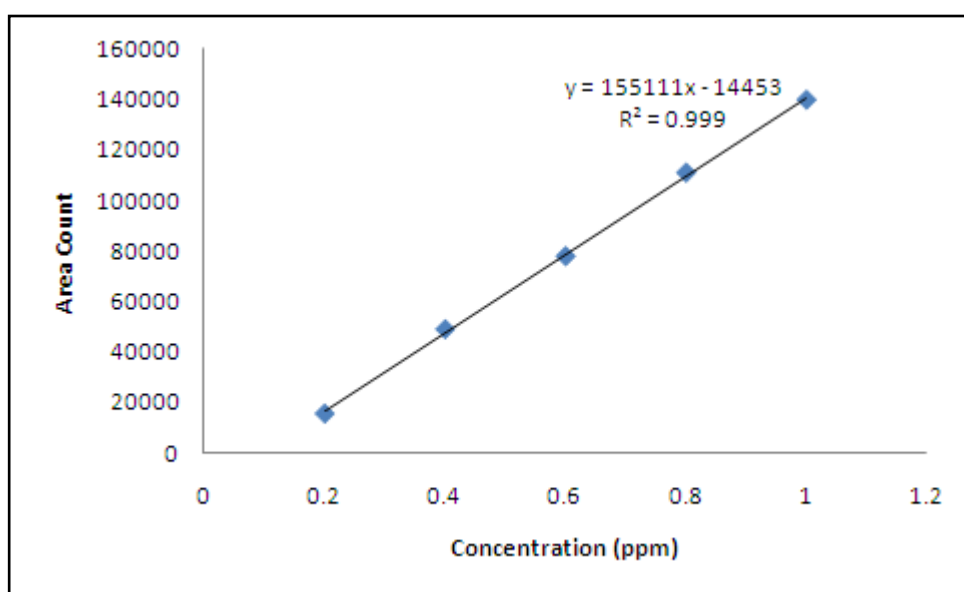
4. Calibration curve of standard syringic acid



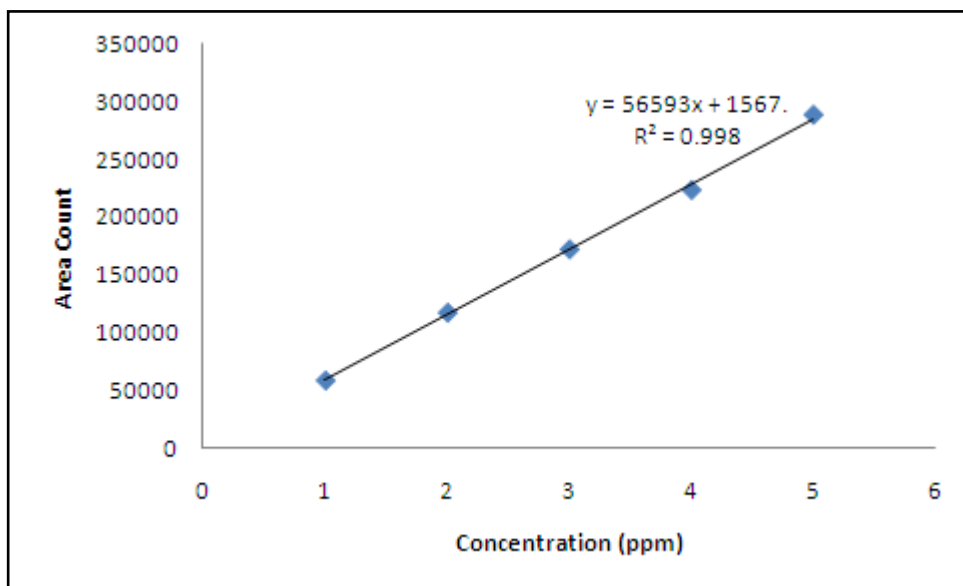
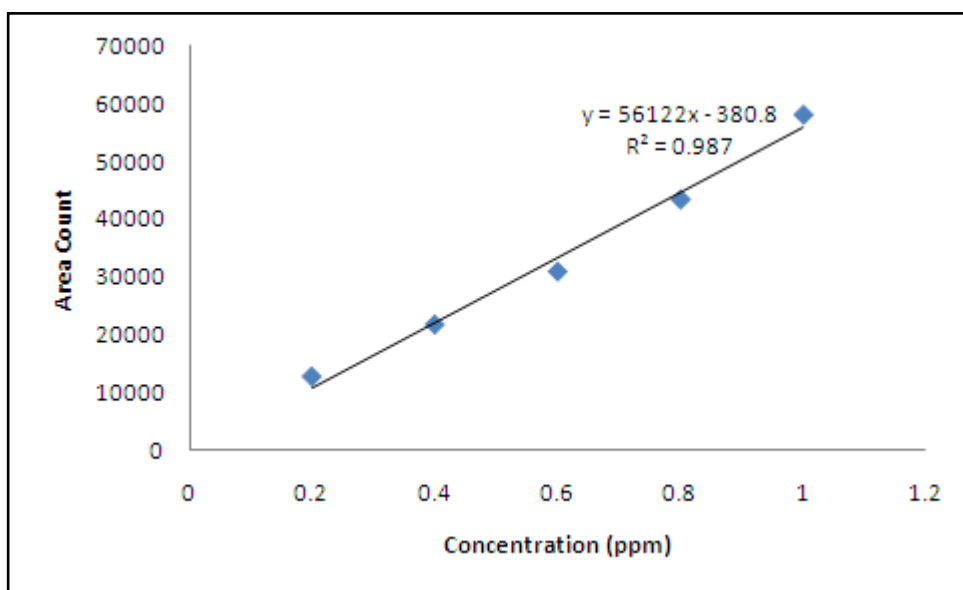
5. Calibration curve of standard p-hydroxybenzaldehyde



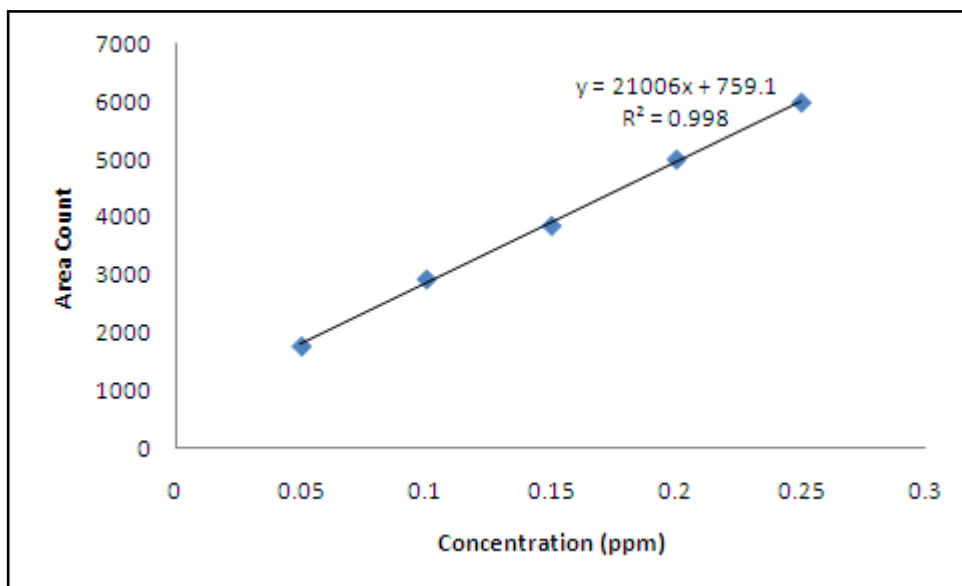
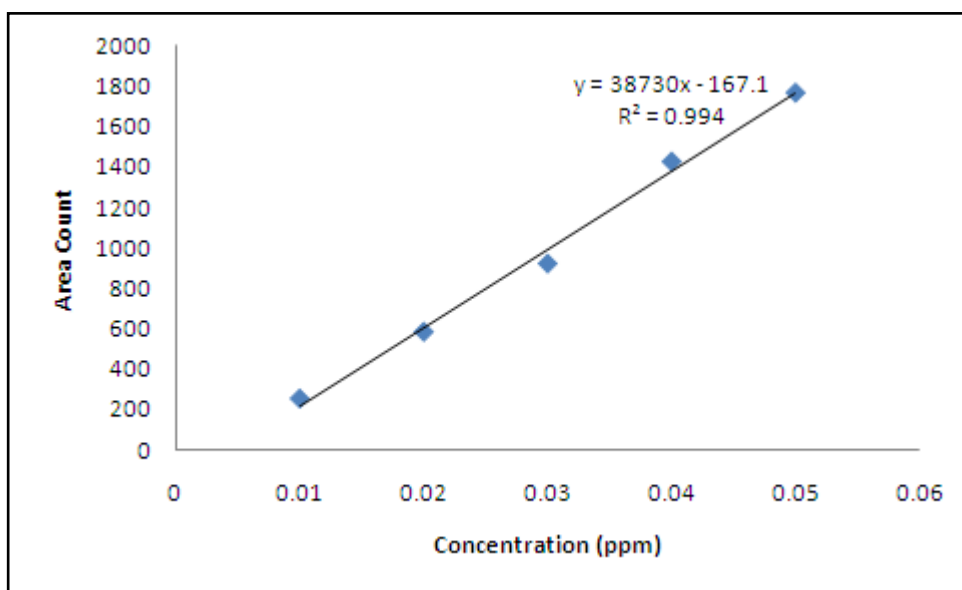
6. Calibration curve of standard vanillin



7. Calibration curve of standard syringaldehyde



8. Calibration curve of standard ferulic acid



Calculations:

e.g: The linear equation for the graph is $y = 155111x + 14453$,

From the equation, y representing the vanillin area, x representing the concentration, while 155111 representing the graph gradient. The HPLC chromatogram shows the area for vanillin as 92815, so, $y = 92815$.

$$\begin{aligned}\text{While, } x &= (92815 - 14453) / 155111 \\ &= 0.5052 \text{ ppm}\end{aligned}$$

Therefore, the concentration of vanillin in 50 mg lignin is 0.5052 ppm.

From the HPLC chromatogram, the area of vanillin in lignin sample is 92815. The concentration of vanillin in the lignin sample is 0.5052 ppm. The percentage of vanillin in lignin was calculated as;

$$M_1 V_1 = M_2 V_2$$

$$0.5052 \text{ ppm (25 mL)} = M_2 (0.25 \text{ mL})$$

$$M_2 = 50.52 \text{ ppm}$$

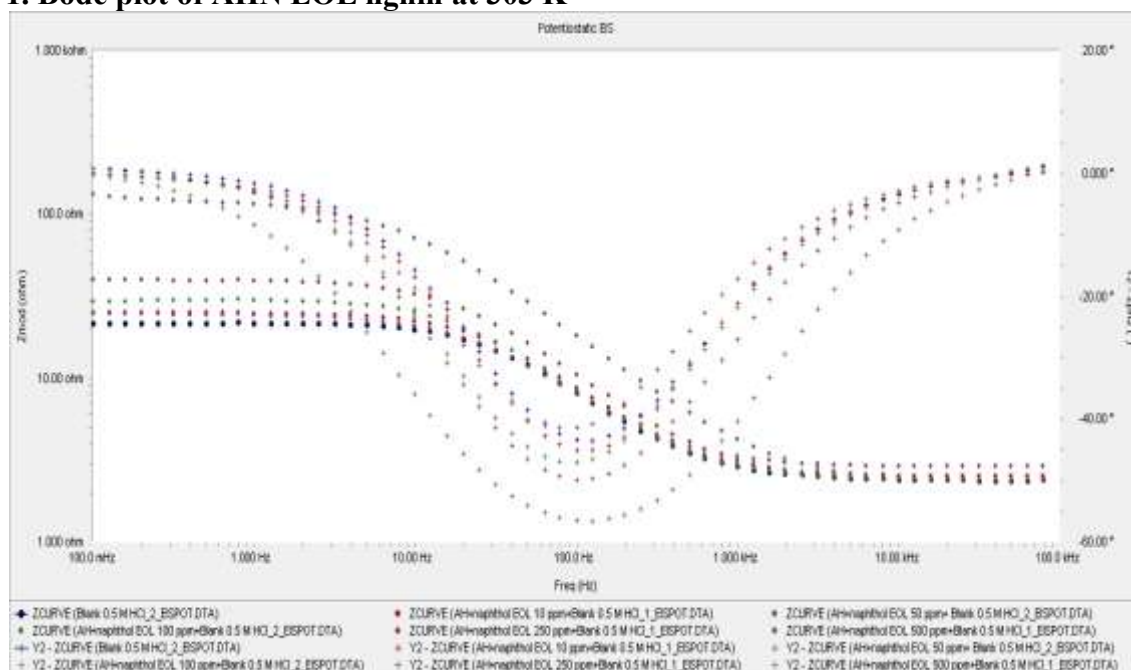
Thus, there are 80.34 μg vanillin in 1 mL of lignin sample. Therefore, 803.4 μg of vanillin can be found in 10 mL lignin sample that has been dilute from 50 mg lignin making the percentage of vanillin in 50 mg of lignin being;

$$= \frac{505.2 \text{ } \mu\text{g vanillin}}{50 \times 10^3 \text{ } \mu\text{g lignin}} \times 100 \%$$

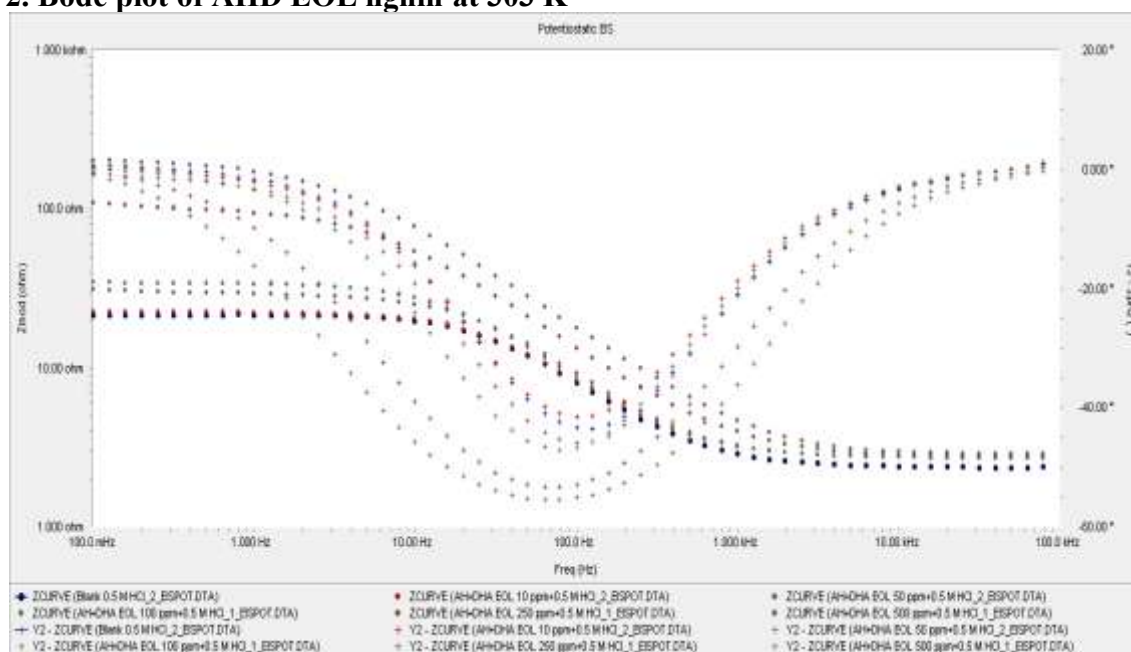
$$= 1.01 \% \text{ vanillin in 50 mg lignin}$$

APPENDIX V: Bode plots of all modified lignin samples obtained from EIS

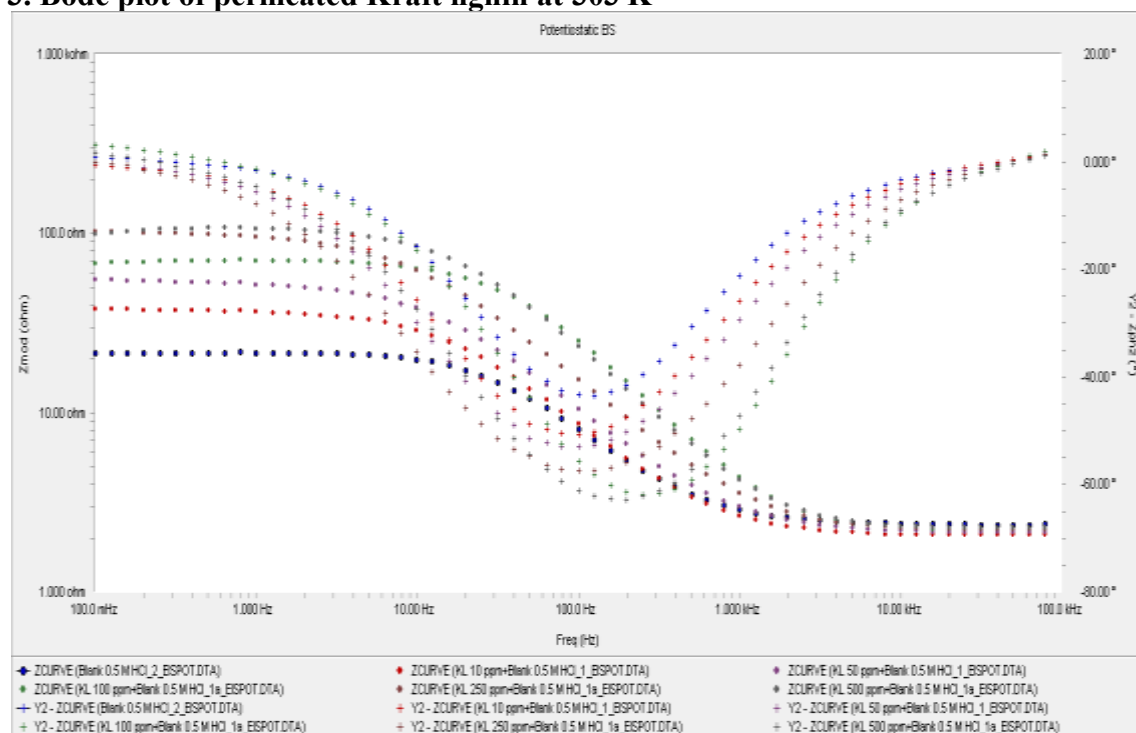
1. Bode plot of AHN EOL lignin at 303 K



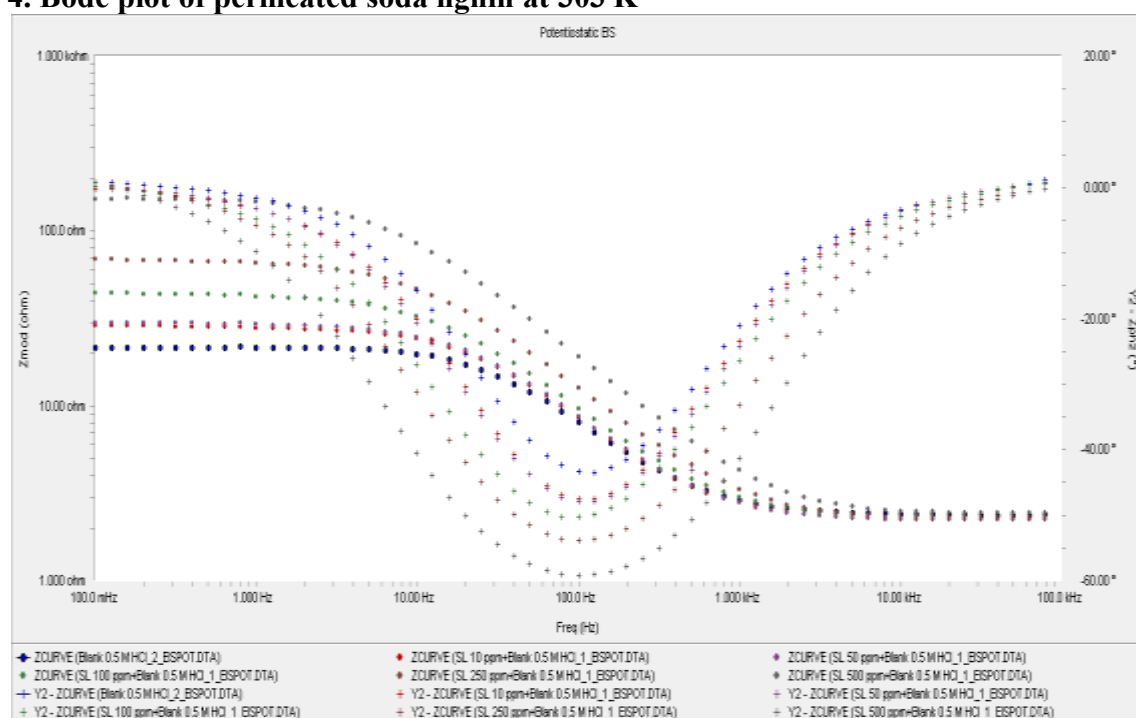
2. Bode plot of AHD EOL lignin at 303 K



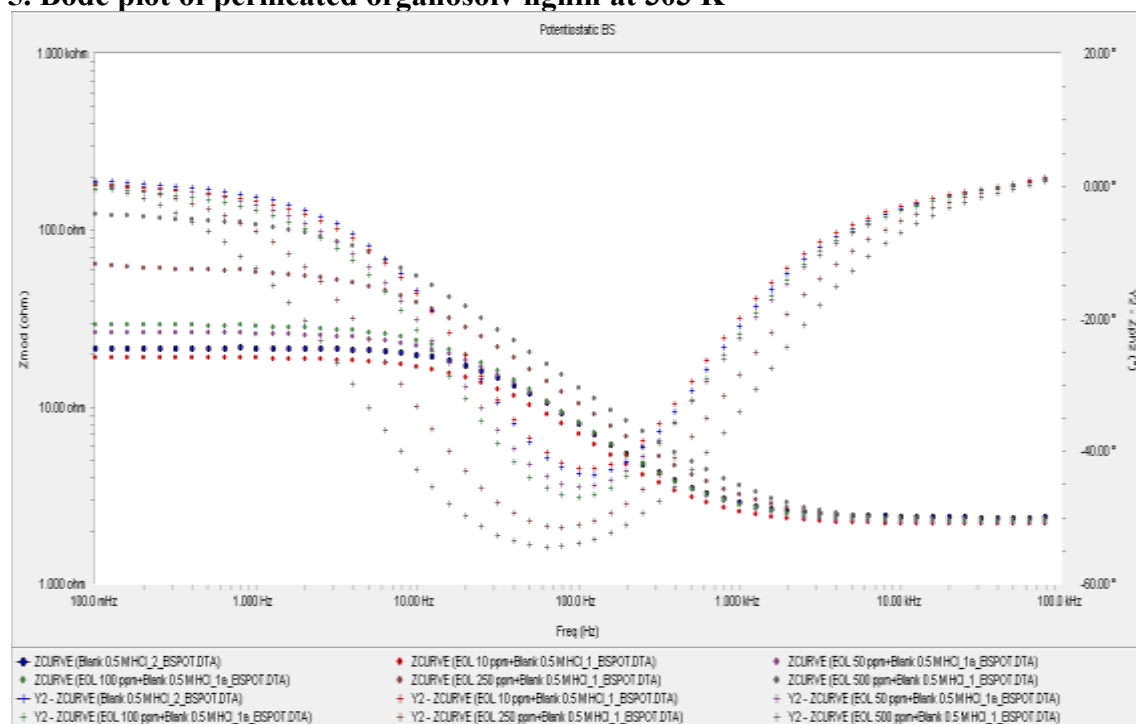
3. Bode plot of permeated Kraft lignin at 303 K



4. Bode plot of permeated soda lignin at 303 K



5. Bode plot of permeated organosolv lignin at 303 K



APPENDIX VI: Effect of temperature on the mild steel corrosion inhibition

1. Effect of temperature on the corrosion of mild steel in 0.5 M HCl at various concentrations of AHN EOL lignin

Temperature (K)	Concentrations (ppm)	W_L (g)	CR ($\text{mg cm}^{-2} \text{ h}^{-1}$)	IE (%)	ϑ	$\vartheta / 1 - \vartheta$
303	0	0.7435	1.2908	0.00	0.00	0.00
	100	0.3695	0.6415	50.30	0.50	1.01
	200	0.1436	0.2493	80.69	0.81	4.18
	300	0.1196	0.2076	83.91	0.84	5.22
	400	0.0920	0.1597	87.63	0.88	7.08
	500	0.0660	0.1146	91.12	0.91	10.27
313	0	0.9597	1.6661	0.00	0.00	0.00
	100	0.4189	0.7273	56.35	0.56	1.29
	200	0.2391	0.4151	75.09	0.75	3.01
	300	0.1934	0.3358	79.85	0.80	3.96
	400	0.1493	0.2592	84.44	0.84	5.43
	500	0.1276	0.2215	86.70	0.87	6.52
323	0	1.2638	2.1941	0.00	0.00	0.00
	100	0.6137	1.0655	51.44	0.51	1.06
	200	0.3997	0.6939	68.37	0.68	2.16
	300	0.3333	0.5786	73.63	0.74	2.79
	400	0.2551	0.4429	79.81	0.80	3.95
	500	0.2383	0.4137	81.14	0.81	4.30
333	0	1.4717	2.5550	0.00	0.00	0.00
	100	0.8166	1.4177	44.51	0.45	0.80
	200	0.5585	0.9696	62.05	0.62	1.64
	300	0.4327	0.7512	70.60	0.71	2.40
	400	0.3999	0.6943	72.83	0.73	2.68
	500	0.3857	0.6696	73.79	0.74	2.82

2. Effect of temperature on the corrosion of mild steel in 0.5 M HCl at various concentrations of AHD EOL lignin

Temperature (K)	Concentrations (ppm)	W_L (g)	CR ($\text{mg cm}^{-2} \text{ h}^{-1}$)	IE (%)	ϑ	$\vartheta / 1 - \vartheta$
303	0	0.7435	1.2908	0.00	0.00	0.00
	100	0.1234	0.2142	83.40	0.83	5.03
	200	0.0630	0.1094	91.53	0.92	10.80
	300	0.0410	0.0712	94.49	0.94	17.13
	400	0.0395	0.0686	94.69	0.95	17.82
	500	0.0383	0.0665	94.85	0.95	18.41
313	0	0.9597	1.6661	0.00	0.00	0.00
	100	0.1894	0.3288	80.26	0.80	4.07
	200	0.1205	0.2092	87.44	0.87	6.96
	300	0.0983	0.1707	89.76	0.90	8.76
	400	0.0951	0.1651	90.09	0.90	9.09
	500	0.0929	0.1613	90.32	0.90	9.33
323	0	1.2638	2.1941	0.00	0.00	0.00
	100	0.2896	0.5028	77.08	0.77	3.36
	200	0.2156	0.3743	82.94	0.83	4.86
	300	0.1913	0.3321	84.86	0.85	5.61
	400	0.1847	0.3207	85.39	0.85	5.84
	500	0.1884	0.3271	85.09	0.85	5.71
333	0	1.4717	2.5550	0.00	0.00	0.00
	100	0.4591	0.7970	68.80	0.69	2.21
	200	0.3722	0.6462	74.71	0.75	2.95
	300	0.3107	0.5394	78.89	0.79	3.74
	400	0.2839	0.4929	80.71	0.81	4.18
	500	0.2723	0.4727	81.50	0.81	4.40

3. Effect of temperature on the corrosion of mild steel in 0.5 M HCl at various concentrations of permeated Kraft lignin

Temperature (K)	Concentrations (ppm)	W_L (g)	CR ($\text{mg cm}^{-2} \text{ h}^{-1}$)	IE (%)	ϑ	$\vartheta / 1 - \vartheta$
303	0	0.6516	1.1313	0.00	0.00	0.00
	100	0.1857	0.3224	71.50	0.72	2.51
	200	0.1466	0.2545	77.50	0.78	3.44
	300	0.1074	0.1865	83.52	0.84	5.07
	400	0.0830	0.1440	87.27	0.87	6.85
	500	0.0731	0.1269	88.78	0.89	7.91
313	0	0.7361	1.2780	0.00	0.00	0.00
	100	0.2602	0.4518	64.65	0.65	1.83
	200	0.2358	0.4094	67.97	0.68	2.12
	300	0.1956	0.3396	73.43	0.73	2.76
	400	0.1572	0.2729	78.64	0.79	3.68
	500	0.1238	0.2149	83.18	0.83	4.95
323	0	0.8455	1.4679	0.00	0.00	0.00
	100	0.3696	0.6417	56.29	0.56	1.29
	200	0.3303	0.5734	60.93	0.61	1.56
	300	0.2956	0.5132	65.04	0.65	1.86
	400	0.2232	0.3875	73.60	0.74	2.79
	500	0.1730	0.3003	79.54	0.80	3.89
333	0	1.1161	1.9377	0.00	0.00	0.00
	100	0.5252	0.9118	52.94	0.53	1.13
	200	0.4931	0.8561	55.82	0.56	1.26
	300	0.4203	0.7297	62.34	0.62	1.66
	400	0.3478	0.6038	68.84	0.69	2.21
	500	0.2916	0.5063	73.87	0.74	2.83

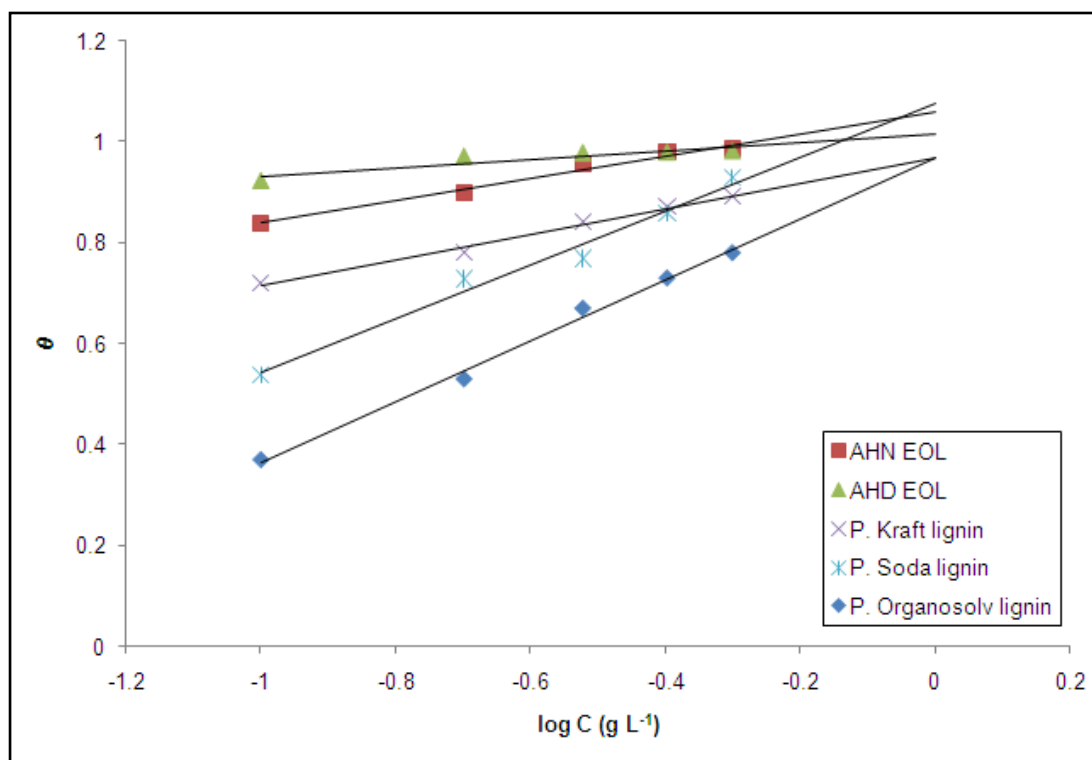
4. Effect of temperature on the corrosion of mild steel in 0.5 M HCl at various concentrations of permeated soda lignin

Temperature (K)	Concentrations (ppm)	W_L (g)	CR ($\text{mg cm}^{-2} \text{ h}^{-1}$)	IE (%)	ϑ	$\vartheta / 1 - \vartheta$
303	0	0.6469	1.1231	0.00	0.00	0.00
	100	0.2956	0.5132	54.31	0.54	1.19
	200	0.1734	0.3010	73.20	0.73	2.73
	300	0.1476	0.2563	77.18	0.77	3.38
	400	0.0881	0.1530	86.38	0.86	6.34
	500	0.0430	0.0747	93.35	0.93	14.04
313	0	0.7921	1.3752	0.00	0.00	0.00
	100	0.3861	0.6703	51.26	0.51	1.05
	200	0.2377	0.4127	69.99	0.70	2.33
	300	0.2078	0.3608	73.77	0.74	2.81
	400	0.1365	0.2370	82.77	0.83	4.80
	500	0.0922	0.1601	88.36	0.88	7.59
323	0	0.8703	1.5109	0.00	0.00	0.00
	100	0.4658	0.8087	46.48	0.46	0.87
	200	0.3106	0.5392	64.31	0.64	1.80
	300	0.2761	0.4793	68.28	0.68	2.15
	400	0.2034	0.3531	76.63	0.77	3.28
	500	0.1396	0.2424	83.96	0.84	5.23
333	0	1.2616	2.1903	0.00	0.00	0.00
	100	0.7463	1.2957	40.84	0.41	0.69
	200	0.5265	0.9141	58.27	0.58	1.40
	300	0.4761	0.8266	62.26	0.62	1.65
	400	0.4368	0.7583	65.38	0.65	1.89
	500	0.2799	0.4859	77.81	0.78	3.51

5. Effect of temperature on the corrosion of mild steel in 0.5 M HCl at various concentrations of permeated organosolv lignin

Temperature (K)	Concentrations (ppm)	W_L (g)	CR ($\text{mg cm}^{-2} \text{ h}^{-1}$)	IE (%)	ϑ	$\vartheta / 1 - \vartheta$
303	0	0.6969	1.2099	0.00	0.00	0.00
	100	0.4388	0.7618	37.04	0.37	0.59
	200	0.3294	0.5719	52.73	0.53	1.12
	300	0.2034	0.3531	70.81	0.71	2.43
	400	0.1732	0.3007	75.15	0.75	3.02
	500	0.0792	0.1374	88.64	0.89	7.80
313	0	0.8977	1.5585	0.00	0.00	0.00
	100	0.6194	1.0753	31.00	0.31	0.45
	200	0.4923	0.8547	45.16	0.45	0.82
	300	0.3029	0.5259	66.26	0.66	1.96
	400	0.2639	0.4582	70.60	0.71	2.40
	500	0.1338	0.2323	85.10	0.85	5.71
323	0	1.2543	2.1776	0.00	0.00	0.00
	100	0.9431	1.6373	24.81	0.25	0.33
	200	0.7342	1.2747	41.47	0.41	0.71
	300	0.5077	0.8814	59.52	0.60	1.47
	400	0.4467	0.7755	64.39	0.64	1.81
	500	0.2443	0.4241	80.52	0.81	4.13
333	0	1.5372	2.6688	0.00	0.00	0.00
	100	1.3028	2.2618	15.25	0.15	0.18
	200	0.9551	1.6582	37.87	0.38	0.61
	300	0.7227	1.2547	52.99	0.53	1.13
	400	0.6418	1.1142	58.25	0.58	1.40
	500	0.3949	0.6856	74.31	0.74	2.89

APPENDIX VII: Temkin adsorption isotherm curves



R^2 : AHN EOL: 0.982; AHD EOL: 0.837; P. Kraft lignin: 0.980; P. Soda lignin: 0.981; P. Organosolv lignin: 0.984.